.

Introduction to Radar
Part I

Scriptum of a lecture at the
Ruhr-Universität Bochum

Dr.-Ing. Joachim H.G. Ender

Honorary Professor of the Ruhr-University Bochum
Head of the Fraunhofer-Institute for High Frequency
Physics and Radar Techniques FHR

Neuenahrer Str. 20, 53343 Wachtberg, Phone 0228-9435-226, Fax 0228-9435-627
E-Mail: joachim.ender@fhr.fraunhofer.de

Contents

Preface

This lecture addresses the basics of modern radar with an emphasis on signal modelling and processing. It is intended to convey the technical and physical background of radar to the students to enable them to understand the mechanisms in depth and so to apply well-founded statistical signal models.

The lecture requires as prerequisites the bases of communications engineering (usual signals, convolution, Fourier transformation, linear systems and filters, sampling theorem, ...). Elementary knowledge of high-frequency technology like wave propagation and antennas is communicated during the lectures.

The emphasis is set on the one hand on the statistical modelling of sensor signals, on the other hand on the multidimensional application of the Fourier transformation in the temporal and spatial domain. Based on these investigations, modern radar techniques are investigated like radar with phased array antennas and synthetic aperture radar (SAR). The lecture is illustrated with many graphics explaining geometrical situations, processing architectures and principles. Also real examples of radar signals are included.

In chapter 1 on radar fundamentals complex valued radar signals for coherent pulse radar are introduced including the Doppler effect caused by target motion, followed by pulse compression techniques. Ambiguities in range and Doppler are studied as well as the design of radar waveforms based on the ambiguity function. Since radar is an ever-lasting fight against noise, statistical parameter estimation is explained in the application to radar; the Cramér-Rao bounds are introduced as means for measuring the information content of statistical signals with respect to the estimation of parameters like direction or Doppler frequency. Radar detectors are derived based on the theory of statistical test, receiver-operating characteristics are calculated as performance measures.

Chapter 2 concerns the processing of vector-valued signals originated from antenna arrays. Beamformers are derived as spatial filters maximizing the signal-to-interference ratio. The monopulse estimator for the direction of a target is deduced using the maximum-likelihood technique. The meaning of the spatial covariance matrix is demonstrated in the context of adaptive beamforming.

The chapter 3 on air and space borne radar platforms describes the geometry of flight and gives insight into the nature of clutter in spatial and frequency domains as a pre-requisite to chapter 4 on synthetic aperture radar (SAR). Here, model signals of point scatterers in two dimensions are presented, ambiguities are derived and the most important SAR processors are investigated. Moreover, this chapter aims to obtaining insights about the meaning of the space of wave number vectors ('k-space') for imaging.

This document is marked as 'part I' since a second part covering also space-time-adaptive processing (STAP) and multi-dimensional SAR is planned.

Remagen, April 2011 Joachim H. G. Ender

Chapter 1

Radar fundamentals

In this chapter we will describe the basics of a *coherent* radar system with the ability to emit an arbitrary wave form and to receive and digitize the backscattered echoes. Afterwards the elementary signal processing units will be built up step by step. The most content of this chapter can be found in books on signal theory or in radar books [1, 2, 3, 5, 6, 7, 8]; nevertheless, we believe that it is very useful for the reader to have all the needed tools together with a unified notation. The concept of matched filter and other matters are dealt in many publications only in the real domain. We describe the signals in the complex domain from the beginning.

1.1 The nature of radar

The main advantages of radar compared to other sensors are its weather and daylight independence, its range-independent resolution and the sensitivity to small displacements and motions, which have led to a triumphal procession especially for remote sensing. The core components of a radar system are: a waveform generator, the transmitter bringing the radio frequency signals to the transmit antenna which radiates the electromagnetic waves into the space, the receiving antenna collecting the waves reflected by objects, the receiver amplifying the weak signals and making them available to the analogue and - above all - digital processing.

A radar system measures the distance and direction to the object, its velocity and some signatures for the purpose of classification. There are two sources for the distance measurement: A coarse but unambiguous information by measurement of the wave travelling time and a fine but ambiguous information by phase measurement. The accuracy is in the order of meters down to decimeters for the first kind and in the order of fractions of the wavelength (millimeters!) for the second. By using the phase modulation over time (Doppler frequency) the radar can measure also the radial velocity with a high accuracy.

There are two different basic concepts of radar: The first aims at the detection and localization of targets; here usually the resolution cell size (range, direction, Doppler) is greater or equal to the extensions generated by the object. Target classification can be achieved via the signal strength (radar cross section, RCS),

Glossary for this chapter

α	Frequency modulation rate of a chirp
α	Time stretch factor (Doppler effect)
α	Level for a statistical test
$\beta = v/c_0$	Ratio of target velocity to velocity of light
η	Threshold
$\chi(\tau, \nu)$	Ambiguity function
φ	Signal parameter (e.g. Doppler phase shift)
Φ	Set of signal parameters
Ψ	Random phase
γ	Signal-to-noise ratio
$\mathbf{P}_U$	Projector to the subspace U
λ	Wavelength
λ_0	Wavelength related to the reference frequency
$\Lambda(\mathbf{z})$	Likelihood ratio
$\psi(\mathbf{z})$	Statistical test
$\rho(s_1, s_2)$	Correlation coefficient
σ^2	Noise variance
$\boldsymbol{\vartheta}$	Parameter vector
$\hat{\boldsymbol{\vartheta}}$	Estimator of parameter vector $\boldsymbol{\vartheta}$
$\boldsymbol{\Theta}$	Set of parameter vectors
τ	Time delay
a	Complex Amplitude
b	Bandwidth
c_0	Velocity of light
$C(x)$	Fresnel integral
$C(T)$	Clutter process
$E[X]$	Expectation of the random variable X
f	Radio frequency
f_0	Reference frequency
f_s	Sampling frequency fast-time
F	Doppler frequency
$F_s = PRF$	Sampling frequency slow-time = Pulse repetition frequency
$F_{\boldsymbol{\vartheta}}(x)$	Distribution function
G_{rx}	Gain of the receive antenna
G_{tx}	Gain of the transmit antenna
$h(t)$	Pulse response
$H(f)$	Transfer function
$H_\eta(k)$	Transfer function of robustified filter
H	Hypothesis (for a statistical test)
$\mathbf{I}_n$	$n \times n$ unit matrix
$I_0(x)$	Modified Bessel function of order 0
$\Im$	Imaginary part
$\mathbf{J}$	Fisher's information matrix
$k_r = 2\pi/\lambda$	Wavenumber
$k_0 = 2\pi/\lambda_0$	Wavenumber related to the reference frequency
$\mathcal{K}$	Wave number set, k-set
K	Alternative (for a statistical test)
$\mathsf{k} = 1.38 \cdot 10^{-23} \quad [Ws/K]$	Boltzmann constant
$\mathsf{kT} = 4 \cdot 10^{-21} \quad [Ws]$	Noise power density at room temparature

$L^{\mathbf{Z}}(\mathbf{z})$	Log-likelihood function
L_{tx}	Power density effected by the transmit antenna
L_{rx}	Power density at the receive antenna
$\mathbf{m}(\boldsymbol{\vartheta})$	Parametrized model for the deterministic signal part
$N(t)$	Noise process
$\mathbf{N}$	Noise vector
$\mathcal{N}_{\mathbb{C}^n}(\boldsymbol{\mu}, \mathbf{R})$	Normal (Gaussian) distribution of a complex random vector
n_f	Noise figure of the receive channel
$p(t), P(f)$	Point spread function and its Fourier transform
$p(R), P(k)$	Point spread scaled to range and its FT
$p^{\mathbf{Z}}(\mathbf{z})$	probability density function (pdf) of $\mathbf{Z}$
$P^{\mathbf{Z}}$	Distribution of $\mathbf{Z}$
P	Power
P_{tx}	Transmit power
P_D	Probability of detection
P_F	Probability of false alarm
$\Pr(A)$	Probability for the event A
q	Radar cross section (RCS) of the target
r	Distance to a scatterer
δr	Range resolution
$R = 2r$	Travelling way of the wave
δR	Travelling way resolution
$\mathsf{r}(t)$	Ramp signal
$\mathbf{R}_Z$	Covariance matrix of $\mathbf{Z}$
$r_{ZZ}(\tau)$	Correlation function of the process $Z(t)$
$R_{ZZ}(f)$	Spectral power density of the process $Z(t)$
$\Re$	Real part
$\mathsf{s}(t), \mathsf{S}(f)$	Transmit wave form and its Fourier transform
$\mathsf{s}(R), \mathsf{S}(k)$	Transmit wave form scaled to range and its FT
$\mathsf{s}_\alpha(t), \mathsf{S}_\alpha(f)$	Chirp and its Fourier transform
s_{RF}	Transmit signal in the RF-domain
$s(t)$	Deterministic receive signal
$\mathbf{s}$	Signal vector
$S(x)$	Fresnel integral
t	Fast time
δt	temporal resolution
T	Slow time
T	Absolute temperature in degree Kelvin
$\Delta T = 1/\Delta F$	Pulse repetition interval
$T(\mathbf{z})$	Test statistics
$\mathrm{Var}[X]$	Variance of the random variable X
$\mathbf{w}$	Weight vector
$x(t), X(f)$	Input signal and its Fourier transform
$y(t), Y(f)$	Filter output and its Fourier transform
$Z(t)$	Received signal
$\mathbf{Z}$	Random vector as model for the measured vector
$\mathbf{z}$	Realization of $\mathbf{Z}$, measurement

Doppler modulations by moving parts of the object, polarization, and the dynamics of motion. The second concept is that of radar imaging. The aim is to generate a quasi optical image (SAR, ISAR). Here the resolution cells have to be much smaller than the objects extension. Information about the target can be extracted from the the two- or three-dimensional images or even one-dimensional images (range profile, micro-Doppler).

1.2 Coherent radar

In this section we will discuss the principle of a coherent pulse radar system including the optimum receive filter. *Coherent* in this context means that the stability of the implemented frequency sources allows to use the phase of the received signals from pulse to pulse.

1.2.1 Quadrature modulation and demodulation

Since the generation of sophisticated waveforms and the adequate processing of the received signals are practically impossible in the radio frequency domain, the parts relevant to signal processing are mostly handled in the baseband. The signals in the baseband are not only mathematically described in the complex number domain; real and imaginary components of the signals are realized in the hardware. The transformation of complex valued baseband signals to real valued radio frequency (RF) signals and vice versa is performed by the *quadrature modulator* (QM) and the *quadrature demodulator* (QDM), respectively.

Let us proceed from an arbitrary complex valued waveform $\mathsf{s}(t)$ generated by a device like an arbitrary waveform generator (AWG) or a direct digital synthesizer (DDS)[1]. This waveform is fed into an QM transforming it into the real valued RF signal $\mathsf{s}_{RF}(t)$ via

$$\begin{aligned} \mathsf{s}_{RF}(t) &= \Re\left\{\mathsf{s}(t)e^{j2\pi f_0 t}\right\} \\ &= \Re\left\{\mathsf{s}(t)\right\}\cos(2\pi f_0 t) - \Im\left\{\mathsf{s}(t)\right\}\sin(2\pi f_0 t). \end{aligned} \tag{1.1}$$

$\mathsf{s}(t)$ is called the *complex envelope* of the RF-signal $\mathsf{s}_{RF}(t)$ with respect to the *reference frequency* f_0. The technical realization of this transformation is depicted in Fig. 1.1 (left), using mixers with local frequency (LO) f_0. The LO-signals $\cos(2\pi f_0 t)$ and $-\sin(2\pi f_0 t)$ are outputs of a stable frequency source, where one is the time delayed version of the other.

The Fourier-transforms of $\mathsf{s}(t)$ and $\mathsf{s}_{RF}(t)$, denoted by $\mathsf{S}(f)$ and $\mathsf{S}_{RF}(f)$, respectively, are related by

$$\mathsf{S}_{RF}(f) = \frac{1}{2}\left(\mathsf{S}(f+f_0) + \mathsf{S}^*(-f-f_0)\right). \tag{1.2}$$

[1] We will use sanserif characters like s to indicate transmit waveforms

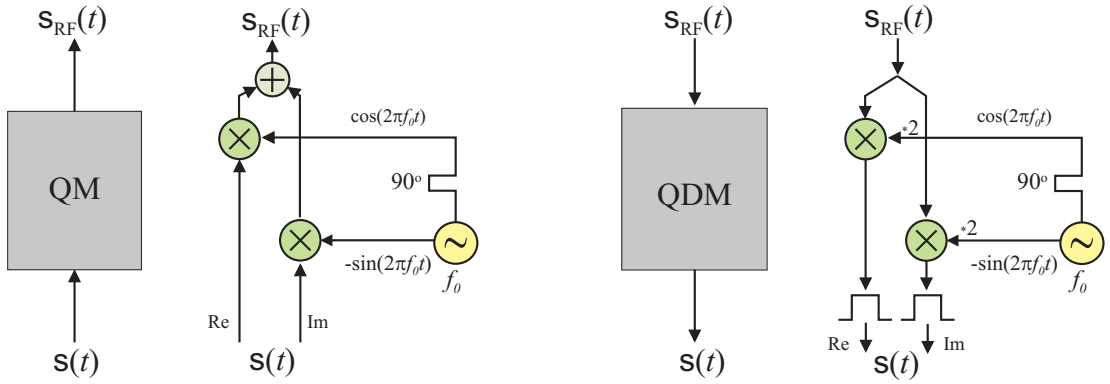

Figure 1.1: *Left: quadrature modulator. Right: quadrature demodulator*

Let the signal $\mathsf{s}(t)$ be bandlimited to the frequency interval $[-b/2, b/2]$ and let $f_0 > b/2$. In this case $\mathsf{S}_{RF}(f)$ is non-zero only over two disjunct intervals $[f_0 - b/2, f_0 + b/2]$ and $[-f_0 - b/2, -f_0 + b/2]$.

For signals with this property the complex envelope $\mathsf{s}(t)$ is uniquely determined by the RF-signal $\mathsf{s}_{RF}(t)$ [4]. Mathematically, the baseband signal $\mathsf{s}(t)$ can be recovered by deleting the negative frequency band $[-f_0-b/2, -f_0+b/2]$ of $\mathsf{S}_{RF}(f)$, shifting the spectrum to the left by f_0, multiplying with the factor 2 and transforming it back to the time domain.

Technically, the recovery of $\mathsf{s}(t)$ is done by the QDM (see Fig. 1.1 right). The RF-signal $\mathsf{s}_{RF}(t)$ is given to two mixers and mixed down with the LO signals $2\cos(2\pi f_0 t)$ and $-2\sin(2\pi f_0 t)$. The outputs of the mixers are filtered by low pass filters with a bandwidth larger than b and lower than $2f_0 - b$ which remove the higher bands centered at $\pm 2f_0$.

If the output of a QM is given directly into a QDM ('bypass'), the resulting output signal of the QDM is identical to the input signal of the QM, see Fig. 1.2, so the QDM performs the inverse operation to that of the QM, the real valued RF-signal may be regarded as a carrier of the base band-signal $s(t)$, able to be transmitted as RF waves over long ranges.

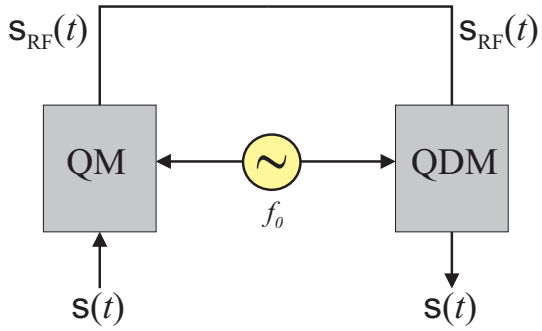

Figure 1.2: *Bypass of quadrature modulator and demodulator*

In real systems, mostly there are several mixing stages with individual local frequencies. Nevertheless, the mathematics remains the same, if all LO-frequencies

are summed up to the reference frequency f_0. f_0 is not necessarily the center frequency; if the spectrum of the base band-signal $\mathsf{s}(t)$ is not centered at zero, the center frequency of the RF-signal and the reference frequency are dislocated by the same amount.

1.2.2 A generic coherent radar

Now we extend the structure shown in Fig. 1.2 to a radar system. The output of the QM is amplified, led over a transmit/receive switch to the antenna and emitted into the free space, see Fig. 1.3. A non moving point target at distance r reflects a part of the wave, the reflected wave reaches the antenna delayed by the time τ, is amplified and put into the QDM. The delay is $\tau = R/c_0$ where $R = 2r$ is the complete travelling way of the wave forward to the scatterer and backward to the receive antenna[2] and c_0 is the velocity of light in the free space.

During the amplification stages noise is added to the received signal which can be taken into account by accumulating all noise contributions to one resulting complex noise signal $N(t)$ superposed to the output of the QDM.

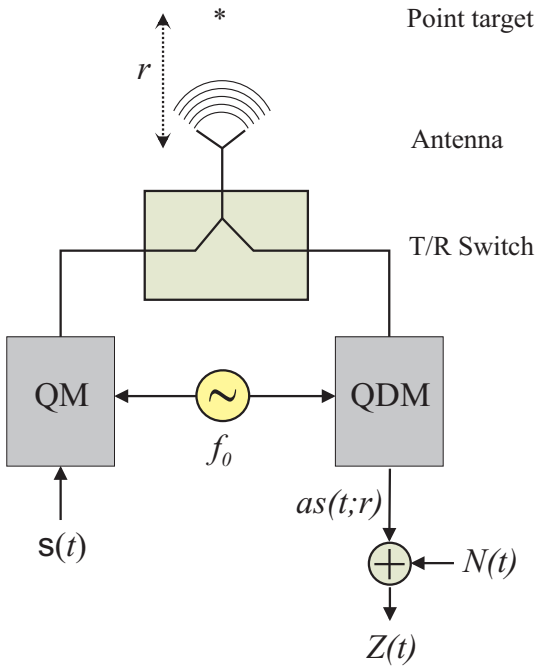

Figure 1.3: *Radar system with baseband signals*

Consequently, the receive signal in the baseband domain $Z(t)$ can be written as

$$Z(t) = as(t;r) + N(t) \tag{1.3}$$

with $s(t;r)$ being the normalized deterministic part of the receive signal and a a complex constant reflecting the system gain, the attenuation over the propagation

[2]The use of the variable R allows to include also bistatic radar systems with the complete travelling way $R = r^{(tx)} + r^{(rx)}$ with different distances from the transmit antenna to the scatterer $r^{(tx)}$ and from the scatterer to the receive antenna $r^{(rx)}$!

path and the reflectivity of the point target. Following a large part of the SAR literature, we discriminate the parameters referring to the radar system (in this situation the receiver time t) and the parameters related to the scene (here: the distance to the scatterer r) by a colon.

The normalized noise-free received RF-signal $s_{RF}(t;r)$ is the delayed transmitted RF-signal:

$$\begin{aligned} s_{RF}(t;r) &= \mathsf{s}_{RF}(t-\tau) \\ &= \Re\left\{\mathsf{s}(t-\tau)e^{j2\pi f_0(t-\tau)}\right\} \\ &= \Re\left\{\mathsf{s}(t-\tau)e^{-j2\pi f_0\tau}e^{j2\pi f_0 t}\right\}. \end{aligned} \tag{1.4}$$

Since the QDM recovers the complex envelope, i.e. the term before the harmonic time function $e^{j2\pi f_0 t}$, the output of it is

$$s(t;r) = \mathsf{s}(t-\tau)e^{-j2\pi f_0\tau}. \tag{1.5}$$

Applying a Fourier transform in the baseband, we get

$$S(f_b;r) = \mathsf{S}(f_b)e^{-j2\pi(f_0+f_b)\tau} = \mathsf{S}(f_b)e^{-j2\pi f\tau} \tag{1.6}$$

with $f = f_0 + f_b$ being the true RF frequency of the transmitted wave component related to the signal component $\mathsf{S}(f_b)$.

If we denote the wavenumber by $k_0 = f_0/c_0 = 2\pi/\lambda_0$, where λ_0 is the wavelength with respect to the reference frequency f_0, we get $2\pi f_0\tau = 2\pi f_0 R/c_0 = 2\pi R/\lambda_0 = k_0 R$ and Eq. (1.5) can be re-written as

$$s(t;r) = \mathsf{s}(t-R/c_0)e^{-jk_0R} \text{ with } R = 2r. \tag{1.7}$$

$$S(f_b;r) = \mathsf{S}(f_b)e^{-jk_rR} \text{ with } k_r = 2\pi(f_0+f_b)/c_0 = k_0 + k_b. \tag{1.8}$$

k_r is the wave number for the electromagnetic wave corresponding to the harmonic decomposition of the transmit signal at baseband frequency f_b.

Apart from the expected time delay in the base band-signal in Eq. (1.7), the important term e^{-jk_rR} in Eq. (1.8) shows the sensitivity of the phase against target motion. If the distance to the scatterer is increased by a half wavelength, the phase rotates by 2π; since also much lower phase changes can be measured, range variations in the order of millimeters are detectable in principle independent of the range which may be 1000 km or more!

1.2.3 Optimum receive filter

Since radar is a continuous fight against noise (and *clutter*, i.e. echoes of unwanted objects), we will optimize the signal-to-noise-ratio (SNR) by filtering the data. First, two related results for the time-discrete case are presented:

Optimum weight vector

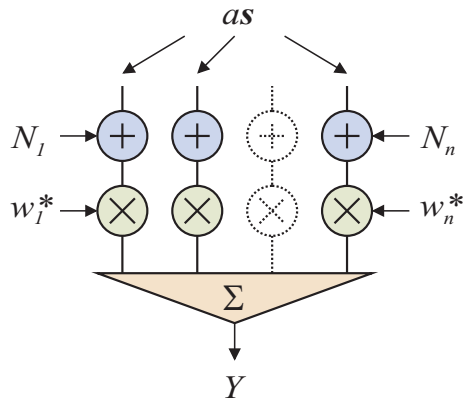

Figure 1.4: *Signal vector superposed by noise and combined by a weight vector*

Problem: Let $\mathbf{s}$ be a complex n-dimensional signal vector, a a complex amplitude and $\mathbf{N}$ a noise vector with expectation zero. The components of $\mathbf{N}$ are assumed to be statistically independent with variance σ^2. To the observer only the noisy data

$$\mathbf{Z} = a\mathbf{s} + \mathbf{N} \tag{1.9}$$

are available. This simple model will come across several times throughout this scriptum. We call this *standard model I*. Now we search for a weighting vector $\mathbf{w}$ for which the scalar product $Y = \mathbf{w}^*\mathbf{Z}$ reaches the maximum SNR (see Fig. 1.4).

Solution: The covariance matrix of the noise is given by $\mathbf{R_N} = E\left[\mathbf{N}\mathbf{N}^*\right] = \sigma^2\mathbf{I}_n$ where $\mathbf{I}_n$ denotes the n-dimensional unit matrix. The SNR of Y is calculated as a function of $\mathbf{w}$ by

$$\gamma(\mathbf{w}) = \frac{|a\mathbf{w}^*\mathbf{s}|^2}{E\left|\mathbf{w}^*\mathbf{N}\right|^2} \tag{1.10}$$

and $\mathbf{w}_{opt} = \operatorname{argmax}\{\gamma(\mathbf{w}) : \mathbf{w} \in \mathbb{C}^n\}$. The denominator of Eq. (1.10) can be developed as

$$E\left|\mathbf{w}^*\mathbf{N}\right|^2 = E\left[\mathbf{w}^*\mathbf{N}\mathbf{N}^*\mathbf{w}\right] = \mathbf{w}^*E\left[\mathbf{N}\mathbf{N}^*\right]\mathbf{w} = \mathbf{w}^*\sigma^2\mathbf{I}_n\mathbf{w} = \sigma^2\|\mathbf{w}\|^2. \tag{1.11}$$

It follows

$$\gamma(\mathbf{w}) = \frac{|a|^2\left|\mathbf{w}^*\mathbf{s}\right|^2}{\sigma^2\|\mathbf{w}\|^2} = \frac{|a|^2\|\mathbf{s}\|^2}{\sigma^2}\frac{|\mathbf{w}^*\mathbf{s}|^2}{\|\mathbf{w}\|^2\|\mathbf{s}\|^2} = \frac{|a|^2\|\mathbf{s}\|^2}{\sigma^2}\left|\rho(\mathbf{w},\mathbf{s})\right|^2. \tag{1.12}$$

$\rho(\mathbf{w},\mathbf{s}) = \frac{\mathbf{w}^*\mathbf{s}}{\|\mathbf{w}\|\|\mathbf{s}\|}$ is the correlation coefficient of $\mathbf{w}$ and $\mathbf{s}$ whose absolute value is always lower or equal to 1, and equal to 1 if $\mathbf{w}$ and $\mathbf{s}$ are collinear (inequality of Cauchy and Schwarz, see A.1.2). So, the maximum SNR for the above problem is achieved for the weight vector

$$\mathbf{w}_{opt} = w\mathbf{s} \tag{1.13}$$

with an arbitrary complex constant $w \neq 0$ and takes the value $\gamma(\mathbf{w}_{opt}) = \frac{|a|^2\|\mathbf{s}\|^2}{\sigma^2}$.

Essence 1.1 *The weight vector optimizing the SNR of its scalar product with* $\mathbf{Z}$ *is the signal vector itself or a complex multiple of it. The obtained SNR is equal to the energy of the deterministic part divided by the noise variance.*

We will meet this property throughout the scriptumfor several times.

Time discrete matched filter

Now it is easy to derive from this solution an optimum filter response to a delayed signal (see Fig. 1.5).

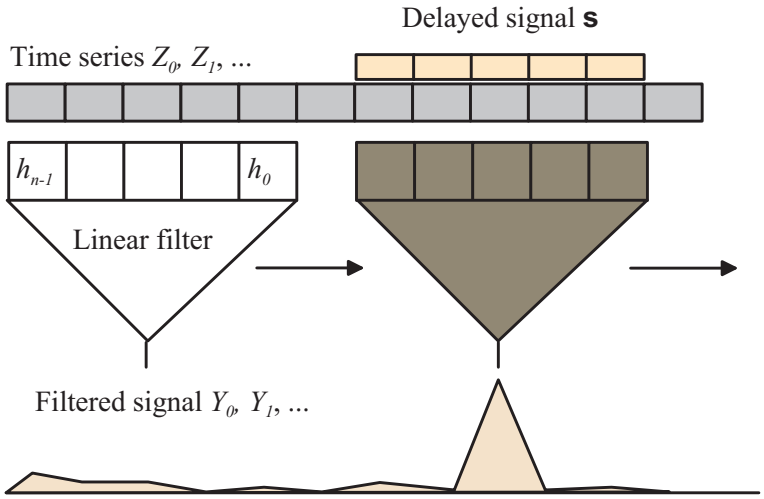

Figure 1.5: *Discrete matched filter*

Problem: Let a be a complex constant,$\mathsf{s} \in \mathbb{C}^n$ a signal vector and $Z_0, Z_1, \ldots$ a complex time series with the following property:

$$Z_\nu = \left\{ \begin{array}{lll} N_\nu & \text{for} & \nu = 0, \ldots, k-1 \\ N_\nu + a\mathsf{s}_{\nu-k} & \text{for} & \nu = k, \ldots, k+n-1 \\ N_\nu & \text{for} & \nu = k+n, \ldots \end{array} \right\}. \tag{1.14}$$

$N_0, N_1, \ldots$ here is a sequence of statistically independent complex noise variables with expectation zero and variance σ^2.
This time series is filtered by a linear time invariant filter with the pulse response h_ν. Which pulse response maximizes the SNR of the filter output at the time index $k+n$?

Solution: Obviously, the signal vector is 'hidden' in the time series and shifted by the amount k. The length of the optimum filter cannot be larger than n, since otherwise only noise will be added without growing signal energy. The filtered

output is the convolution with the pulse response:

$$Y_\nu = \sum_{\mu=0}^{n-1} Z_{\nu-\mu} h_\mu \tag{1.15}$$

$$Y_{k+n} = \sum_{\mu=0}^{n-1} (a\mathsf{s}_{n-\mu} + N_{k+n-\mu}) h_\mu \tag{1.16}$$

Following the essence 1.1, Eq.(1.13), the optimum filter coefficients are $h_\mu = ws^*_{n-\mu}$ with a non-zero constant w.

Essence 1.2 *The pulse response of the optimum filter is equal to the time-inverted, complex conjugated signal:*

$$h_\mu = w\mathsf{s}^*_{n-\mu} \text{ for } \mu = 0, \ldots, n-1 \tag{1.17}$$

The maximum SNR is $\gamma(h_{opt}) = \frac{|a|^2 \|\mathsf{s}\|^2}{\sigma^2}$. *This filter is called matched filter.*

Time continuous matched filter

This time discrete optimization task can easily be transferred to the time continuous case. Let $\mathsf{s}(t)$ be a bandlimited complex signal with Fourier transform $\mathsf{S}(f)$ and $N(t)$ be a wide sense stationary noise process[3] with expectation zero. Let $r_{NN}(\tau) = E\left[N(t+\tau)N^*(t)\right]$ be the correlation function of $N(t)$ (= covariance function, since the expectation is zero) and its Fourier transform $R_{NN}(f) = \int \exp\{-j2\pi f\tau\} r_{NN}(\tau) d\tau$ the spectral noise density.

Problem: We assume that the noise process is white over the signal bandwidth, i.e. $R_{NN}(f) = \sigma^2$ for all f with $\mathsf{S}(f) \neq 0$. $Z(t)$ is the superposition of the delayed signal $\mathsf{s}(t-\tau)$ and the noise process $N(t)$. $Z(t)$ is given into a filter with pulse response $h(t)$, the output of the filter is $Y(t)$.

$$Z(t) = a\mathsf{s}(t-\tau) + N(t) \tag{1.18}$$

$$Y(t) = (h \star Z)(t) \tag{1.19}$$

Which $h(t)$ optimizes the SNR $\gamma(h)$ at time $t = \tau$?

Solution: The noise related part of the output signal is again a wide sense stochastic process. The SNR of $Z(\tau)$ is given by

$$\gamma(h) = \frac{\left|a \int \mathsf{s}(t-\tau) h(\tau - t) dt\right|^2}{E|(h \star N)(0)|^2}. \tag{1.20}$$

[3] A stochastical process is called stationary, if its statistical properties are invariant against time shifts; it is called wide sense stationary, if its correlation properties are invariant against time shifts.

If we define a new signal by $q(t) := \mathsf{s}^*(-t)$, the nominator is easily calculated to

$$|a|^2 \left| \int \mathsf{s}(t-\tau)h(\tau-t)dt \right|^2 = |a|^2 \left| \int q(t)h^*(t)dt \right|^2 \quad (1.21)$$

$$= |a|^2 |< q, h >|^2 . \quad (1.22)$$

The denominator is given by (see appendix A.7)

$$E\,|(h \star N)(0)|^2 = \sigma^2 \|h\|^2. \quad (1.23)$$

Since $\|\mathsf{s}\|^2 = \|q\|^2$, we get

$$\gamma(h) = \frac{|a|^2 |< q, h >|^2}{\sigma^2 \|h\|^2} \quad (1.24)$$

$$= \frac{|a|^2 \|\mathsf{s}\|^2}{\sigma^2} |\rho(h,q)|^2 \quad (1.25)$$

where $\rho(h,q)$ denotes the correlation coefficient of h and q. Following Cauchy-Schwarz's inequality for continuous signals (see appendix A.2), the optimum filter is given by $h_{opt}(t) = wq(t) = w\mathsf{s}^*(-t)$ with any non-zero constant w.

Essence 1.3 *The pulse response of the optimum filter is equal to the time-inverted, complex conjugated signal*

$$h_{opt}(t) = w\mathsf{s}^*(-t). \quad (1.26)$$

The maximum SNR is $\gamma(h_{opt}) = \frac{|a|^2\|\mathsf{s}\|^2}{\sigma^2}$. *This filter is called matched filter.*

In the foregoing, we have derived the optimum way to filter the output signal of the QDM in the generic radar system sketched in Fig. 1.3. There are two possible ways to implement it: Either an analogue filter is attached to the receive chain with a pulse response close to Eq.(1.26) and the filter output is converted to the digital domain, or the signal is first sampled by an analogue-to-digital converter (ADC) and digitally filtered according to Eq.(1.17). The latter is the more modern method and will be followed throughout the scriptum.

1.2.4 The point spread function

If any signal $x(t)$ is given into the filter matched to $s(t)$, the output $y(t)$ is

$$y(t) = (h_{opt} \star x)(t) \quad (1.27)$$

$$= \int h_{opt}(\tau)x(t-\tau)d\tau \quad (1.28)$$

$$= \int \mathsf{s}^*(-\tau)x(t-\tau)d\tau \quad (1.29)$$

$$= \int \mathsf{s}^*(\tau)x(t+\tau)d\tau. \quad (1.30)$$

Obviously the matched filtering is identical to a *correlation* with the transmit signal. In the frequency domain, we get

$$Y(f) = \mathsf{S}^*(f)X(f). \quad (1.31)$$

If the transmit signal itself is given into an arbitrary filter with pulse response $h(t)$, the output is called *point spread function*

$$p(t) = (h \star \mathsf{s})(t), P(f) = H(f) \cdot \mathsf{S}(f). \tag{1.32}$$

The radar system plus receive filter reacts on a point scatterer at distance r with the deterministic part $y(t) = ap(t - 2r/c_0) \exp\{-j2k_0 r\}$.

For the matched filter, the output is given by

$$\begin{aligned} p(t) &= (h_{opt} \star \mathsf{s})(t) && (1.33)\\ &= \int \mathsf{s}^*(\tau)\mathsf{s}(t+\tau)d\tau && (1.34)\\ &= r_{\mathsf{ss}}(t) && (1.35) \end{aligned}$$

and in the frequency region we get

$$P(f) = |\mathsf{S}(f)|^2. \tag{1.36}$$

We summarize:

Essence 1.4 *Matched filtering means correlation with the transmit signal. The point spread function is the reaction of the receive filter to the transmit signal. The point spread function is equal to the autocorrelation of the transmit signal, if a matched filter is used. In this case it is the Fourier back transform of the magnitude-squared of the signal spectrum.*

1.2.5 Two time scales for pulse radar

The analogue signal outputs of the receiver unit have to be sampled and A/D-converted as input to digital signal processing. After transmission of a pulse the system is switched to receive. A receive window is opened starting at the time corresponding to the minimum desired range. Now the sampling is performed at a sampling rate $f_s = 1/\Delta t$ a bit larger than the signal bandwidth. Sampling stops at the time of desired maximum range. The samples fill a *rangeline* which can be arranged as a column in a two-dimensional array (*sample field*), as illustrated in Fig. 1.6. The next pulse is emitted after the *pulse repetition interval* ΔT, the samples of the echoes build a new rangeline which is inserted in the two-dimensional field and so on. The frequency $F_s = 1/\Delta T$ is called *pulse repetition frequency (PRF)*.

In this way, the sample field is filled from pulse to pulse and is the starting point for further signal processing. This two-dimensional raw-data structure is used for the most modern radar systems. If there are more than one receive channel in parallel, for each of the channels a sample field is generated effecting a three-dimensional raw data structure.

Both of the two dimensions of the sample field have the original dimension 'time'; the vertical axis (t) is called *fast-time* controlling the interval between the pulses and the horizontal axis (T) *slow-time* related to the pulse-to-pulse clock.

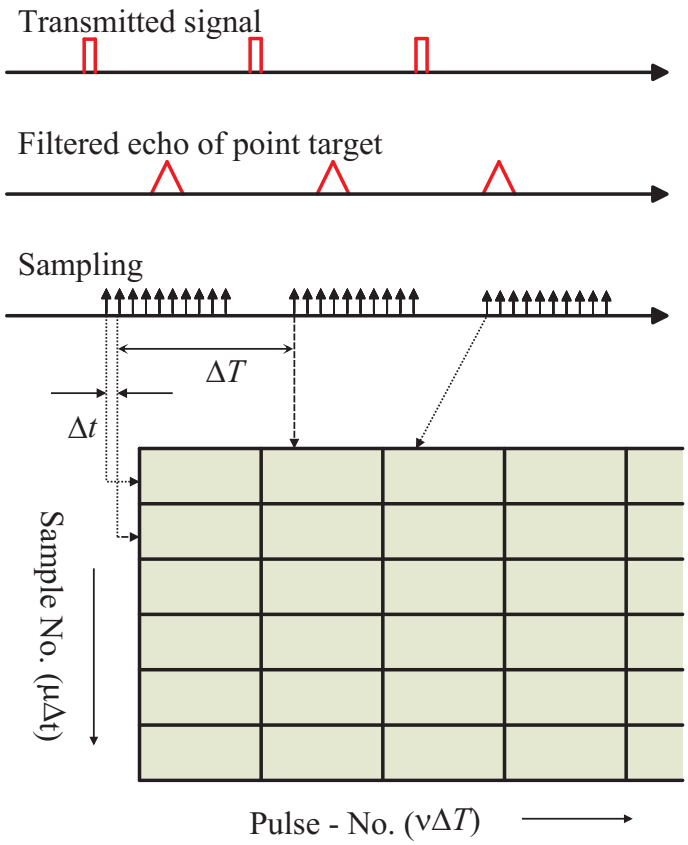

Figure 1.6: *Two time scales for pulse radar*

In the fast-time domain the sampling frequency $f_s = 1/\Delta t$ ranges in general from some MHz to a few GHz, related to a range sampling interval $c_0/(2f_s)$ of about 150 m (1 MHz) downto 15 cm (1GHz). The sampling frequency in the slow-time domain $F_s = 1/\Delta T$ normally is in the order of hundreds of Hz to a MHz leading to an unambiguous range interval $c_0/(2F_s)$ of some hundred kilometers downto some hundred meters.

1.3 Doppler effect

Moving targets change the frequency of the backscattered waveform due to the Doppler effect. Let us assume that the distance to the target $r(t)$ is time varying and $v_r(t) = \frac{d}{dt}r(t)$ denotes the radial velocity.

Due to the motion of the target, the delay of the wave $\tau(t)$ becomes time-dependent where t is defined at the time at the receiver. The RF receive signal will be the time-delayed transmit signal according to Eq. (1.4) from which the complex baseband signal is determined:

$$\begin{aligned} s_{RF}(t; r(.)) &= \mathsf{s}_{RF}(t - \tau(t)) \\ &= \Re\left\{\mathsf{s}(t - \tau(t))e^{-j2\pi f_0 \tau(t)} e^{j2\pi f_0 t}\right\} \end{aligned} \tag{1.37}$$

$$s(t; r(.)) = \mathsf{s}(t - \tau(t))e^{-j2\pi f_0 \tau(t)}. \tag{1.38}$$

The rotating phase in the exponential term constitutes the basic component of the Doppler frequency:

$$F_0(t) = \frac{1}{2\pi}\frac{d}{dt}[-2\pi f_0 \tau(t)] = -f_0 \frac{d}{dt}\tau(t). \tag{1.39}$$

Since the varying time delay in the base band signal introduces additional phase rotations, we resolve the waveform in its spectral components and get

$$S(f_b; r(.)) = \mathsf{S}(f_b)e^{-j2\pi f_b \tau(t)}e^{-j2\pi f_0 \tau(t)} = \mathsf{S}(f_b)e^{-j2\pi(f_0+f_b)\tau(t)}. \tag{1.40}$$

So, the Doppler frequency related to the baseband frequency f_b is

$$F(t, f_b) = -(f_0 + f_b)\frac{d}{dt}\tau(t) = F_0(t) - f_b \frac{d}{dt}\tau(t). \tag{1.41}$$

Object motion negligible during the wave's travelling time If the radial velocity of the target is so low that its position at the time point of transmission and its position at the time point of receive are small against the wavelength, the motion of the target during the wave's travelling time can be neglected. Often this situation is called *stop and go approximation*. The idea behind is that the target stops for a moment where a pulse is transmitted, reflected and received and then proceeds to the next position according to its radial velocity.

In this case, $\tau(t) \approx 2r(t)/c_0$, neglecting that the range of the target at the time of reflection is slightly different to $r(t)$. Under this approximation, $\frac{d}{dt}\tau(t) = 2v_r(t)/c_0$ and from Eq.(1.39) the Doppler frequency is

$$F(t, f_b) = -\frac{2(f_0 + f_b)}{c_0}v_r(t) = -\frac{2v_r(t)}{\lambda} \text{ with } \lambda = \frac{c_0}{f_0 + f_b}. \tag{1.42}$$

Exact expression For targets with a large radial velocity this approximation may not be sufficient. We are looking for an exact solution. At time t the echo is received from a pulse which was emitted at time $t - \tau(t)$ and hit the target at time $t' = t - \tau(t)/2$. The distance at this point was $r(t')$, so the time for forward and backward travelling is $\tau(t) = 2r(t')/c_0$. We get the following equation

$$\tau(t) = \frac{2r\left(t - \frac{\tau(t)}{2}\right)}{c_0}, \tag{1.43}$$

which implicitly determines the time delay $\tau(t)$.

For a linear time dependence $r(t) = r_0 + v_r t$ the delay $\tau(t)$ and its temporal derivative are easily calculated from Eq. (1.43):

$$\tau(t) = \frac{2(r_0 + v_r t)}{c_0 + v_r} = \frac{1}{1+\beta}\frac{2(r_0 + v_r t)}{c_0} \tag{1.44}$$

$$\frac{d}{dt}\tau(t) = \frac{1}{1+\beta}\frac{2v_r}{c_0} \tag{1.45}$$

with $\beta = v_r/c_0$. The resulting Doppler frequency is calculated to

$$F(t, f_b) = -(f_0 + f_b)\frac{d}{dt}\tau(t) = -\frac{1}{1+\beta}\frac{2(f_0+f_b)v_r}{c_0} = -\frac{1}{1+\beta}\frac{2v_r}{\lambda}. \tag{1.46}$$

This result differs from the stop-and-go approximation by the factor $\frac{1}{1+\beta}$ which is normally very close to 1.

Essence 1.5 *The Doppler frequency of a moving target is given by* $F = -\frac{1}{1+\beta}\frac{2v_r}{\lambda}$ *with* $\beta = v_r/c_0$. *For the stop-and-go approximation this is simplified to* $F = -2v_r/\lambda$.

We go back to the received signal Eq. (1.38). With $g(t) = t - \tau(t)$ we get

$$\begin{aligned} s(t) &= \mathsf{s}(t - \tau(t))e^{-j2\pi f_0 \tau(t)} && (1.47)\\ &= \mathsf{s}(g(t)) \exp\{-j2\pi f_0 (t - g(t))\} && (1.48) \end{aligned}$$

For constant radial velocity $g(t)$ is computed from Eq. (1.44) to

$$\begin{aligned} g(t) &= t - \frac{1}{1+\beta}\frac{2(r_0 + v_r t)}{c_0} && (1.49)\\ &= \frac{1-\beta}{1+\beta}t - \frac{1}{1+\beta}\frac{2r_0}{c_0} && (1.50)\\ &= \alpha t - \tau' && (1.51) \end{aligned}$$

with $\alpha = \frac{1-\beta}{1+\beta}$ and $\tau' = \frac{1}{1+\beta}\frac{2r_0}{c_0}$ and by inserting this expression into Eq. (1.47) the received signal is

$$s(t) = \mathsf{s}(\alpha t - \tau') \exp\{-j2\pi f_0(\tau' + (1-\alpha)t)\}. \tag{1.52}$$

We draw the following conclusions:

- The time scale of the receive signal has been stretched by the factor α with respect to the transmitted signal.
- The signal has been modulated by the Doppler frequency $F_0 = -f_0(1-\alpha)$.
- The initial time delay and initial phase have been modified to τ' and $-2\pi f_0 \tau'$.

The effects of the Doppler modulation on a sequence of rectangular pulses are illustrated in Fig. 1.7. The time-continuous receive signal can be split into the fast and slow-time domains and sorted into the two dimensional array of samples. There are three main effects: Firstly the phase modulation during one received pulse, secondly the phase shift from pulse to pulse and thirdly the increasing delay from pulse to pulse. The latter is called *range migration* or *range walk* . The effects are of different importance. Most significant is the phase change from pulse to pulse which is the first to be exploited in signal processing. The Doppler modulation within the received single pulse often can be neglected, if the pulse duration is not too long. The range migration effect is negligible for short pulse trains and coarse range resolution, but in general not for imaging radars.

1.4 Definitions of resolution

Let us return to the point spread function $p(t)$, Eq. 1.32. It has a maximum at $t = 0$ and a certain *width* of the main beam which expresses how the response to a point like target is smeared. Obviously this width is related to the ability of the radar system to *resolve* point like targets which are close together. So, the value 'resolution' should be a measure how far two point targets have to be separated to be recognized as two. A general mathematical definition does not exist. The simplest way is to measure the width of the main beam. Since this is not uniquely defined, we mention different approaches:

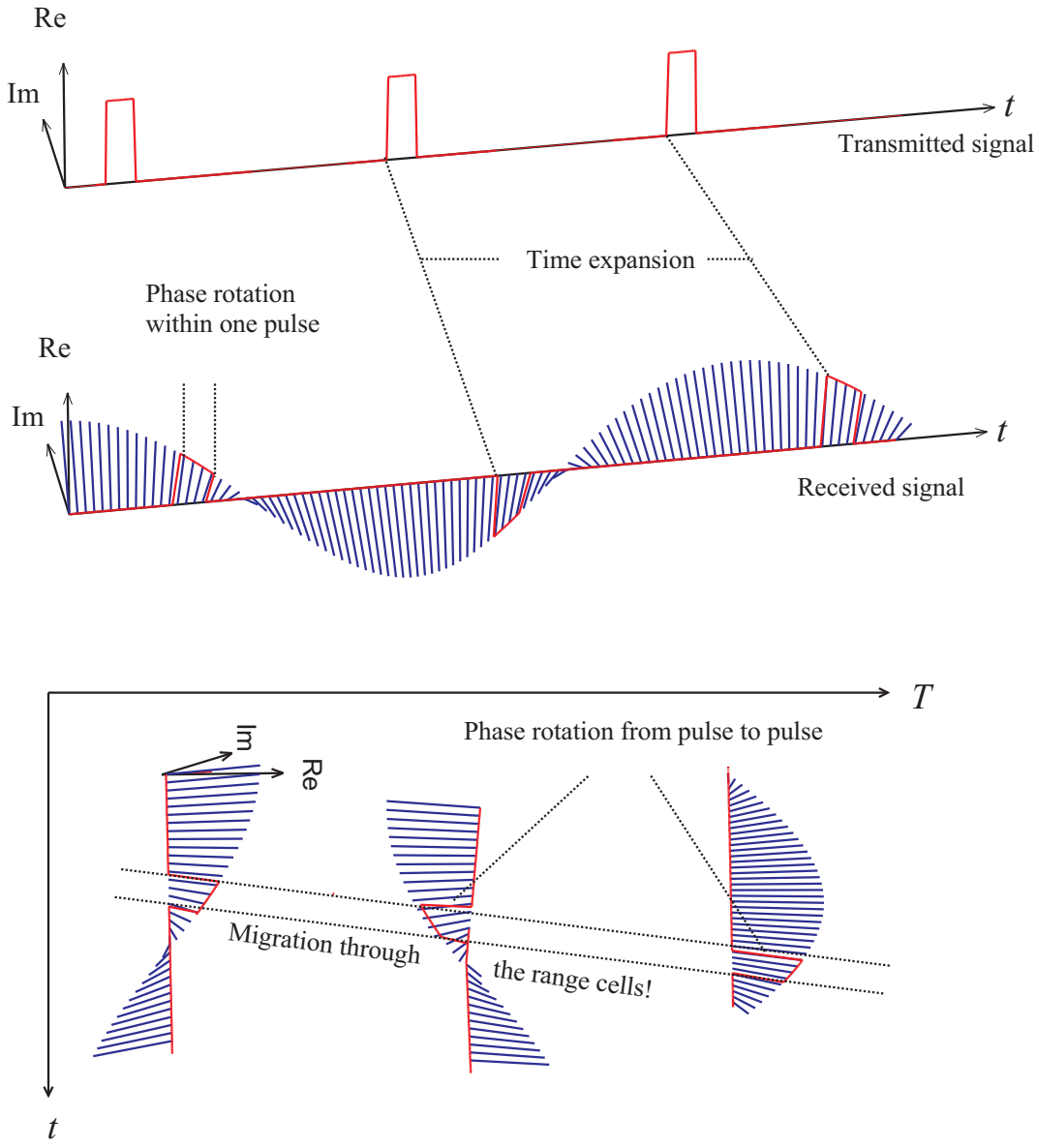

Figure 1.7: *Doppler effect for a pulse train; bottom: After transformation to the $T - t$ plane*

3dB-resolution: The temporal resolution δt is defined by $t_+ - t_-$ where t_+ and t_- are that points of time closest to $t = 0$ where the power of the point spread function has decreased to the half of the maximum value:

$$|p(t_-)|^2 = |p(t_+)|^2 = \frac{1}{2}|p(0)|^2 . \tag{1.53}$$

The 3dB-resolution is a more technical value which for example is given in data sheets to systems and units. More feasible in our context is the

Distance of the maximum to the first zero: For many wave forms the main beam of the point spread function is bounded by a clear zero. The distance from the maximum to this zero is a measure of width, too. If a rectangular pulse of length t_s is used, the response of the matched filter is a triangular pulse with the first zero at $t = t_s$. So the temporal resolution in this sense is $\delta t = t_s$.

Rayleigh resolution: If the spectrum of the pulse is represented by a rectangular function with bandwidth b, the point spread function for matched filtering is a sin x/x function with first zero at $t = 1/b$. Following the preceding definition, the resolution in this case is $\delta t = 1/b$. This definition can be used also for spectra which are not rectangular, if the bandwidth is measured in another way, for instance as a 3dB-bandwidth.

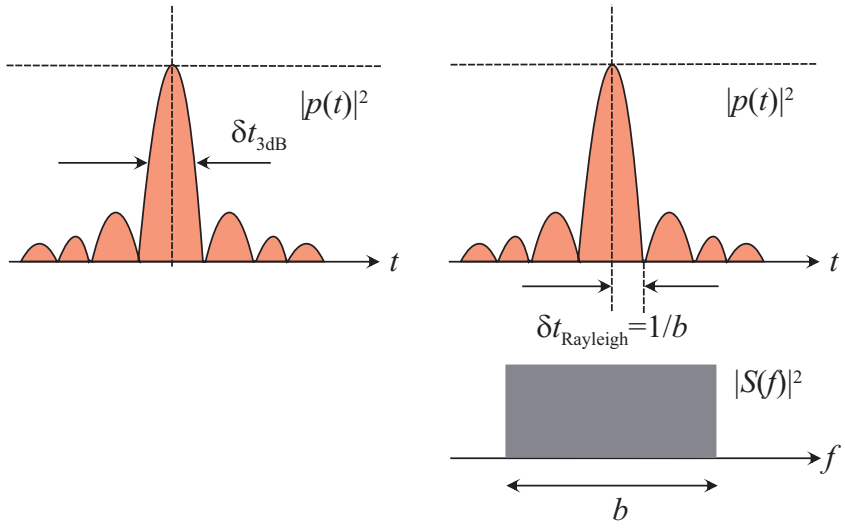

Figure 1.8: *Definitions of resolution*

From the temporal resolution δt immediately the *range resolution* results in $\delta R = c_0 \delta t$, where R is the complete travelling way of the wave, and consequently

$$\delta r = \frac{c_0}{2}\delta t \tag{1.54}$$

for monostatic radars with $R = 2r$.

If the range-axis is partitioned into intervals of length δr, these are called *range resolution cells*.

Similar conditions can be found in other dimensions of the radar like Doppler frequency or angle. In general a radar resolution cell is a multidimensional body whose extensions along the axes are the range resolution, Doppler resolution, angular resolution and so on.

1.5 Pulse compression

1.5.1 The idea of pulse compression

The range resolution achieved with a rectangular pulse of length t_s is given by $\delta r = c_0 t_s/2$. The energy $\|\mathsf{s}\|^2$ of the pulse, which determines the maximum range, is $\|\mathsf{s}\|^2 = t_s P$ where P denotes the power. This is - especially if semiconductors are used for the high power amplifier - limited.

Problem: How can a finer range resolution be achieved without loss of pulse energy?

The solution is to expand the bandwidth by modulation of the pulse. From Eq. 1.54 the Rayleigh range resolution of a waveform with a rectangular spectrum $\mathsf{S}(f)$ of bandwidth b is given by

$$\delta r = \frac{c_0}{2b} \tag{1.55}$$

without direct dependence on the pulse length.

If the original waveform $\mathsf{s}(t)$ with Fourier transform $\mathsf{S}(f)$ is passed through a filter with transfer function $H(f) = \exp\{j\varphi(f)\}$ the spectrum of the filtered waveform $\mathsf{s}_{RF}(t)$ is given by $\mathsf{S}_{RF}(f) = H(f)\mathsf{S}(f)$ and $|\mathsf{S}_{RF}(f)|^2 = |\mathsf{S}(f)|^2$. Since the point spread function for matched filtering is the Fourier back transform of the squared magnitude of the signal spectrum, the point spread functions corresponding to $\mathsf{s}(t)$ and $\mathsf{s}_{RF}(t)$ are the same. If for instance the primary waveform is a rectangular pulse with a C times shorter pulse length t_s/C is passed through a filter with transfer function $H(f) = \exp\{-j2\pi\tau(f)f\}$, the delay $\tau(f)$ is frequency dependent causing a time stretch of the original signal. Assume that a time stretch by a factor C is achieved. Then the resulting wave form can again be amplified to the power P resulting in the same energy content as the rectangular pulse with duration t_s. But the spectrum is stretched by the factor C effecting a C times better range resolution. C is called *compression factor* . The *time-bandwidth product* of the rectangular pulse is $t_s \cdot \frac{1}{t_s} = 1$, that of the expanded pulse $t_s \cdot \frac{C}{t_s} = C$, so the time-bandwidth product is equal to the compression factor.

Essence 1.6 *For the range resolution the bandwidth of the transmitted waveform is decisive:* $\delta r = \frac{c_0}{2b}$. *The gain in range resolution with respect to a rectangular pulse of same duration is called compression rate, which is equal to the time-bandwidth product. Two different waveforms* $\mathsf{s}(t)$ *and* $\mathsf{s}_{RF}(t)$ *effect the same point spread function for matched filtering, if* $\mathsf{s}_{RF}(t)$ *is generated by* $\mathsf{s}(t)$ *by passing it through a filter with a transfer function with magnitude 1.*

1.5.2 The chirp waveform, anatomy of a chirp I

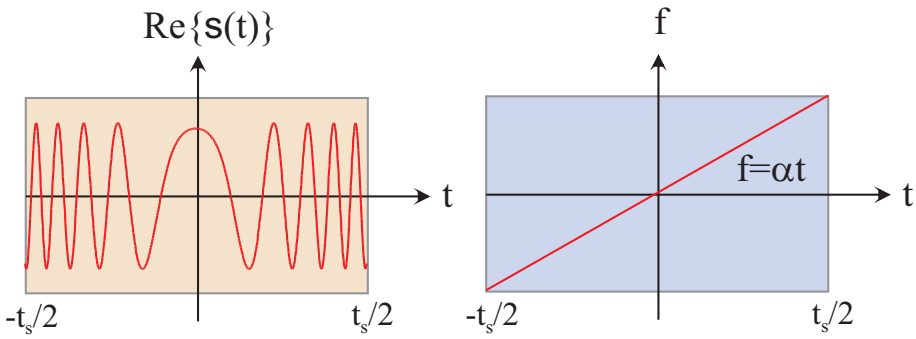

Figure 1.9: *Chirp*

An outstanding role in coded waveforms plays the linearly frequency modulated pulse with constant amplitude, in radar jargon called 'chirp' , defined by

$$\mathsf{s}_\alpha(t) = \exp\{j\pi\alpha t^2\}w(t) \tag{1.56}$$

We call α frequency modulation rate or simply 'rate'. If the window $w(t)$ is rectangular ($w(t) = \mathrm{rect}(t/t_s)$), the instantaneous frequency $f(t) = \alpha t$ runs through the interval $[-\alpha t_s/2, \alpha t_s/2]$ (see Fig. 1.9) effecting a bandwidth which is close to the instantaneous frequency span αt_s. So the time-bandwidth product (=compression rate!) is approximately equal to αt_s^2.

Exactly, the Fourier transform of this rectangular chirp is given by

$$\mathsf{S}_\alpha(f) = \int_{-t_s/2}^{t_s/2} \exp\{j\pi\alpha t^2 - j2\pi ft\}dt \tag{1.57}$$

$$= \sqrt{\frac{1}{2\alpha}} e^{-j\pi\frac{1}{\alpha}f^2} \left[C(x_1) + C(x_2) + j(S(x_1) + S(x_2))\right] \tag{1.58}$$

with

$$x_1 = \sqrt{\frac{\alpha}{2}} t_s \left(1 + \frac{2f}{\alpha t_s}\right), \quad x_2 = \sqrt{\frac{\alpha}{2}} t_s \left(1 - \frac{2f}{\alpha t_s}\right)$$

and the Fresnel-Integrals

$$S(x) = \int_0^x \sin\left(\frac{\pi}{2}t^2\right) dt, \quad C(x) = \int_0^x \cos\left(\frac{\pi}{2}t^2\right) dt. \tag{1.59}$$

If t_s is small, the phase modulation is negligible and the Fourier transform tends to a $\sin x/x$ function whose main beam becomes narrower if t_s grows, see Fig. 1.10. At a point where the time-bandwidth product exceeds 1, the main beam splits and broadens more and more and takes approximately the form of a rectangular function with a bandwidth close to the frequency span αt_s. Anticipating the chapter on SAR, we observe exactly this behavior of the point spread function in azimuth if the motion compensation is not perfect leaving a quadratic phase error.

When t_s tends to infinity, x_1 and x_2 also tend to infinity and integral cosine and integral sine tend to 1/2, so the limiting form of the Fourier transform is

$$\mathsf{S}_\alpha(f) \to \frac{1+j}{\sqrt{2\alpha}} e^{-j\pi\frac{1}{\alpha}f^2} = \frac{1+j}{\sqrt{2\alpha}} \quad \mathsf{s}_{-1/\alpha}(f). \tag{1.60}$$

Essence 1.7 *The magnitude of the Fourier transform of a rectangular chirp with rate α has the approximate shape of a rectangular function with bandwidth close to the frequency span αt_s. For infinite duration the Fourier transform is again a chirp with rate $-1/\alpha$.*

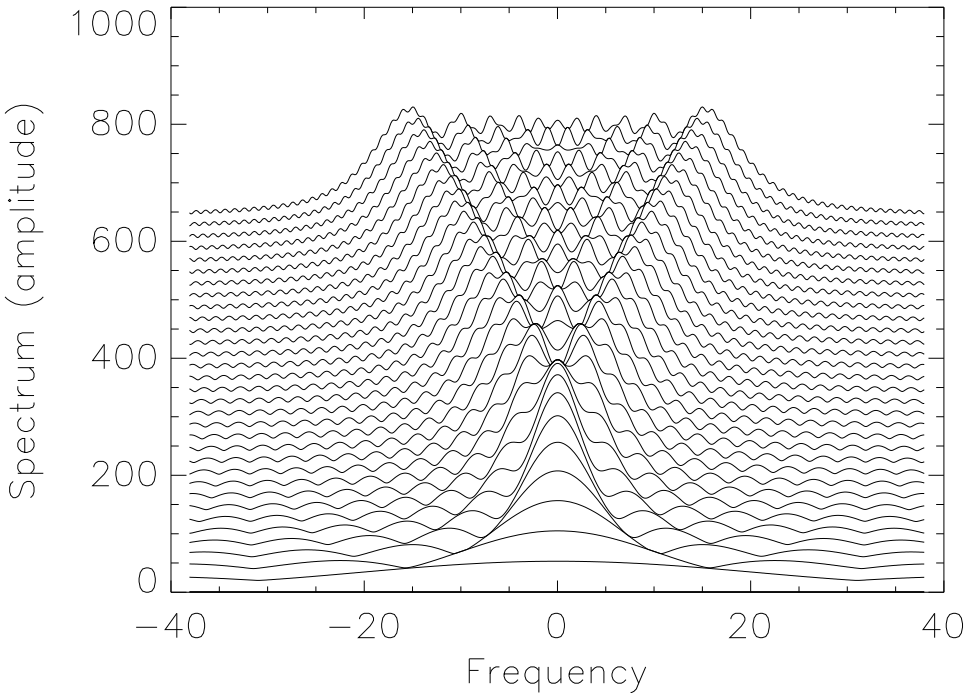

Figure 1.10: *Magnitude of the Fourier transforms of chirps with growing time basis*

Fig. 1.11 shows the steps of the compression of a chirp in the time-domain and the frequency domain.

1.5.3 Spatial interpretation of the radar signal and the receive filter

In this section, we pass to the spatial domain. From the viewpoint of focussing to images (SAR), the spatial domain is the primary one.

We transform the temporal transmit signal, the pulse response of the receive filter and the point spread function into spatial signals, dependent on the spatial

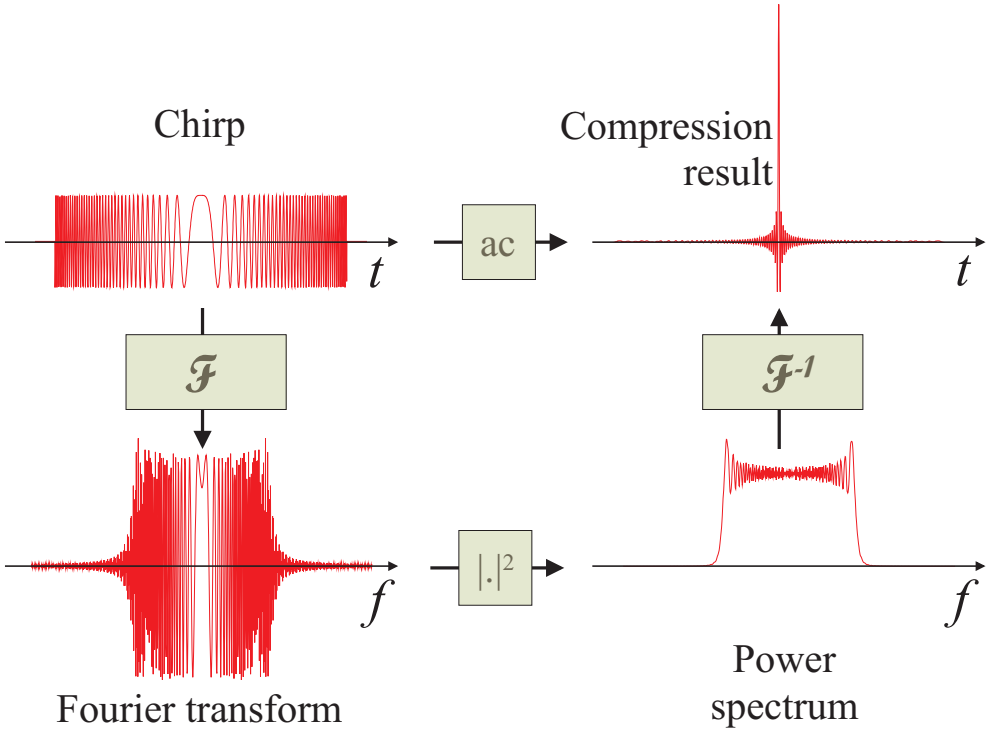

Figure 1.11: *Compression of a chirp signal*

variable $R = 2r$ via $t \to R = c_0 t$. In this section we will use the symbols s, h, p as functions of R.

The Fourier transforms are referring now to spatial frequencies, the wave-number replaces the circular frequency:

$$\mathsf{S}(k) = \int \mathsf{s}(R) e^{-jkR} dR \tag{1.61}$$

$$H(k) = \int h(R) e^{-jkR} dR \tag{1.62}$$

$$P(k) = \int p(R) e^{-jkR} dR \tag{1.63}$$

Note that these relations are formulated in the baseband, so $k = 2\pi f_b / c_0$ is that part to the physical effective wavenumber $k_r = k_0 + k = \frac{2\pi}{\lambda}$ contributed by the base band frequencies.

$p(R)$ is the point spread function of the signal, now in the spatial domain. Its width determines the range resolution in the variable R, for monostatic radars the range resolution in r is half of that in R.

For matched filtering, we get:

$$p(R) = \frac{1}{2\pi} \int |\mathsf{S}(k)|^2 e^{jkR} dk. \tag{1.64}$$

The power of the signal spectrum $\mathcal{W}(k) := |\mathsf{S}(k)|^2$ can be interpreted as a *weighting* in the k-domain, and we conclude:

Essence 1.8 *The point spread function for matched filtering in the range domain is given by the inverse Fourier transform of the power of the signal spectrum in the wave number domain.*

1.5.4 Inverse and robust filtering

The matched filter achieves the optimum signal-to-noise ratio. On the other hand, the sidelobes of the matched filter may be unacceptable. For an arbitrary receive filter $h(R)$ we introduce the following quantities:

$$\begin{aligned} L_s(h) &= |p(0)|^2 \\ L_n(h) &= \int |h(R)|^2 dR \\ L_p(h) &= \int |p(R)|^2 dR. \end{aligned} \tag{1.65}$$

$L_s(h)$ is the power of the point spread function at its maximum, $L_n(h)$ the noise power density at the output of the filter for normalized white noise at its input, and $L_p(h)$ is the total energy of the point spread function, containing also the power spread to the sidelobes. The maximization of the ratio $L_s(h)/L_n(h)$ leads to the matched filter, the maximization of $L_s(h)/L_p(h)$ to the *inverse filter*, as we will see in the following. To get any state in between, we define a weighted quantity of unwanted power by $L_i(h) := \eta L_n(h) + L_p(h)$ and solve the optimization task

$$h_\eta = \operatorname{argmax} \left\{ \frac{L_i(h)}{L_n(h)} : h \in L_2(\mathbb{C}) \right\} \tag{1.66}$$

The result in the wave number domain is[4]

$$H_\eta(k) = w \frac{\mathsf{S}^*(k)}{\eta + |\mathsf{S}(k)|^2} \tag{1.67}$$

with an arbitrary non-zero constant w.

The Fourier transform of the related point spread function takes the form

[4]Derivation: In the wavenumber domain we have $L_s(h) = \left|\int H(k)\mathsf{S}(k)dk/(2\pi)\right|^2$, $L_n(h) = \int |H(k)|^2 dk/(2\pi)$, $L_p(h) = \int |H(k)|^2 |\mathsf{S}(k)|^2 dk/(2\pi)$. By defining $H'(k) := H(k)\sqrt{\eta + |\mathsf{S}(k)|^2}$ and $S'(k) := \mathsf{S}(k)/\sqrt{\eta + |\mathsf{S}(k)|^2}$ we get $L_s(h) = \left|\int H'(k)S'(k)dk/(2\pi)\right|^2$ and $\eta L_n(h) + L_p(h) = \int |H'(k)|^2 dk$. From the inequality of Cauchy-Schwarz follows for the maximization of the ratio $H'_{opt}(k) = wS'^*(k)$ and from that immediately the statement.

$$P_\eta(k) = H_\eta(k)\mathsf{S}(k) = w\frac{|\mathsf{S}(k)|^2}{\eta + |\mathsf{S}(k)|^2} \tag{1.68}$$

For $\eta = 0$ (noise neglected) and $w = 1$ we get $H_0(k) = 1/\mathsf{S}(k)$ which defines the inverse filter. For $w = \eta$ and η tending to infinity (only noise regarded) $H_\eta(k) \to \mathsf{S}^*$ results in the matched filter.

Let $\mathcal{K} := \left\{k : |\mathsf{S}(k)|^2 > 0\right\}$ be the carrier of the baseband signal spectrum which we will call in the following 'k-set'. Here, the k-set is placed at the baseband. Later we will consider also the related k-set in the physical wave number domain.

The application of the inverse filter is defined on $\mathcal{K}$. Outside this set the transfer function $H_0(k)$ may be set equal to zero.

We get for the point spread function $p_0(k)$ in this case:

$$P_0(k) = \begin{cases} \frac{\mathsf{S}(k)}{\mathsf{S}(k)} = 1 \text{ for } k \in \mathcal{K} \\ 0 \quad \text{else} \end{cases} \tag{1.69}$$

Obviously, $P_0(k)$ is the *indicator function* of the set $\mathcal{K}$ where the indicator function $I_M(x)$ of an arbitrary set M is defined as 1, if $x \in M$ and 0 else. From Eq. (1.69) it follows

$$p_0(R) = \frac{1}{2\pi}\int I_\mathcal{K} e^{jkR} dk = \frac{1}{2\pi}\int_\mathcal{K} e^{jkR} dk. \tag{1.70}$$

Essence 1.9 *For the application of the inverse filter, the point spread function is equal to the Fourier back transform of the indicator function of the carrier of the signal spectrum (k-set)*

If the signal power spectrum $|\mathsf{S}(k)|^2$ itself is 1 for $k \in \mathcal{K}$ and zero else, i.e. a uniform power distribution over the carrier, matched filter and inverse filter coincide. In this case, there is no SNR loss.

For the arbitrary case we get a normalized SNR of

$$SNR = \frac{\left|\int_\mathcal{K} \frac{|\mathsf{S}(k)|^2}{\eta+|\mathsf{S}(k)|^2} dk\right|^2}{2\pi \int_\mathcal{K} \frac{|\mathsf{S}(k)|^2}{\left(\eta+|\mathsf{S}(k)|^2\right)^2} dk} \tag{1.71}$$

$$= \begin{cases} \frac{1}{2\pi}\int_\mathcal{K} |\mathsf{S}(k)|^2 dk \text{ for } \eta \to \infty \\ \frac{\left(\int_\mathcal{K} dk\right)^2}{2\pi \int_\mathcal{K} |\mathsf{S}(k)|^{-2} dk} \text{ for } \eta = 0 \end{cases} \tag{1.72}$$

If $|\mathsf{S}(k)|^2$ takes in $\mathcal{K}$ values close to zero, the denominator in the second case may be very large or even infinity effecting a high loss in SNR. If the robustified filter for a suitable choice of η is used, this can be avoided. The robustified filter behaves like the matched filter for small values of the spectral signal power and like the inverse filter for large values. It is able to correct variations of the spectral signal power as illustrated in Fig. 1.12.

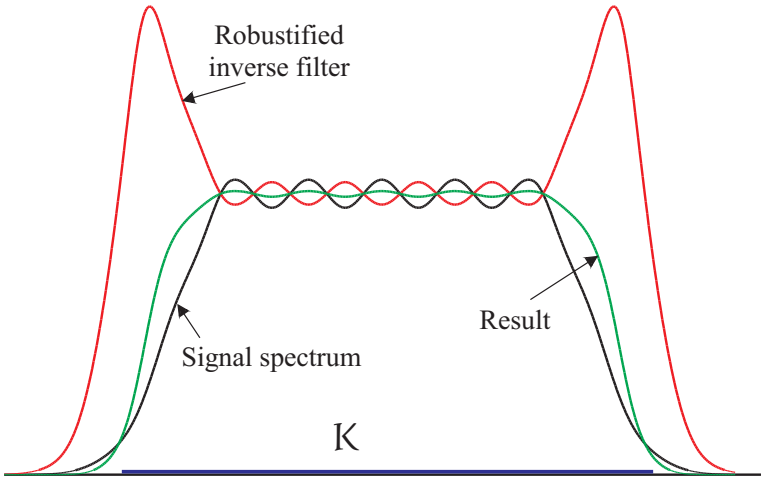

Figure 1.12: *Robustified filter*

1.5.5 Range processing and the normal form

For radar engineers it is convenient to think in processing schemes. Starting point is always the array of complex samples as introduced in section 1.2.5. We assume that the analogue filtering before sampling reduces to a low path filter limiting the noise bandwidth to a value smaller than the sampling frequency according to the Nyquist condition. Clearly the sampling frequency should be larger than the bandwidth of the useful signal. Under these conditions, range compression can be done in the digital domain.

Fig. 1.13 shows the processing scheme in the temporal and frequency domain. For each range line the compression filter has either to be applied as convolution in the temporal domain or as multiplication with the transfer function in the frequency domain.

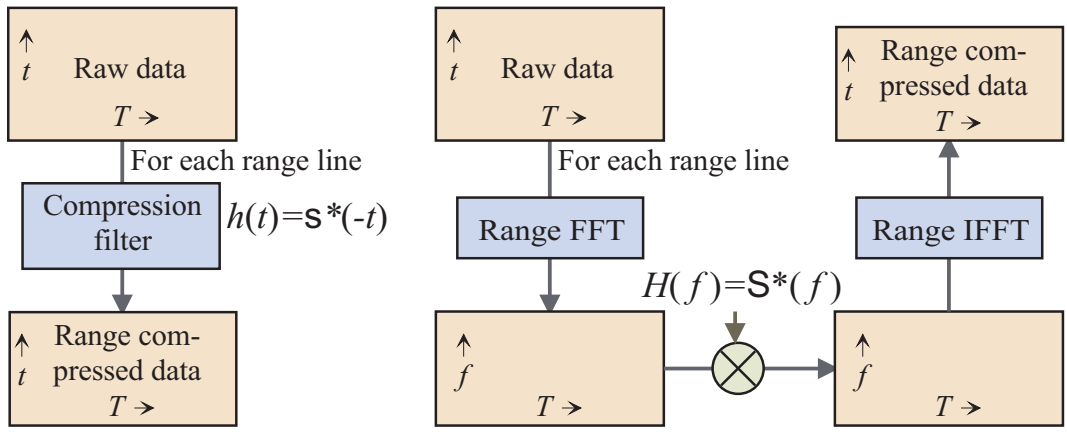

Figure 1.13: *Range compression with the matched filter. Left: direct convolution, right: processing in the frequency domain*

Regarding the transformation to the wavenumber domain and the inverse filtering we can come to an elegant signal representation, called *normal form* :

First, the fast-time variable is substituted as range variable. Let the measured signal along one range line be $z(R)$. The first step of range compression is to apply the Fourier transform yielding $Z(k) = \int z(R) \exp\{-jkR\} dR$. Now the inverse filter is applied resulting in $y(k) = Z(k)/\mathsf{S}(k)$. We call the output *pre-processed data*.

A following inverse Fourier transform (IFFT) would yield the range compressed data. Nevertheless, in some applications, the next step is not the IFFT but a processing along the slow-time variable. If $z(R)$ is the noise-free echo of a point scatterer at $R = R_0$, we get

$$z(R) = a\mathsf{s}(R - R_0) \exp\{-jk_0R_0\} \tag{1.73}$$
$$Z(k) = a\mathsf{S}(k) \exp\{-j(k_0 + k)R_0\}. \tag{1.74}$$

After application of the inverse filter, the signal is

$$y(k; R_0) = Z(k)/\mathsf{S}(k) \tag{1.75}$$
$$= a \exp\{-j(k_0 + k)R_0\} \tag{1.76}$$

for all k in the measured baseband k-set. Obviously, the dependance on the wave form has been eliminated by the inverse filtering.

Regarding $k_r = k_0 + k$ we can define the model signal as function of k_r by $s(k_r; R_0) := y(k_r - k_0; R_0)$ and get the following *normal form* for a point scatterer at range R:

$$s(k_r; R) = \exp\{-jk_rR\}. \tag{1.77}$$

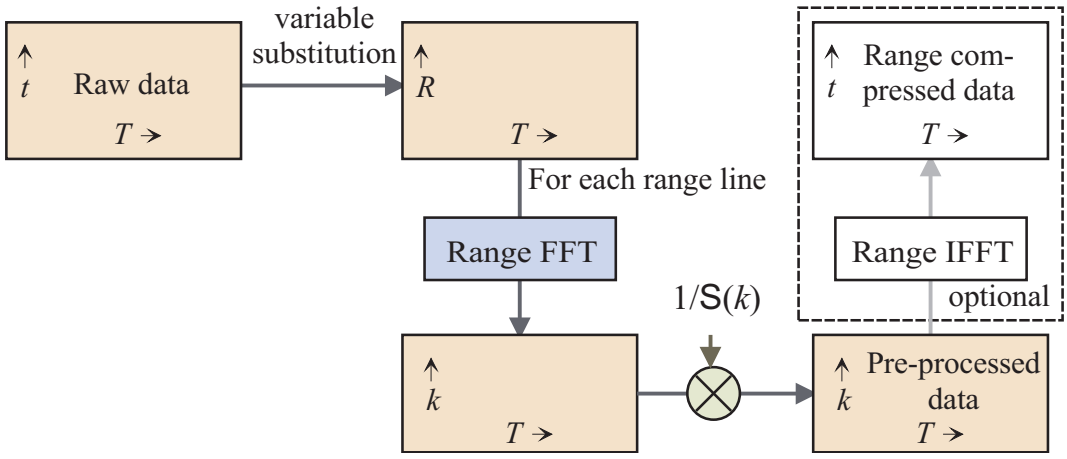

Figure 1.14: *Pre-processing to the k domain*

1.5.6 The de-ramping technique

We return to the representation in time. If the received echoes are sampled with the Nyquist-rate according to the signal bandwidth the A/D conversion technique is soon

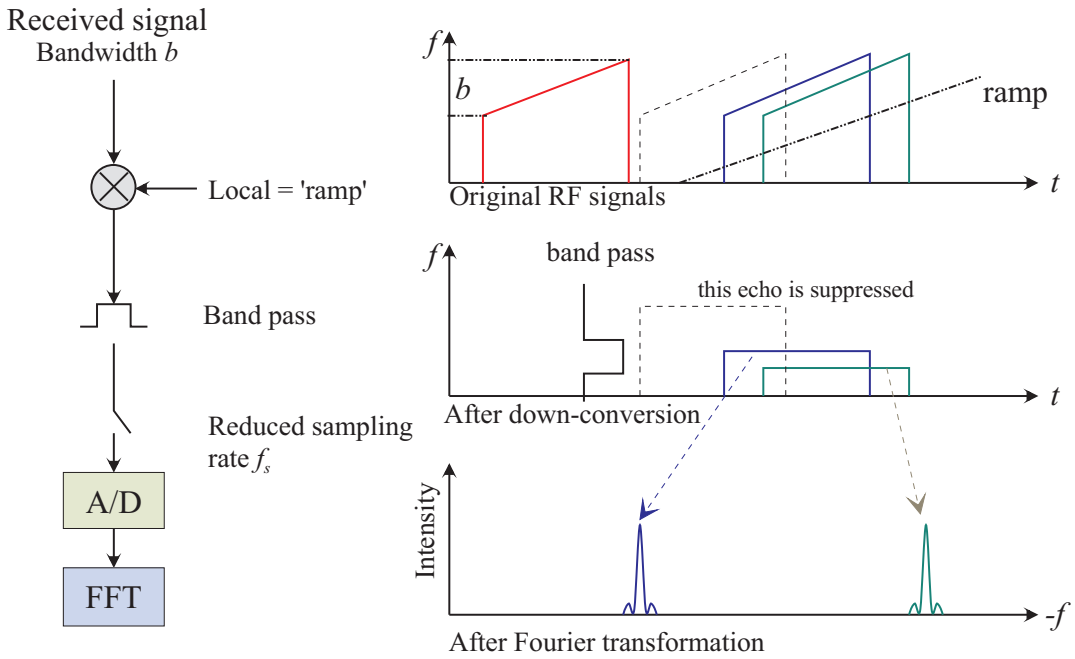

Figure 1.15: *De-Ramping*

at its limits, if the bandwidth advances into the GHz area. An elegant possibility to avoid this bottle neck is the *de-ramping*-method, see Fig. 1.15. A linearly frequency modulated waveform with the baseband representation $\mathsf{s}(t) = \exp\{j\pi\alpha t^2\}\mathrm{rect}(t/t_s)$ is used as transmit pulse. The returning echoes $\mathsf{s}(t-\tau)$ are down-converted by a 'ramp' $\mathsf{r}(t) = \exp\{j\pi\alpha(t-t_0)^2\}$ resulting in

$$\mathsf{r}^*(t)\mathsf{s}(t-\tau) = \exp\{j\pi\alpha(t_0^2+\tau^2)\}\exp\{j\pi\alpha 2(\tau-t_0)t\}\mathrm{rect}((t-\tau)/t_s). \qquad (1.78)$$

This mixing product has the constant frequency $\alpha(\tau - t_0)$. This frequency corresponds to the range of the scatterer $f(r) = \alpha(2r/c_0 - t_0)$. Now a bandpass is applied letting only the frequencies in the interval $[f_1, f_2]$ pass. This is equivalent to cut the range of scatterers which are not suppressed by the filter to a range window $[r_1, r_2]$. Subsequently the filtered echoes can be sampled at a lower sampling frequency obeying the Nyquist condition with respect to the pass band. A following Fourier transform effects a range compression; the frequency axis can be re-scaled to range. A simple calculation shows that the original range resolution $\delta r = c_0/(2b)$ is preserved. The price payed for the reduced sampling rate is the abandonment of ranges outside the 'zoom' interval.

If the duration of the chirp is large compared to the used range-interval, the down-converted sampled signals can be used directly as entries in the normal form Eq. (1.77), if the axis is re-scaled from f to k_r.

1.6 Range-Doppler processing

The relative radial motion of a target (i.e. either the target or the radar is moving or both of them) is described by a time-dependent range $r(T)$ to the antennas phase

center. $r(T)$ is called *range history*. The complete travelling way of the wave then is $R(T) = 2r(T)$ when we use the stop-and-go approximation.

Under this approximation, the signal of a target moving relatively to the radar in the (k, T)-domain can be idealized in the normal form as

$$s^{(k_r,T)}(k_r, T; R(.)) = \exp\{-jk_r R(T)\}. \tag{1.79}$$

If the range history is time-linear or can be approximated as time-linear during the duration of a sequence of pulses: $r(T) = r_0 + v_r T$, the double way is $R(T) = R_0 + v_R T$ with $R_0 = 2r_0, v_R = 2v_r$ and the signal in two dimensions is given by

$$\begin{aligned} s^{(k_r,T)}(k, T; R_0, v_R) &= \exp\{-jk_r(R_0 + v_R T)\} && (1.80)\\ &= \exp\{-jk_r R_0\} \exp\{-jk_r v_R T\} && (1.81)\\ &= \exp\{-jk_r R_0\} \exp\{j2\pi F(k_r)T\} && (1.82) \end{aligned}$$

where $F(k_r) = -\frac{1}{2\pi} k_r v_R = -\frac{1}{\lambda} v_R$ is the Doppler frequency which is proportionally to k_r.

1.6.1 Separated processing

Conventionally, range-Doppler processing is done in two separated steps. First, the range-compression of the pre-processed data $z^{(k,T)}(k, T)$ is performed by the Fourier back transformation:

$$z^{(R,T)}(R, T) = \frac{1}{2\pi} \int z^{(k,T)}(k, T) \exp\{-jkR\} dk. \tag{1.83}$$

Then follows a Fourier transform into the Doppler domain

$$z^{(R,F)}(R, F) = \int z^{(R,T)}(R, T) \exp\{-j2\pi FT\} dT. \tag{1.84}$$

While the radial motion of the target mostly can be neglected for the first step, it often is a problem for the second, since for the Fourier transformation along the rows of the sample field it has to be assumed that the target remains in the same range resolution cell during the time of coherent integration. This is often not the case especially for long pulse sequences and/or fine range resolution (range migration). In this case the output of separated processing will show a response smeared along range corresponding to the change of range during the slow-time interval. Also the Doppler resolution will suffer since the effective time basis decreases. Additionally a variation of the target's radial velocity during the time of integration leads to a smear in the Doppler domain.

1.6.2 Range-velocity processing

The effect of range migration can be compensated in its linear term by *Range-velocity processing* . For a fixed radial velocity v_r the Doppler frequency is proportional to the

RF frequency, or the wave number: $F(k_r) = -k_r v_r/\pi$. At a reference wavenumber k_0 we will observe the Doppler frequency $F(k_0)$ leading to a periodicity $\Delta T_0 = 1/F(k_0)$ in the slow-time domain. If the time axis for the other wavenumbers is re-scaled by a factor k_r/k_0, the periodicity at all wavenumbers will also be T_0 instead of $\Delta T = 1/F(k_r)$. If this re-scaling is done before the last step of range compression, the inverse Fourier transformation along k, the range walk will be compensated since the final data are no longer arranged in wavenumber/Doppler but in fact in wavenumber/radial velocity. The re-scaling can be done by re-sampling to a new raster ('re-formatting') with an interpolator or by aids of the *chirp scaling algorithm*, see [14]. This approach is state-of the art in SAR-systems but can be applied also to other systems like airspace surveillance radars, if range walk is a problem. In Fig. 1.16 both approaches are illustrated.

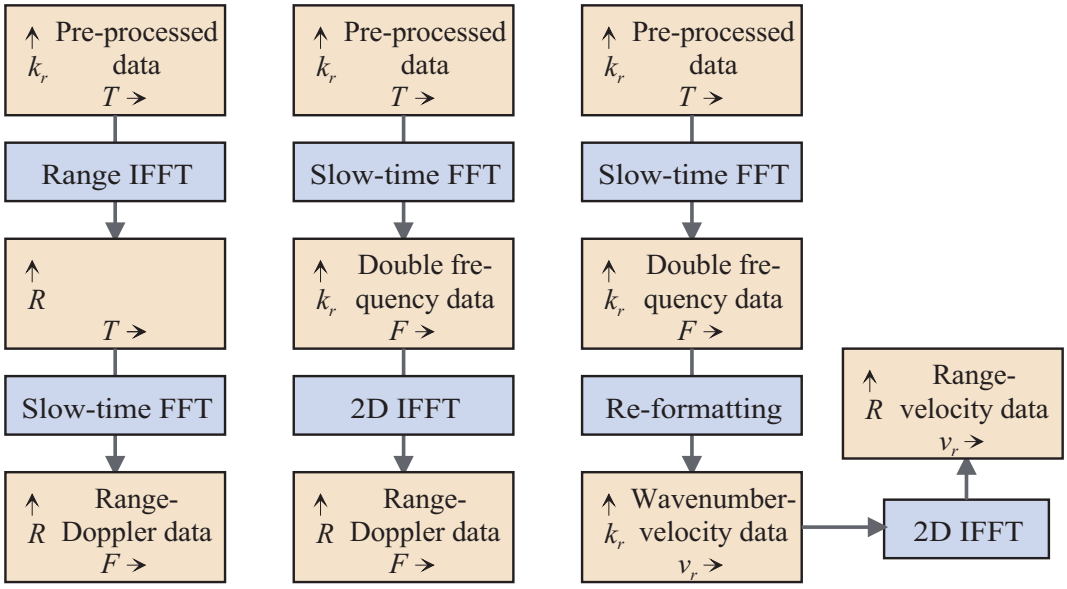

Figure 1.16: *Range Doppler processing and Range velocity processing*

1.6.3 Ambiguity function

The choice of a specific waveform $\mathsf{s}(t)$is not only decisive for the range resolution but also for the response to Doppler shifts. To judge the performance of a waveform in both dimensions, the *ambiguity function* was introduced in the 1950th as the square magnitude of the function

$$\chi(\tau, \nu) := \int \mathsf{s}(t)\mathsf{s}^*(t-\tau)e^{j2\pi\nu t}dt. \tag{1.85}$$

Obviously, $\chi(\tau, \nu)$ represents the reaction of a filter matched to Doppler frequency F_0 to a signal with Doppler frequency $F_0 + \nu$ in a simplified form. The maximum of the magnitude is at the origin. A peak at another place in the (τ, ν)-plane (*ambiguity plane*) indicates that at the corresponding temporal-frequency shift the

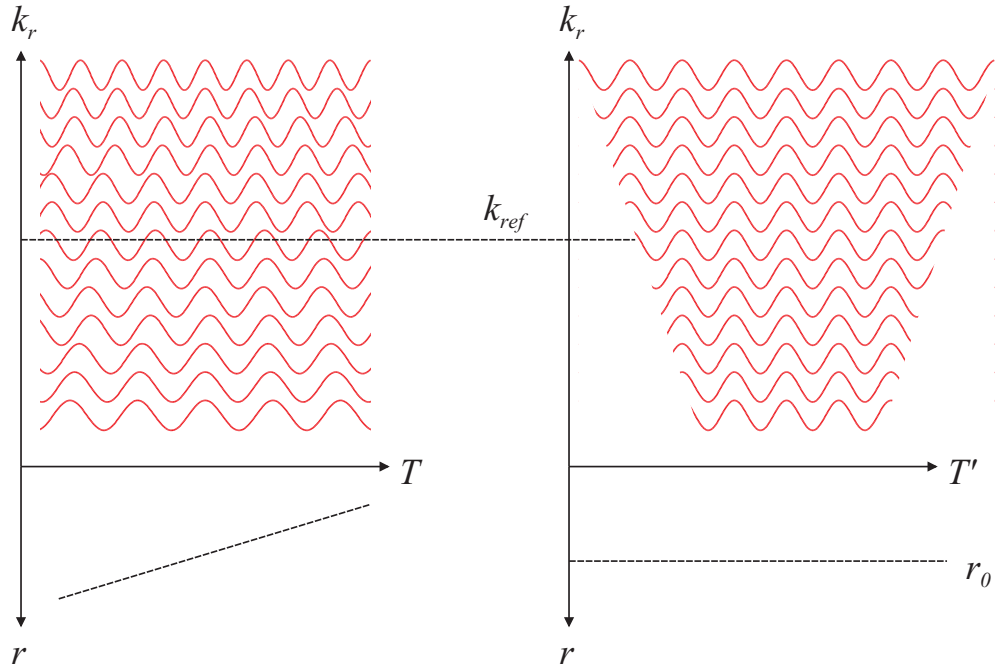

Figure 1.17: *Re-formatting for the range velocity processing. For each wavenumber, the time axis is scaled to yield the same slow-time frequency as at a reference wavenumber. At the same time, the range frequency becomes constant along T leading to a fixed range, the linear range walk is removed.*

signal is difficult to discriminate from the signal at $\tau = \nu = 0$: obviously there is an ambiguity.

Transformed to the frequency domain, we get

$$\chi(\tau, \nu) := \int \mathsf{S}(f - \nu)\mathsf{S}^*(f)e^{2\pi j f \tau} df. \tag{1.86}$$

The one-dimensional cuts along the time and Doppler axes are given by

$$\chi(\tau, 0) = r_{\mathsf{ss}}(\tau) \tag{1.87}$$
$$\chi(0, \nu) = r_{\mathsf{SS}}(-\nu). \tag{1.88}$$

Along the τ axis we recognize the autocorrelation function of the temporal signal, along the ν axis the mirrored autocorrelation function of the frequency representation.

If $|\chi(\tau, \nu)|^2$ is integrated over the whole ambiguity plane the following rule about the *volume invariance* of the ambiguity function is obtained:

$$\int \int |\chi(\tau, \nu)|^2 d\tau d\nu = \|\mathsf{s}\|^4. \tag{1.89}$$

Essence 1.10 *The volume under the ambiguity function does not depend on the shape of the waveform but only on the signal energy.*

This means that it is not possible to reduce the sidelobe energy completely over the whole ambiguity plane without change to the main lobe, but that only a shift of the energy to other regions is possible, for instance to places in which ambiguities are not severe, since they are e.g. outside of the practically to expect range-Doppler area, an aim of *wave form design*.

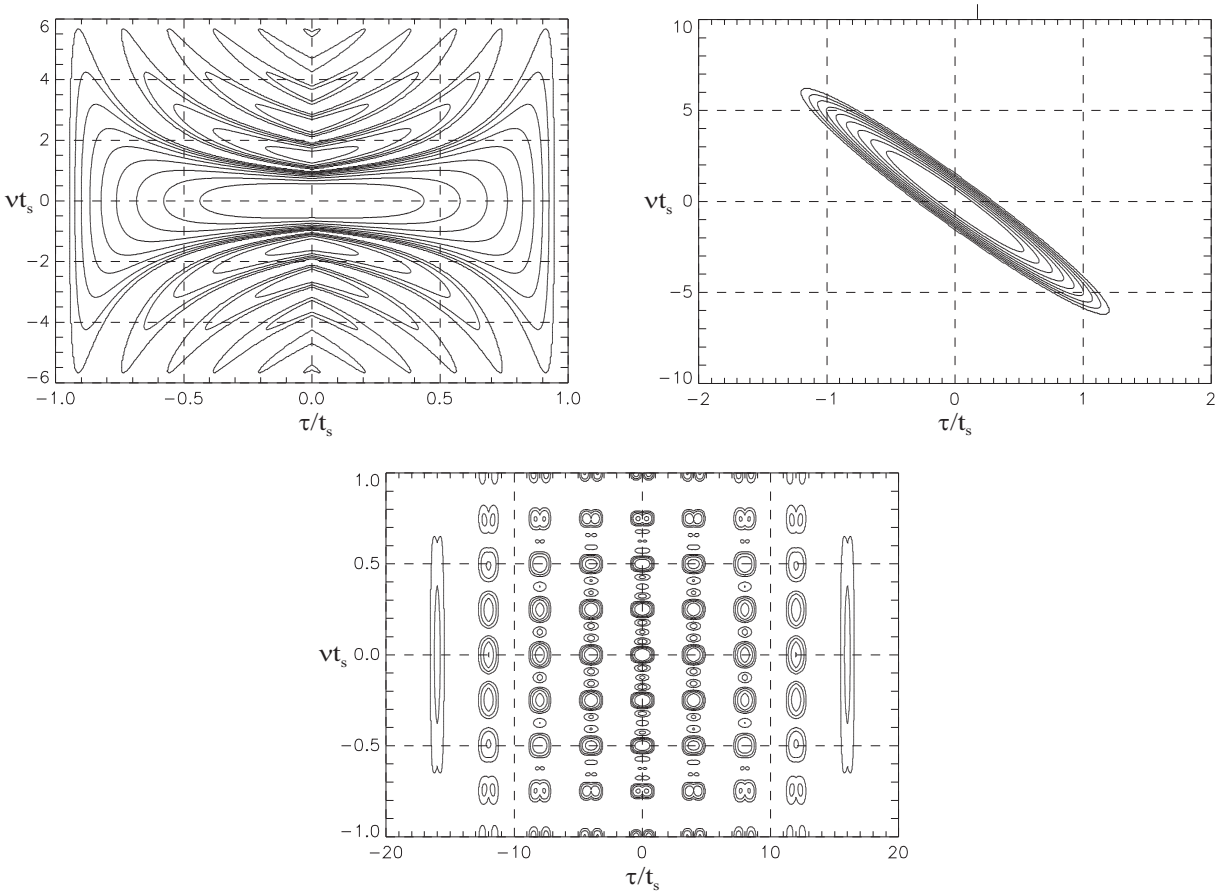

Figure 1.18: *Ambiguity functions of three waveforms in level plot representation. Top left: rectangular pulse, top right: chirp with Gaussian envelope, bottom: train of five rectangular pulses*

Ambiguity function of important waveforms

Rectangular pulse: If $\mathsf{s}(t) = rect(t/t_s)$ the ambiguity function is given by $\chi(\tau,\nu) = e^{j\pi\nu\tau}(t_s - |\tau|)si(\pi\nu(t_s - |\tau|))$ for $|\tau| \leq t_s$ and zero else. In the temporal variable we recognize the triangular function as autocorrelation function of the rectangular pulse, in the Doppler frequency the expected *si* function.

Chirp with Gaussian envelope: For a chirp with Gaussian envelope:

$$\mathsf{s}(t) = \exp\left\{-\frac{t^2}{2\sigma^2} + j\pi\alpha t^2\right\}, \tag{1.90}$$

the ambiguity function is

$$\chi(\tau,\nu) = \sqrt{\pi\sigma^2}e^{j\pi\nu\tau}\exp\left\{-\frac{\tau^2}{4\sigma^2} - (\pi\sigma)^2(\alpha\tau+\nu)^2\right\}. \tag{1.91}$$

For fixed τ the magnitude of the ambiguity function is at $\nu = -\alpha\tau$, so the 'ridge of the ambiguity mountain' is tilted against the axes. This can be heuristically explained as follows (see Fig. 1.19):

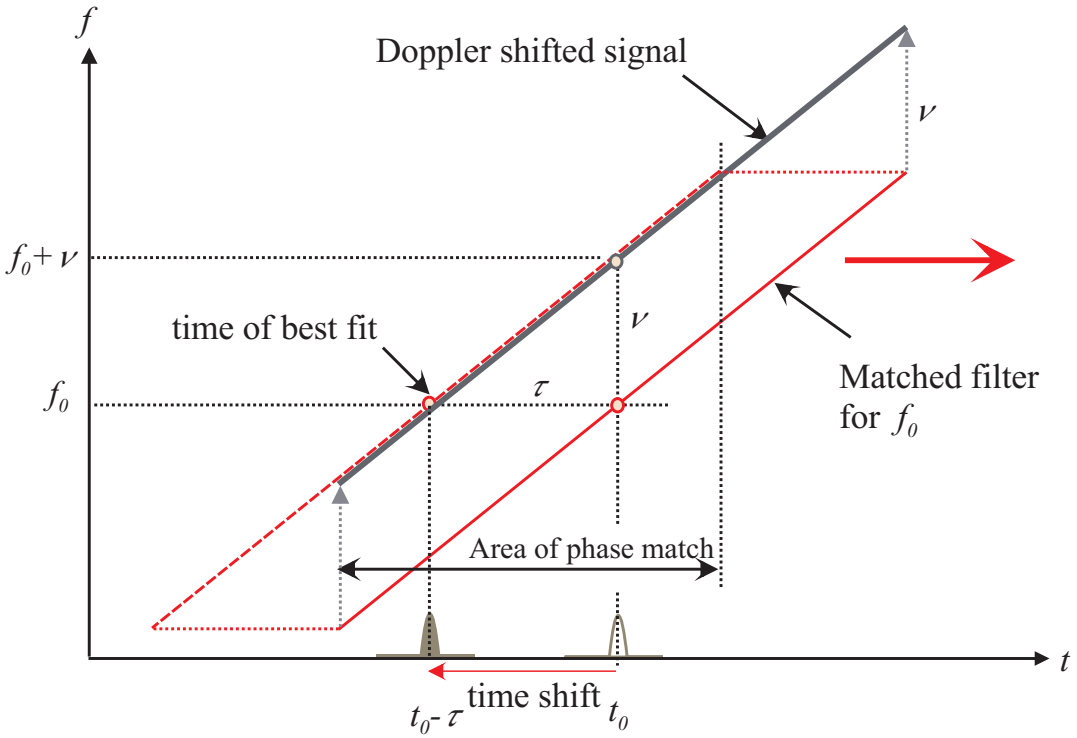

Figure 1.19: *TimeShift*

The matched filter for a mean Doppler frequency f_0, which is represented by a straight line in the time-frequency plain, moves along the time axis. If it is congruent with a signal at the same mean Doppler, at the output of the filter there will arise a peak at the time $t = t_0$, if the echo signal is centered at t_0. But if the same echo signal is shifted in Doppler by the amount ν, the filter will match a part of the signal at the time $t = t_0 - \tau$ with $\tau = \nu/\alpha$. So the peak will occur at the time shift τ and with a widened and lowered main beam due to the shorter time base.

On the one hand, this is a disadvantage, since the position of the range response is changed due to a Doppler shift effecting a wrong range information. On the other hand, the chirp waveform matches the Doppler shifted signal nevertheless over a part of the pulse duration, accumulating SNR and making detection possible. This property is called *Doppler tolerance*. Other waveforms, e.g. a pseudo-noise coded pulse, don't have this property, slight Doppler shifts cause a complete mismatch along the whole time axis, detection is prevented. In this case, pulse compression has to be performed with a bank of filters matched to a selection of Doppler frequencies.

Obviously, for the chirp waveform there is an ambiguity between Doppler and range. If one of the two is known, the other variable can be measured with high

accuracy. The Doppler frequency may be measured over a sequence of pulses and used for a correction of range.

Essence 1.11 *The chirp wave form is Doppler tolerant, i.e. a Doppler shift of the echo with respect to the reference chirp leads only to a moderate SNR loss corresponding to the non-overlapping part of the signal spectra. A time shift is effected which is proportional to the Doppler shift.*

Train of rectangular pulses If a train of N equal pulses $\mathsf{s}(t)$ is transmitted with a temporal period ΔT, the resulting wave form is $\mathsf{q}(t) = \sum_{n=0}^{N-1} \mathsf{s}(t - n\Delta T)$ and the ambiguity function χ_q of q is evaluated from the ambiguity function χ_s of s by

$$\begin{aligned} \chi_q(\tau,\nu) &= \frac{1}{N}\sum_{n=0}^{N-1}\sum_{m=0}^{N-1} e^{j2\pi\nu n\Delta T}\chi_s(\tau-(n-m)\Delta T,\nu) \qquad (1.92)\\ &= \frac{1}{N}\sum_{p=-(N-1)}^{N-1}\frac{\sin(\pi\nu(N-|p|)\Delta T)}{\sin(\pi\nu\Delta T)}e^{j\pi\nu\Delta T(N-1+p)}\chi_s(\tau-p\Delta T,\nu). \end{aligned}$$

For a train of rectangular pulses the ambiguity function is shown in Fig. 1.18. The range resolution is the same as for the single pulse, while the Doppler resolution is decreased to $1/t_q$, where t_q is the duration of the whole pulse train. In the ambiguity plane we recognize a temporal ambiguity with period ΔT leading to a range ambiguity $\frac{c}{2}\Delta T$ and a Doppler ambiguity with a period $PRF = 1/\Delta T$. If we define a *ambiguity rectangle* with the edges ΔT and $1/\Delta T$, its area is for any choice of the PRF equal to 1. This leads to the following

Essence 1.12 *For a pulse train repeated with ΔT, the product of temporal and frequency ambiguity is equal to 1. The product of range ambiguity and Doppler ambiguity is equal to $c_0/2$. The product of range ambiguity and radial velocity ambiguity is $c_0/\lambda = f$.*

So the choice of the PRF will changes the ambiguities, but not their product. For the most radar designs, it is not possible to place both ambiguities simultaneously into areas where they are harmless. Three cases can be discriminated:

- **Low-PRF mode**: After the transmission of a pulse, the next pulse is transmitted not before all echoes of the first pulse have arrived, also from the maximum range r_{max} with non-negligible echo power. So the PRF for range-unambiguous operation is limited by $PRF_{max} = c_0/(2r_{max})$.
- **High-PRF mode**: To evaluate also the highest expected radial velocity $\pm v_{max}$ unambiguously from the Doppler frequency, this has to be at least $PRF_{min} = 4v_{max}/\lambda$.
- **Medium-PRF mode**: The PRF lies in between, there are ambiguities in range as well as in Doppler

1.6.4 Towards 1D imaging

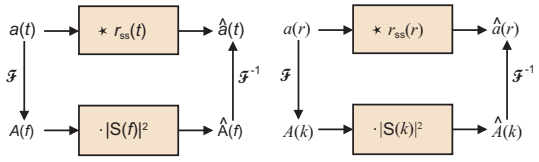

Figure 1.20: *1DImaging*

Pulse compression can be regarded as one-dimensional imaging, see Fig. 1.20. If the reflectivity in range is given by $a(r)$, the result of transmission of a waveform $\mathsf{s}(r)$ scaled to the range domain and matched filtering of the echoes is the convolution of $a(r)$ with the autocorrelation function of $\mathsf{s}(r)$. This can be regarded as the imperfect 'reconstruction' $\hat{a}(r)$ of the range reflectivity, the *range profile*. In the wavenumber domain $A(k)$ - the Fourier transform of $a(r)$ - is multiplied by the squared magnitude of the signal spectrum resulting in $\hat{A}(k)$ whose back transform is again $\hat{a}(r)$. Since $|\mathsf{S}(k)|^2$ is unequal to zero only over an interval determined by the RF band of the transmitted signal, the multiplication effects a cutting of the reflectivity spectrum, which limits the bandwidth of $\hat{a}(r)$, resulting in an 'unsharp' image.

1.7 Estimation

1.7.1 Estimation problem for a standard signal model

If the model for the distribution of a random variable X contains an unknown parameter vector $\boldsymbol{\vartheta} \in \boldsymbol{\Theta}$, the basic problem is to estimate this parameter vector with an estimator $\hat{\boldsymbol{\vartheta}}(x)$ for a given realization x of X. For each $\boldsymbol{\vartheta}$ the distribution $P^X_{\boldsymbol{\vartheta}}$ of X and the probability distribution function (pdf) $p^X_{\boldsymbol{\vartheta}}(x)$ are parametrized by this parameter vector.

General basics of the estimation theory proceeding from this problem are described in the mathematical appendix A.6. Here, we start with an estimation problem which often arises in radar signal processing (we call this *standard model II*):

Example : Let the n-dimensional random vector $\mathbf{Z}$ be modelled by

$$\mathbf{Z} = a\mathbf{s}(\varphi) + \mathbf{N}, \mathbf{N} \sim \mathcal{N}_{\mathbb{C}^n}(\mathbf{0}, \sigma^2\mathbf{I}_n). \tag{1.93}$$

The complex amplitude a and the parameter φ are unknown and have to be estimated. The signal vector is dependant on φ. For instance, the coefficients of $\mathbf{s}(\varphi)$ could describe the signal along slow-time, while $\varphi = 2\pi F \Delta T$ is the phase increment from pulse to pulse due to Doppler modulation. Or $\mathbf{s}(\varphi)$ denotes the signals at an antenna array, while φ describes the angle of arrival of an impinging wave.
For this example, the parameter vector is $\boldsymbol{\vartheta} = (a, \varphi)^t$ with values in $\boldsymbol{\Theta} = \mathbb{C} \times \Phi$, where Φ is e.g. the interval $[0, 2\pi]$. The related probability distribution of Z is $P^Z_{a,\varphi} = \mathcal{N}_{\mathbb{C}^n}(a\mathbf{s}(\varphi), \sigma^2\mathbf{I}_n)$.

1.7.2 Maximum likelihood estimator

This problem is of the form

$$\mathbf{Z} = \mathbf{m}(\boldsymbol{\vartheta}) + \mathbf{N} \tag{1.94}$$

with $\mathbf{N} \sim \mathcal{N}_{\mathbb{C}^n}(\mathbf{0}, \sigma^2\mathbf{I}_n)$. $\mathbf{m}(\boldsymbol{\vartheta})$ describes the deterministic part in dependance on the parameter vector $\boldsymbol{\vartheta}$.

The related set of pdf's is

$$p^{\mathbf{Z}}_{\boldsymbol{\vartheta}}(\mathbf{z}) = \frac{1}{\pi^n \sigma^{2n}} \exp\left\{-\frac{1}{\sigma^2} \|\mathbf{z} - \mathbf{m}(\boldsymbol{\vartheta})\|^2\right\} \tag{1.95}$$

and their logarithm (*log-likelihood function*)

$$L^{\mathbf{Z}}_{\boldsymbol{\vartheta}}(\mathbf{z}) = -\ln(\pi^n \sigma^{2n}) - \frac{1}{\sigma^2} \|\mathbf{z} - \mathbf{m}(\boldsymbol{\vartheta})\|^2 \tag{1.96}$$

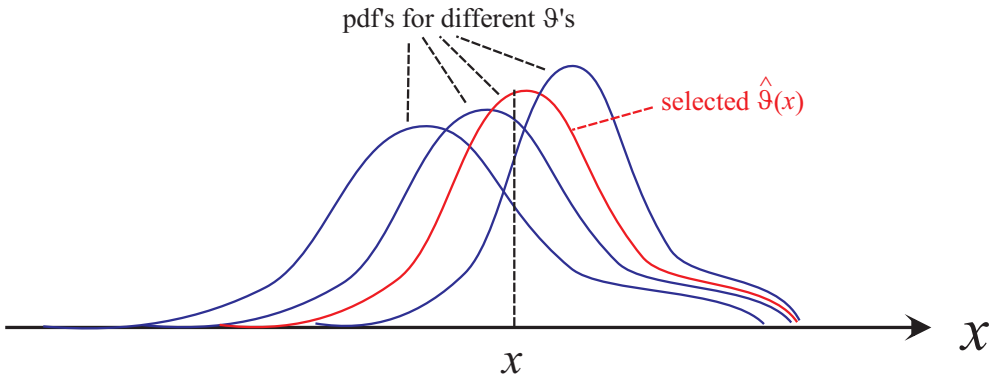

Figure 1.21: *Principle of Maximum Likelihood estimation*

The *maximum likelihood estimator* (ML estimator) for this problem is given as the maximum of the pdf with respect to $\boldsymbol{\vartheta}$ as illustrated in Fig. 1.21 - or its logarithm (see appendix A.6.2) and results in the minimization task

$$\hat{\boldsymbol{\vartheta}}(\mathbf{z}) = \operatorname{argmin}\left\{\|\mathbf{z} - \mathbf{m}(\boldsymbol{\vartheta})\|^2 : \boldsymbol{\vartheta} \in \boldsymbol{\Theta}\right\}. \tag{1.97}$$

Obviously, for the assumption of a Gaussian probability distribution, the ML estimate is equivalent to the *minimum mean square estimator*.

If we return to the signal model in Eq.(1.93), we have to solve

$$\begin{pmatrix} \hat{a} \\ \hat{\varphi} \end{pmatrix}(\mathbf{z}) = \operatorname{argmin}\left\{\|\mathbf{z} - a\mathbf{s}(\varphi)\|^2 : a \in \mathbb{C}, \varphi \in \Phi\right\}. \tag{1.98}$$

The solution can be done in two steps. First, we minimize with respect to a and get

$$\hat{a}_\varphi(\mathbf{z}) = \frac{\mathbf{s}^*(\varphi)\mathbf{z}}{\|\mathbf{s}(\varphi)\|^2} \tag{1.99}$$

$$\|\mathbf{z} - \hat{a}_\varphi(\mathbf{z})\mathbf{s}(\varphi)\|^2 = \|\mathbf{z}\|^2 - \frac{|\mathbf{s}^*(\varphi)\mathbf{z}|^2}{\|\mathbf{s}(\varphi)\|^2}. \tag{1.100}$$

If we define the normalized signal by $\tilde{\mathbf{s}}(\varphi) = \mathbf{s}(\varphi)/\|\mathbf{s}(\varphi)\|$, the ML estimation of φ and a are obtained by

$$\hat{\varphi}(\mathbf{z}) = \operatorname{argmax}\left\{|\tilde{\mathbf{s}}^*(\varphi)\mathbf{z}|^2 : \varphi \in \Phi\right\} \tag{1.101}$$

$$\hat{a}(\mathbf{z}) = \tilde{\mathbf{s}}^*(\hat{\varphi}(\mathbf{z}))\mathbf{z} \tag{1.102}$$

Essence 1.13 *For estimating the unknown variables in the signal model Eq.(1.93), first the maximum magnitudes of the matched filter outputs with respect to the normalized signal is to be determined, then the amplitude estimate is given as the result of the related matched filter.*

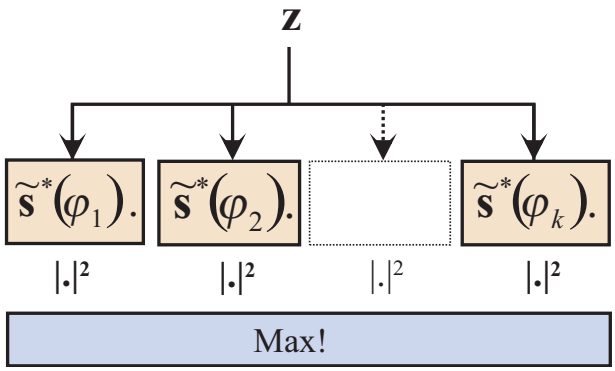

Figure 1.22: *Maximum likelihood estimator for a signal with unknown parameter (signal model Eq.(1.93))*

If the set $\Phi = \{\varphi_1, \ldots, \varphi_k\}$ is finite, this can be accomplished by a filter bank, as illustrated in Fig. 1.22.

For the signal model of unknown Doppler frequency $\mathbf{s}(\varphi) = \begin{pmatrix} \exp\{\cdot j\varphi\} \\ \dots \\ \exp\{n \cdot j\varphi\} \end{pmatrix}$ and $\Phi = \{0 \cdot 2\pi/n, \dots, (n-1) \cdot 2\pi/n\}$ the filter bank is equivalent to the discrete Fourier transform and the ML estimator searches for the maximum of the magnitude of the Doppler spectrum.

Maximum likelihood estimator for colored noise

Now, let the noise in the more general model

$$\mathbf{Z} = \mathbf{m}(\boldsymbol{\vartheta}) + \mathbf{N} \tag{1.103}$$

be 'colored', i.e. not white. Let the noise have the distribution $\mathbf{N} \sim \mathcal{N}_{\mathbb{C}^n}(\mathbf{0}, \mathbf{R})$ with a general non-singular covariance matrix $\mathbf{R}$. Now the pdf is

$$p^{\mathbf{Z}}_{\boldsymbol{\vartheta}}(\mathbf{z}) = \frac{1}{\pi^n \det \mathbf{R}} \exp\left\{-(\mathbf{z} - \mathbf{m}(\boldsymbol{\vartheta}))^* \mathbf{R}^{-1} (\mathbf{z} - \mathbf{m}(\boldsymbol{\vartheta}))\right\} \tag{1.104}$$

and we get analogue to the preceding

$$\begin{aligned} \hat{\boldsymbol{\vartheta}}(\mathbf{z}) &= \operatorname{argmin} \left\{ (\mathbf{z} - \mathbf{m}(\boldsymbol{\vartheta}))^* \mathbf{R}^{-1} (\mathbf{z} - \mathbf{m}(\boldsymbol{\vartheta})) : \boldsymbol{\vartheta} \in \boldsymbol{\Theta} \right\} && (1.105) \\ &= \operatorname{argmin} \left\{ \left\| \mathbf{R}^{-1/2} (\mathbf{z} - \mathbf{m}(\boldsymbol{\vartheta})) \right\|^2 : \boldsymbol{\vartheta} \in \boldsymbol{\Theta} \right\}. && (1.106) \end{aligned}$$

The application of $\mathbf{R}^{-1/2}$ has 'whitened' the random vector, as can seen by

$$E\left[\left(\mathbf{R}^{-1/2}\mathbf{N}\right) \left(\mathbf{R}^{-1/2}\mathbf{N}\right)^* \right] = \mathbf{R}^{-1/2}\mathbf{R}\mathbf{R}^{-1/2} = \mathbf{I}_n. \tag{1.107}$$

1.7.3 Cramér-Rao Bounds

A widely method used for the analysis of possible performance of estimators are the *Cramér-Rao Bounds* (CRB) which are treated in the appendix A.6.3. At this point, we will present the CRB for the model Eq.(1.94). *Fisher's information matrix* is defined by

$$\mathbf{J}(\boldsymbol{\vartheta}) = E_{\boldsymbol{\vartheta}} \left[\left(\frac{\partial}{\partial \boldsymbol{\vartheta}} \ln p^{\mathbf{Z}}_{\boldsymbol{\vartheta}}(\mathbf{Z}) \right) \left(\frac{\partial}{\partial \boldsymbol{\vartheta}} \ln p^{\mathbf{Z}}_{\boldsymbol{\vartheta}}(\mathbf{Z}) \right)^t \right]. \tag{1.108}$$

In Eq.(1.96) the logarithm of the pdf was presented, from which we can compute its partial derivatives

$$\begin{aligned} \frac{\partial}{\partial \boldsymbol{\vartheta}} L^{\mathbf{Z}}_{\boldsymbol{\vartheta}}(\mathbf{z}) &= -\frac{1}{\sigma^2} \frac{\partial}{\partial \boldsymbol{\vartheta}} \|\mathbf{z} - \mathbf{m}(\boldsymbol{\vartheta})\|^2 && (1.109) \\ &= \frac{2}{\sigma^2} \Re\left\{ \mathbf{m}^*_{\boldsymbol{\vartheta}}(\boldsymbol{\vartheta}) (\mathbf{z} - \mathbf{m}(\boldsymbol{\vartheta})) \right\} && (1.110) \end{aligned}$$

where $\mathbf{m}_{\boldsymbol{\vartheta}} = \left(\frac{\partial}{\partial\vartheta_1}\mathbf{m}, \ldots, \frac{\partial}{\partial\vartheta_k}\mathbf{m}\right)$ denotes the partial derivatives of $\mathbf{m}$. Since the second factor in the brackets is the noise contribution, Fisher's information matrix is easily calculated:

$$\begin{aligned}
\mathbf{J}(\boldsymbol{\vartheta}) &= \frac{4}{\sigma^4} E_{\boldsymbol{\vartheta}} \left[\Re\left\{\mathbf{m}^*_{\boldsymbol{\vartheta}}(\boldsymbol{\vartheta})\mathbf{N}\right\} \left(\Re\left\{\mathbf{m}^*_{\boldsymbol{\vartheta}}(\boldsymbol{\vartheta})\mathbf{N}\right\}\right)^t \right] && (1.111)\\
&= \frac{2}{\sigma^4} \Re\left\{ E_{\boldsymbol{\vartheta}} \left[\mathbf{m}^*_{\boldsymbol{\vartheta}}(\boldsymbol{\vartheta})\mathbf{N}\mathbf{N}^*\mathbf{m}_{\boldsymbol{\vartheta}}(\boldsymbol{\vartheta}) \right] \right\} && (1.112)\\
&= \frac{2}{\sigma^2} \Re\left\{ \mathbf{m}^*_{\boldsymbol{\vartheta}}(\boldsymbol{\vartheta})\mathbf{m}_{\boldsymbol{\vartheta}}(\boldsymbol{\vartheta}) \right\}. && (1.113)
\end{aligned}$$

So under the assumptions of the signal model Eq.(1.94) the partial derivatives of the deterministic part of the signal constitute the information matrix. Under slight conditions, the covariance matrix of any unbiased estimator is bounded by the inverse of Fisher's information matrix. If there is only one real parameter ϑ, this is simplified to

$$\mathrm{Var}_\vartheta \left[\hat{\vartheta}(\mathbf{Z}) \right] \geq \mathbf{J}^{-1}(\vartheta) = \frac{\sigma^2}{2\|\mathbf{m}_\vartheta(\vartheta)\|^2} \tag{1.114}$$

for any unbiased estimator $\hat{\vartheta}(\mathbf{z})$ of ϑ.

If, for example, $\mathbf{m}(\varphi) = a(\exp\{j(\nu - \bar{\nu})\varphi\})_{\nu=1,\ldots,n}$ models a signal with Doppler angular increment φ and a is assumed to be known, we get

$$\mathbf{J}^{-1}(\varphi) = \frac{\sigma^2}{2|a|^2 \sum_{\nu=1}^{n} (\nu - \bar{\nu})^2} \tag{1.115}$$

$\bar{\nu}$ has to be chosen as the mean value of all subscripts $\bar{\nu} = (n+1)/2$ to achieve the phase of a being independent on φ. Otherwise the assumed knowledge of a would also include an information on φ. The resulting CRB is

$$\mathbf{J}^{-1}(\varphi) = \frac{6\sigma^2}{|a|^2 n(n^2-1)} = \frac{6}{(n^2-1)\mathrm{SNR}} \tag{1.116}$$

where SNR is the accumulated signal-to-noise ratio.

Recall, that this result is obtained without specifying a concrete estimator. It reflects the information content of the data with respect to the parameter to be estimated. This analysis can often be used for the design of system parameters without going into details of estimation.

1.8 Target detection

1.8.1 The target detection problem

We regard the radar measurement $\mathbf{z}$ which can be interpreted as a realization of the random vector $\mathbf{Z}$. It is not known from the beginning, if the measurement includes a

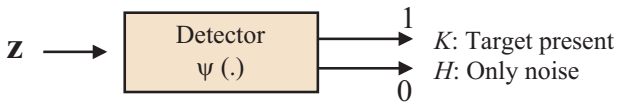

Figure 1.23: *A target detector*

target signal, or if it is produced by noise only. A device would be of great interest, which automatically decides if a target is supposed to be present or not. Such a device (as illustrated in Fig. 1.23) is called *detector* in this context and can be described by a function $\psi(\mathbf{z})$ taking values in $\{0, 1\}$ with the result 1, if the detector decides for 'target present' and 0 else. In the general mathematical background, this detector is called *test*.

The two possibilities for the origin of data are called *hypothesis* H for the 'normal' or 'uninteresting' case that there was only noise, and *alternative* K for the 'important' and 'interesting' case that a target echo is hidden in the measurement. In mathematical language, it has to be tested the alternative K (target present) against the hypothesis H (only noise).

Since $\mathbf{Z}$ is a random vector, the decision cannot be made with absolute certainty, wrong decisions are possible with certain probabilities. If the detector decides for 'K: target present' though there was only noise (H), this is called *false alarm*, if it decides for 'H: only noise' though there is indeed a target (K), we call this *target miss*.

The probability for the first kind of error is called *false alarm probability* P_F, that for the second kind of error *target miss probability*. More usual as the latter is the expression *detection probability* P_D for the opposite case, that the detector decides correctly for K, if a target is present. Clearly, P_D is equal to 1 minus the probability of target miss.

To compute these probabilities we need models for the distribution of $\mathbf{Z}$.

Example 1: detector for a signal with known phase As an example we proceed from the standard model I with Gaussian noise:

$$\mathbf{Z} = a\mathbf{s} + \mathbf{N}, \quad \mathbf{N} \sim \mathcal{N}_{\mathbb{C}^n}\left(\mathbf{0}, \sigma^2\mathbf{I}_n\right), \mathrm{a} \in \mathbb{C} \tag{1.117}$$

For a fixed $a \in \mathbb{C}$ the distribution of $\mathbf{Z}$ is $P^{\mathbf{Z}}(a) = \mathcal{N}_{\mathbb{C}^n}\left(a\mathbf{s}, \sigma^2\mathbf{I}_n\right)$ with the pdf

$$p^{\mathbf{Z}}(a; \mathbf{z}) = \frac{1}{(\pi\sigma^2)^n} \exp\left\{-\frac{1}{\sigma^2}\left\|\mathbf{z} - a\mathbf{s}\right\|^2\right\} \tag{1.118}$$

1.8.2 Simple alternatives

A stringent solution for an optimum detector is possible, if there are exactly two probability distributions for the two alternatives (*simple alternatives*). For the noise-only case we have for this model a simple hypothesis $P_0 = P^{\mathbf{Z}}(0) = P^{\mathbf{N}}$. For the

alternative the possible values for the amplitude a have - for the present - to be limited to a fixed value $a = a_0 \neq 0$ leading to the distribution $P_1 = P^{\mathbf{Z}}(a_0)$. The corresponding pdf's are $p_0(\mathbf{z})$ and $p_1(\mathbf{z})$.

So the detection problem reduces to test the alternative $K : \mathbf{Z} \sim P_1$ against the hypothesis $H : \mathbf{Z} \sim P_0$.

If a certain detector ψ is used, the two basic probabilities are

$$P_F = \Pr\{\text{decision for } K|H\} = P_0(\psi(\mathbf{Z}) = 1) \tag{1.119}$$
$$P_D = \Pr\{\text{decision for } K|K\} = P_1(\psi(\mathbf{Z}) = 1) \tag{1.120}$$

The approach of Neyman and Pearson

Radar detection follows the *approach of Neyman and Pearson*[12]: The two alternatives are not symmetrical. The error of the first kind (here: a target is indicated, though only noise is present) possibly induces unwanted activities. Its probability P_F has to be controlled, it shall not be larger than a pre-given *level* α. Among all tests fulfilling this demand, a test ψ_{opt} is called *best test for the level* α , if it has the maximum detection probability P_D.

Likelihood ratio test

Neyman and Pearson have not only proofed that such a best test exists, but they have constructively given how it has to be performed. For continuous distributions like in the example, it is given by

$$\psi(\mathbf{z}) = \begin{cases} 1 & \text{if } \Lambda(\mathbf{z}) > \eta \\ 0 & \text{if } \Lambda(\mathbf{z}) \leq \eta \end{cases} \tag{1.121}$$
$$\text{with } \Lambda(\mathbf{z}) = \frac{p_1(\mathbf{z})}{p_0(\mathbf{z})}. \tag{1.122}$$

$\Lambda(\mathbf{z})$ is called *likelihood ratio*, and the *threshold* η has to be determined to achieve $P_F = \alpha$. This test (detector) is called *likelihood ratio test (likelihood ratio detector).*

If $f : \mathbb{R} \to \mathbb{R}$ is a strictly monotonic increasing function, then the comparison of $T(\mathbf{z}) := f(\Lambda(\mathbf{z}))$ with the new threshold $\eta' = f(\eta)$ defines a best test, too. For the regarded example, we use the logarithm as such a monotonic function, resulting in the *log likelihood ratio*

$$\ln \Lambda(\mathbf{z}) = \ln \left\{ \frac{p^{\mathbf{Z}}(a_0; \mathbf{z})}{p^{\mathbf{Z}}(0; \mathbf{z})} \right\} \tag{1.123}$$

$$= \ln \left\{ \frac{\frac{1}{(\pi\sigma^2)^n} \exp\left\{-\frac{1}{\sigma^2} \left|\mathbf{z} - a_0\mathbf{s}\right|^2\right\}}{\frac{1}{(\pi\sigma^2)^n} \exp\left\{-\frac{1}{\sigma^2} \left|\mathbf{z}\right|^2\right\}} \right\} \tag{1.124}$$

$$= \frac{1}{\sigma^2} \left(-\|a_0\mathbf{s}\|^2 + 2Re\left\{a_0^*\mathbf{s}^*\mathbf{z}\right\}\right) \tag{1.125}$$

Let $a_0 = |a_0|e^{j\phi}$. Applying the second strictly monotonic increasing function $g(x) = \frac{\sigma^2}{2|a_0|}x + \frac{|a_0|}{2}\|\mathbf{s}\|^2$ we finally get the function $T(\mathbf{z}) = Re\left\{e^{-j\phi}\mathbf{s}^*\mathbf{z}\right\}$ and the best test

$$\psi(\mathbf{z}) = \begin{cases} 1 & \text{if} \quad \Re\left\{e^{-j\phi}\mathbf{s}^*\mathbf{z}\right\} > \eta' \\ 0 & \text{else} \end{cases} \tag{1.126}$$

$$\tag{1.127}$$

Obviously the best test is achieved if the filter matched to $\mathbf{s}$ is applied followed by a phase compensation of the phase of a_0. Then the deterministic part of the measurement is rotated to the real part. Only this is compared to a threshold, see Fig. 1.24 top. See Fig. 1.27.

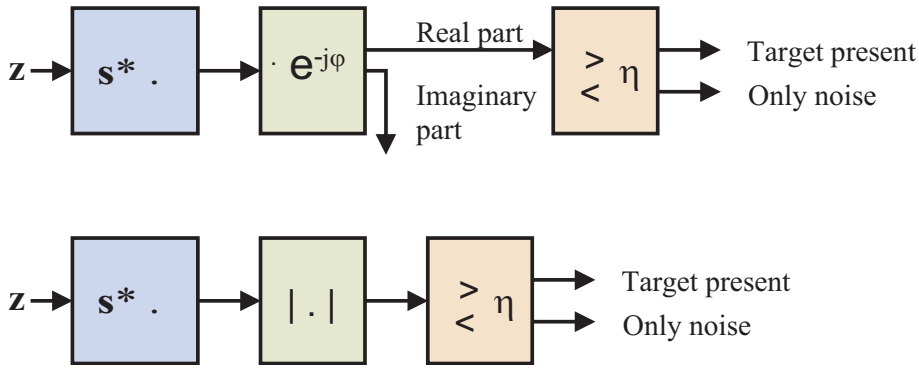

Figure 1.24: *Top: detector for known phase. Bottom: detector for unknown phase*

Example 2: detector for a signal with random phase In general, the phase of the signal will not be known in the radar application, since it depends on the exact range of the scatterer in the accuracy of fractions of a wavelength. So in this example we model the phase Ψ as rectangular distributed over $(0, 2\pi)$:

$$\begin{aligned} &\mathbf{Z} = \gamma e^{j\Psi}\mathbf{s} + \mathbf{N}, \quad \mathbf{N} \sim \mathcal{N}_{\mathbb{C}^n}\left(\mathbf{0}, \sigma^2\mathbf{I}_n\right), \gamma \in \mathbb{R} \\ &\qquad\qquad\quad \Psi \sim \mathcal{R}\left(0, 2\pi\right), \\ &\qquad\qquad\quad \mathbf{N} \text{ and } \Psi \text{ statistical independent.} \qquad (1.128) \\ &H : \gamma = 0 \\ &K : \gamma > 0 \end{aligned}$$

We search for a best test for K against H for the level α.

Solution: For arbitrary γ we find the pdf $p_\gamma^{\mathbf{Z}}(\mathbf{z})$ by integrating over the conditioned distribution for $\Psi = \psi$:

$$\begin{aligned} p_\gamma^{\mathbf{Z}}(\mathbf{z}) &= \int_0^{2\pi} p_\gamma^{\mathbf{Z}|\Psi=\psi}(\mathbf{z}) p^{\Psi}(\psi) d\psi & (1.129) \\ &= \left(\pi\sigma^2\right)^{-n} \frac{1}{2\pi} \int_0^{2\pi} \exp\left\{ -\frac{\left\|\mathbf{z} - \gamma e^{j\psi}\mathbf{s}\right\|^2}{\sigma^2} \right\} d\psi & (1.130) \\ &= \left(\pi\sigma^2\right)^{-n} e^{-(\|\mathbf{z}\|^2 + \|\gamma\mathbf{s}\|^2)/\sigma^2} \frac{1}{2\pi} \int_0^{2\pi} \exp\left\{ \frac{2\Re\{\gamma \mathbf{s}^* \mathbf{z} e^{-j\psi}\}}{\sigma^2} \right\} d\psi & (1.131) \\ &= \left(\pi\sigma^2\right)^{-n} e^{-(\|\mathbf{z}\|^2 + \|\gamma\mathbf{s}\|^2)/\sigma^2} \frac{1}{2\pi} \int_0^{2\pi} \exp\left\{ \frac{2|\gamma \mathbf{s}^* \mathbf{z}|}{\sigma^2} \cos\psi \right\} d\psi & (1.132) \\ &= \left(\pi\sigma^2\right)^{-n} e^{-(\|\mathbf{z}\|^2 + \|\gamma\mathbf{s}\|^2)/\sigma^2} I_0\left(\frac{2|\gamma \mathbf{s}^* \mathbf{z}|}{\sigma^2} \right). & (1.133) \end{aligned}$$

$I_0(x)$ here denotes the *modified Bessel function of order 0*, see appendix Eq. (A.60). The distribution described by the pdf evaluated in Eq. (1.128) is called *Rician distribution*, see appendix Eq. (A.94) and *Rayleigh distribution*, if $\gamma = 0$.

The likelihood ratio now is computed to

$$\Lambda(\mathbf{z}) = \frac{p_\gamma^{\mathbf{Z}}(\mathbf{z})}{p_0^{\mathbf{Z}}(\mathbf{z})} = e^{-\|\gamma\mathbf{s}\|^2/\sigma^2} I_0\left(\frac{2|\gamma \mathbf{s}^* \mathbf{z}|}{\sigma^2} \right). \qquad (1.134)$$

Since $I_0(x)$ is a strictly monotonic increasing function, we can replace $\Lambda(\mathbf{z})$ by

$$T(\mathbf{z}) = |\mathbf{s}^* \mathbf{z}|. \qquad (1.135)$$

The parameter γ has disappeared, so this test function is optimum for arbitrary $\gamma > 0$, it leads to an *uniform best test* which simply compares the amplitude of the matched filter to the threshold, see Fig. 1.24 bottom.

The dependance of the probability of detection on the SNR is depicted in Fig. 1.27. Compared to the detection with known phase, a loss of about 1 dB at representative parameters can be stated.

1.8.3 Composed alternatives

Unfortunately, uniform best tests don't exist in general. Often a test problem extends to two sets of distributions instead of only two single distributions. Like in the estimation problem section 1.7 the model for a random variable X contains an unknown parameter vector $\boldsymbol{\vartheta} \in \boldsymbol{\Theta}$ for the distribution $P_{\boldsymbol{\vartheta}}^X$ and the pdf $p_{\boldsymbol{\vartheta}}^X(x)$. Let $\boldsymbol{\Theta}_0$ and $\boldsymbol{\Theta}_1$ be two disjunct subsets of $\boldsymbol{\Theta}$. Now, the test problem is to decide for a realization x of X, to which of the two classes the parameter vector belongs:

$$H : \boldsymbol{\vartheta} \in \boldsymbol{\Theta}_0 \tag{1.136}$$
$$K : \boldsymbol{\vartheta} \in \boldsymbol{\Theta}_1 \tag{1.137}$$

Maximum likelihood ratio tests

A practical way is to insert the maximum likelihood estimators for the two alternatives $\hat{\boldsymbol{\vartheta}}_i(x) = \operatorname{argmax}\left\{p_{\boldsymbol{\vartheta}}^X(x) : \boldsymbol{\vartheta} \in \boldsymbol{\Theta}_i\right\}$ for $i = 1, 2$ and form with these the *maximum likelihood ratio*:

$$\tilde{\Lambda}(x) : = \frac{p_{\hat{\boldsymbol{\vartheta}}_1(x)}^X(x)}{p_{\hat{\boldsymbol{\vartheta}}_0(x)}^X(x)} \tag{1.138}$$
$$= \frac{\max\left\{p_{\boldsymbol{\vartheta}}^X(x) : \boldsymbol{\vartheta} \in \boldsymbol{\Theta}_1\right\}}{\max\left\{p_{\boldsymbol{\vartheta}}^X(x) : \boldsymbol{\vartheta} \in \boldsymbol{\Theta}_0\right\}}. \tag{1.139}$$

Example 3: Detector for a signal in colored noise Throughout this scriptumthis test problem is of great importance.

$$\begin{aligned} &\mathbf{Z} = a\mathbf{s} + \mathbf{N}, \quad \mathbf{N} \sim \mathcal{N}_{\mathbb{C}^n}\left(\mathbf{0}, \mathbf{R}\right), \mathrm{a} \in \mathbb{C} \\ &H : a = 0 \\ &K : a \neq 0. \end{aligned} \tag{1.140}$$

We search for a maximum likelihood ratio test.

Solution: For arbitrary a the pdf. is given by

$$p_a^{\mathbf{Z}}(\mathbf{z}) = \frac{1}{\pi^n \det \mathbf{R}} \exp\left\{-(\mathbf{z}-a\mathbf{s})^* \mathbf{R}^{-1} (\mathbf{z}-a\mathbf{s})\right\} \tag{1.141}$$

The maximum likelihood ratio is given by

$$\begin{aligned} \tilde{\Lambda}(\mathbf{z}) &= \max_a \frac{p_a^{\mathbf{Z}}(\mathbf{z})}{p_0^{\mathbf{Z}}(\mathbf{z})} && (1.142)\\ &= \exp\left\{\mathbf{z}^*\mathbf{R}^{-1}\mathbf{z} - \min_a (\mathbf{z}-a\mathbf{s})^* \mathbf{R}^{-1} (\mathbf{z}-a\mathbf{s})\right\} && (1.143) \end{aligned}$$

The amplitude $\hat{a}$ leading to the extremum is a maximum likelihood estimator of a for the conditions of the alternative, and is computed to

$$\hat{a} = \frac{\mathbf{s}^*\mathbf{R}^{-1}\mathbf{z}}{\mathbf{s}^*\mathbf{R}^{-1}\mathbf{s}}. \tag{1.144}$$

The logarithm of the maximum likelihood ratio now is

$$\begin{aligned} \ln \tilde{\Lambda}(\mathbf{z}) &= \mathbf{z}^*\mathbf{R}^{-1}\mathbf{z} - (\mathbf{z}-\hat{a}\mathbf{s})^* \mathbf{R}^{-1} (\mathbf{z}-\hat{a}\mathbf{s}) && (1.145)\\ &= \mathbf{z}^*\mathbf{R}^{-1}\mathbf{z} - \mathbf{z}^* \left(\mathbf{I}_n - \frac{\mathbf{R}^{-1}\mathbf{s}\mathbf{s}^*}{\mathbf{s}^*\mathbf{R}^{-1}\mathbf{s}}\right) \mathbf{R}^{-1} \left(\mathbf{I}_n - \frac{\mathbf{s}\mathbf{s}^*\mathbf{R}^{-1}}{\mathbf{s}^*\mathbf{R}^{-1}\mathbf{s}}\right) \mathbf{z} && (1.146)\\ &= \mathbf{z}^*\mathbf{R}^{-1}\mathbf{z} - \mathbf{z}^* \left(\mathbf{R}^{-1} - \frac{\mathbf{R}^{-1}\mathbf{s}\mathbf{s}^*\mathbf{R}^{-1}}{\mathbf{s}^*\mathbf{R}^{-1}\mathbf{s}}\right) \mathbf{z} && (1.147)\\ &= \frac{\left|\mathbf{z}^*\mathbf{R}^{-1}\mathbf{s}\right|^2}{\mathbf{s}^*\mathbf{R}^{-1}\mathbf{s}} && (1.148) \end{aligned}$$

Equivalent to this is the test function

$$T(\mathbf{z}) = \left|\mathbf{z}^*\mathbf{R}^{-1}\mathbf{s}\right|^2. \tag{1.149}$$

Example 4: Detector for a signal with unknown parameter An example for the maximum likelihood ratio test is the detection of a signal with unknown parameter according to standard model II:

$$\begin{aligned} &\mathbf{Z} = a\mathbf{s}(\varphi) + \mathbf{N}, \quad \mathbf{N} \sim \mathcal{N}_{\mathbb{C}^n}(\mathbf{0}, \sigma^2\mathbf{I}_n), \mathrm{a} \in \mathbb{C} \\ &\qquad\qquad \varphi \in \Phi \text{ unknown parameter} \\ &\qquad\qquad \|\mathbf{s}(\varphi)\|^2 > 0 \text{ for all } \varphi \in \Phi \qquad (1.150)\\ &H : a = 0 \\ &K : a \neq 0. \end{aligned}$$

We search for a maximum likelihood ratio test.

Solution: The test problem is parametrized by $\boldsymbol{\vartheta} = (a, \varphi)$, $\boldsymbol{\Theta}_0 = \{(0, \varphi) : \varphi \in \Phi\}$, $\boldsymbol{\Theta}_1 = \{(a, \varphi) : a \in \mathbb{C} \setminus \{0\}, \varphi \in \Phi\}$.

For $a = 0$ the pdf does not depend on φ:

$$p_0^{\mathbf{Z}}(\mathbf{z}) = (\pi\sigma^2)^{-n} \exp\left\{-\|\mathbf{z}\|^2/\sigma^2\right\}, \tag{1.151}$$

while for the alternative the maximum likelihood estimator has to be inserted:

$$p_{\hat{a},\hat{\varphi}}^{\mathbf{Z}}(\mathbf{z}) = (\pi\sigma^2)^{-n} \exp\left\{-\frac{\|\mathbf{z} - \hat{\mathbf{a}}\mathbf{s}(\hat{\varphi})\|^2}{\sigma^2}\right\} \tag{1.152}$$

$$= (\pi\sigma^2)^{-n} \exp\left\{-\frac{\|\mathbf{z}\|^2 - |\tilde{\mathbf{s}}^*(\hat{\varphi})\mathbf{z}|^2}{\sigma^2}\right\}, \tag{1.153}$$

where $\tilde{\mathbf{s}}$ is the signal $\mathbf{s}$ normalized to norm equal to one, and $\hat{\varphi}(\mathbf{z}) = \operatorname{argmax}\left\{|\tilde{\mathbf{s}}^*(\varphi)\mathbf{z}|^2 : \varphi \in \Phi\right\}$ according to Eq. (1.99).

Consequently, the maximum likelihood ratio is given by

$$\tilde{\Lambda}(x) = \frac{\exp\left\{-\frac{\|\mathbf{z}\|^2 - |\tilde{\mathbf{s}}^*(\hat{\varphi})\mathbf{z}|^2}{\sigma^2}\right\}}{\exp\left\{-\frac{\|\mathbf{z}\|^2}{\sigma^2}\right\}} \tag{1.154}$$

$$= \exp\left\{\frac{\max\left\{|\tilde{\mathbf{s}}^*(\varphi)\mathbf{z}|^2 : \varphi \in \Phi\right\}}{\sigma^2}\right\} \tag{1.155}$$

Equivalent to this, since monotonic increasing depending, is the test function

$$T(\mathbf{z}) = \max\left\{|\tilde{\mathbf{s}}^*(\varphi)\mathbf{z}|^2 : \varphi \in \Phi\right\}. \tag{1.156}$$

For a finite set $\Phi = \{\varphi_1, \ldots, \varphi_k\}$ the detector is builded as illustrated in Fig. 1.25.

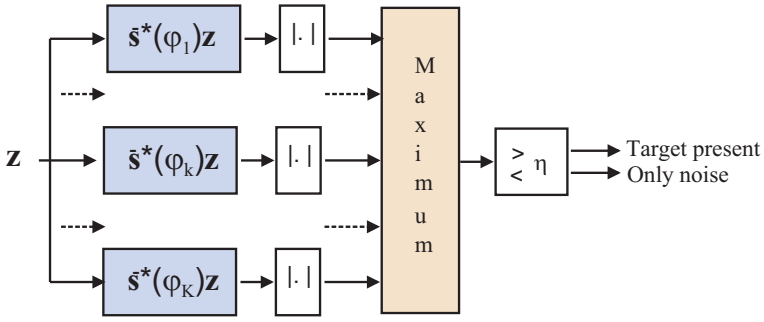

Figure 1.25: *Maximum likelihood ratio test*

As in the section on maximum likelihood estimators, for the signal model of unknown Doppler frequency $\mathbf{s}(\varphi) = \begin{pmatrix} \exp\{0 \cdot j\varphi\} \\ \ldots \\ \exp\{(n-1) \cdot j\varphi\} \end{pmatrix}$ and $\Phi = \{0 \cdot 2\pi/n, \ldots, (n-1) \cdot 2\pi/n\}$ the filter bank is equivalent to the discrete Fourier transform. The maximum amplitude of the Fourier spectrum now has to be compared to a threshold.

For the case of orthogonal signals (as in the discrete Fourier transformation), the probability of detection is plotted against the SNR in Fig. 1.27.

1.8.4 Probability of detection for basic detectors

Probability of detection versus Signal-to-noise-ratio

Following the approach of Neyman and Pearson, a fixed upper bound α for the false alarm probability P_F is specified.

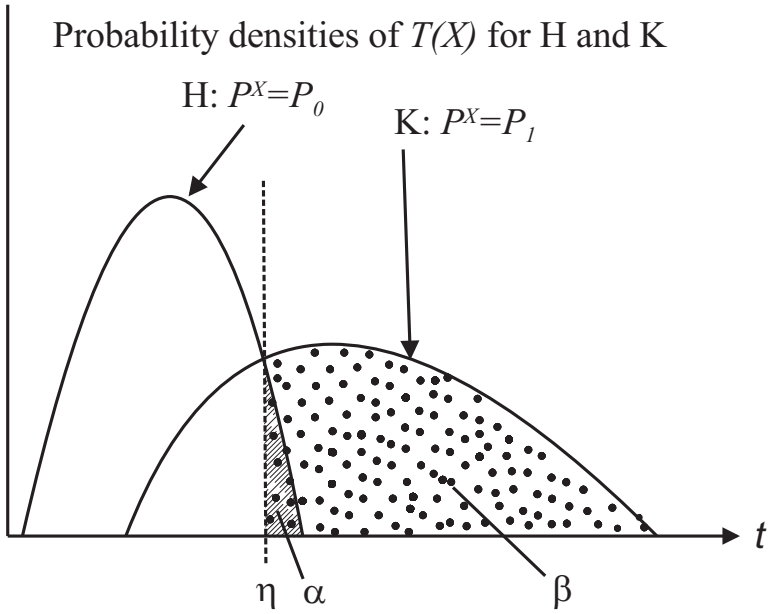

Figure 1.26: *False alarm probability and detection probability as areas below the probability density functions of the test statistics*

If an arbitrary test function $T(X)$ is used for the general test problem Eq. (1.136) the threshold η has to be determined by

$$\eta := \min \left\{ t : P_{\boldsymbol{\vartheta}}^{(X)}(T(X) > t) \leq \alpha \text{ for all } \boldsymbol{\vartheta} \in \boldsymbol{\Theta}_0 \right\}. \tag{1.157}$$

If $F_{\boldsymbol{\vartheta}}(t) := P_{\boldsymbol{\vartheta}}^{(X)}(T(X) \leq t)$ denotes the distribution function of $T(X)$ for an arbitrary $\boldsymbol{\vartheta}$, η can be found by

$$\eta := F_0^{-1}(1-\alpha) \text{ with } F_0(t) := \min \{ F_{\boldsymbol{\vartheta}}(t) : \boldsymbol{\vartheta} \in \boldsymbol{\Theta}_0 \} \tag{1.158}$$

if F_0 is bijective. Then the detection probability can be derived by

$$P_D(\boldsymbol{\vartheta}) = F_{\boldsymbol{\vartheta}}(\eta). \tag{1.159}$$

The dependance of the detection probability on the SNR is depicted in Fig. 1.27 for different conditions.

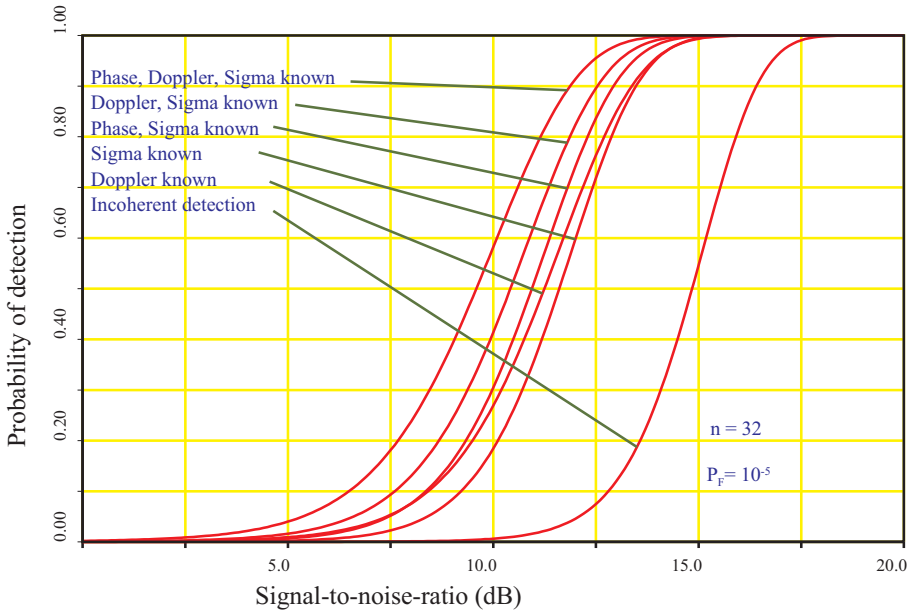

Figure 1.27: *Detection probability in dependence on the SNR. The false alarm probability is fixed at* 10^{-5} *and the number of samples is 32.*

Receiver operating characteristics

For a fixed SNR the dependence $P_D(P_F)$ is called *receiver operating characteristics*, plotted in Fig. 1.28 for the test problem example 2. If the SNR is zero, $P_D = P_F$ and we get the diagonal. For growing SNR the curves are vaulted upwards but retaining the points (0,0) and (1,1). A best test is characterized by the property that its ROC curve is the upper bound for the ROC of any test for this problem at each value of P_F.

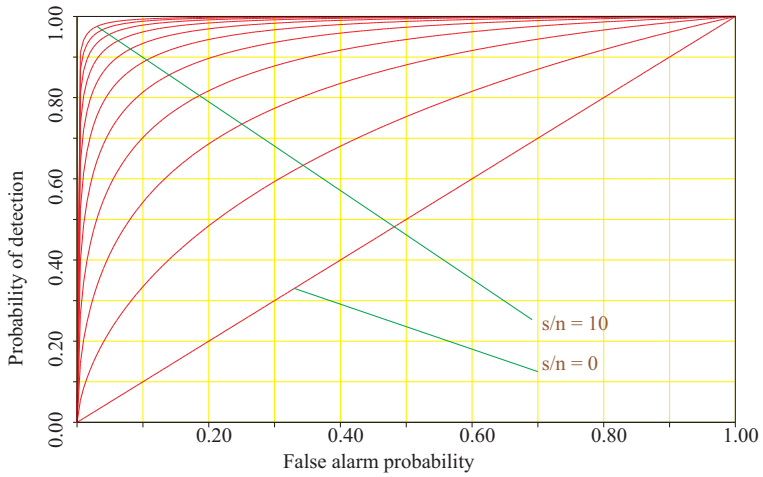

Figure 1.28: *Receiver operating characteristics (ROC)*

Constant false alarm rate detectors

All detectors regarded up to now assume that the noise variance is known. If a threshold was computed for a certain σ^2 and the real noise variance becomes larger - for instance because of variations of the amplification factor - the false alarm probability can increase dramatically. To anticipate this, a test can be constructed with a P_F independent on σ^2. For instance, example 2 can be expanded to this situation:

Example 5: detector for unknown noise variance

$$\begin{array}{ll} \mathbf{Z} = \gamma e^{j\Psi}\mathbf{s} + \mathbf{N}, & \mathbf{N} \sim \mathcal{N}_{\mathbb{C}^n}\left(\mathbf{0}, \sigma^2\mathbf{I}_n\right), \gamma \in \mathbb{R} \\ & \Psi \sim \mathcal{R}\left(0, 2\pi\right), \\ & \mathbf{N} \text{ and } \Psi \text{ statistical independent,} \\ & \sigma^2 \text{ unknown.} \\ H : \gamma = 0 & \\ K : \gamma > 0 & \end{array} \tag{1.160}$$

The statistical model is invariant against a multiplication with a scalar. In the mathematical test theory a method was developed to construct *best invariant tests*. We relinquish going into detail, but give directly the solution:

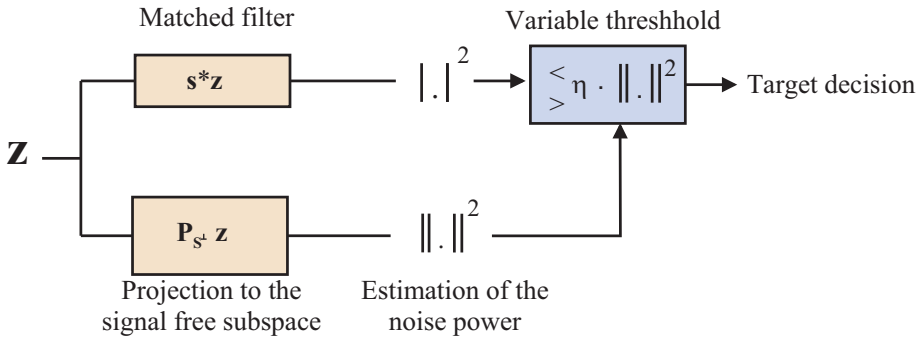

Figure 1.29: *CFAR*

Without loss of generality we can assume that the signal vector $\mathbf{s}$ is normalized to $\|\mathbf{s}\|^2 = 1$. Then,

$$T\left(\mathbf{z}\right) = \frac{\left|\mathbf{s}^*\mathbf{z}\right|^2}{\left\|\mathbf{z}\right\|^2 - \left|\mathbf{s}^*\mathbf{z}\right|^2} = \frac{\left\|\mathbf{P}_{<\mathbf{s}>}\mathbf{z}\right\|^2}{\left\|\mathbf{P}_{<\mathbf{s}>^\perp}\mathbf{z}\right\|^2} \tag{1.161}$$

is a best invariant test (without proof). $\mathbf{P}_{<\mathbf{s}>} = \mathbf{s}\mathbf{s}^*$ and $\mathbf{P}_{<\mathbf{s}>^\perp} = \mathbf{I}_n\mathbf{s}\mathbf{s}^*$ denote the projections into the signal subspace and the subspace orthogonal to it, respectively. $\mathbf{P}_{<\mathbf{s}>^\perp}\mathbf{Z}$ blends out the deterministic part of the signal, and only the noise part is left: $\mathbf{P}_{<\mathbf{s}>^\perp}\mathbf{Z} = \mathbf{P}_{<\mathbf{s}>^\perp}\mathbf{N}$. The expectation of its square norm is $E[\mathbf{P}_{<\mathbf{s}>^\perp}\mathbf{N}] = (n-1)\sigma^2$, so $\left\|\mathbf{P}_{<\mathbf{s}>^\perp}\mathbf{z}\right\|^2/(n-1)$ can be regarded as a bias-free estimate of the noise variance. Instead of dividing by this, the threshold can be obtained by multiplication of a fixed value η with this estimator, to 'adjust' the threshold to the varying noise power. This is illustrated in Fig. 1.29.

Besides example 4 there are many other CFAR detectors, which are invariant against special transformations, e.g. *nonparameteric* tests like *sign tests* or *rank tests*.

Incoherent detection

If there is no phase information available - as it is the case for very old or very cheap systems - only the amplitude values $A_\nu, \nu = 1..n$ can be observed.

Example 6: Incoherent detector

$$\begin{array}{ll} \mathbf{Z} = \gamma\mathbf{s} + \mathbf{N}, & \mathbf{N} \sim \mathcal{N}_{\mathbb{C}^n}\left(\mathbf{0}, \sigma^2\mathbf{I}_n\right), \gamma \in \mathbb{R} \\ & A_\nu = |Z_\nu|, \nu = 1..n, \\ H : \gamma = 0 & \\ K : \gamma = \gamma_0 > 0 & \end{array} \tag{1.162}$$

For a realization $\mathbf{a}$ of the random vector $\mathbf{A}$ containing this amplitudes, the likelihood ratio is given by the product of the likelihood ratios for the individual amplitudes, which are Rician distributed for the alternative and Rayleigh distributed for the hypothesis. With the densities given in the appendix App. A.92 and A.94 it is evaluated as

$$\Lambda(\mathbf{a}) = \prod_{\nu=1}^{n} \frac{2a_\nu e^{-(a_\nu^2 - \gamma_0^2|s_\nu|^2)/\sigma^2} I_0\left(2\gamma_0|s_\nu|a_\nu/\sigma\right)}{2a_\nu e^{-a_\nu^2/\sigma^2}} \tag{1.163}$$

$$= e^{\gamma_0^2|s_\nu|^2/\sigma^2} \prod_{\nu=1}^{n} I_0\left(2\gamma_0|s_\nu|a_\nu/\sigma\right). \tag{1.164}$$

Equivalent is the test statistic

$$T(\mathbf{a}) = \sum_{\nu=1}^{n} \ln\left(I_0\left(2\gamma_0|s_\nu|a_\nu/\sigma\right)\right). \tag{1.165}$$

In this case, the test statistics really depends on the *construction parameter* γ_0. Only for $\gamma = \gamma_0$ it will result in the maximum detection probability. For small argument the logarithm of the modified Bessel function can be approximated by its absolute and quadratic Taylor expansion resulting in the simple equivalent form

$$T'(\mathbf{a}) = \sum_{\nu=1}^{n} |s_\nu|^2 a_\nu^2. \tag{1.166}$$

Compared to the coherent detectors mentioned before, this has a much worse performance which can be recognized in Fig. 1.27. While for $n \to \infty$ the SNR of

a single component tends to zero like $1/n$ to achieve a fixed detection probability with a coherent detector, it behaves like $1/\sqrt{n}$ for the incoherent detector. So the performance difference grows with the number of samples.

1.9 MTI for ground based radar

One of the most important goals of a radar system is to detect a moving target against *clutter*. The expression 'clutter' comprises all echoes of unwanted reflectors on ground like woods and fields and in the air (clouds, rain, ...).

As we know from the previous, radar is an excellent instrument to sense also small changes of the distance from pulse to pulse independent on range. The radial motion of a target induces the Doppler modulation, as described in section 1.3, resulting in a phase change from pulse to pulse.

To detect the moving target against the clutter background, it is necessary to suppress or cancel the clutter returns with as small suppression of the target signal as possible.

1.9.1 Temporal stable clutter

If the clutter echoes don't change from pulse to pulse, as it is the case e.g. for buildings and rocks, and for calm wind, the Doppler frequency of the clutter is equal to zero and it is easy to cancel the clutter. Heuristical methods use recursive filters with a zero at Doppler=0, e.g. the *two-pulse canceller* $Y_\nu = Z_\nu - Z_{\nu-1}$. For a pulse train of N pulses, we introduce the following standard model III:

$$\mathbf{Z} = a\mathbf{s} + c\mathbf{1} + \mathbf{N}, \quad \mathbf{N} \sim \mathcal{N}_{\mathbb{C}^N}\left(\mathbf{0}, \sigma^2 \mathbf{I}_N\right). \tag{1.167}$$

Here, $\mathbf{1}$ is the vector with all components equal to 1, and c is an unknown constant reflecting the clutter amplitude. To find an optimum method we could derive a best test based on this model, or we may search for a maximum likelihood estimate of a and c, given a realization $\mathbf{z}$ of $\mathbf{Z}$. The latter is given by the best fit minimizing the mean square error

$$\begin{pmatrix} \hat{a} \\ \hat{c} \end{pmatrix}(\mathbf{z}) \;=\; \begin{pmatrix} \mathbf{s}^*\mathbf{s} & \mathbf{s}^*\mathbf{1} \\ \mathbf{1}^*\mathbf{s} & \mathbf{1}^*\mathbf{1} \end{pmatrix}^{-1} \begin{pmatrix} \mathbf{s}^* \\ \mathbf{1}^* \end{pmatrix} \mathbf{z} \tag{1.168}$$

It follows

$$\hat{a}(\mathbf{z}) = \frac{\mathbf{s}^*\mathbf{P}_{<\mathbf{1}>^\perp}\mathbf{z}}{\mathbf{s}^*\mathbf{P}_{<\mathbf{1}>^\perp}\mathbf{s}}, \quad \hat{c}(\mathbf{z}) = \frac{\mathbf{1}^*\mathbf{P}_{<\mathbf{s}>^\perp}\mathbf{z}}{\mathbf{1}^*\mathbf{P}_{<\mathbf{s}>^\perp}\mathbf{1}}. \tag{1.169}$$

$\mathbf{P}_{<\mathbf{1}>^\perp} = \mathbf{I}_N - \frac{\mathbf{1}\mathbf{1}^*}{\mathbf{1}^*\mathbf{1}}$ is the projector to the subspace orthogonal to $\mathbf{1}$, similar for $\mathbf{P}_{<\mathbf{s}>^\perp}$. Note that the application of $\mathbf{P}_{<\mathbf{1}>^\perp}$ means to subtract the mean value of all components from each component. Clearly this operation cancels the clutter and produces a zero for a signal at Doppler=0. After clutter cancellation the target

match is performed. The result for $\hat{a}$ can directly be used for detection by comparing its magnitude to a threshold.

Now, we further investigate the relevant expression $T(\mathbf{z}) = \mathbf{s}^* \mathbf{P}_{<\mathbf{1}>^\perp} \mathbf{z}$. Let $\mathbf{d}(F) = (\exp\{j2\pi F \Delta T\}, \ldots, \exp\{jN2\pi F \Delta T\})$ denote the signal vector effected by Doppler frequency F (Note that $\mathbf{d}(0) = \mathbf{1}$). Further let $\mathbf{s} = \mathbf{d}(F_0)$ be the signal for a chosen Doppler frequency F_0.

Then $D(F; F_0) = |\mathbf{d}^*(F_0) \mathbf{P}_{<\mathbf{1}>^\perp} \mathbf{d}(F)|^2$ describes the filter gain if the filter is matched to frequency F_0 and a signal at frequency F comes in. The resulting gain curves for a bank of filters for varying F_0 is shown in Fig. 1.30. The gain $D(F_0; F_0)$ at matching frequency shows a notch at $F_0 = 0$.

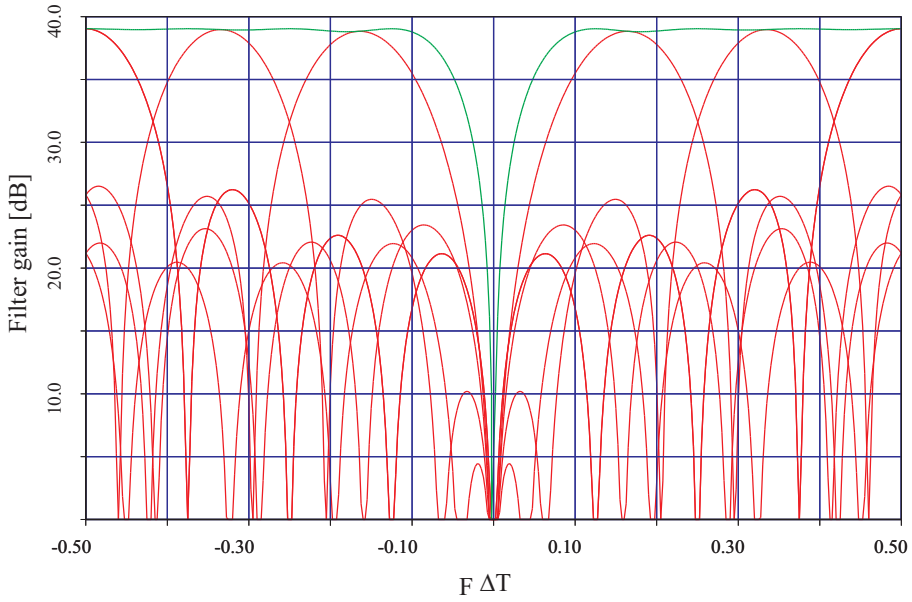

Figure 1.30: *Red: Doppler filter gains for varying center frequencies; green: gain at matching frequency*

1.9.2 Temporal variation of clutter

If the wind is moving the trees, or if clouds are passing the sky, the clutter is no longer temporal stable. In this case, the clutter echoes have to be described by a stochastic process $C(T)$. The samples of this process are collected in the clutter vector $\mathbf{C} = (C(1 \cdot \Delta T), \ldots, C(N \cdot \Delta T))$. The model for the random vector of the measured data is now

$$\mathbf{Z} = a\mathbf{s} + \mathbf{C} + \mathbf{N}, \quad \mathbf{N} \sim \mathcal{N}_{\mathbb{C}^N}\left(\mathbf{0}, \sigma^2 \mathbf{I}_N\right) \tag{1.170}$$

$$\mathbf{C}, \mathbf{N} \text{ stoch. independent }, E[\mathbf{C}] = \mathbf{0}, E[\mathbf{C}\mathbf{C}^*] = \mathbf{R}_C. \tag{1.171}$$

The distribution of $\mathbf{C}$ is left open intentional. It can be a normal distribution or a more sophisticated distribution with a better fit to the reality. The linear processing

of the data $Y = \mathbf{w}^*\mathbf{Z}$ with the optimum resulting *signal-to-clutter-plus-noise ratio* SCNR is obtained with the weight vector

$$\mathbf{w}_{opt} = \mathbf{R}_C^{-1}\mathbf{s}. \tag{1.172}$$

This will be shown in the context of array processing, see Eq. (2.27).

Often $C(T)$ can be modelled as a *stationary stochastic process*, i.e. the statistical properties don't change with time. A weaker condition is the property to be a *wide sense stationary stochastic process*, that means that the correlation properties don't change with time.

Since the phase of $C(T)$ will be uniformly distributed over $(0, 2\pi)$, its expectation is zero. Then, its correlation properties are described by the correlation function (which is in this case equal to the covariance function)

$$r_{CC}(\tau) = E[C(T+\tau)C^*(\tau)]. \tag{1.173}$$

If the common distribution of each sample vector of $C(T)$ is Gaussian, the covariance function completely determines the statistical properties of $C(T)$.

The Fourier transform of $r_{CC}(T)$ is called *power spectrum* or *spectral power density*:

$$R_{CC}(F) = \int \exp\{-j2\pi FT\} r_{CC}(T) dT. \tag{1.174}$$

The power spectrum is always larger or equal to zero and represents the spectral distribution of the clutter power.

If we regard an infinite sequence of samples $C_\nu = C(\nu\Delta T)$, they form a time discrete stationary process and have the correlations $E[C_{\nu+\mu}C_\nu^* = R_C(\mu\Delta T)$. The power spectrum for the discrete process is defined by the discrete Fourier transform

$$P_C^{(d)}(F) = \sum_\mu \exp\{-j2\pi\mu F\Delta T\} R_C(\mu\Delta T). \tag{1.175}$$

Let $\Delta F = 1/\Delta T$ be the pulse repetition frequency. If $P_C(F) = 0$ for $F \notin (-\frac{\Delta F}{2}, \frac{\Delta F}{2})$ the sampling fulfills the Nyquist condition and we get

$$P_C^{(d)}(F) = P_C(F)\Delta F \text{ for } F \in \left[-\frac{\Delta F}{2}, \frac{\Delta F}{2}\right]. \tag{1.176}$$

Now we regard the normalized Fourier transform of the clutter echoes:

$$C^{(F)}(F) = \frac{1}{\sqrt{N}} \sum_{n=1}^{N} C_\nu \exp\{-j2\pi nF\Delta T\} \tag{1.177}$$

The magnitude squared of $C^{(F)}(F)$ is called *periodogram* and is often used for the estimation of the power spectrum.

Its expectation is

$$E\left[\left|C^{(F)}(F)\right|^2\right] = \frac{1}{N}\sum_{\nu=1}^{N}\sum_{\mu=1}^{N} E\left[C_\nu C_\mu^*\right]\exp\{-j2\pi(\nu-\mu)F\Delta T\} \quad (1.178)$$

$$= \frac{1}{N}\sum_{\kappa=-(N-1)}^{N-1}\sum_{\nu=\max\{1,1+\kappa\}}^{\min\{N,N+\kappa\}} R_C(\kappa\Delta T)\exp\{-j2\pi\kappa F\Delta T\} \quad (1.179)$$

$$= \sum_{\kappa=-(N-1)}^{N-1}\left(1-\frac{|\kappa|}{N}\right)R_C(\kappa\Delta T)\exp\{-j2\pi\kappa F\Delta T\}. \quad (1.180)$$

This is a windowed version of the discrete power spectrum. If the correlation vanishes for $|\tau| > \tau_0$ or, equivalently for $|\kappa| > \kappa_0$, then for $n > \kappa_0$

$$E\left[\left|C^{(F)}(F)\right|^2\right] = \sum_{\kappa=-\kappa_0}^{\kappa_0}\left(1-\frac{|\kappa|}{N}\right)R_C(\kappa\Delta T)\exp\{-j2\pi\kappa F\Delta T\} \quad (1.181)$$

$$\rightarrow \sum_{\kappa=-\kappa_0}^{\kappa_0} R_C(\kappa\Delta T)\exp\{-j2\pi\kappa F\Delta T\} \text{ for } N\rightarrow\infty \quad (1.182)$$

$$= P_C^{(d)}(F) \quad (1.183)$$

The covariance matrix of $\mathbf{C}$ takes the form

$$\mathbf{R}_C = E\left[\mathbf{C}\mathbf{C}^*\right] \quad (1.184)$$

$$= \begin{pmatrix} R_0 & R_1 & \dots & R_{N-2} & R_{N-1} \\ R_{-1} & R_0 & \dots & R_{N-3} & R_{N-2} \\ \dots & \dots & \dots & \dots & \dots \\ R_{-(N-2)} & R_{-(N-1)} & \dots & R_0 & R_1 \\ R_{-(N-1)} & R_{-(N-2)} & \dots & R_{-1} & R_0 \end{pmatrix} \quad (1.185)$$

$$\text{with } R_\nu = R_C(-\nu\Delta T). \quad (1.186)$$

A matrix of that structure is called *Toeplitz matrix*; the rows are shifted by one position from row to row.

1.10 Radar equation, SNR, CNR, SCNR

Now we tie the results from section 1.8 together with physical facts to calculate the maximum range of a radar.

1.10.1 Power budget for the deterministic signal

Power density generated by the transmit antenna Let the power of the transmit signal at the input of the transmit antenna be P_{tx} $[W]$. If the complete

power is transferred to the emitted wave, the integral of the power density over the surface of each sphere enclosing the transmit antenna will be P_{tx}, too, if no absorption in the atmosphere is present. For an omnidirectional lossless antenna this leads in the range r to the power density $L_{tx} = P_{tx}/(4\pi r^2) \quad [W/m^2]$.

If a directed antenna with gain G_{tx} (antenna losses taken into account) in the direction to the scatterer is used, the power density has to be multiplied by the factor G_{tx}, so we get $L_{tx} = G_{tx}P_{tx}/(4\pi r^2)$.

Power of the reflected wave The *radar cross section* (RCS) of the reflected object is defined by $q = P_{refl}/L_{tx}$ where P_{refl} is the virtual power of an omnidirectional radiator generating the same power density in direction of the receive antenna as the wave reflected by the object. So q is the virtual area capturing the power $P_{refl} = qL_{tx}$ which replaces the object in order to generate the reflected power density[5].

We get $P_{refl} = qG_{tx}P_{tx}/(4\pi r^2)$ and the power density at the receive antenna $L_{rx} = P_{refl}/(4\pi r^2)$, combined in

$$L_{rx} = qG_{tx}P_{tx}/(4\pi r^2)^2 \tag{1.187}$$

Power of the receive signal Following antenna theory ([9]), a perfectly matched omnidirectional receive antenna has an effective cross section $q_{rx} = \lambda^2/(4\pi)$ and would yield the power $L_{rx}\lambda^2/(4\pi)$ at its output, if the power density of the incoming wave is L_{rx}. If we instead of this we use a directed antenna with gain G_{rx} in the direction to the scatterer the effective cross section is enlarged to $q_{rx} = G_{rx}\lambda^2/(4\pi)$ and the power at the output is $P_{rx} = L_{rx}G_{rx}\lambda^2/(4\pi)$. If we insert this into Eq. (1.177) we get

$$P_{rx} = S_{21}P_{tx} \quad \text{with} \quad S_{21} = \frac{G_{tx}G_{rx}\lambda^2 q}{(4\pi)^3 r^4} \tag{1.188}$$

S_{21} is the transmission coefficient between transmit and receive antenna via the way to the reflector and back which is normally extremely small. If the RF transmit signal $\mathsf{s}_{RF}(t)$ is normalized in that way that $|\mathsf{s}_{RF}(t)|^2$ is the effective power feeded into the transmit antenna at time t and $s_{RF}(t)$ is the received signal from the backscattering object at the antenna output, we get the same proportionality for the energies

[5] A metallic sphere with radius $d \gg \lambda$ has an RCS of approximately its geometrical area $q = \pi d^2$ in the projection to a plane. Radar cross sections of targets range from about $10^{-4}m^2$ (fly) to $10^5 m^2$ (large ship) for usual radar frequencies, see [6]. If the extension of the target is smaller than a wavelength, its backscattering is sited in the *Rayleigh region*, the RCS is approximately proportional to the forth power of the frequency. For instance, the leaves in a forest which may have an extension in the order of a decimeter, reflect strongly at frequencies of 10 and more GHz and are more or less transparent for frequencies lower than 1 GHz (*foliage penetration*).

$$\int |s_{RF}(t)|^2 dt = S_{21} \int |\mathsf{s}_{RF}(t)|^2 dt \tag{1.189}$$

and the spectral power densities

$$|S_{RF}(f)|^2 = S_{21} |\mathsf{S}_{RF}(f)|^2. \tag{1.190}$$

1.10.2 Spectral power density of the noise

The spectral power density of the natural noise at the absolute temperature T of the receiver (in Kelvin degrees $[K]$) is given by $C_{noise} = \mathsf{kT}$, where $\mathsf{k} = 1.38065 \cdot 10^{-23}$ $[Ws/K]$ is the *Boltzmann constant*, see [6]. For room temperature this value is about $\mathsf{kT} \approx 4 \cdot 10^{-21}$ $[Ws]$. Each receiving system has additional noise sources increasing the spectral power density by a factor f_n (*noise figure*) resulting in

$$C_{noise} = \mathsf{kT} n_f \quad [Ws]. \tag{1.191}$$

Depending on the frequency and the bandwidth, a noise figure of below 1 dB (X-band) or 3 dB (W-band) can be realized.

If the white noise is given into a filter with transfer function $H(f)$, the resulting spectral power density of the output noise is

$$C^{out}_{noise}(f) = |H(f)|^2 C_{noise}. \tag{1.192}$$

In this context the filter is called *form filter*. The total power of the noise output is

$$\sigma_n^2 = C_{noise} \int |H(f)|^2 df \tag{1.193}$$

and for a filter matched to the wave form we get

$$\sigma_n^2 = C_{noise} \int |\mathsf{S}_{RF}(f)|^2 df \tag{1.194}$$

For a rectangular signal spectrum of bandwidth b we get a noise power of

$$\sigma_n^2 = \mathsf{kT} b n_f \quad [W]. \tag{1.195}$$

1.10.3 Signal-to-noise ratio and maximum range

Let γ_{min} be the minimum SNR to obtain a detection probability P_F for a target with fixed RCS q at a false alarm probability P_F. Representative is the coherent detection of a target with unknown phase (see problem Eq. (1.128)). Here we need for $P_F = 10^{-5}$ and $P_E = 0.9$ an SNR of about $\gamma_{min} \approx 20$ (13 dB).

From Eq.(1.188) together with Eq.(1.195) we get an SNR of

$$\gamma = \frac{P_{tx} G_{tx} G_{rx} \lambda^2 q}{(4\pi)^3 r^4 \mathsf{k}\mathsf{T} b n_f} \eta. \tag{1.196}$$

Here the new inserted constant η subsumes all the remaining losses on the way to the detector. The total loss can be distributed to the units in different ways. We prefer the way that the antenna losses including electromagnetic mismatch is included in the antenna gain, and that the additional noise in the RF part, decreasing the SNR, is contained in the noise figure n_f of the receiver. The remaining losses can be found in the mismatch of the receive filter, sampling losses, suboptimum detectors, and so on.

To obtain the minimum SNR, the inequality $\gamma \geq \gamma_{min}$ has to be fulfilled and can be resolved to get the maximum range according to Eq. (1.196):

$$r \leq r_{max} = \sqrt[4]{\frac{P_{tx} G_{tx} G_{rx} \lambda^2 q \eta}{(4\pi)^3 \mathsf{k}\mathsf{T} b n_f \gamma_{min}}} \tag{1.197}$$

Eq. (1.197) is known in this or a similar form as the *radar equation*.

For coherent integration of N pulses the SNR is increased by a factor N. This can be taken into account, if for b the bandwidth according to the whole coherent integration time is inserted:

$$b = \frac{1}{T_{int}} = \frac{1}{N t_s} = \frac{1}{d T_{compl}} \tag{1.198}$$

where $d = t_s / \Delta T$ is the *duty factor* and T_{compl} the whole observation time.

Essence 1.14 *The maximum range to obtain a minimum SNR is given by Eq. (1.197) which is called the 'radar equation'. It is proportional to the forth root of the transmit power, the gain of the antennas, and the RCS of the target.*

In this form, the maximum range is proportional to the square root of the wavelength for fixed antenna gain. To keep the gain constant, the antenna dimensions have to be scaled proportional to the wave length. On the other hand, if the antenna's size is fixed, the gain for transmit and receive will be proportional to $1/\lambda^2$, resulting in the maximum range being proportional to $1/\sqrt{\lambda}$. Further, if the time to scan a given spatial sector is fixed, the necessary number of beams grows proportionally to $1/\lambda^2$, so the illumination time for each beam will decrees at the same rate. Under these conditions, λ cancels out and the maximum range is independent on the frequency.

Instead of the forth root for SAR in the stripmap mode we will get the third root, since the illumination time here is proportional to the range, see Eq.(4.113).

Chapter 2

Signal processing for real arrays

In this chapter we summarize the facts and tools for array processing as pre-requisites for the air- and spaceborne clutter suppression. We start with beamforming for array antennas, deal the spatial interference suppression, regard the estimation of the target direction and present the Cramér-Rao Bounds (CRB) for this estimation task.

2.1 Beamforming for array antennas

2.1.1 The SNR-optimum beamformer

Linear arrays

We regard a *linear array antenna* with M omnidirectional single elements at the positions x_m (see Fig. 2.1).

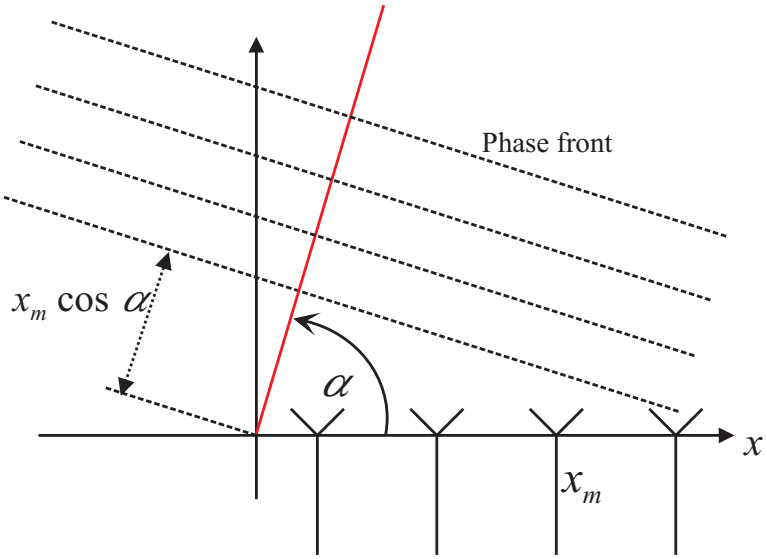

Figure 2.1: *Travelling way differences for a linear array*

Glossary for this chapter

α	Direction angle with respect to the array axis
α	Magnitude of the signal's amplitude
δu	Resolution of directional cosine
δu	Deviation of focusing direction
$\delta(\mathbf{x})$	Difference beam
Δu	Ambiguity of directional cosine
Δx	Element spacing
η	Interference-to-noise-ratio
γ	Signal-to-noise ratio
λ	Wavelength
λ	Eigen value
$\Delta\psi$	Phase increment from element to element
$\rho(s_1, s_2)$	Correlation coefficient of the two signals s_1 and s_2
σ^2	Variance of noise
$\sigma(\mathbf{x})$	Sum beam
a	Complex amplitude
$a(x)$	Complex amplitude along a linear aperture
$a(\vec{x})$	Element distribution function
$A(\vec{k})$	Fourier transform of the element distribution function
$A(u)$	Complex amplitude of a wave from direction u
b	Bandwidth
$\mathbf{b}$	Beamformer vector
$\mathbf{B}$	Random vector of interference amplitudes
$\mathbf{d}(\vec{u})$	Direction of arrival (DOA) vector
$D(\vec{u}, \vec{u}_0)$	Characteristics for the array focused to $\vec{u}_0$
$Di(u, M)$	Dirichlet function
$\mathbf{e}(u)$	Normalized DOA vector
$F(\vec{u}, \vec{u}_0)$	Array factor for focusing to $\vec{u}_0$
$G_{\vec{u}_0}(.)$	Physical characteristics for focusing direction $\vec{u}_0$
$\mathbf{H}$	Interference suppression operator
$\mathbf{I}_n$	Identity matrix of dimension n
$\mathbf{J}$	External interference at array output
J	Amplitude of external interference source
$\mathbf{J}(\vartheta)$	Fisher's information matrix
$k_r = 2\pi/\lambda$	Wavenumber
$\vec{k} = k_r\vec{u}$	Wavenumber vector
l_x	Length of a linear array
$\mathbf{m}(\vartheta)$	Signal including amplitude dependent on parameter vector ϑ
M	Number of single elements
$\mathbf{P}_U$	Projector to the subspace U
$\mathbf{Q}$	External interference plus noise
$\mathbf{R}$	Covariance matrix of interference plus noise
$\mathbf{R}_N$	Covariance matrix of noise
$\mathbf{R}_J$	Covariance matrix of interference
$\widehat{\mathbf{R}}$	Sample matrix or empirical covariance matrix
$\mathbf{S}$	Matrix of signal column vectors

u	Directional cosine
u_{max}	Maximum scan
$\vec{u}$	Unit vector in line-of-sight
$\vec{u}_0$	Unit vector in focusing direction
$u = \cos\alpha$	Directional cosine with respect to the array axis
u_0	Directional cosine for focusing direction
x_m	x-Position of mth array element
$\vec{x}_m$	3D-Position of mth array element
$\mathbf{Z}$	Random vector of array outputs

A plane wave coming in from a direction which encloses an angle α with the array-axis, has to travel a way to the mth single element which is shorter by the amount ux_m than the way to the origin, where $u = \cos\alpha$ denotes the *directional cosine* .

The vector collecting the voltage outputs at the elements obtains the form

$$\mathbf{d}(u) = c \begin{pmatrix} e^{jk_r u x_1} \\ \vdots \\ e^{jk_r u x_M} \end{pmatrix}. \tag{2.1}$$

This signal vector depending on the direction of the incoming wave, is called *direction of arrival vector* or shortly *DOA-vector*. c is a constant which can be chosen by convenience. [1]

Note that the DOA vector only depends on the angle α or - equivalent - the directional cosine u. In the three-dimensional space, all directions with the same angle with respect to the x-axis define a cone surface. We will call this cone late *iso-DOA cone*.

For each component we may assume a superposition of statistically independent noise with variance σ^2 leading to the following model of the spatial sample vector:

$$\mathbf{Z} = a\mathbf{d}(u) + \mathbf{N}. \tag{2.2}$$

A linear combination $Y = \mathbf{b}^*\mathbf{Z}$ with an arbitrary complex vector $\mathbf{b}$ will lead to a certain antenna pattern, for this reason the vector $\mathbf{b}$ is called *beamformer*. Fig. 1.4 may serve as an illustration. Now we derive the SNR-optimum beamformer to a selected direction u_0.

Analogue to Eq.(1.12) for an arbitrary $\mathbf{b}$ the output of the array will have the SNR

$$\gamma(\mathbf{b}) = \frac{|a|^2 \left\|\mathbf{d}\left(u_0\right)\right\|^2}{\sigma^2} \left|\rho\left(\mathbf{b}, \mathbf{d}\left(u_0\right)\right)\right|^2. \tag{2.3}$$

Like in the section 1.2.3 the optimum solution turns out to be the beamformer $\mathbf{b}_{opt}(u_0) = w\mathbf{d}(u_0)$ with any non-zero complex constant w. For convenience, we take $w = 1$.

[1] If the antenna characteristics $D_m(u)$ of the single elements are not equal, they have to be incorporated into the DOA-vector: $\mathbf{d}(u) = c\left(D_1(u)\exp\{jk_r u x_1\}, \ldots, D_M(u)\exp\{jk_r u x_M\}\right)^t$.

Essence 2.1 *For white noise, the maximum SNR for a source in direction u_0 is obtained by the beamformer $\mathbf{b}_{opt}(u_0) = \mathbf{d}(u_0)$ equal to the DOA-vector to u_0. The maximum obtains the value $|a|^2 \|\mathbf{d}(u_0)\|^2/\sigma^2$, i.e. the ratio of the received power accumulated over all elements and the noise variance at a single element.*

So, by adding elements, the SNR can be increased proportional to the number of elements.

In the transmit case the same beamformer (with $c = 1$) produces the maximum power density in direction u_0, if all single elements have the same antenna characteristics and radiate with the same power.

Two- and three-dimensional arrays

It is easy to transfer this to the two- and three-dimensional case.

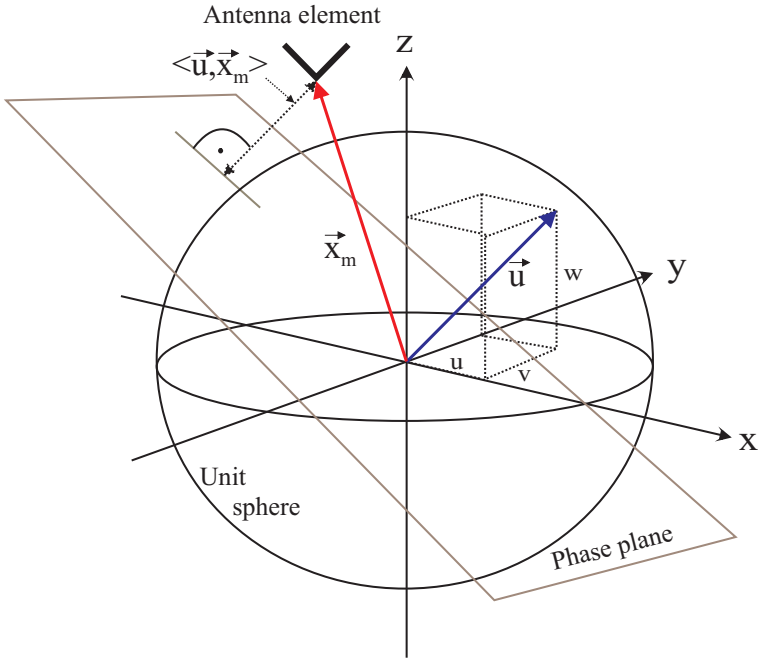

Figure 2.2: *Three dimensional array*

Let the element positions be $\vec{x}_m, m = 1, \ldots, M$ in a Cartesian three dimensional coordinate system. A plane wave comes in from a direction defined by the unit vector $\vec{u} = (u, v, w)^t$. The variables u, v, w are directional cosines with respect to the x, y, z axes, see Fig. 2.2. Further, the travelling distance to the element position $\vec{x}_m$, normalized to that to the origin, is given by $\langle \vec{u}, \vec{x}_m \rangle$. Consequently, the following DOA vector is generated:

$$\mathbf{d}(\vec{u}) = c \begin{pmatrix} e^{jk_r\langle \vec{u},\vec{x}_1\rangle} \\ \vdots \\ e^{jk_r\langle \vec{u},\vec{x}_M\rangle} \end{pmatrix} = c \begin{pmatrix} e^{j\langle \vec{k},\vec{x}_1\rangle} \\ \vdots \\ e^{j\langle \vec{k},\vec{x}_M\rangle} \end{pmatrix}. \tag{2.4}$$

Here $\vec{k} = k_r \vec{u}$ is a wave number vector (but with the opposite sign as the physical wave number vector of the incoming wave). Again, SNR-optimum beamforming in a selected direction $\vec{u}_0$ is achieved with the beamformer

$$\mathbf{b}_{opt}(\vec{u}_0) = \mathbf{d}(\vec{u}_0). \tag{2.5}$$

2.1.2 Characteristics of the array

In the following we will use as normalization constant $c = 1/\sqrt{M}$. In this case, DOA vector and optimum beamformer have unit norm.

Let the array be focused to direction $\vec{u}_0$. An incoming wave with normalized power from an arbitrary direction $\vec{u}$ will produce at the output of the array a signal $D(\vec{u}, \vec{u}_0)$. For fixed focusing direction the array has the (physical) characteristics

$$G_{\vec{u}_0}(.) = \frac{D(., \vec{u}_0)}{C_{\vec{u}_0}} \tag{2.6}$$

where $C_{\vec{u}_0}$ is the normalization constant $C_{\vec{u}_0} = \sqrt{\frac{1}{4\pi\eta} \int_\Omega |D(\vec{u}', \vec{u}_0)|^2 dO(\vec{u}')}$, the integration area is the surface Ω of the unit sphere, $dO(\vec{u}')$ denotes the infinitesimal surface element, and η the efficiency of the antenna array (which might also be dependent on the focusing direction).

On the other hand, the direction to the source can be fixed, and only the beamformer focusing direction is varied. This leads to another kind of characteristics, let us call this *scan characteristics* $D(\vec{u}_0, .)$.

While the physical characteristics Eq.(2.6) obeys the physical laws like energy preservation, the scan characteristics is a mathematical tool happening exclusively in the computer, if the array is fully digital, and in the phase shifters for a phased array.

If the array is composed of identical identically orientated single elements with the common characteristics $D_0(\vec{u})$, we get from the direction $\vec{u}$ the signal vector $D_0(\vec{u})\mathbf{d}(\vec{u})$. If the array is focused to the direction $\vec{u}_0$ with the beamformer $\mathbf{b}(\vec{u}_0) = \mathbf{d}(\vec{u}_0)$, we get the array output

$$\begin{aligned} D(\vec{u}, \vec{u}_0) &= D_0(\vec{u})\mathbf{d}^*(\vec{u}_0)\mathbf{d}(\vec{u}) && (2.7) \\ &= D_0(\vec{u})F(\vec{u}, \vec{u}_0). && (2.8) \end{aligned}$$

with

$$\begin{aligned} F(\vec{u}, \vec{u}_0) &= \mathbf{d}^*(\vec{u}_0)\mathbf{d}(\vec{u}) && (2.9) \\ &= \frac{1}{M} \sum_{m=1}^{M} e^{jk_r \langle \vec{u} - \vec{u}_0, \vec{x}_m \rangle}. && (2.10) \end{aligned}$$

$F(\vec{u}, \vec{u}_0)$ is called *array factor* and depends only on the geometry of the phase center positions; the influence on the single elements has been factored out. For the performed choice $c = 1/\sqrt{M}$ the magnitude of the array factor is for running $\vec{u}$ maximum at $\vec{u} = \vec{u}_0$ and assumes there the value 1.

Essence 2.2 *The characteristics of an array antenna with identical identically orientated single elements is the product of the array factor with the single element characteristics.*

The array characteristics as spatial Fourier transform

With $\vec{k}_0 = k_r\vec{u}_0, \vec{k} = k_r\vec{u}$ it follows

$$F(\vec{u}, \vec{u}_0) = \int e^{-jk_r\langle\vec{u}_0-\vec{u},\vec{x}\rangle} \frac{1}{M} \sum_{m=1}^{M} \delta(\vec{x} - \vec{x}_m)\, d\vec{x} \tag{2.11}$$

$$= A(\vec{k}_0 - \vec{k}), \tag{2.12}$$

where $A(\vec{k})$ is the Fourier transform of the element distribution function $a(\vec{x}) = \frac{1}{M}\sum_{m=1}^{M} \delta(\vec{x} - \vec{x}_m)$.

Essence 2.3 *The array factor is the Fourier transform of the spatial element distribution.*

Now we regard a linear array with equidistant spacing Δx, the positions on the x-axis are $x_m = m\Delta x$. For the case of a linear array, only the first component u of a general direction vector $\vec{u}$ is necessary, so the DOA-vectors and array-factors will be written as functions of the directional cosine u. The array factor is given by

$$F(u, u_0) = \frac{1}{M} \sum_{m=1}^{M} e^{jm\Delta\psi} \tag{2.13}$$

$$= e^{j\bar{m}\Delta\psi} \frac{\sin\left(M\frac{\Delta\psi}{2}\right)}{M\sin\left(\frac{\Delta\psi}{2}\right)} \tag{2.14}$$

$$= e^{j\bar{m}\Delta\psi} \mathrm{Di}\left(\frac{\Delta\psi}{\pi}, M\right) \tag{2.15}$$

with $\Delta\psi = k_r\Delta x(u - u_0)$ and $\bar{m} = \frac{1}{M}\sum_{m=1}^{M} m$ and the *Dirichlet function* Di, defined by $\mathrm{Di}(u, M) := \frac{\sin\left(M\frac{\pi}{2}u\right)}{M\sin\left(\frac{\pi}{2}u\right)}$.

Resolution and beamwidth

The mainbeam with its maximum at $u = u_0$ decreases to zero at $\Delta\psi = 2\pi/M$. This is equivalent to a directional cosine difference of

$$\delta u = \frac{\Delta\psi}{(k_r\Delta x)} = \frac{\lambda}{M\Delta x} = \frac{\lambda}{l_x} \tag{2.16}$$

where l_x is the length of the array. It is a Rayleigh measure for the resolution in the directional cosine, or the beamwidth, respectively.

Essence 2.4 *The beamwidth of an SNR-optimum focused linear antenna array in the directional cosine domain is given by* λ/l_x.

2.1.3 Ambiguities of the array characteristics

Secondary mainlobes for a linar array

We proceed from a linear array with equidistant elements with inter-element distance Δx. The scan characteristics $\frac{1}{M}F_s(u,\mathbf{z}) = \sum e^{-jk_r um\Delta x} z_m$ obviously is periodical in the directional cosine with the period Δu determined by $k_r \Delta u \Delta x = 2\pi$ leading to

$$\Delta u \;=\; \lambda/\Delta x. \tag{2.17}$$

The same behavior can be observed for an arbitrary beamformer $\mathbf{b}$ at the characteristics $F_p(\mathbf{b},u) = \mathbf{b}^*\mathbf{d}(u)$. The periodicity is illustrated in Fig. 2.3. A main beam focused to direction u_1 is repeated at the direction $u_2 = u_1 + \Delta u$. If u_2 falls into the visible area $u \in [-1,1]$ a secondary main beam arises at $u = u_2$.

To avoid secondary main beams for any main beam direction $u_1 \in [-1,1]$, the condition

$$\lambda/\Delta x \geq \max\{|u_2 - u_1| : u_1, u_2 \in [-1,1]\} = 2 \tag{2.18}$$

has to be fulfilled, i. e. the inter-element distance Δx has to be smaller or equal to $\lambda/2$.

If the array shall be steered only in the restricted interval $[-u_{max}, u_{max}]$, the spatial sampling condition is given by

$$\Delta x \leq \lambda/(1+u_{max}). \tag{2.19}$$

Nyquist criterium for unambiguous sampling

The condition $\Delta x \leq \lambda/2$ for unambiguous array characteristics corresponds to another important result: If waves with the complex amplitudes $A(u)$ impinge from all directions $u \in [-1,1]$ on an infinite aperture along the x-axis, they superimpose to the complex amplitude function

$$a(x) = \int_{-1}^{1} A(u) e^{jk_r ux} du = \frac{1}{k_r} \int_{-k_r}^{k_r} A(k_x/k_r) e^{jk_x x} dk_x. \tag{2.20}$$

Obviously, $a(x)$ is expressed as the Fourier transform of a signal with the variable 'directional cosine' over a finite interval, i. e. it is a bandlimited signal where

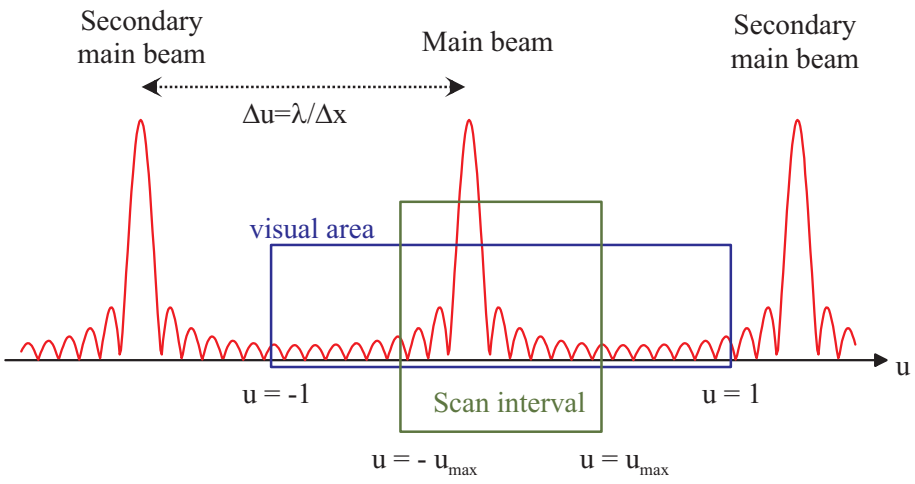

Figure 2.3: *Ambiguity of the array factor, secondary main lobes*

the spatial bandwidth is given by $b = 2k_r/(2\pi) = 2/\lambda$. Following the Nyquist-Shannon sampling theorem, the signal has to be sampled at a sampling interval $\Delta x \leq 1/b = \lambda/2$ to reconstruct the signal $A(u)$ perfectly.

Essence 2.5 *To avoid secondary main beams, the spatial sampling interval of a linear array has to be smaller or equal to the half wavelength, if the whole visibility area shall be scanned, and equal or smaller to* $\lambda/(1 + u_{max})$*, if only the interval* $[-u_{max}, u_{max}]$ *has to be covered. For an infinite linear aperture, the spatial sampling interval has to be smaller or equal to* $\lambda/2$ *to reconstruct the complex amplitudes of the impinging waves unambiguously.*

Secondary mainlobes for a planar array

The mostly used phased array antenna is a *planar phased array*. Here the two directional cosines u and v corresponding to the x and y dimensions of the array determine uniquely the direction $\vec{u}$, if the half space backwards of the antenna can be neglected. A rectangular raster $\Delta x \times \Delta y$ in the aperture plane leads to a rectangular ambiguity grid $\Delta u = \lambda/\Delta x, \Delta v = \lambda/\Delta y$ in the directional cosine plane, see Fig. 2.4. Unambiguity in the visible area can be forced by a quadratic grid with spacing $\lambda/2$. For other grid shapes (e.g. triangular) already a slightly minor element density leads to the disappearance of secondary sidelobes in the visible area, see Fig. 2.4.

2.2 Interference suppression

If apart from the noise there are external interferences like clutter returns (or active external emitters of electromagnetic waves), the model of the received signal vector takes the form

$$\mathbf{Z} = a\mathbf{d}(\vec{u}) + \mathbf{J} + \mathbf{N} \tag{2.21}$$

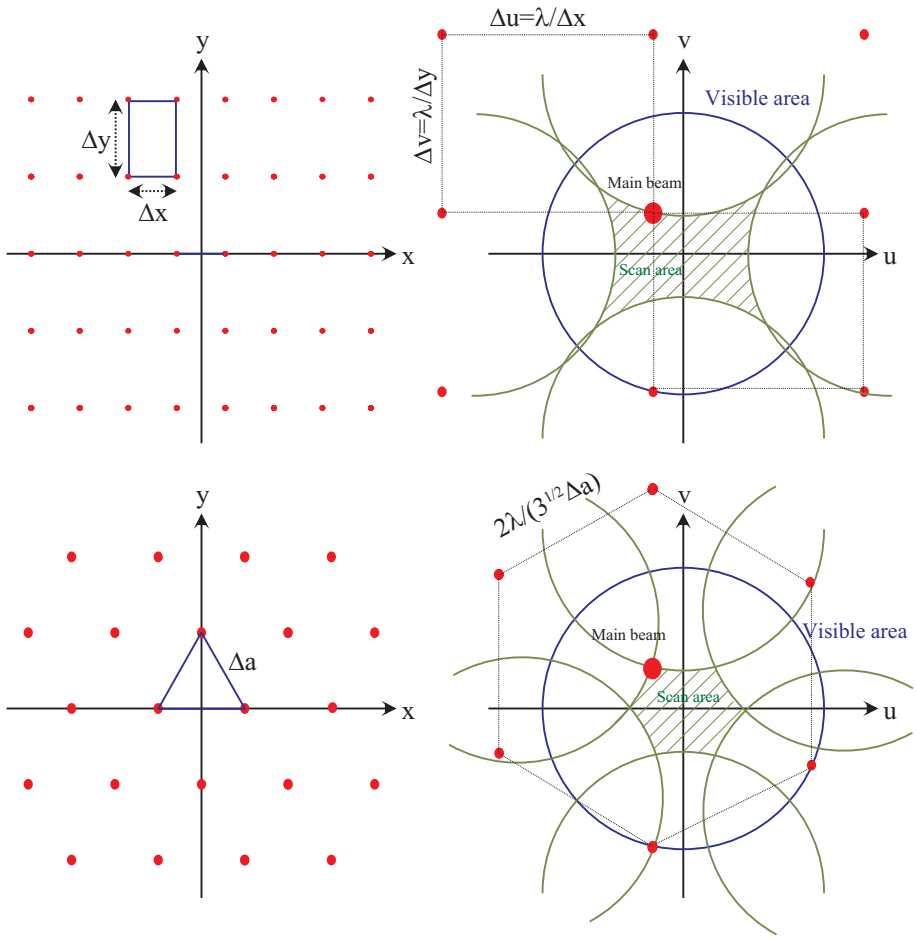

Figure 2.4: *Secondary mainlobes of a planar array. Left: rectangular grid, right: triangular grid*

where $\mathbf{d}(\vec{u})$ is the DOA-vector from a source in direction $\vec{u}$ and $\mathbf{J}$ denotes the received external interference which will be modelled as a random vector statistically independent on the noise and with expectation $\mathbf{0}$. The DOA-vector can be arbitrary, also including different amplitudes due to non identical elements.

Interference and noise are summarized to one random vector $\mathbf{Q} = \mathbf{J} + \mathbf{N}$ with the covariance matrix

$$\mathbf{R} = \mathbf{R_Q} = E\left[(\mathbf{J}+\mathbf{N})(\mathbf{J}+\mathbf{N})^*\right] = E[\mathbf{J}\mathbf{J}^*] + E[\mathbf{N}\mathbf{N}^*] = \mathbf{R_J} + \sigma^2\mathbf{I}_M. \qquad (2.22)$$

This is a situation with 'colored' interference.

2.2.1 Test for the detection of the useful signal

First we regard the problem to detect the deterministic signal $\mathbf{d}(\vec{u})$ and formulate the

Test problem: Let $\mathbf{Z} = a\mathbf{d}(\vec{u}) + \mathbf{Q}$ be Gaussian distributed: $\mathbf{Z} \sim \mathcal{N}_{\mathbb{C}^M}(a\mathbf{d}(\vec{u}), \mathbf{R})$. Decide between

H: $a = 0$ (only interference)
and
K: $|a| > 0$ (Useful signal superposed by interference)

Solution: We know the solution from the test example in section 1.8, Eq. (1.149). The maximum likelihood ratio test for this problem is given by comparing the test statistic

$$T(\mathbf{z}) = \left|\mathbf{z}^*\mathbf{R}^{-1}\mathbf{s}\right|^2 \tag{2.23}$$

to a threshold.

2.2.2 Optimum beamformer for colored interference

Alternative, we can search for an SNR-optimum beamformer. In contrary to the preceding test problem, no explicit probability distribution is demanded. We only need the properties that the expectation of the interference plus noise is zero and that the covariance matrix is given as before.

Problem: For a selected direction $\vec{u}_0$, find a beamformer $\mathbf{b}(\vec{u}_0)$ for which $Y = \mathbf{b}^*(\vec{u}_0)\mathbf{Z}$ achieves a maximum signal-to-noise-plus-interference ratio (SNIR)!

Solution: Since $\mathbf{R}$ is hermitian and positive definite, we can form the matrix $\mathbf{R}^{-1/2}$. The covariance matrix of $\widetilde{\mathbf{Q}} = \mathbf{R}^{-1/2}\mathbf{Q}$ is the $M \times M$ unit matrix, since

$$E\left[\mathbf{R}^{-1/2}\mathbf{Q}\left(\mathbf{R}^{-1/2}\mathbf{Q}\right)^*\right] = \mathbf{R}^{-1/2}E\left[\mathbf{Q}\mathbf{Q}^*\right]\mathbf{R}^{-1/2} = \mathbf{R}^{-1/2}\mathbf{R}\mathbf{R}^{-1/2} = \mathbf{I}_M. \tag{2.24}$$

Obviously, $\mathbf{R}^{-1/2}$ 'whitens' the interference. If this 'whitener' is applied to the random vector $\mathbf{Z}$, we get

$$\widetilde{\mathbf{Z}} = \mathbf{R}^{-1/2}\mathbf{Z} = a\tilde{\mathbf{d}}(\vec{u}_0) + \widetilde{\mathbf{Q}} \tag{2.25}$$

with the deterministic component $\tilde{\mathbf{d}}(\vec{u}_0) = \mathbf{R}^{-1/2}\mathbf{d}(\vec{u}_0)$ and the stochastic component $\widetilde{\mathbf{Q}} = \mathbf{R}^{-1/2}\mathbf{Q}$. The random vector $\widetilde{\mathbf{Z}}$ bears the same information as the original vector, since the transformation is reversible by multiplying with $\mathbf{R}^{1/2}$.

Now the optimum beamformer for $\widetilde{\mathbf{Z}}$ is easily found using Essence 2.1 which is valid since $\widetilde{\mathbf{Z}}$ contains only white interference: $\tilde{\mathbf{b}}_{opt}(\vec{u}_0) = \tilde{\mathbf{d}}(\vec{u}_0)$. If this beamformer is applied to $\widetilde{\mathbf{Z}}$, the result is

$$Y = \tilde{\mathbf{d}}^*(\vec{u}_0)\tilde{\mathbf{Z}} = \left(\mathbf{d}^*(\vec{u}_0)\mathbf{R}^{-1/2}\right)\left(\mathbf{R}^{-1/2}\mathbf{Z}\right) = \mathbf{d}^*(\vec{u}_0)\mathbf{R}^{-1}\mathbf{Z} = \left(\mathbf{R}^{-1}\mathbf{d}(\vec{u}_0)\right)^*\mathbf{Z}. \quad (2.26)$$

Obviously, the optimum beamformer to be applied to $\mathbf{Z}$ is

$$\mathbf{b}_{opt}(\vec{u}_0) = \mathbf{R}^{-1}\mathbf{d}(\vec{u}_0). \quad (2.27)$$

This is in good agreement with the result for the optimum detector given in Eq.(2.23).

Essence 2.6 *The SNIR-optimum beamformer for colored interference can be found by the principle of 'pre-whiten and match'. It is given by the inverse noise+interference covariance matrix applied to the DOA-vector in the desired direction. For Gaussian distribution, also the maximum likelihood ratio test is based on the output of this beamformer.*

The 'pre-whiten and match principle' for adaptive arrays is illustrated in Fig. 2.5

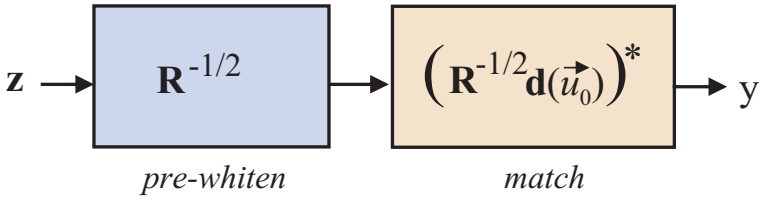

Figure 2.5: *Pre-whiten and match principle*

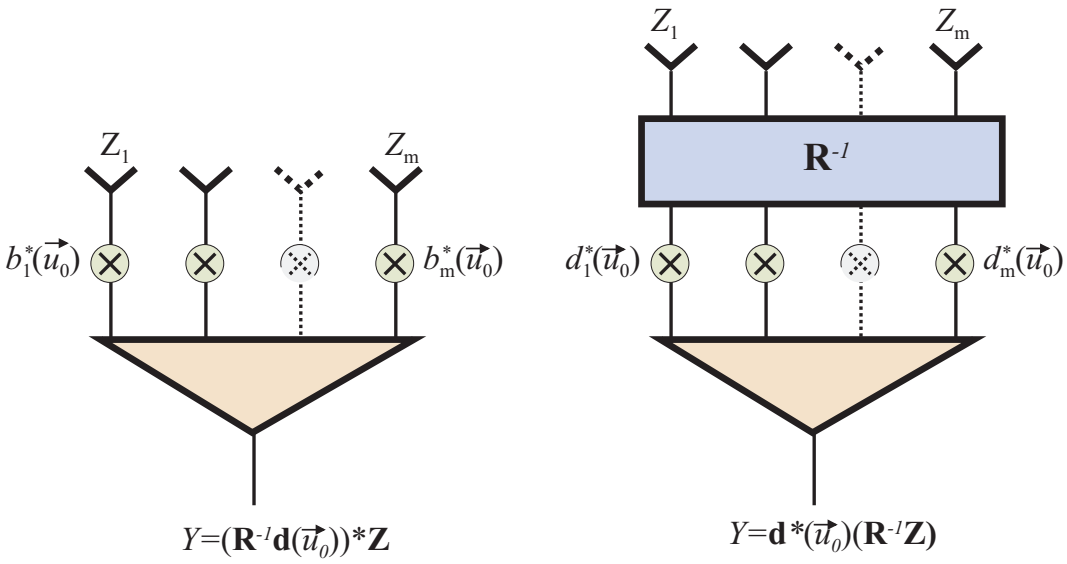

Figure 2.6: *Two realizations of an adaptive array*

The operation $Y = \mathbf{d}^*(\vec{u}_0)\mathbf{R}^{-1}\mathbf{Z}$ can be put into brackets in different ways which are mathematical equivalent but not the same in the technical realization, see Fig.

2.6. If we put together the two first factors, we get the optimum beamformer $\mathbf{b}_{opt}(\vec{u}_0) = \mathbf{R}^{-1}\mathbf{d}(\vec{u}_0)$ leading to the realization shown on the left side of Fig. 2.6. For each new direction the beamformer has to be calculated again. If the right two terms are bracketed, we get the situation depicted at the right side of the figure. First the element outputs are transformed by the matrix $\mathbf{R}^{-1}$ (suppression of interference) and then the classical beamformer is applied to the resulting vector for any direction.

2.2.3 SNIR before and after optimum filtering

For an arbitrary beamformer $\mathbf{b}$ the SNIR is calculated to

$$\gamma(\mathbf{b}) = |a|^2 \frac{|\mathbf{b}^*\mathbf{d}(\vec{u}_0)|^2}{E\,|\mathbf{b}^*\mathbf{Q}|^2} \tag{2.28}$$

$$= |a|^2 \frac{|\mathbf{b}^*\mathbf{d}(\vec{u}_0)|^2}{\mathbf{b}^*\mathbf{R}\mathbf{b}} \tag{2.29}$$

For the optimum beamformer, $\mathbf{b}_{opt} = \mathbf{R}^{-1}\mathbf{d}(\vec{u}_0)$, and it follows

$$\gamma(\mathbf{b}_{opt}) = |a|^2 \frac{|\mathbf{d}^*(\vec{u}_0)\mathbf{R}^{-1}\mathbf{d}(\vec{u}_0)|^2}{\mathbf{d}^*(\vec{u}_0)\mathbf{R}^{-1}\mathbf{R}\mathbf{R}^{-1}\mathbf{d}(\vec{u}_0)} \tag{2.30}$$

$$= |a|^2 \mathbf{d}^*(\vec{u}_0)\mathbf{R}^{-1}\mathbf{d}(\vec{u}_0) \tag{2.31}$$

If the conventional beamformer is used, we get

$$\gamma(\mathbf{d}(\vec{u}_0)) = |a|^2 \frac{\|\mathbf{d}(\vec{u}_0)\|^4}{\mathbf{d}^*(\vec{u}_0)\mathbf{R}\mathbf{d}(\vec{u}_0)}. \tag{2.32}$$

The gain of the optimum beamformer compared to the conventional beamformer is expressed by

$$\frac{\gamma(\mathbf{b}_{opt}(\vec{u}_0))}{\gamma(\mathbf{d}(\vec{u}_0))} = \frac{\mathbf{d}^*(\vec{u}_0)\mathbf{R}^{-1}\mathbf{d}(\vec{u}_0)}{\|\mathbf{d}(\vec{u}_0)\|^2} \frac{\mathbf{d}^*(\vec{u}_0)\mathbf{R}\mathbf{d}(\vec{u}_0)}{\|\mathbf{d}(\vec{u}_0)\|^2}. \tag{2.33}$$

Moreover, it is usual to compare the SNIR to the SNR obtained without external interference with the conventional beamformer. This is expressed by

$$\frac{SNIR}{SNR} = \frac{\sigma^2\mathbf{d}^*(\vec{u}_0)\mathbf{R}^{-1}\mathbf{d}(\vec{u}_0)}{\|\mathbf{d}(\vec{u}_0)\|^2}. \tag{2.34}$$

2.2.4 The case of a single source of interference

The general form of interference suppression as treated in the foregoing section is valid for any kind of interference which can be modelled as a random vector with

fixed covariance matrix. We regard an array with identical identically orientated elements and an interference coming from a distinct direction $\vec{v}$.

Let the complex amplitude J of the interference be random with expectation zero and variance σ_J^2. Then

$$\mathbf{Z} = a\mathbf{d}(\vec{u}) + \mathbf{J} + \mathbf{N} = a\mathbf{d}(\vec{u}) + J\mathbf{d}(\vec{v}) + \mathbf{N}. \tag{2.35}$$

The covariance matrices of interference $\mathbf{J}$ and interference plus noise $\mathbf{Q} = \mathbf{J} + \mathbf{N}$ are given by

$$\mathbf{R_J} = E[\mathbf{J}\mathbf{J}^*] = \sigma_J^2 \mathbf{d}(\vec{v})\mathbf{d}^*(\vec{v}) \tag{2.36}$$

$$\mathbf{R} = E[\mathbf{Q}\mathbf{Q}^*] = \sigma^2 \mathbf{I}_M + \sigma_J^2 \mathbf{d}(\vec{v})\mathbf{d}^*(\vec{v}). \tag{2.37}$$

A normalization to the noise variance yields

$$\frac{1}{\sigma^2}\mathbf{R} = \mathbf{I}_M + \eta \frac{\mathbf{d}(\vec{v})\mathbf{d}^*(\vec{v})}{\|\mathbf{d}(\vec{v})\|^2} \tag{2.38}$$

$$= \mathbf{I}_M + \eta \widetilde{\mathbf{d}}(\vec{v})\widetilde{\mathbf{d}}^*(\vec{v}) \tag{2.39}$$

with $\eta = \sigma_J^2 \|\mathbf{d}(\vec{v})\|^2/\sigma^2$ being the *interference-to-noise-ratio (INR)* and using the normalized DOA-vector $\widetilde{\mathbf{d}}(\vec{v}) = \mathbf{d}(\vec{v})/\|\mathbf{d}(\vec{v})\|$.

Shape of the inverse covariance matrix: Using the matrix equality

$$(\mathbf{I} + \eta \mathbf{v}\mathbf{v}^*)^{-1} = \mathbf{I} - \frac{\eta}{1 + \eta \mathbf{v}^*\mathbf{v}} \mathbf{v}\mathbf{v}^* \tag{2.40}$$

(see Annex Eq.(A.28)) $\frac{1}{\sigma^2}\mathbf{R}$ can be inverted to

$$\sigma^2 \mathbf{R}^{-1} = \mathbf{I}_M - \zeta \widetilde{\mathbf{d}}(\vec{v})\widetilde{\mathbf{d}}^*(\vec{v}) \quad \text{with} \quad \zeta = \frac{\eta}{1+\eta}. \tag{2.41}$$

Now the application of the interference suppression operator $\mathbf{H} = \sigma^2\mathbf{R}^{-1}$ to the measured array output $\mathbf{z}$ can be written as

$$\mathbf{H}\mathbf{z} = \mathbf{z} - \zeta \widetilde{\mathbf{d}}(\vec{v})\widetilde{\mathbf{d}}^*(\vec{v})\mathbf{z} = \mathbf{z} - \zeta \hat{J}(\mathbf{z})\widetilde{\mathbf{d}}(\vec{v}) = \mathbf{z} - \zeta \hat{\mathbf{J}}(\mathbf{z}) \tag{2.42}$$

with $\hat{J}(\mathbf{z}) = \widetilde{\mathbf{d}}^*(\vec{v})\mathbf{z}$ and $\widehat{\mathbf{J}}(\mathbf{z}) = \hat{J}(\mathbf{z})\widetilde{\mathbf{d}}(\vec{v})$.

It is illuminating to interpret this formula. $\hat{J}(\mathbf{z}) = \widetilde{\mathbf{d}}^*(\vec{v})\mathbf{z}$ means to form a beam into the direction $\vec{v}$ of the interference. Since $\|\widetilde{\mathbf{d}}(\vec{v})\| = 1$ the output $\hat{J}(\mathbf{z})$ is an unbiased estimator of the complex interference amplitude. (see Annex Eq.(A.31))

$\widehat{\mathbf{J}}(\mathbf{z}) = \hat{J}(\mathbf{z})\widetilde{\mathbf{d}}(\vec{v})$ is a reconstruction of the interference vector. [2]

Obviously a complex multiple w of the signal $\mathbf{d}(\vec{v})$ expected from the interference direction v is subtracted from the original sample vector $\mathbf{z}$. To determine the factor, a beam is formed into this direction: $y = \mathbf{d}^*(\vec{v})\mathbf{z}$ and the output is scaled with $w = \frac{\eta y}{1+\eta \mathbf{d}^*(\vec{v})\mathbf{d}(\vec{v})}$.

[2] To be worked over from here on

Adaptive characteristics The characteristics of the array for fixed beamformer $\mathbf{b}(\vec{u}_0) = \mathbf{R}^{-1}\mathbf{d}(\vec{u}_0)$ is calculated to $D(\vec{u}, \vec{u}_0) = \beta \mathbf{d}^*(\vec{u}_0)\mathbf{R}^{-1}\mathbf{d}(\vec{u})$. Here, β is a normalization factor which is chosen in that way that $D(\vec{u}_0, \vec{u}_0) = 1$, if only noise is present. We assume further that the single elements are omnidirectional and that the DOA vectors are normalized to unit vectors. Under these circumstances it follows $\beta = \sigma^2$. We get

$$\begin{aligned} D(\vec{u}, \vec{u}_0) &= \beta \mathbf{d}^*(\vec{u}_0)\mathbf{R}^{-1}\mathbf{d}(\vec{u}) && (2.43)\\ &= \mathbf{d}^*(\vec{u}_0)\left(\mathbf{I}_M - \gamma \mathbf{d}(\vec{v})\mathbf{d}^*(\vec{v})\mathbf{d}(\vec{u})\right) && (2.44)\\ &= \mathbf{d}^*(\vec{u}_0)\mathbf{d}(\vec{u}) - \gamma \mathbf{d}^*(\vec{u}_0)\mathbf{d}(\vec{v})\mathbf{d}^*(\vec{v})\mathbf{d}(\vec{u}) && (2.45)\\ &= F(\vec{u}, \vec{u}_0) - \gamma F^*(\vec{v}, \vec{u})F(\vec{v}, \vec{u}_0). && (2.46) \end{aligned}$$

$F(\vec{u}, \vec{u}_0)$ is the array factor as defined in Eq. (2.9) with $F(\vec{u}, \vec{u}) \equiv 1$,

In direction of the interfering source we get

$$\begin{aligned} D(\vec{v}, \vec{u}_0) &= F(\vec{v}, \vec{u}_0) - \gamma F^*(\vec{v}, \vec{u})F(\vec{v}, \vec{u}_0) && (2.47)\\ &= F(\vec{v}, \vec{u}_0)\left(\frac{\eta F(\vec{v}, \vec{v})}{1 + \eta F(\vec{v}, \vec{v})}\right). && (2.48) \end{aligned}$$

$$\begin{aligned} D(\vec{v}, \vec{v}) &= F(\vec{v}, \vec{v})\left(\frac{\eta F(\vec{v}, \vec{v})}{1 + \eta F(\vec{v}, \vec{v})}\right) && (2.49)\\ &= \frac{\eta}{1 + \eta}. && (2.50) \end{aligned}$$

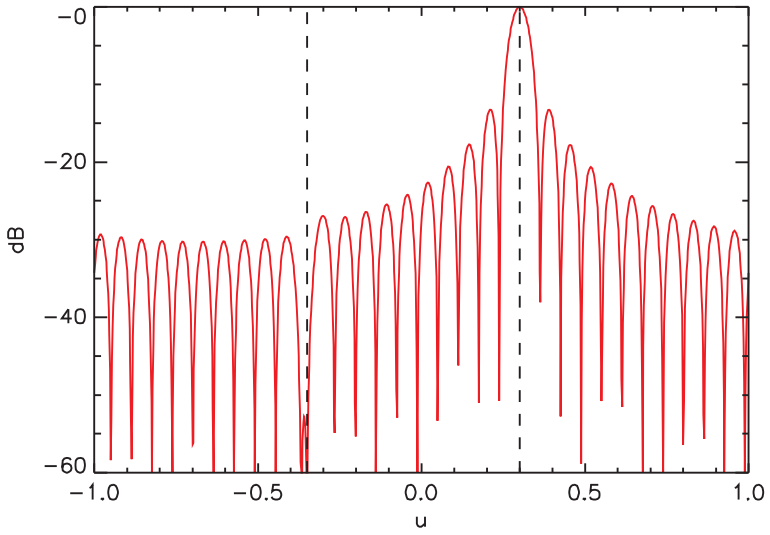

Figure 2.7: *Adaptive Null*

Obviously a minimum is obtained in the direction of interference, that for $\eta \to \infty$ tends to a null, see Fig. 2.7. The optimum beamformer is a linear combination from the two classical beamformers in target- and interference direction:

$$\begin{aligned}\mathbf{b}(\vec{u}_0) &= \sigma^2\mathbf{R}^{-1}\mathbf{d}(\vec{u}_0) && (2.51)\\ &= (\mathbf{I}_M - \gamma\mathbf{d}^*(\vec{v})\mathbf{d}(\vec{v}))\,\mathbf{d}(\vec{u}_0) && (2.52)\\ &= \mathbf{d}(\vec{u}_0) - \gamma\mathbf{d}^*(\vec{v})\mathbf{d}(\vec{u}_0)\mathbf{d}(\vec{v}) && (2.53)\end{aligned}$$

(The factor σ^2 is allowed since the SNIR is invariant against multiplication of the beamformer by a scalar).

The signal to noise plus interference ratio (SNIR) in dependence on the target direction The *signal to noise plus interference ratio (SNIR)* at the output of the beamformer focused to the target direction $\vec{u}_0 = \vec{u}$ is given by

$$\begin{aligned}SNIR(\vec{u}) &= \frac{|a\mathbf{d}^*(\vec{u})\mathbf{R}^{-1}\mathbf{d}(\vec{u})|^2}{E\,|\mathbf{d}^*(\vec{u})\mathbf{R}^{-1}(\mathbf{J}+\mathbf{N})|^2} && (2.54)\\ &= |a|^2\,\mathbf{d}^*(\vec{u})\mathbf{R}^{-1}\mathbf{d}(\vec{u}) && (2.55)\\ &= \frac{|a|^2}{\sigma^2}\mathbf{d}^*(\vec{u})\,(\mathbf{I}_M - \gamma\mathbf{d}(\vec{v})\mathbf{d}^*(\vec{v})\mathbf{d}(\vec{u})) && (2.56)\\ &= \frac{|a|^2}{\sigma^2}\left(1 - \frac{\gamma}{M}\,|F(\vec{v},\vec{u})|^2\right). && (2.57)\end{aligned}$$

From the value without outer interference $|a|^2/\sigma^2$ the characteristics with focusing to the interference direction is subtracted, see Fig. 2.8.[3]

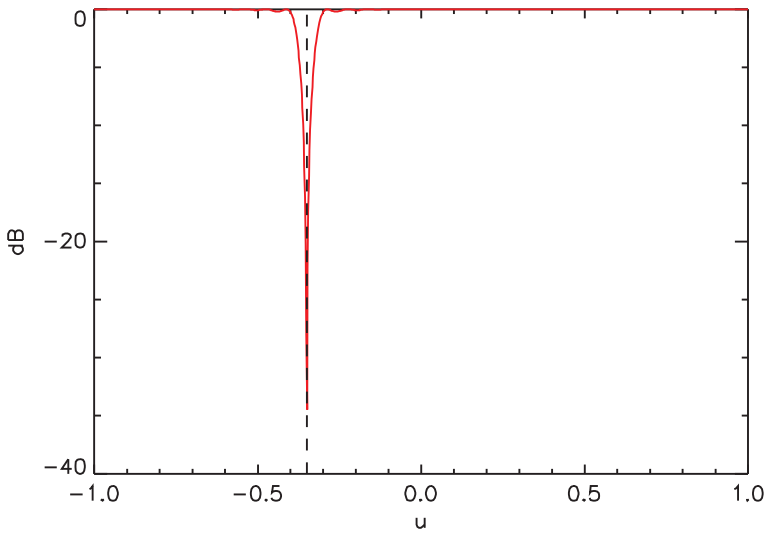

Figure 2.8: *SNIR curve for one interference direction*

Limit for large INR For a large η tends γ to $\gamma = 1/(\mathbf{d}^*(\vec{v})\mathbf{d}(\vec{v}))$, the limiting form of $\mathbf{R}^{-1}$ is

[3] A further illustration could show the subtsction of the pattern

$$\sigma^2\mathbf{R}^{-1} \to \mathbf{I}_M - \frac{\mathbf{d}(\vec{v})\mathbf{d}^*(\vec{v})}{\mathbf{d}^*(\vec{v})\mathbf{d}(\vec{v})} = \mathbf{I}_M - \mathbf{P}_{<\mathbf{d}(\vec{v})>}, \tag{2.58}$$

where $\mathbf{P}_{<\mathbf{d}(\vec{v})>}$ denotes the projector to the linear subspace spanned by $\mathbf{d}(\vec{v})$. The characteristics tends to null in direction of the interference.

2.2.5 Several sources of interference

Again, we regard the model $\mathbf{Z} = a\mathbf{d}(\vec{u}_0) + \mathbf{Q}, \mathbf{Q} = \mathbf{J} + \mathbf{N}$ with the covariance matrix $\mathbf{R}$ of the sum $\mathbf{Q}$ of internal and external interference.

Let in the directions $\vec{v}_1, \ldots, \vec{v}_k$ be interfering sources with the complex random amplitudes $B_1, \ldots, B_k$, collected in the vector $\mathbf{B} = (B_1, \ldots, B_k)^t$ with zero expectations and covariances described by the covariance matrix $\mathbf{R_B} = E[\mathbf{B}\mathbf{B}^*]$.

The related DOA-vectors are the columns of the $M \times k$ - Matrix $\mathbf{D} = (\mathbf{d}(\vec{v}_1), \cdots, \mathbf{d}(\vec{v}_k))$. For $\mathbf{D}$ we presume regularity, i.e. the DOA-vectors to the interfering sources are linearly independent.

Then we get

$$\mathbf{J} = \sum_{\kappa=1}^{k} B_\kappa \mathbf{d}(\vec{v}_\kappa) = \mathbf{D}\mathbf{B} \tag{2.59}$$

and

$$\mathbf{Z} = a\mathbf{d}(\vec{u}_0) + \mathbf{D}\mathbf{B} + \mathbf{N}. \tag{2.60}$$

Let U_J be the linear subspace spanned by $\mathbf{d}(\vec{v}_1), \cdots, \mathbf{d}(\vec{v}_k)$ and $U_J^\perp$ the subspace orthogonal to U_J. Then

$$\mathbf{R_J} = \mathbf{D}E\left[\mathbf{B}\mathbf{B}^*\right]\mathbf{D}^* = \mathbf{D}\mathbf{R_B}\mathbf{D}^* \tag{2.61}$$

$$\mathbf{R} = \sigma^2\mathbf{I}_M + \mathbf{D}\mathbf{R_B}\mathbf{D}^*. \tag{2.62}$$

If the number of external interference sources k is smaller than the number of channels M, the matrix $\mathbf{R_J}$ is not regular, its rank is maximal equal to k. The inverse of the $M \times M$ dimensional matrix $\mathbf{R}$ can be reduced to an equivalent matrix operation in the k-dimensional subspace U_J according to [4]

$$\sigma^2\mathbf{R}^{-1} = \mathbf{I}_M - \mathbf{D}\mathbf{E}\mathbf{D}^*. \tag{2.63}$$

The $k \times k$ dimensional matrix $\mathbf{E}$ is given by

$$\mathbf{E} = \left(\sigma^2\mathbf{R}_B^{-1} + \mathbf{D}^*\mathbf{D}\right)^{-1}. \tag{2.64}$$

So we get

[4] This identity is known as the 'matrix inversion lemma', see Appendix

$$\sigma^2\mathbf{R}^{-1} = \mathbf{I}_M - \mathbf{D}\left(\sigma^2\mathbf{R}_B^{-1} + \mathbf{D}^*\mathbf{D}\right)^{-1}\mathbf{D}^*. \tag{2.65}$$

Limit for large INR If the noise is negligible with respect to the interference, i.e. the INR in all channels tends to infinity, $\sigma^2\mathbf{R}_B^{-1}$ will approach $\mathbf{0}$ resulting in

$$\sigma^2\mathbf{R}^{-1} \to \mathbf{I}_M - \mathbf{D}\left(\mathbf{D}^*\mathbf{D}\right)^{-1}\mathbf{D}^* = \mathbf{I} - \mathbf{P}_{U_J} = \mathbf{P}_{U_J}^{\perp}. \tag{2.66}$$

Essence 2.7 *For the limiting case of negligible noise, the optimum interference suppression results in the projection to the subspace orthogonal to the subspace spanned by the DOA vectors to the sources of interference (interference space).*

2.2.6 Signal subspace, interference subspace, noise subspace

As long as linearity can be assumed, for the case of simultaneous useful signals, interference, and noise the following general model can be applied:

$$\mathbf{Z} = \mathbf{S}\mathbf{a} + \mathbf{D}\mathbf{B} + \mathbf{N}, \tag{2.67}$$

with the useful signals $\mathbf{S} = (\mathbf{s}_1, \cdots, \mathbf{s}_l)$, the interfering signals $\mathbf{D} = (\mathbf{d}_1, \cdots, \mathbf{d}_k)$ and the noise $\mathbf{N}$. The complex amplitudes of the useful signals are collected in the deterministic vector $\mathbf{a}$, and those of the interfering signals in the random vector $\mathbf{B}$. We assume that the signal vectors as well as the interference vectors are linearly independent, i. e. the matrix $\mathbf{S}$ has the full rank l and the matrix $\mathbf{D}$ has the rank k.

Useful signals and noise If $\mathbf{Z}$ consists of only useful signals and noise, we have seen in the preceding that the projection $\mathbf{P}_{U_S} := \mathbf{S}(\mathbf{S}^*\mathbf{S})^{-1}\mathbf{S}^*$ to the space of useful signals $U_S = Lin\{\mathbf{s}_1, \cdots, \mathbf{s}_l\}$ reconstructs the signals in terms of minimum mean square optimally. The noise looses l degrees of freedom due to the projection, so the remaining complete noise power will be equal to $l\sigma^2$. The useful signals are not affected by the projection.

Useful signals, interfering signals, and noise The interfering signals are contained in the interference subspace $U_J = Lin\{\mathbf{d}_1, \cdots, \mathbf{d}_l\}$. To remove the whole interference (necessary, if the noise is negligible with respect to the interference), the projector $\mathbf{P}_{U_J^{\perp}} := \mathbf{I}_M - \mathbf{D}(\mathbf{D}^*\mathbf{D})^{-1}\mathbf{D}^*$ has to be applied. This projector eliminates completely the interference, but also a part of the useful signals. The remaining parts of the useful signals are $\left(\mathbf{P}_{U_J^{\perp}}\mathbf{s}_1, \cdots, \mathbf{P}_{U_J^{\perp}}\mathbf{s}_l\right)$, the optimal reconstruction is obtained by the projection $\mathbf{P}_{U_S}\mathbf{P}_C^{\perp} = \mathbf{P}_{U_J^{\perp}}\mathbf{P}_{U_S}$. This is the projector to the subspace $U_S \cap U_J^{\perp}$.

Essence 2.8 *For the model of linearly superposed useful signals, and interfering signals the related subspaces can be identified. The projection to the signal subspace does not decrease the performance of detection and estimation, it is a sufficient statistics. To remove the whole interference a subsequent projector to the subspace orthogonal to the interference subspace may be applied, which may decrease the signal power. The two projections - which can be subsumed to only one projection - also reduce the noise power.*

2.2.7 A basic data reduction retaining optimal detection- and estimation properties for signals in interference

2.2.8 An example for continuous distributed interference

As an example we examine a linear array composed of omnidirectional elements with an external interference coming continuously and uniformly from all directions.

Problem: We regard a linear array of M elements with inter-element distance d, arranged along the z-axis of a Cartesian coordinate system. We assume external interference coming from all three-dimensional directions uniformly and independent (Interference being white over the set of directions on the unit sphere). Determine the covariance matrix of the vector of the element outputs!
Solution: Let the z-coordinates of the phase centers be $z_m = m\Delta z, m = 1,\ldots,M$, the other components are equal to zero. The normalized DOA vector to an arbitrary direction $\vec{u} = (\sin\vartheta\cos\varphi, \sin\vartheta\sin\varphi, \cos\vartheta)^t$ characterized in spherical coordinates is given by

$$\mathbf{d}(\vec{u}) = \begin{pmatrix} \exp\{jk_r\Delta z\cos\vartheta\} \\ \vdots \\ \exp\{jk_rM\Delta z\cos\vartheta\} \end{pmatrix}, \tag{2.68}$$

the received signal is $C = \int_\Omega A(\vec{u})\mathbf{d}(\vec{u})dO(\vec{u})$ and the covariance matrix is calculated to

$$\begin{aligned}
\mathbf{R_J} &= E\left[\int_\Omega\int_\Omega A(\vec{u})A^*(\vec{u'})\mathbf{d}(\vec{u})\mathbf{d}^*(\vec{u'})dO(\vec{u})dO(\vec{u'})\right] && (2.69)\\
&= \sigma_A^2\int_\Omega \mathbf{d}(\vec{u})\mathbf{d}^*(\vec{u})dO(\vec{u}) && (2.70)\\
&= \sigma_A^2\left(\int_0^{2\pi}\int_0^{\pi}\exp\{jk_r(m-\mu)\Delta z\cos\vartheta\}\sin\vartheta d\vartheta d\varphi\right)_{m,\mu=1}^{M} && (2.71)\\
&= \sigma_A^2\left(2\pi\int_{-1}^{1}\exp\{jk_r(m-\mu)\Delta z u\}du\right)_{m,\mu=1}^{M} && (2.72)\\
&= \pi\sigma_A^2\left(\mathrm{si}(k_r(m-\mu)\Delta z)\right)_{m,\mu=1}^{M}. && (2.73)
\end{aligned}$$

If $\Delta z = \lambda/2$, then $k_r\Delta z = \pi$ and

$$\mathbf{R_J} = \pi\sigma_A^2\mathbf{I}_M. \tag{2.74}$$

Essence 2.9 *The outputs of a linear array with spacing $\lambda/2$ are uncorrelated for spatial white interference uniformly distributed over the unit sphere.*

2.3 Eigenspaces and sample matrix

Eigenvalues of a covariance matrix If $\mathbf{u}$ is a normalized eigenvector of the covariance matrix $\mathbf{R_Z}$ of an arbitrary random vector $\mathbf{Z}$ with expectation $\mathbf{0}$ with respect to the eigenvalue λ, then

$$\mathbf{R_Z u} = \lambda \mathbf{u} \tag{2.75}$$
$$\mathbf{u}^* \mathbf{R_Z u} = \lambda \mathbf{u}^* \mathbf{u} = \lambda, \tag{2.76}$$

it follows

$$E[\|\mathbf{u}^* \mathbf{Z}\|^2] = \lambda. \tag{2.77}$$

Now we return to the interfering part of Eq. (2.60). The vector combining external and internal interference is $\mathbf{Q} = \mathbf{DB} + \mathbf{N}$ with the covariance matrix $\mathbf{R}$, the subspace of external interference is $U_J = \langle \mathbf{d}_1, \ldots, \mathbf{d}_k \rangle$. For each $\mathbf{u} \in U_J^\perp$ we have:

$$\mathbf{Ru} = (\mathbf{DR}_B \mathbf{D}^* + \sigma^2 \mathbf{I})\mathbf{u} = \sigma^2 \mathbf{u}, \tag{2.78}$$

so $\mathbf{u}$ is an eigenvector of $\mathbf{R}$ to the eigenvalue σ^2. Since $U_J^\perp$ has the dimension $M-k$, $M-k$ eigenvectors $\mathbf{u}_{k+1}, \cdots, \mathbf{u}_m$ can be found spanning $U_J^\perp$. The remaining k eigenvectors to the eigenvalues $\lambda_1, \cdots, \lambda_k$ are orthogonal to $U_J^\perp$, are consequently elements of U_J. For these the following equation is valid

$$\mathbf{u}_\kappa^* \mathbf{R} \mathbf{u}_\kappa = \mathbf{u}_\kappa^* (\mathbf{DR}_B \mathbf{D}^* + \sigma^2 \mathbf{I}) \mathbf{u}_\kappa \geq \sigma^2. \tag{2.79}$$

If the columns of $\mathbf{D}$ are linearly independent is $\mathbf{R}_B$ regular, even the greater sign is valid.

Essence 2.10 *The eigenvectors to the k largest eigenvalues span the interference subspace, while the remaining eigenvectors are related to the remaining noise subspace and have the eigenvalues* σ^2.

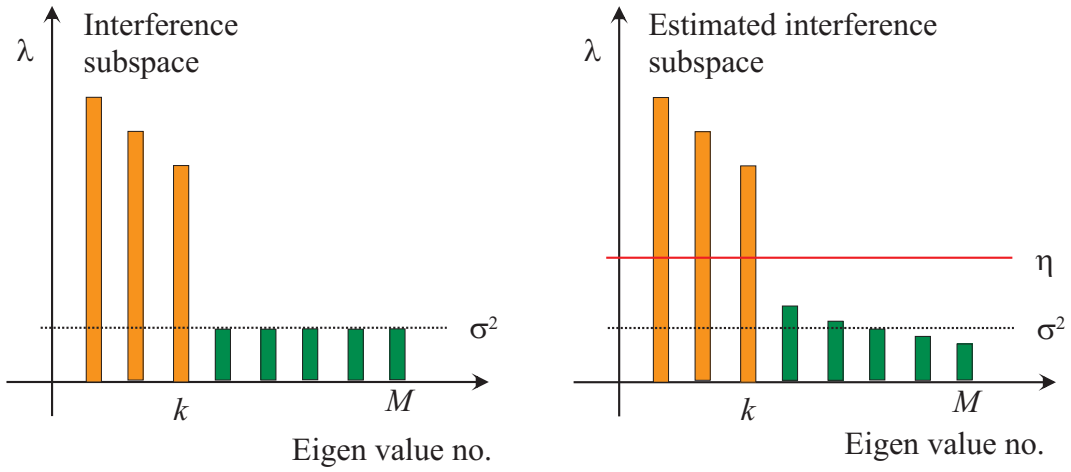

Figure 2.9: *The eigenvalues of the covariance matrix ('eigen spectrum')*

2.3.1 Determination of the weights

In the most applications the covariance matrix is unknown. An adaptive determination of the coefficients of the beamformer is based on a learning sequence $\mathbf{q}_1, \ldots, \mathbf{q}_n$ which are ideally independent realizations of interference plus noise $\mathbf{Q}$. In this context, the terminus 'snapshot' is often used.

In the literature, many methods to determine the weights are described; we only mention a few of them. Generally, we apply an $M \times M$ filter matrix $\mathbf{H}$ to the data. To maximize the SNIR, $\mathbf{H}$ has to be chosen as a multiple of $\mathbf{R}$. Since the true covariance matrix is not available other matrices have to be used. The loss is calculated to

$$loss = \frac{\gamma(\mathbf{H})}{\gamma(\mathbf{R}^{-1})} \tag{2.80}$$

$$= \frac{|\mathbf{d}^*(\vec{u}_0)\mathbf{H}\mathbf{d}(\vec{u}_0)|^2}{\mathbf{d}^*(\vec{u}_0)\mathbf{H}^*\mathbf{R}\mathbf{H}\mathbf{d}(\vec{u}_0)\mathbf{d}^*(\vec{u}_0)\mathbf{R}^{-1}\mathbf{d}(\vec{u}_0)}. \tag{2.81}$$

The sample matrix: The matrix

$$\widehat{\mathbf{R}} = \frac{1}{n}\sum_{\nu=1}^{n} \mathbf{q}_\nu \mathbf{q}_\nu^* \tag{2.82}$$

is called *sample matrix* or *empirical covariance matrix*. Its expectation is equal to the wanted covariance matrix $\mathbf{R}$, so $\widehat{\mathbf{R}}$ is an unbiased estimate of $\mathbf{R}$.

Sample matrix inversion: Instead of $\mathbf{R}$ the estimate $\widehat{\mathbf{R}}$ is inverted. This method is called *sample matrix inversion (SMI)*.

Diagonal loading: Since $\widehat{\mathbf{R}}$ is a random variable, $\mathbf{H} = \widehat{\mathbf{R}}^{-1}$ fluctuates especially if the number n of snapshots is low. The robustness of this technique can be increased by using *diagonal loading*: To the diagonal of $\widehat{\mathbf{R}}$ a small constant ϵ is added before inversion: $\mathbf{H} = (\widehat{\mathbf{R}} + \epsilon \mathbf{I}_M)^{-1}$.

Projection method: If $\hat{U}_J$ is an estimate of the interference subspace, the projector $\mathbf{H} = \mathbf{P}_{\hat{U}_J}^{\perp}$ is applied. The estimation $\hat{U}_J$ can be extracted from the sample matrix: The eigenvalues $\lambda_1, \ldots, \lambda_M$ of the sample matrix are ordered. According to the behavior of the eigenvalues of the true covariance matrix, we expect k large eigenvalues related to the interference subspace and $M - k$ eigenvalues related to the remaining noise subspace. A comparison with a suitable threshold yields the k largest eigenvalues to the eigenvectors $\mathbf{u}_1, \ldots, \mathbf{u}_k$. The span of these vectors is the estimation of the interference subspace. The remaining eigenvectors span the subspace $\hat{U}_J^{\perp}$ which is asymptotically free from interference.

2.4 DOA-estimation and Cramér-Rao Bounds

If the parallel signals of an antenna array or subapertures of an array are available, the possibility to estimate the direction of arrival with a high accuracy is opened. In contrary to finding the maximum of the main beam by scanning this is possible in principle by processing the echoes of only one pulse. For this reason, these methods are called *monopulse estimators*. In the following, we will have a closer look at the general angular estimation problem, derive its *Cramér-Rao Bounds (CRB)* as a means to judge the estimation accuracy, and present an algorithm for a generalized monopulse estimator for colored interference.

2.4.1 Estimation problem and signal model

We start by formulating the general signal model and the estimation problem. The basic model is the same as in Eq.(2.21), except for restricting it to the case of a linear array.

Problem: Based on a realization $\mathbf{z}$ of

$$\mathbf{Z} = a\mathbf{d}(u) + \mathbf{Q} \quad \text{(model A)} \tag{2.83}$$

with unknown complex constant a and known covariance matrix $\mathbf{R}$, u has to be estimated.

This is a well known problem in array processing theory (see e.g. [13] or [15]). Nevertheless, for the application on moving platforms, this has rarely been addressed, e.g. in [10], [11].

2.4.2 Cramér-Rao Bounds for the general problem

The Cramér-Rao Bounds offer the possibility to calculate a bound for the expected quadratic deviation of an arbitrary estimator of the true value. They are based on *Fisher's information matrix*, see Annex section A.6.3. In section 1.7.3 we have already derived the Cramér-Rao Bounds for the estimation of the direction, if only noise is present.

If we use the statistical model

$$\mathbf{Z} = \mathbf{m}(\boldsymbol{\vartheta}) + \mathbf{Q} \tag{2.84}$$

with a deterministic complex vector $\mathbf{m}(\boldsymbol{\vartheta})$ and interference $\mathbf{Q} \sim \mathcal{N}_{\mathbb{C}^n}(\mathbf{0}, \mathbf{R})$, Fisher's information matrix is given by

$$\mathbf{J}(\boldsymbol{\vartheta}) = \frac{2}{\sigma^2} Re\left\{\mathbf{m}^*_{\boldsymbol{\vartheta}}(\boldsymbol{\vartheta})\mathbf{R}^{-1}\mathbf{m}_{\boldsymbol{\vartheta}}(\boldsymbol{\vartheta})\right\} \tag{2.85}$$

where $\mathbf{m}_{\boldsymbol{\vartheta}}(\boldsymbol{\vartheta})$ means the gradient of $\mathbf{m}_{\boldsymbol{\vartheta}}$ with respect to $\boldsymbol{\vartheta}$ written as $n \times k$ matrix, see appendix **??**.

If the unknowns in Eq. (2.83) are combined into the real-valued parameter vector $\vartheta = (u, \alpha, \varphi)$ with $a = \alpha \exp\{j\varphi\}$, the vector $\mathbf{m}$ is expressed as

$$\mathbf{m}(\boldsymbol{\vartheta}) = \alpha e^{j\varphi}\mathbf{d}(u). \tag{2.86}$$

The Fisher information matrix is calculated starting from Eq.(A.111) to

$$\mathbf{J} = 2\Re\begin{pmatrix} \alpha^2\mathbf{d}_u^*\mathbf{R}^{-1}\mathbf{d}_u & \alpha\mathbf{d}_u^*\mathbf{R}^{-1}\mathbf{d} & j\alpha^2\mathbf{d}_u^*\mathbf{R}^{-1}\mathbf{d} \\ \alpha\mathbf{d}^*\mathbf{R}^{-1}\mathbf{d}_u & \mathbf{d}^*\mathbf{R}^{-1}\mathbf{d} & 0 \\ -j\alpha^2\mathbf{d}^*\mathbf{R}^{-1}\mathbf{d}_u & 0 & \alpha^2\mathbf{d}^*\mathbf{R}^{-1}\mathbf{d} \end{pmatrix} \tag{2.87}$$

For simplicity, the dependence on u was omitted, and the subscript u denotes the derivation with respect to u. The variance of the estimation error of the directional cosine is limited by the first component of the inverse Fisher matrix, which can be analytically calculated from Eq. (2.87) using the representation of sub-determinants:

$$(\mathbf{J}^{-1})_{11} = \frac{1}{2|a|^2}\frac{p}{q} \tag{2.88}$$

with

$$\begin{aligned} p &= \mathbf{d}^*\mathbf{R}^{-1}\mathbf{d} \\ q &= \mathbf{d}^*\mathbf{R}^{-1}\mathbf{d}\mathbf{d}_u^*\mathbf{R}^{-1}\mathbf{d}_u - \left|\mathbf{d}_u^*\mathbf{R}^{-1}\mathbf{d}\right|^2. \end{aligned} \tag{2.89}$$

Fig. 2.10 shows the SNIR and CRB curves for two sources of interference.

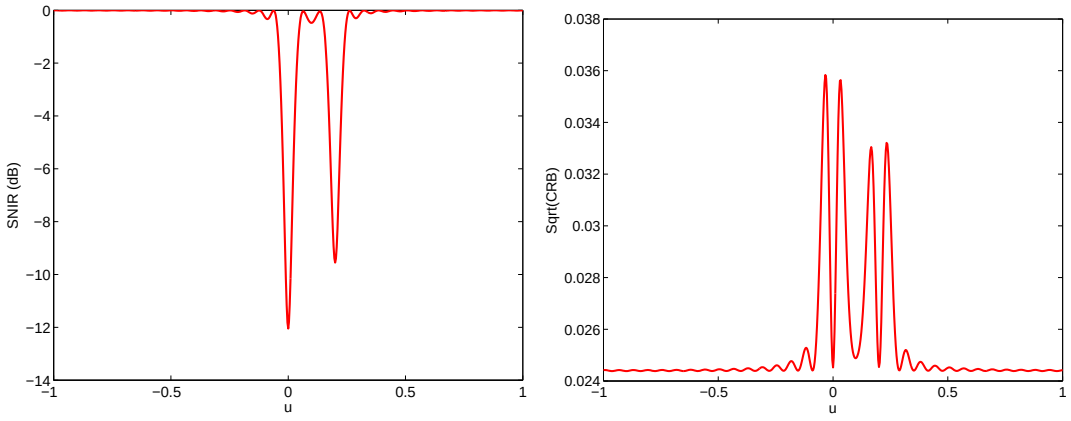

Figure 2.10: *SNIR- and CRB plot for two external sources of interference*

Essence 2.11 *For colored interference, the expected quadratic error of any estimator of the directional cosine for the signal model Eq.(2.83) is bounded by the first coefficient of the inverse Fisher matrix given in Eq.(2.88).*

2.4.3 The basic estimation problem

As we will see, the general problem can be reduced to a much simpler basic problem:

$$\mathbf{X} = b\mathbf{e}(u) + \mathbf{N} \quad \text{(model B)} \tag{2.90}$$

with the properties

$$\begin{aligned} \|\mathbf{e}(u)\|^2 &\equiv 1 && (2.91)\\ \mathbf{e}_u^*(u)\mathbf{e}(u) &= 0 && (2.92)\\ \mathbf{R}_N &= \mathbf{I}_M. && (2.93) \end{aligned}$$

Again, the complex amplitude b and the parameter u are unknown, the task is to estimate u based on a realisation $\mathbf{x}$ of $\mathbf{X}$.

Cramér-Rao-Bounds

From Eq. (2.83) we see that under these conditions the Fisher information matrix is diagonal, i.e. the estimation of the three parameters is decoupled. The inverse of the element of $\mathbf{J}$ dedicated to u is simply given by

$$J_{11}^{-1} = \frac{1}{2|b|^2\|\mathbf{e}_u(u)\|^2}. \tag{2.94}$$

Maximum-Likelihood estimator

Under the assumption that $\mathbf{N}$ is Gaussian distributed, the ML estimator of u is given to

$$\hat{u} = \text{argmax}_u \left\{ |\mathbf{e}^*(u)\mathbf{x}|^2 : u \in [-1, 1] \right\}, \tag{2.95}$$

while $\hat{b} = \mathbf{e}^*(\hat{u})\mathbf{x}$ is the corresponding ML estimate of b. The first derivative of Eq. (2.95) with respect to u yields the necessary condition:

$$\Re\left\{ (\mathbf{e}_u^*(\hat{u})\mathbf{x}) \left(\mathbf{e}^*(\hat{u})\mathbf{x}\right)^* \right\} = 0. \tag{2.96}$$

Monopulse estimator

In order to reduce computational complexity, we may approximate the ML equation (2.96). Let u_0 be a direction close to the unknown direction u, e.g. the main look direction of the phased array, and $\Delta u = u - u_0$. By Taylor-expansion

$$\begin{aligned} \mathbf{e}(u) &\approx \mathbf{e}(u_0) + \Delta u \mathbf{e}_u(u_0) && (2.97)\\ \mathbf{e}_u(u) &\approx \mathbf{e}_u(u_0) + \Delta u \mathbf{e}_{uu}(u_0). && (2.98) \end{aligned}$$

around u_0 we get as the approximation of the ML equation:

$$\Re\left\{ \left(\sigma(\mathbf{x}) + \widehat{\Delta u}\delta(\mathbf{x})\right)^* \left(\delta(\mathbf{x}) + \widehat{\Delta u}\gamma(\mathbf{x})\right) \right\} = 0, \tag{2.99}$$

with the abbreviations

$$\sigma(\mathbf{x}) = \mathbf{e}^*(u_0)\mathbf{x},\ \delta(\mathbf{x}) = \mathbf{e}_u^*(u_0)\mathbf{x},\ \gamma(\mathbf{x}) = \mathbf{e}_{uu}^*(u_0)\mathbf{x}. \tag{2.100}$$

Omitting terms of the order $\widehat{\Delta u}^2$ yields

$$\Re\left\{\sigma^*(\mathbf{x})\delta(\mathbf{x}) + \widehat{\Delta u}\left(|\delta(\mathbf{x})|^2 + \sigma^*(\mathbf{x})\gamma(\mathbf{x})\right)\right\} = 0. \tag{2.101}$$

For sufficient SNR and small $\widehat{\Delta u}^2$ the terms in the brackets right from $\widehat{\Delta u}$ can be replaced by $|\delta(\mathbf{x})|^2 \approx 0, \gamma(\mathbf{x}) \approx \sigma(\mathbf{x})\mathbf{e}_{uu}^*(u_0)\mathbf{e}(u_0) = -\sigma(\mathbf{x})\|\mathbf{e}_u(u_0)\|^2$ resulting in

$$\widehat{\Delta u} \approx \frac{1}{\|\mathbf{e}_u(u_0)\|^2}\Re\left\{\frac{\delta(\mathbf{x})}{\sigma(\mathbf{x})}\right\}. \tag{2.102}$$

This is the well-known monopulse estimator for white noise interference; $\sigma(\mathbf{x})$ is the *sum channel*, $\delta(\mathbf{x})$ the *difference channel*.

Essence 2.12 *For white Gaussian noise under the assumptions of the basic estimation problem of model B Eq.(2.90 the approximate maximum likelihood estimator is given in Eq. (2.102). In principle, only one pulse is necessary to estimate the deviation Δu from the focusing direction, if two beamformers are used: The sum channel $\sigma(\mathbf{x})$ and the difference channel $\delta(\mathbf{x})$.*

Unfortunately, this estimator possesses an infinite variance, since the probability that the denominator takes values in the area around 0 is extremely low for sufficient SNR but not zero. Nevertheless, this can be avoided by blending out these values with a clipping function $g(x)$ tending to 1 for $x \to \infty$ and $g(x)/x$ bounded for $x \to 0$.

$$\widehat{\Delta u} := \frac{1}{\|\mathbf{e}_u(u_0)\|^2}\Re\left\{\frac{\delta(\mathbf{x})}{\sigma(\mathbf{x})}\right\} g(|\sigma(\mathbf{x})|). \tag{2.103}$$

It can be shown that for this version the estimator is efficient in the limit $|b| \to \infty$ and $\Delta u \to 0$, that means the expectation of the quadratic error approaches the CRB.

2.4.4 Transformation of the general problem to the basic problem

Reduction equations

Model A Eq. (2.83) can be transformed into model B Eq. (2.90) in the following way: First, the random vector is multiplied by the 'whitening filter' $\mathbf{R}^{-1/2}$:

$$\mathbf{X} = \mathbf{R}^{-1/2}\mathbf{Z} \tag{2.104}$$

resulting in a identity covariance matrix for $\mathbf{X}$. During this operation also the DOA vector is distorted. We can further normalize the DOA vector by changing the amplitude a appropriately:

$$\mathbf{X} = \tilde{b}\tilde{\mathbf{e}}(u) + \mathbf{N} \tag{2.105}$$

with

$$\mathbf{N} = \mathbf{R}^{-1/2}\mathbf{Q} \tag{2.106}$$

$$\tilde{\mathbf{e}}(u) = \frac{\mathbf{R}^{-1/2}\mathbf{d}(u)}{\|\mathbf{R}^{-1/2}\mathbf{d}(u)\|} \tag{2.107}$$

$$\tilde{b} = a\|\mathbf{R}^{-1/2}\mathbf{d}(u)\|. \tag{2.108}$$

To force the condition $\mathbf{e}_u^*(u)\mathbf{e}(u) = 0$ in Eq. (2.91), the phase of the signal vector is normalised to zero derivation at $u = u_0$:

$$\mathbf{e}(u) := \frac{\tilde{\mathbf{e}}^*(u)\tilde{\mathbf{e}}(u_0)}{|\tilde{\mathbf{e}}^*(u)\tilde{\mathbf{e}}(u_0)|}\tilde{\mathbf{e}}(u) \tag{2.109}$$

This phase shift can be compensated by an opposite phase shift of $\tilde{b}$ to the final amplitude b. Hence the transformations in Eq. (2.104)-(2.109) yield $\mathbf{X} = b\mathbf{e}(u) + \mathbf{N}$ with the desired properties that is identical to model B.

Generalised Monopulse estimator

The monopulse estimator Eq. (2.102) can be expanded to a general monopulse estimator for the model A. At $u = u_0$, we get with the abbreviations $d_{00} = \mathbf{d}^*(u)\mathbf{R}^{-1}\mathbf{d}(u)$, $d_{u0} = \mathbf{d}_u^*(u)\mathbf{R}^{-1}\mathbf{d}(u)$, $d_{uu} = \mathbf{d}_u^*(u)\mathbf{R}^{-1}\mathbf{d}_u(u)$ and omitting the dependance on u:

$$|b|^2 = |a|^2 d_{00} \tag{2.110}$$

$$\tilde{\mathbf{e}} = d_{00}^{-1/2}\mathbf{R}^{-1/2}\mathbf{d} \tag{2.111}$$

$$\tilde{\mathbf{e}}_u = d_{00}^{-1/2}\mathbf{R}^{-1/2}\mathbf{d}_u - d_{00}^{-3/2}\Re\{d_{u0}\}\mathbf{R}^{-1/2}\mathbf{d} \tag{2.112}$$

$$\begin{aligned}\mathbf{e}_u &= \tilde{\mathbf{e}}_u + (\tilde{\mathbf{e}}_u^*\tilde{\mathbf{e}})\tilde{\mathbf{e}} \\ &= d_{00}^{-1/2}\mathbf{R}^{-1/2}\mathbf{d}_u - d_{00}^{-3/2}d_{u0}^*\mathbf{R}^{-1/2}\mathbf{d}\end{aligned} \tag{2.113}$$

$$\|\mathbf{e}_u\|^2 = \|\tilde{\mathbf{e}}_u\|^2 - |\tilde{\mathbf{e}}_u^*\tilde{\mathbf{e}}|^2 = d_{00}^{-1}d_{uu} - d_{00}^{-2}|d_{u0}|^2 \tag{2.114}$$

As verification of the consistency of the CRB for the basic form (Eq. 2.94) with the general form, we may compute

$$\frac{1}{2|b|^2\|\mathbf{e}_u\|^2} = \frac{d_{00}}{2|a|^2(d_{00}d_{uu} - |d_{u0}|^2)}, \tag{2.115}$$

which in fact is consistent with Eq. (2.88).

We are now left with the derivation of the general forms of the sum and difference channels:

$$\begin{aligned}\sigma(\mathbf{x}) &= \mathbf{e}^*(u_0)\mathbf{x} \\ &= d_{00}^{-1/2}\left(\mathbf{d}^*(u_0)\mathbf{R}^{-1/2}\right)\mathbf{R}^{-1/2}\mathbf{z} = d_{00}^{-1/2}\mathbf{\Sigma}(\mathbf{z})\end{aligned} \tag{2.116}$$

$$\begin{aligned}\delta(\mathbf{x}) &= \mathbf{e}_u^*(u_0)\mathbf{x} \\ &= \left(d_{00}^{-1/2}\mathbf{d}_u^*\mathbf{R}^{-1/2} - d_{00}^{-3/2}d_{u0}\mathbf{d}^*\mathbf{R}^{-1/2}\right)\mathbf{R}^{-1/2}\mathbf{z} \\ &= d_{00}^{-1/2}\mathbf{\Delta}(\mathbf{z}) - d_{00}^{-3/2}d_{u0}\mathbf{\Sigma}(\mathbf{z})\end{aligned} \tag{2.117}$$

with $\mathbf{\Sigma}(\mathbf{z}) := \mathbf{d}^*(u_0)\mathbf{R}^{-1}\mathbf{z}$ and $\mathbf{\Delta}(\mathbf{z}) := \mathbf{d}_u^*(u_0)\mathbf{R}^{-1}\mathbf{z}$. Using (Eq. 2.102) we can derive the generalized monopulse estimator to

$$\begin{aligned}\widehat{\Delta u} &= \frac{1}{\|\mathbf{e}_u(u_0)\|^2}\Re\left\{\frac{\delta(\mathbf{x})}{\sigma(\mathbf{x})}\right\} \\ &= \frac{d_{00}^2}{d_{00}d_{uu}-|d_{u0}|^2}\Re\left\{\frac{\mathbf{\Delta}(\mathbf{z})}{\mathbf{\Sigma}(\mathbf{z})}-\frac{d_{u0}}{d_{00}}\right\}. \qquad (2.118)\end{aligned}$$

Finally, by using the beamformer vectors $\mathbf{b}_\Sigma = \mathbf{R}^{-1}\mathbf{d}(u_0)$ and $\mathbf{b}_\Delta = \mathbf{R}^{-1}\mathbf{d}_u(u_0)$, the estimator can be expressed as

$$\widehat{\Delta u} = \frac{|\mathbf{b}_\Sigma^*\mathbf{d}(u_0)|^2}{\mathbf{b}_\Sigma^*\mathbf{d}(u_0)\mathbf{b}_\Delta^*\mathbf{d}_u(u_0)-|\mathbf{b}_\Delta^*\mathbf{d}(u_0)|^2} \qquad (2.119)$$

$$\times\Re\left\{\frac{\mathbf{b}_\Delta^*\mathbf{z}}{\mathbf{b}_\Sigma^*\mathbf{z}}-\frac{\mathbf{b}_\Delta^*\mathbf{d}(u_0)}{\mathbf{b}_\Sigma^*\mathbf{d}(u_0)}\right\}. \qquad (2.120)$$

This form is exactly identical to that given in [13], where it was called 'corrected adaptive monopulse'. However, therein it was derived from another viewpoint, namely to linearly correct a monopulse quotient $Q = \Re\{\mathbf{b}_\Delta^*\mathbf{z}/\mathbf{b}_\Sigma^*\mathbf{z}\}$ to eliminate bias and slope of the interference-less quotient. In our derivations we have shown, that the generalized monopulse estimator Eq. (2.119) is a natural expansion of the simple monopulse estimator Eq. (2.102), therefore clearly possessing the same property of asymptotic efficiency. For u close to u_0, large SNR and a clipping prohibiting that the denominator comes close to zero, the variance of the generalized monopulse estimator approaches the CRB in Eq. (2.89) and (2.115).

2.5 Linear transformations

To reduce the technical and computational effort, transformations into a lower-dimensional data space is of interest. Starting from the standard model $\mathbf{Z} = a\mathbf{s}+\mathbf{Q}$ we regard a linear transformation described by the $K \times M$ dimensional matrix $\mathbf{T}$ transforming the data into a new K-dimensional data space via $\mathbf{Z}_{tr} = \mathbf{TZ}$. The resulting deterministic part is $\mathbf{s}_{tr} = \mathbf{Ts}$ and the interference is transformed by $\mathbf{J}_{tr} = \mathbf{TJ}$ leading to the new model $\mathbf{Z}_{tr} = a\mathbf{s}_{tr} + \mathbf{Q}_{tr}$. The transformed covariance matrix is given by $\mathbf{R}_{tr} = \mathbf{TRT}^*$.

2.5.1 Gain loss by linear transformations

The SNIR before transformation is $\gamma = |a|^2\mathbf{s}^*\mathbf{R}^{-1}\mathbf{s}$. Now we calculate the new SNIR γ_T after transformation:

$$\begin{aligned}\gamma_T &= |a|^2\mathbf{s}_{tr}^*\mathbf{R}_{tr}^{-1}\mathbf{s}_{tr} \qquad (2.121)\\ &= |a|^2\mathbf{s}^*\mathbf{T}^*\left(\mathbf{TRT}^*\right)^{-1}\mathbf{Ts}. \qquad (2.122)\end{aligned}$$

The loss induced by the transformation is

$$\text{Loss}_T = \frac{\gamma_T}{\gamma} = \frac{\mathbf{s}^*\mathbf{T}^*\left(\mathbf{T}\mathbf{R}\mathbf{T}^*\right)^{-1}\mathbf{T}\mathbf{s}}{\mathbf{s}^*\mathbf{R}^{-1}\mathbf{s}}. \tag{2.123}$$

2.5.2 Special transformations

Invertible transformation If $K = M$ and $\mathbf{T}$ is invertible, $\mathbf{T}$ and $\mathbf{T}^*$ can be shifted out of the brackets as their inverse yielding after cancellation with $\mathbf{T}$ and $\mathbf{T}^*$ the same expression as without transformation, there is no loss.

Transformation using the optimum beamformer If $K = 1$ and $\mathbf{T} = \left(\mathbf{R}^{-1}\mathbf{s}\right)^*$ we get no loss, too, which is easily varified. This is an extreme reduction of dimensionality, nevertheless it does not really spare computation since the inverse of the full covariance matrix has to be calculated.

Transformation into the subspace spanned by interference plus signal If the vectors $\mathbf{v}_1, \ldots, \mathbf{v}_k$ span the interference subspace, the transformation matrix

$$\mathbf{T} = \left(\mathbf{v}_1, \ldots, \mathbf{v}_K, \mathbf{s}\right)^* \tag{2.124}$$

also will not lead to a loss [5].

[5] Proof follows

Chapter 3

Air- and spaceborne radar

The aim of this chapter is to introduce the special situation of a radar mounted on an airplane or satellite. The main specific problem is that the radar itself is moving. All ground scatterers are moving relative to the radar, different radial velocities of fixed scatterers are the consequence. We will concentrate on the properties of the echoes from the temporal stable ground surface for an airborne radar - where the earth surface can be approximated by a plane - and for space based radar with an appropriate model of ta curved surface and a satellite orbit. The results are useful for synthetic aperture imaging as well as for moving target recognition. Throughout this chapter, the regarded time interval is short enough to justify a time-linear approximation of the phase.

3.1 Definition of basic angles

Before treating the ground echoes of an air- or spaceborne radar, let us define some angles which apply for flat as well as curved earth surface, see Fig. 3.1. The angle ϵ between the horizontal plane at the radar and the line-of-sight (LOS) to a point on the ground, characterized by the unit vector $\vec{u}$ is called *depression angle*. The angle $\vartheta = \epsilon + \pi/2$ is used for a mathematical description in a spherical coordinate system. On the earth surface the wave comes in at the *incidence angle* β with respect to the vertical axis at this point. It is also usual to measure the direction of the incoming wave relative to the horizontal plane. This angle $\gamma = \pi/2 - \beta$ is called *grazing angle*. In the literature, there are different definitions of the *elevation angle*. We will use this expression only in the relation to the antenna surface. For the approximation of a flat earth - which is usual for airborne radar with medium range - the grazing angle and the depression angle are equal $\gamma = \epsilon$ and for the incidence angle we get $\beta = \pi - \vartheta$.

Let the radar be moving in direction of the x-axis, see Fig. 3.1 right. The angle α between x-axis and the LOS is called *coneangle*, the angle φ between the x-axis and the projection of the LOS to the (x, y)-plane is called *azimuthangle*. Cone- and azimuth angle are related by

Glossary for this chapter

α	Cone angle
β	Incidence angle
$\delta r, \delta v, \delta F$	Resolutions in range, velocity and Doppler
δu	Resolution in directional cosine
ΔT	Pulse repetition period
Δx	Spacing of synthetic array
$\vec{\delta}_r, \vec{\delta}_v$	Edges of a resolution patch on ground
ϵ	Depression angle
φ	Azimuth angle
γ	Grazing angle
λ	Wavelength
ω_E	Rotation velocity of the earth
Ω_{BA}	Angular velocity matrix
σ_0	Terrain scattering coefficient
ϑ	Angle between z axis and look direction
A	Area of a ground resolution patch
B_{main}, B_{tot}	Main beam and total Doppler bandwidths
$D(u), D(\vec{u})$	Two-way characteristics of antenna
F	Doppler frequency
F_s	Sampling frequency in slow time = PRF
$F_{max} = 2V/\lambda$	Maximum clutter Doppler frequency
$\mathbf{G}, \mathbf{H}$	Mappings from the earth surface to the range-velocity plane
h	Flight altitude over ground
l_x	Length of antenna in flight direction
L_x	Length of synthetic array
$\mathbf{L}_{BA}$	Rotation matrix from the system A to the system B
$\vec{p}$	Position of a scatterer
$P_C(F)$	Doppler power spectrum of clutter
$PRF = F_s$	Pulse repetition frequency
r	Range to scatterer
r_g	Ground range
$\vec{r}, \vec{r}_g$	Vector from the antenna to a scatterer and its ground projection
$\vec{R}, \vec{R}_g$	Position of the antennas phase center and its ground projection
$u = \cos\alpha$	Cosine of cone angle
$\vec{u} = (u, v, w)^t$	Unit vector pointing from the antenna to a scatterer
$\vec{V}$	Platform velocity vector
V	Platform velocity
v_r	Radial velocity
$W(\sin\gamma)$	Weighting function for reflectivity
(x_A, y_A, z_A)	Antenna coordinate system
(x_e, y_e, z_e)	Earth fixed coordinate system with origin at the surface
(x_E, y_E, z_E)	Earth fixed coordinate system with origin at the center
(x_I, y_I, z_I)	Inertial coordinate system
(x_P, y_P, z_P)	Platform coordinate system

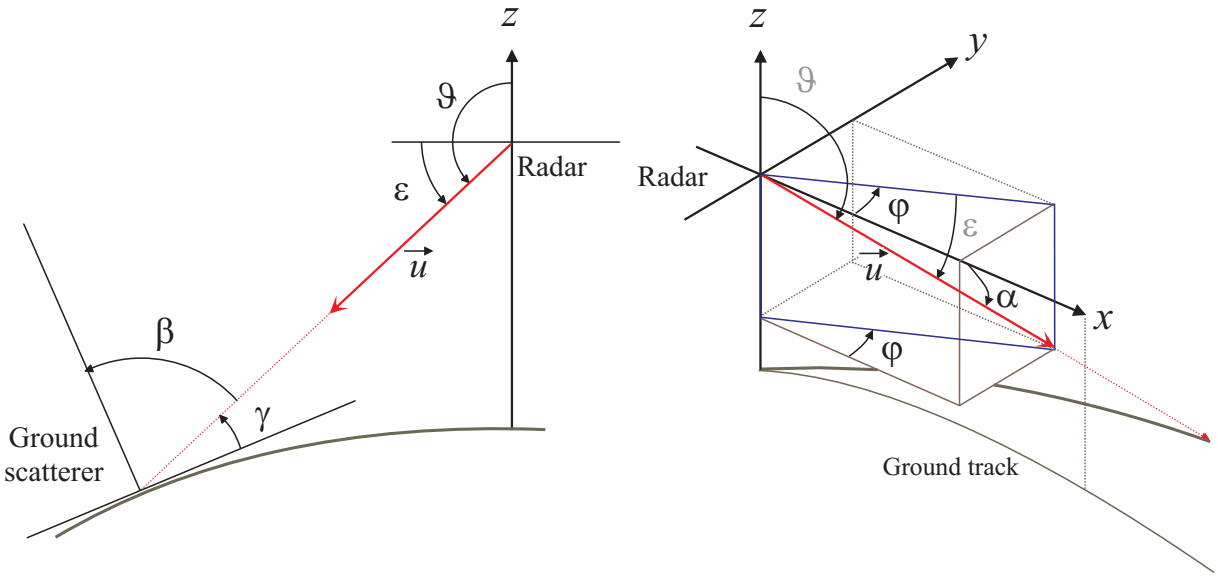

Figure 3.1: *Left: Definition of angles in the vertical plane: β: Incidence angle, ϵ: Depression angle, γ: Grazing angle, ϑ: Angle used for spherical coordinate system. Right: φ: Azimuth angle, α: Cone angle*

$$\cos\alpha = \cos\varphi\cos\epsilon. \tag{3.1}$$

3.2 Airborne radar

3.2.1 Energy distribution in range and Doppler

To get a feeling of the expected ground returns, in Fig. 3.2 a coarse distribution of the energy of the ground-returns is depicted for a forward looking configuration. If the flight altitude is h, the first return in range comes from the surface patch directly under the airplane containing the *nadir* , i.e. the projection of the antennas phase center to the ground plane. Since the range is minimum, and the area of this patch is relatively large, and since the wave comes in perpendicular to the surface producing a *specular reflection*, this echo is very strong and appears normally also in the data, if the nadir direction is outside the main beam of the antenna. In the area of illumination of the ground by the main beam, the mean echo power is - apart from the modulation by the antenna pattern - decreasing proportional to r^{-4} according to the range law Eq.(1.188).

In the Doppler domain also a strong nadir return is observed at the Doppler frequency zero, since the radial velocity of a scatterer directly under the platform vanishes according to the LOS being perpendicular to the flight path. In the main beam illumination area the radial velocities of the ground scatterers with respect to the platform vary between $v_r^{(1)} = -V\cos\alpha_1$ and $v_r^{(2)} = -V\cos\alpha_2$ where α_1 and α_2 are the cone angles at the boundaries of the main beam. This leads to

a Doppler spread over the interval $[F_{max}\cos\alpha_1, F_{max}\cos\alpha_2]$ with $F_{max} = 2V/\lambda$. Doppler frequencies with magnitudes larger then F_{max} can never appear for non moving scatterers. Also the power of the spectrum is governed by the elevation pattern of the antenna and the r^{-4} law.

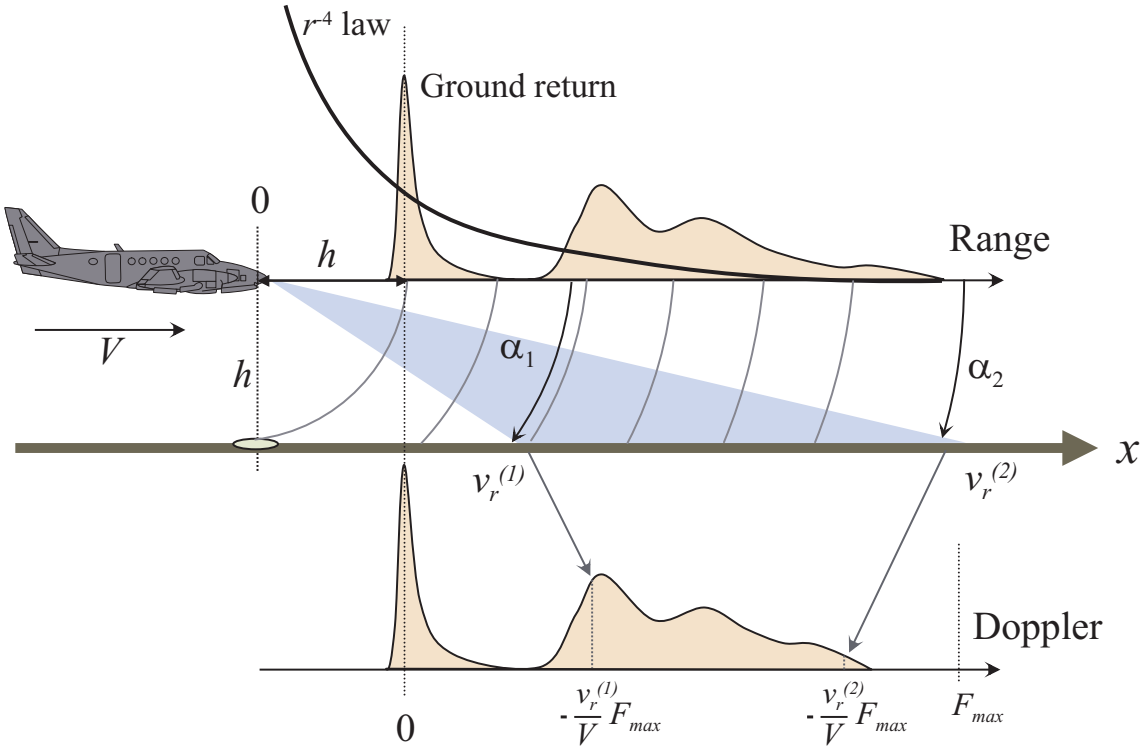

Figure 3.2: *Energy distribution of the ground-returns in range and Doppler*

3.2.2 Three dimensional geometry for horizontal flight

For airborne radar, we may assume the earth surface to be flat. Let the platform - with the antenna's phase center as the reference point - move along a straight flight path with constant velocity $\vec{V}$. Fig. 3.3 shows the geometrical situation for horizontal flight at the altitude h above ground. At a fixed point of time the position of the antenna's phase center is $\vec{R}$.

We discriminate three identically orientated cartesian coordinate systems, one fixed to the platform (x_P, y_P, z_P) with the antennas phase center at its origin and x_P arranged to the direction of motion and one to the earth (x_e, y_e, z_e) where $z_e = 0$ at the earth's surface and the last $(x_{e'}, y_{e'}, z_{e'})$ centered to the ground point directly beneath the platform, the nadir. The vector $\vec{r}$ from the antenna's phase center to a ground scatterer at the position $\vec{p}$ is given by $\vec{r} = \vec{p} - \vec{R}$. The unit vector $\vec{u} = \vec{r}/\|\vec{r}\|$ represents the LOS-vector.

The ground range vector $\vec{R}_g$ is the projection of the platform vector $\vec{R}$ to the earth plane, $\vec{r}_g$ the projection of the vector $\vec{r}$. The lengths of the latter vectors are denoted by r and $r_g = \sqrt{r^2 - h^2}$, respectively.

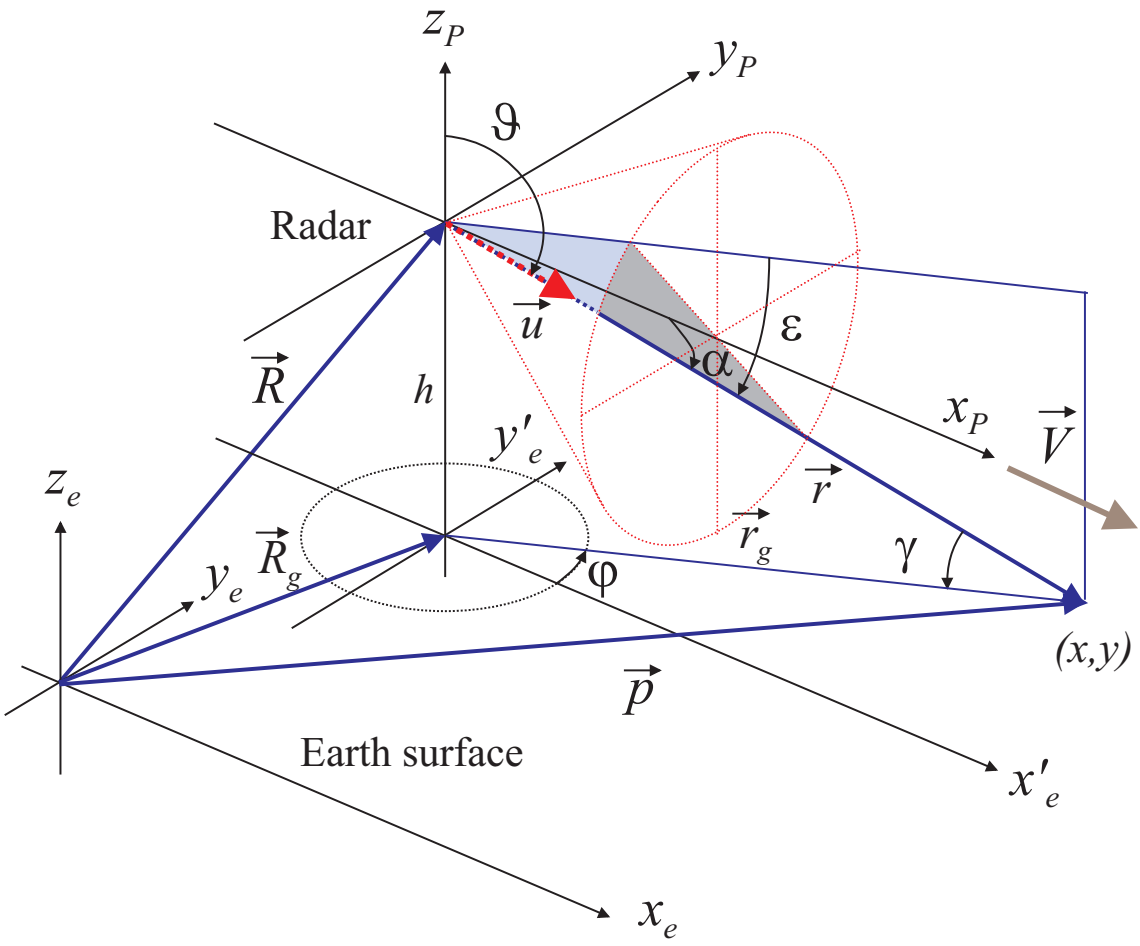

Figure 3.3: *Three dimensional geometry for horizontal flight*

The LOS-vector $\vec{u}$ can be expressed by spherical polar coordinates with respect to the platform coordinate system:

$$\vec{u} = \begin{pmatrix} \sin\vartheta\cos\varphi \\ \sin\vartheta\sin\varphi \\ \cos\vartheta \end{pmatrix} = \begin{pmatrix} \cos\epsilon\cos\varphi \\ \cos\epsilon\sin\varphi \\ -\sin\epsilon \end{pmatrix}. \tag{3.2}$$

Since the earth surface is assumed to be flat, the grazing angle γ is equal to the depression angle φ and related to the range via $\sin\gamma = \sin\epsilon = h/r$. The radial velocity of any point scatter with respect to the antenna's phase center is given by $v_r =< \vec{V}, \vec{u} >= V\cos\alpha$ where α is the cone angle.

3.2.3 ISO-Range and ISO-Doppler contours

In Fig. 3.4 the correspondence of the radar parameters range and Doppler in the three dimensional space and on the earth surface is illustrated. Clearly, the points of equal range r to the antenna's phase center are placed on the surface of a sphere with radius r centered at $\vec{R}$ and the points of equal radial velocity of non moving

scatterers on the surface of a cone with the cone angle α and its corner at $\vec{R}$. The lines in the three-dimensional space with equal range and radial velocity are cuts of that spheres with that cones: They are circles orientated perpendicular to the flight path.

The lines on the earth surface with the same distance to the phase center (*ISO-range lines*) are the cuts of the range sphere with the earth planes, i.e. circles with its center at the nadir. The lines with the same radial velocity are the cuts of the above mentioned cone surfaces with the earth plane, i.e. parabulae. At a fixed RF the radial velocity is proportional to the Doppler frequency, so the cone can also be called *Doppler cone* and the cone cuts with the earth surface *ISO-Doppler lines* .

Also in the case of non-horizontal flight the ISO-Doppler lines are cone-cuts: for ascending flight directions they are hyperbolae, for descending flight they also can be ellipses.

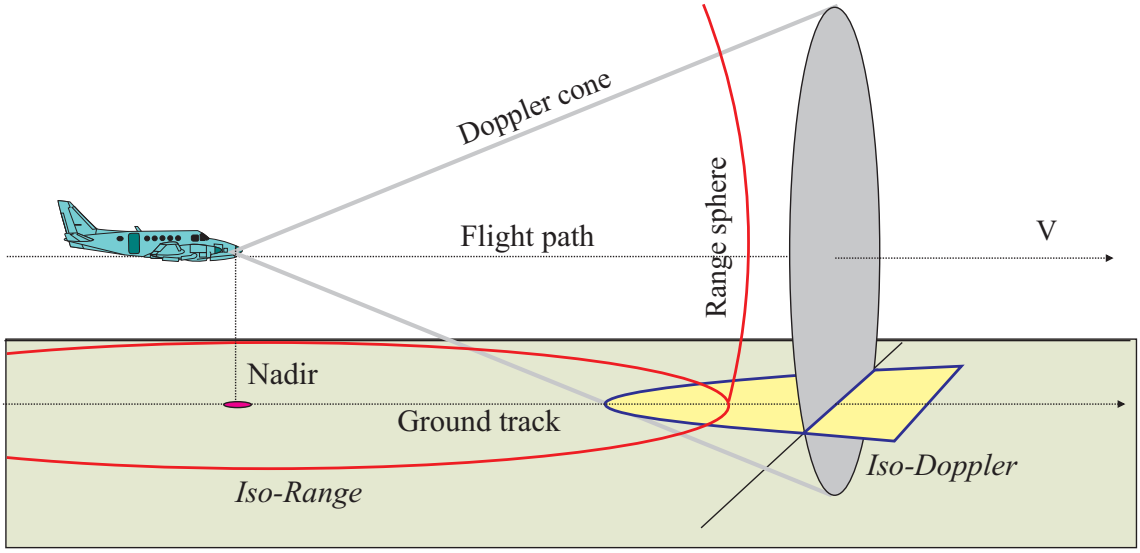

Figure 3.4: *Range sphere and Doppler cone*

Fig. 3.5 shows a projection of the ISO-range and ISO-Doppler contours to the earth plane for a side-looking radar. In this figure, also the antenna pattern as it illuminates the earth surface is indicated. Already by inspecting this figure it becomes clear that the Doppler spectrum of a homogeneous area is related to the antenna pattern. We will deepen this fact in the following.

Essence 3.1 *The ISO-range lines on the surface are circles centered at the nadir, the ISO-Doppler lines are cuts of the Doppler-cone with the surface. The Doppler-cone has its axis in flight direction and its corner at the antennas phase center, the cone angle α is related to the radial velocity by $v_r = -V \cos \alpha$.*

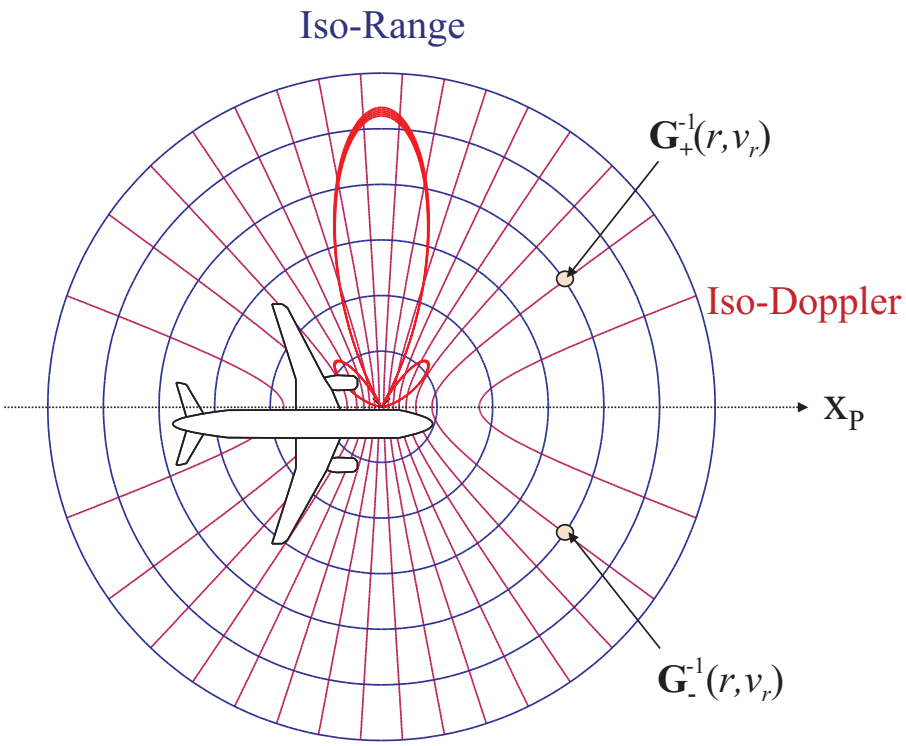

Figure 3.5: *ISO-range and ISO-Doppler contours*

3.2.4 Mapping between range - radial velocity and earth surface

In the following we will investigate the mapping from a position on the ground to the radar parameters range/radial velocity (range/Doppler, respectively), and vice versa. For each point $(x, y)^t$ on the ground surface measured in nadir-centered coordinates $(x_{e'}, y_{e'}, z_{e'})$, see Fig. 3.3, range and radial velocity are determined by the mapping

$$\mathbf{G}(x,y) \;=\; \begin{pmatrix} r \\ v_r \end{pmatrix}(x,y) = \begin{pmatrix} \sqrt{x^2+y^2+h^2} \\ \\ -V\frac{x}{\sqrt{x^2+y^2+h^2}} \end{pmatrix}. \tag{3.3}$$

The mapping is symmetric in y, i.e. $\mathbf{G}(x,-y) = \mathbf{G}(x,y)$. It is unique on the half space $y > 0$. The inverses of the restrictions to the positive and the negative half space, respectively, are given by the functions $\mathbf{G}_+$ and $\mathbf{G}_-$, defined by

$$\mathbf{G}_{\pm}^{-1}(r,v_r) \;=\; \begin{pmatrix} x \\ y_\pm \end{pmatrix}(r,v_r) = \begin{pmatrix} -r\frac{v_r}{V} \\ \\ \pm\sqrt{r^2\left(1-\left(\frac{v_r}{V}\right)^2\right)-h^2} \end{pmatrix}. \tag{3.4}$$

ISO-range and ISO-Doppler lines in (x, y)-coordinates are easily derived by

Eq. (3.4), considering the unique relation between radial velocity and Doppler $F = -\frac{v_r}{V} F_{max}$, as long as no Doppler ambiguities arise. A range-Doppler pair (r, F) is related to the two points $\mathbf{G}_+^{-1}(r, v_r)$ and $\mathbf{G}_-^{-1}(r, v_r)$ on the earth with $v_r = -VF/F_{max}$, see Fig. 3.5.

Consequently, the range-Doppler map generated in the radar processor according to Fig. 1.16 can be regarded as a first coarse radar image of the earth surface which is left-right ambiguous with respect to the flight path. If a side-looking antenna is used as in Fig. 3.5 where the antenna gain to the back plane can be neglected, this ambiguity vanishes and a one-to-one correspondence between range-Doppler map and the half space on the earth surface is established.

Analogue to Eq. (3.3) we may express these relations also using polar coordinates (r_g, φ) on ground with $(x, y) = (r_g \cos\varphi, r_g \sin\varphi)$ defining a referring mapping $\mathbf{H}$ by

$$\mathbf{H}(r_g, \varphi) = \begin{pmatrix} r \\ v_r \end{pmatrix}(r_g, \varphi) = \begin{pmatrix} \sqrt{r_g^2 + h^2} \\ -V \frac{r_g}{\sqrt{r_g^2+h^2}} \cos\varphi \end{pmatrix}. \tag{3.5}$$

Again, $\mathbf{H}$ is unambiguous in the half spaces, and the inverses are given by

$$\mathbf{H}_\pm^{-1}(r, v_r) = \begin{pmatrix} r_g \\ \varphi_\pm \end{pmatrix}(r, v_r) = \begin{pmatrix} \sqrt{r^2 - h^2} \\ \pm \arccos\left(\frac{v_r r}{V\sqrt{r^2-h^2}}\right) \end{pmatrix}. \tag{3.6}$$

Essence 3.2 *For each range-velocity pair (r, v_r) there are two points on the earth surface generating echo signals at (r, v_r). Their positions are symmetric to the flight path projected on the ground.*

3.3 Real and synthetic arrays

There are many correspondences between a real array and sampling during the flight: The sampling interval $\Delta T = 1/F_s$ in slow time is transferred by the platform's motion into a spatial sampling $\Delta x = V\Delta T$ along the flight path. In this way, a *synthetic array* is generated whose properties are quite similar to a real array, see Tab. 3.3.

The signal model for a sequence of N pulses assuming a scatterer in direction u is given by

$$\mathbf{s}(u) = \begin{pmatrix} e^{j2k_r u\Delta x} \\ \vdots \\ e^{j2k_r uN\Delta x} \end{pmatrix}. \tag{3.7}$$

This is mathematically identical to the model of a DOA-vector for a real array, Eq. (2.1) apart from an additional factor 2 in the exponent regarding the two-way

	Real array	Synthetic array	Temporal interpretation
Spatial sampling Array length Directional cosine resolution	Δx_a l_x $\delta u_a = \lambda/l_x$	$\Delta x = V\Delta T$ $L_x = VT_{int}$ $\delta u = \lambda/(2L_x)$	
Maximum spatial frequency Maximum Doppler frequency	$k_{xmax} = 2\pi/\lambda$	$k_{xmax} = 4\pi/\lambda$	 $F_{max} = 2V/\lambda$
Spatial frequency Doppler frequency	$k_x = uk_{xmax}$	$k_x = uk_{xmax}$	 $F = -uF_{max}$
k-ambiguity Doppler ambiguity	$\Delta k_x = 2\pi/\Delta x_a$	$\Delta k_x = 2\pi/\Delta x$	 $\Delta F = 1/\Delta T$
Directional cosine ambiguity Nyquist condition to cover $[u_1, u_2]$	$\Delta u = \lambda/\Delta x$ $\Delta x \leq \frac{\lambda}{u_2 - u_1}$	$\Delta u = \lambda/(2\Delta x)$ $\Delta x \leq \frac{\lambda}{2(u_2 - u_1)}$	$\Delta u = \Delta F/F_{max}$ $\Delta T \leq \frac{\lambda}{2V(u_2 - u_1)}$

Table 3.1: Relations for real and synthetic arrays

travelling of the wave. So the properties of a real array can be transferred to the synthetic array analogue.

Spatial frequency A Doppler frequency F can also be regarded as a spatial frequency along the flight path with $k_x = (2\pi F/V)F$. Clutter Doppler frequencies $F(u) = -2uV/\lambda$ are transferred to clutter spatial frequencies via $k_x(u) = -4\pi u/\lambda = -2uk_r$.

Beamforming Doppler processing can be interpreted as the formation of a *synthetic beam* for each Doppler cell with Doppler frequency F to that direction $u(F) = -F/F_{max}$ corresponding to the clutter Doppler frequency F. If the Doppler filter is applied over a time interval of length T_{int}, the platform has moved over a distance $L_x = VT_{int}$. This is the length of the synthetic array, the *synthetic aperture*. Though this expression is used mainly related to the SAR technique, it can be applied with meaning also for air- or space borne MTI. In this chapter, we presume that L_x is small enough to approximate the wavefronts to be planar, i.e. the phase propagation along the synthetic aperture can be assumed to be linear. In other words: The synthetic array is small enough to accept the far field condition given for real antennas (Eq. (**??**)) and considering a factor 2: $L_x \leq \sqrt{r\lambda}$ with an allowed phase deviation from a linear function not larger than $\pm\pi/4$.

Ambiguities Due to the finite sampling along the aperture with period Δx, ambiguities arise in the directional cosine according to $\Delta u = \lambda/(2\Delta x)$ like that of a real array (see Eq. (2.17)). These are directly related to the Doppler ambiguity $\Delta F = F_s$ via $\Delta u = \Delta F/F_{max}$. Therefore, to cover a directional cosine interval $[u_1, u_2]$ unambiguously the spatial sampling period according to the Nyquist condition must not be larger than $\Delta x = \lambda/(2(u_2 - u_1))$.

Interaction between real and synthetic characteristics The Doppler ambiguities can be suppressed, if the main beam of the real array is smaller than the ambiguities in the directional cosine caused by Doppler ambiguities. This means, the beamwidth of the real array δu_a has to be smaller than the ambiguity of the synthetic beam Δu. It follows

$$\begin{aligned} \delta u_a &\leq \Delta u && (3.8)\\ \frac{\lambda}{l_x} &\leq \frac{\Delta F}{F_{max}} && (3.9)\\ l_x &\geq \frac{\lambda F_{max}}{\Delta F} = 2V\Delta T. && (3.10) \end{aligned}$$

This means that the antenna length has to be larger or equal to twice the way the platform moves from pulse to pulse.

The output of a Doppler filter for frequency F_0 forms a beam to the direction $u_0 = -F_0/F_{max}$. So the response $h(F, F_0)$ of this Doppler filter to other frequencies F can also be regarded as a spatial characteristics $D_{dop}(u, u_0) = h(-uF_{max}, -u_0F_{max}$ of the synthetic array. If $D(u)$ is the two-way characteristics of the real antenna, the sensitivity of the Doppler filter output to clutter echoes from direction u is given by the product of the two characteristics:

$$H(u, u_0) = D(u)D_{dop}(u, u_0). \tag{3.11}$$

This is illustrated in Fig. 3.6.

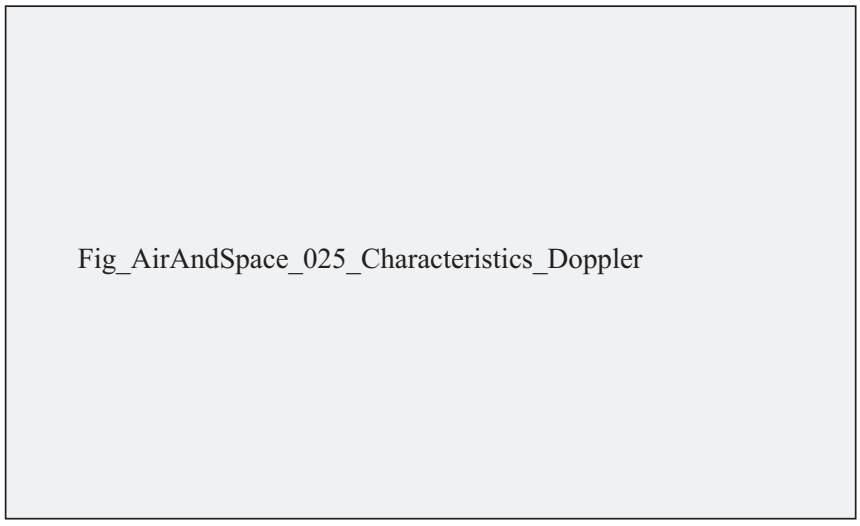

Figure 3.6: *The combination of Dopper filter transfer function and spatial characteristics for clutter*

Range-Doppler resolution patch on the earth surface

By the radar processor range-Doppler cells are generated with the resolutions δr and δF. Range - radial velocity resolution cells are derived from this with the resolutions δr and $\delta v = \delta F \lambda/2$. We now look for the area on the earth surface corresponding to δr and δv? These are areas with the form of grid cells shown in Fig. 3.5 if the spacing between the ISO-range and the ISO-Doppler lines are chosen as the relating resolutions.

Inspecting Eq. (3.4) the derivations with respect to r and v_r are given by

$$\vec{g}_r := \frac{\partial}{\partial r}\mathbf{G}_+^{-1}(r, v_r) = \begin{pmatrix} -\frac{v_r}{V} \\ \frac{r\left(1-\left(\frac{v_r}{V}\right)^2\right)}{\sqrt{r^2\left(1-\left(\frac{v_r}{V}\right)^2\right)-h^2}} \end{pmatrix} = \begin{pmatrix} -\cos\alpha \\ \frac{r}{y}\sin^2\alpha \end{pmatrix} \tag{3.12}$$

$$\vec{g}_v := \frac{\partial}{\partial v_r}\mathbf{G}_+^{-1}(r, v_r) = \begin{pmatrix} -\frac{r}{V} \\ \frac{-r^2\frac{v_r}{V^2}}{\sqrt{r^2\left(1-\left(\frac{v_r}{V}\right)^2\right)-h^2}} \end{pmatrix} = -\frac{r}{V}\begin{pmatrix} 1 \\ \frac{r}{y}\cos\alpha \end{pmatrix}. \tag{3.13}$$

So, as long as linearity is justified, the resolution cell in range and radial velocity on the earth surface is approximately given by a parallelogram with the edges determined by the vectors $\vec{\delta}_r = \delta r \vec{g}_r$ and $\vec{\delta}_v = \delta v \vec{g}_v$, see Fig. 3.7.

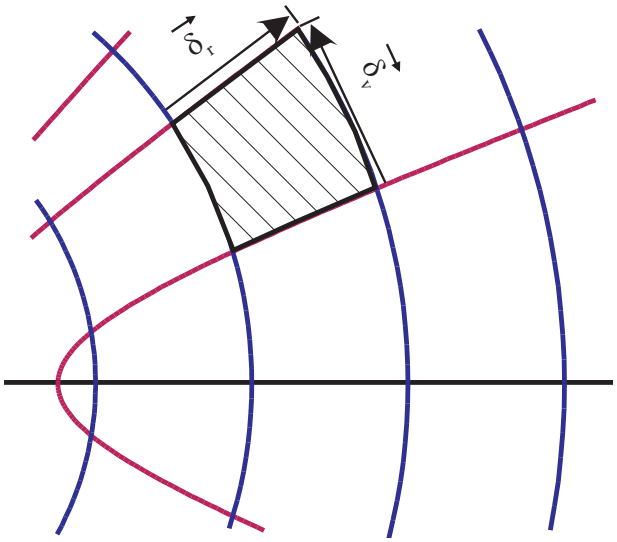

Figure 3.7: *A range Doppler resolution patch*

The area of this patch is easily determined from Eq. (3.12):

$$A_{res} = \|\vec{\delta}_r \times \vec{\delta}_v\| = \frac{r^2}{|y|V}\delta r \delta v = \frac{r^2}{|y|V} a_{res} \tag{3.14}$$

with the resolution area $a_{res} = \delta r \delta v = \frac{c_0}{2b}\frac{\lambda}{2T_{int}}$ in the original (r, v_r) plane. Obviously, the grid degenerates in the vicinity of $y = 0$. The reason is that the slope of the

radial velocity (Doppler) in the y-direction is zero for $y = 0$. We will find this property also in the application to SAR imaging.

3.3.1 The Doppler spectrum of clutter

Coarse consideration in two dimensions

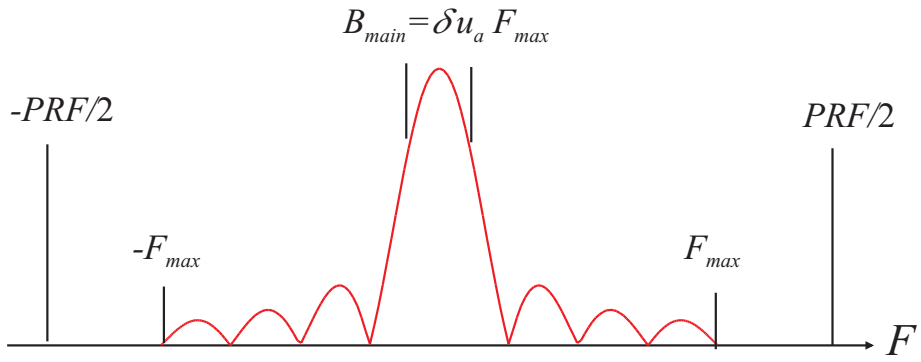

Figure 3.8: *Doppler Spectrum of clutter*

Let's go back to Fig. 3.5 and assume that the antenna pattern is zero on the half space $y < 0$. Let the two-way antenna characteristics $D(u)$ be dependent in the first place only on the directional cosine u. In direction u the radial velocity of the stationary ground scatterers is given by the linear relation $F(u) = -uF_{max}$ or $u(F) = -F/F_{max}$, vice versa. So in this direction the ground echoes at Doppler F are weighted by the antenna characteristics $D(u(F))$. From this, we can derive the coarse form of the Doppler spectrum of the ground echoes:

If the reflectivity of the ground is homogeneous, or if the Doppler power spectrum is averaged over a long time, we get

$$P_C(F) \approx const \left| D\left(\frac{F}{F_{max}}\right)\right|^2 . \tag{3.15}$$

In other words, the Doppler power spectrum is a *scaled version of the two-way antenna pattern.* This fact is illustrated in Fig. 3.8. In the application of moving target indication, the ground echoes are regarded as *clutter* and their Doppler spectrum are called *clutter spectrum.* It can be divided into three areas:

- *The main beam clutter.* It's bandwidth is given by $B_{main} = \delta u_a F_{max}$, where δu_a denotes the beamwidth of the two-way characteristics.
- *The sidelobe clutter.* The spectrum is sharply bounded by the condition $-1 \leq u \leq 1$. So we have for the bandwidth of the whole clutter spectrum: $B_{tot} = 2F_{max}$.

- *The clutter free region.* This is outside the bandwidth B_{tot}.

For most airborne radar systems, it is impossible to cover all of the sidelobe clutter or even parts of the clutter free region unambiguously by the sampling frequency F_s = PRF. This can be achieved only if $\Delta T > 1/B_{tot} = \lambda/(4V)$, i.e. the pulse repetition interval has to be shorter than the time needed by the platform to fly the distance of $\lambda/4$. For GHz frequencies and normal airspeed this would require a PRF larger than allowed to avoid range ambiguities. As a consequence, normally at least the sidelobe part of the clutter will be aliased, so there will hardly be any completely clutter-free region! Common SAR systems apply an azimuth sampling frequency equal to or a little above B_{main}, MTI-systems should use a considerably higher PRF!

To sample the main beam clutter according to the Nyquist criterium F_s has to be larger or equal to B_{main}. For the way the airplane is allowed to fly between two pulses follows $V\Delta T \leq V/B_{main} = \lambda/(2\delta u_a)$. If we insert the main beam width $\delta u_a = \lambda/l_x$ of an antenna of length l_x, we get

$$B_{main} = \frac{V}{l_x/2}, \quad V\Delta T \leq \frac{l_x}{2}, \tag{3.16}$$

so the airplane should not move more than a half antenna length between two pulses.

Essence 3.3 *The clutter spectrum can be approximated as the two way antenna pattern scaled via $u = -F/F_{max}$ with $F_{max} = 2V/\lambda$. Three areas of the clutter spectrum can be discriminated: the main beam clutter, the sidelobe clutter and the clutter free region $|F| > F_{max}$.*

Clutter spectrum - three dimensional derivation

Let us have a closer look to the clutter spectrum taking all three dimensions into account! The two-way antenna characteristics $D(\vec{u})$ now is expressed as function of the LOS-vector $\vec{u}$. For a certain fixed range r there are two patches on the earth surface effecting the Doppler frequency F, namely at $\mathbf{G}_+^{-1}(r, -VF/F_{max})$ and $\mathbf{G}_-^{-1}(r, -VF/F_{max})$, see Eq. (3.4). There are two LOS-vectors $\vec{u}_\pm(r, F)$ pointing to these points which can be evaluated to

$$\vec{u}_\pm(r, F) = \begin{pmatrix} u \\ \pm\sqrt{1-u^2-w^2} \\ -w \end{pmatrix} \tag{3.17}$$

$$\text{with } u = \cos\alpha = -\frac{F}{F_{max}} \tag{3.18}$$

$$w = \sin\epsilon = \sin\gamma = h/r. \tag{3.19}$$

The areas of the patches have been calculated to $A = \frac{r^2}{|y|V}\delta r\delta v$, see Eq. (3.12), which can be further expressed as

$$A(r,F) = \frac{r^2}{V\sqrt{1-\left(\frac{F}{F_{max}}\right)^2-\left(\frac{h}{r}\right)^2}}\delta r\delta v. \tag{3.20}$$

For homogeneous 'spatial white' clutter the energy coming from the directions $\vec{u}_\pm(r,F)$ will be proportional to the patch area. Summarizing, the power of the clutter spectrum at range r can be approximated by

$$P_C(r,F) \approx const\left(|D(\vec{u}_+(r,F))|^2+|D(\vec{u}_-(r,F))|^2\right)A(r,F)r^{-4}W(h/r)\sigma_0. \tag{3.21}$$

Here, σ_0 - sometimes written in texts simply as '*sigma zero*' - denotes the *terrain scattering coefficient*, i. e. the *reflectivity* of the surface, which is defined by the property that an area a of that type of surface has the RCS $q = a\sigma_0$. Tables of σ_0 for different kinds of vegetation depending on the frequency and the grazing angle have been published. $W(\sin\gamma)$ is a weighting function reflecting the influence of the grazing angle. In the simplest case, set $W(w) = w$ to take into account that the effective area perpendicular to the LOS is equal to $\sin\gamma$ times the ground area. Remind that the approximation for $A(r,F)$ is not valid in the vicinity of $y = 0$!

3.4 Ambiguities and the critical antenna size

In this section we will have a closer look to the ambiguities in range and radial velocity. To suppress ambiguities, the antenna's main beam must not cover more than one ambiguity rectangle. This leads to a condition to the minimum size of the real aperture.

3.4.1 Range ambiguities

Let's first study range ambiguities $\Delta r = \frac{c_0}{2}\Delta T$ effected by a low pulse repetition interval $\Delta T = 1/F_s$. That means that in a range resolution cell dedicated to the primary range r also the echoes from all the ranges $r_\nu = r + \nu\Delta r$ with $\nu \in \mathbb{Z}$ and $r_\nu \geq h$ are superposed. From Eq. (3.6) follows for the ambiguous ground ranges:

$$r_g^{(\nu)} = \sqrt{r_\nu^2 - h^2}. \tag{3.22}$$

This is illustrated in Fig. 3.9. The desired range r might be in a secondary range ambiguity interval like indicated in the illustration. The range ambiguities cause elevation angle ambiguities according to

$$\epsilon_\nu = \arcsin\left(\frac{h}{r_\nu}\right). \tag{3.23}$$

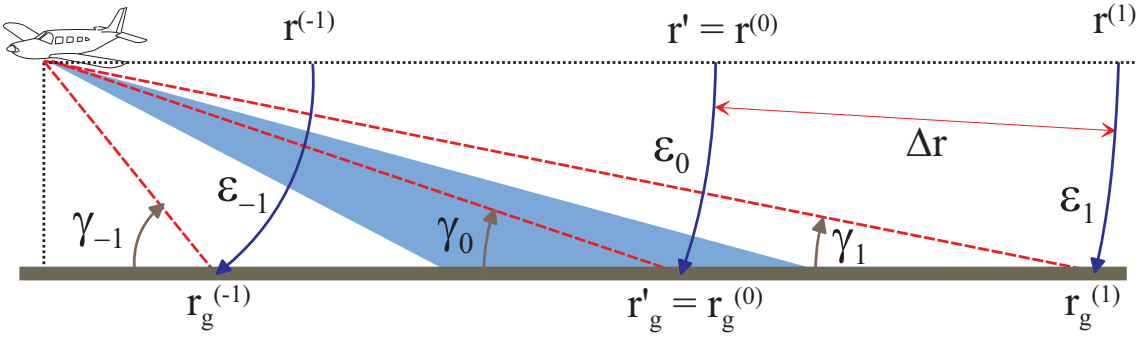

Figure 3.9: *Range ambiguities*

3.4.2 Azimuth ambiguities

Due to low PRF sampling, ambiguities in the Doppler frequency are introduced with the period $\Delta F = 1/\Delta T$ resulting in a velocity ambiguity with the period $\Delta v = \lambda/(2\Delta T)$. So the Doppler filter for the radial velocity v_r also receives signals from scatterers with the radial velocities $v_\mu = v_r + \mu\Delta v$, $\mu \in \mathbb{Z}$. That means that we receive not only echoes from points on the Doppler cone with the cone angle α with $\cos\alpha = v_r/V$, but also from all those cones with the cone angles $\cos\alpha_\mu = v_\mu/V$ for which $|v_\mu| \leq V$, see Fig. 3.10.

Since $\cos\alpha = \cos\varphi\cos\epsilon$, there follows for fixed depression angle ϵ, i.e. for a fixed range, an ambiguity of the azimuth angle:

$$\varphi_\mu = \pm\arccos\left(\frac{v_\mu}{V\cos\epsilon}\right) = \pm\arccos\left(\frac{v_\mu r}{V\sqrt{r^2-h^2}}\right). \tag{3.24}$$

3.4.3 Full description of ambiguities

We can fit together the two types of ambiguities by inserting $r_\nu = r + \nu\Delta r$ and $v_\mu = v_r + \mu\Delta v$ into Eq. (3.6) and we get

$$\begin{pmatrix} r_g \\ \varphi_\pm \end{pmatrix}_{\nu\mu} = \begin{pmatrix} \sqrt{r_\nu^2 - h^2} \\ \pm\arccos\left(\frac{v_\mu r_\nu}{V\sqrt{r_\nu^2-h^2}}\right) \end{pmatrix}. \tag{3.25}$$

The result is a grid on the earth surface, which is principally the same as in Fig. 3.5, if the ISO-range and ISO-Doppler contours are drawn in the raster of Δr and ΔF.

An area bounded by the lines $r_\nu \leq r \leq r_{\nu+1}$ and $v_\mu \leq v_r \leq v_{\mu+1}$ forms an *ambiguity facet* on the earth surface. In the range-Doppler map generated by the processor, the contributions of all ambiguity facets are superposed, weighted by the antenna characteristics and the r^{-4}-law.

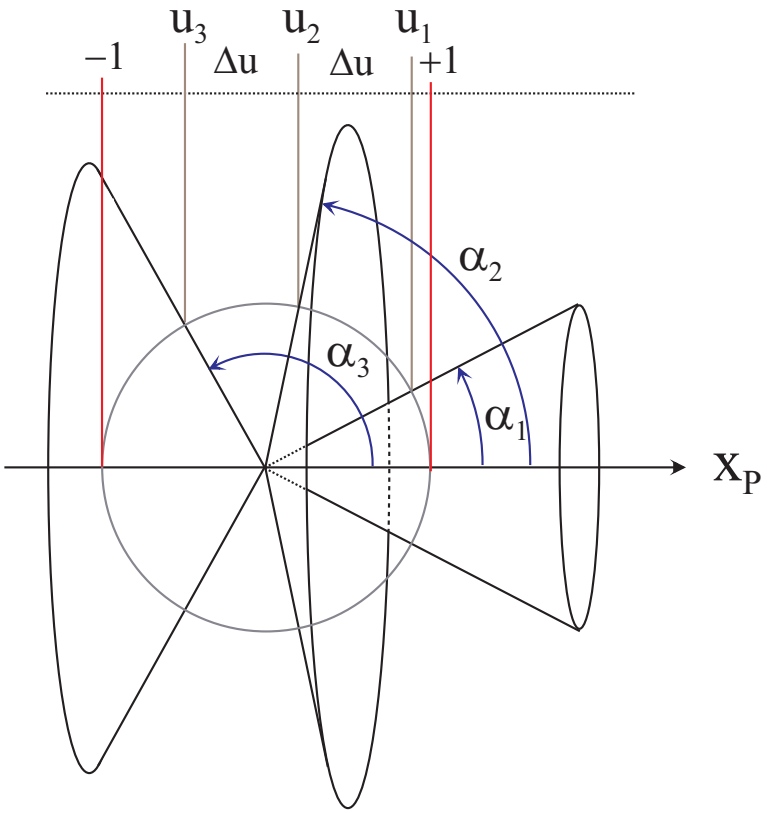

Figure 3.10: *Azimuth ambiguities*

For a side-looking configuration we regard the main ambiguity facet around the line perpendicular to the flight path, see Fig. 3.11. A rectangular in the (v, r) plane with the lateral lengths Δv and Δr corresponds to a circular ring segment bounded by parabulae on the earth surface. The extensions in x- and y-direction are approximately given by

$$\Delta\xi \approx r\frac{\Delta v}{V} \text{ and } \Delta y \approx \frac{\Delta r}{\cos\epsilon} \tag{3.26}$$

where ϵ is the depression angle at the reference point $(\sqrt{r^2 - h^2}, 0)$. From this we get the area of the ambiguity facet

$$A_{amb} \approx \Delta\xi\Delta y \approx \frac{r}{V\cos\epsilon}\Delta v\Delta r = \frac{r}{V\cos\epsilon}\frac{\lambda c_0}{4}. \tag{3.27}$$

Note that this expression is independent on the PRF and is given only by a few basic parameters.

As a numerical example we regard the following figures: $r = 700$ km, $V = 7600$ m/s, $\lambda = 3$ cm, $\epsilon = 45$ deg. It follows an ambiguity area of 293 km^2. For earth observation satellites this number can only be changed significantly by choosing another wavelength since the other parameters are more or less given.

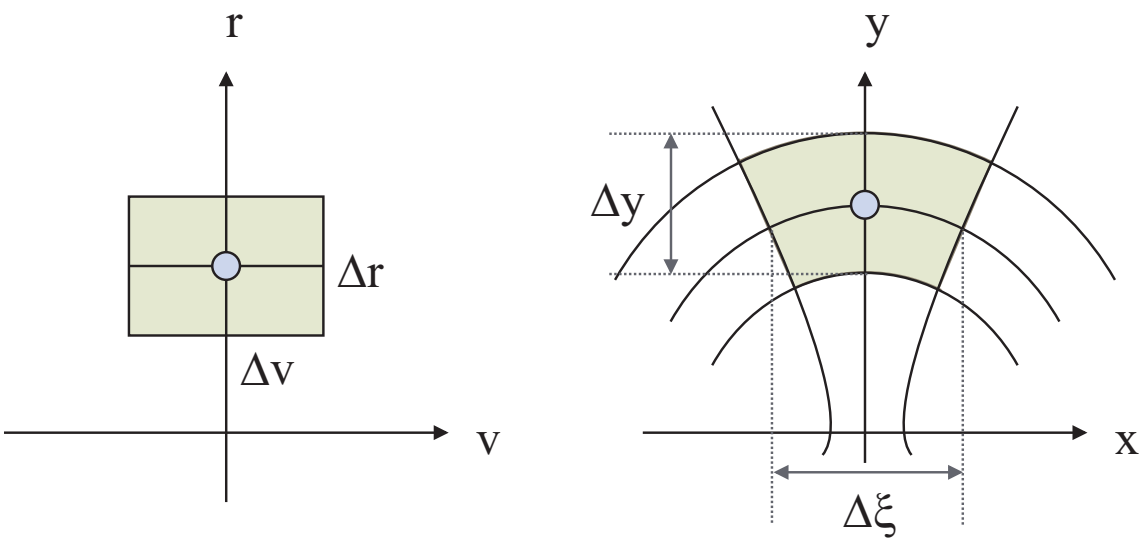

Figure 3.11: *Ambiguity facet in the sidelooking situation*

This ambiguity area covers a spatial angle as seen by the antenna of

$$\Omega_{amb} = \frac{A_{amb}}{r^2} \sin\epsilon \approx \frac{\lambda c_0}{4rV} \tan\epsilon. \tag{3.28}$$

3.4.4 Minimum antenna size

For SAR as well as for MTI it is desired that the main beam illuminates only one ambiguity facet in order to exclude the superposition of secondary returns within the main beam. The spatial angle of the main beam of an antenna with the effective area a_{ant} perpendicular to the look direction is approximately given by $\Omega_{ant} = \lambda^2/a_{ant}$. To fulfill the condition that the main beam has illuminate an area smaller or equal to the ambiguity facet From Eq. (3.28) we conclude directly

$$\Omega_{ant} \leq \Omega_{amb} \tag{3.29}$$

$$\frac{\lambda^2}{a_{ant}} \leq \frac{\lambda c_0}{4rV} \tan\epsilon \tag{3.30}$$

$$a_{ant} \geq \frac{4\lambda rV}{c_0 \tan\epsilon} \tag{3.31}$$

For the before mentioned numerical example we get a minimum antenna area of about a_{ant}=2.1 m^2. It should be noted, that this area just covers the ambiguity facet in the sense of Rayleigh's resolution. In order to fit the whole main beam from zero to zero into this area, the dimensions of the antenna have to be increased by a factor two, i. e. the antenna area has to be four times as large; for the example we get a minimum area of 8.5 m^2.

This result is independent on the PRF. To get a feeling about minimum length and height for a given PRF, we recapitulate Eq. (3.8), where the minimum antenna length was derived to $l_{x,min} = 2V\Delta T$.

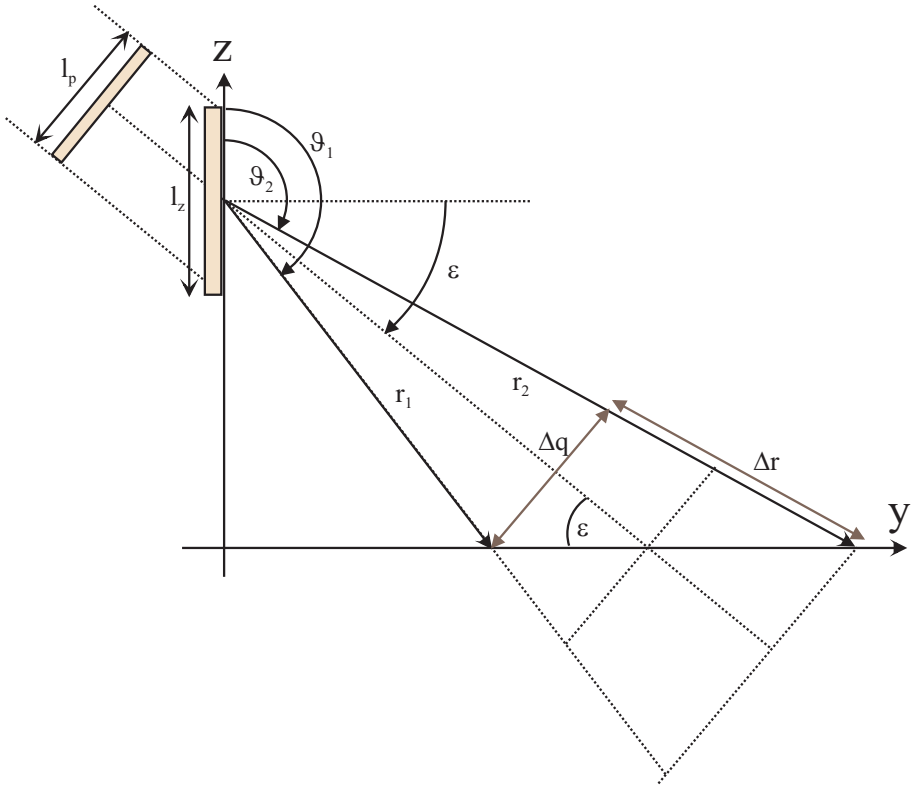

Figure 3.12: *Minimum antenna height*

The minimum antenna extension perpendicular to LOS and flight path is easily evaluated, see Fig. 3.12: The length Δq between two ambiguous range radials perpendicular to the LOS is $\Delta q = \tan\epsilon \Delta r$. On the other hand, if l_p is the projected antenna length perpendicular to the LOS, in range r the extension of the main beam perpendicular to the LOS is $\delta q = r\lambda/l_p$. It follows from the condition $\delta q \leq \Delta q$ for the minimum projected antenna length: $l_{p,min} = \lambda r/(\Delta r \tan\epsilon)$. From these two minimum lengths we get the minimum projected antenna area:

$$a_{ant} \geq l_{x,min} l_{p,min} = \frac{2V\Delta T\lambda r}{\Delta r \tan\epsilon} \tag{3.32}$$

$$= \frac{4\lambda r V}{c_0 \tan\epsilon} \tag{3.33}$$

which is the same result as in Eq. (3.29). Of course, there are additional conditions for the antenna size, for example to get a sufficient antenna gain for the power budget, but also with respect to mechanical constraints.

Essence 3.4 *If range and azimuth ambiguities shall be avoided by the illumination by the antenna main beam, the antenna area has to fulfill the inequation Eq. (3.32).*

3.5 Spacebased geometry

The most of the studied properties of a radar moving over ground can be transferred to the spacebased situation. The most important difference is that the curvature of the earth has to be taken into account. In this section the geometry describing the flight path of the radar platform in relation to the curved earth surface is considered, followed by the analysis of ambiguous clutter directions due to discrete sampling in range and azimuth.

3.5.1 Coordinate systems and transformations

[1]

If (x_A, y_A, z_A) and (x_B, y_B, z_B) are two cartesian coordinate systems with identical origin, any vector $\vec{R}_A$ can be transformed into the B-system according to

$$\vec{R}_B = \mathbf{L}_{BA}\vec{R}_A, \tag{3.34}$$

where $\mathbf{L}_{BA}$ is an orthonormal rotational matrix, i.e. $\mathbf{L}_{BA}^t\mathbf{L}_{BA} = \mathbf{Id}$ and $\mathbf{L}_{AB} = \mathbf{L}_{BA}^{-1} = \mathbf{L}_{BA}^t$. Two subsequent transformations L_{BA} and L_{CB} can be combined to a single via $L_{CA} = L_{CB}L_{BA}$.

$\mathbf{L}_{BA}$ can be described by the three *Euler angles*:

$$\begin{aligned}
\mathbf{L}_{BA} &= \mathbf{L}_1(\Phi)\mathbf{L}_2(\Theta)\mathbf{L}_3(\Psi) \\
&= \begin{pmatrix} 1 & 0 & 0 \\ 0 & \cos\Phi & \sin\Phi \\ 0 & -\sin\Phi & \cos\Phi \end{pmatrix} \begin{pmatrix} \cos\Theta & 0 & -\sin\Theta \\ 0 & 1 & 0 \\ \sin\Theta & 0 & \cos\Theta \end{pmatrix} \begin{pmatrix} \cos\Psi & \sin\Psi & 0 \\ -\sin\Psi & \cos\Psi & 0 \\ 0 & 0 & 1 \end{pmatrix} \\
&= \begin{pmatrix} \cos\Theta\cos\Psi & \cos\Theta\sin\Psi & -\sin\Theta \\ \sin\Phi\sin\Theta\cos\Psi - \cos\Phi\sin\Psi & \sin\Phi\sin\Theta\sin\Psi + \cos\Phi\cos\Psi & \sin\Phi\cos\Theta \\ \cos\Phi\sin\Theta\cos\Psi + \sin\Phi\sin\Psi & \cos\Phi\sin\Theta\sin\Psi - \sin\Phi\cos\Psi & \cos\Phi\cos\Theta \end{pmatrix}
\end{aligned} \tag{3.35}$$

where three simple rotations (*Euler rotations*) are performed subsequently: First, a rotation about the z-axis by the angle Ψ, for the second, a rotation about y-axis by the angle Θ, and for the third, a rotation about x-axis by the angle Φ[2]. The signs for the rotation about the y-axis seem to be inverted compared to the other two rotations. The reason is that all rotations are counted positive for left-turning if we look along the rotation axis to the origin.

If the vector $\vec{r}_A(t)$ and the transformation matrix $\mathbf{L}_{BA}(t)$ are time-dependent, we obtain

[1] Could be shifted to annex

[2] In the literature, different variations of the Euler rotations can be found. We use a type common in the field of aero-space engineering

$$\begin{aligned}\vec{v}_B(t) &= \frac{d}{dt}\vec{r}_B(t) \\ &= \left(\frac{d}{dt}\mathbf{L}_{BA}(t)\right)\vec{r}_A(t) + \mathbf{L}_{BA}(t)\frac{d}{dt}\vec{r}_A(t) \\ &= \Omega_{BA}(t)\vec{r}_A(t) + \mathbf{L}_{BA}(t)\vec{v}_A(t) \end{aligned} \tag{3.36}$$

Since $\mathbf{L}_{BA}^t(t)\mathbf{L}_{BA}(t) = \mathbf{Id}$, the time derivative of this expression is zero, resulting in

$$\Omega_{BA}^t(t)\mathbf{L}_{BA}(t) + \mathbf{L}_{BA}^t(t)\Omega_{BA}(t) = \mathbf{0} \tag{3.37}$$

$$\mathbf{L}_{BA}^t(t)\Omega_{BA}(t) = -\left(\mathbf{L}_{BA}^t(t)\Omega_{BA}(t)\right)^t \tag{3.38}$$

that means the matrix $\mathbf{L}_{BA}^t(t)\Omega_{BA}(t)$ is antisymmetrical and $\Omega_{BA}(t)$ can be written in the form

$$\Omega_{BA}(t) = \mathbf{L}_{BA}(t)\begin{pmatrix} 0 & -\omega_z(t) & \omega_y(t) \\ \omega_z(t) & 0 & -\omega_x(t) \\ -\omega_y(t) & \omega_x(t) & 0 \end{pmatrix} \tag{3.39}$$

3.5.2 Coordinate systems for earth observation

Let the path of the satellite with respect to an Cartesian inertial coordinate system (x_I, y_I, z_I) with its origin at the earth's center and the z_I-axis directed along the earth rotational axis be described by a vector valued time function $\vec{R}_I(T)$ with time derivative $\vec{V}_I(T)$, i.e. the history of the velocity vector.

An earth fixed coordinate system (x_E, y_E, z_E) with origin and z_E-axis identical to the inertial system rotates with the angular velocity ω_E with respect to the latter, which can be described by a time dependent transformation matrix $\mathbf{L}_{EI}(T)$ from the I-system to the E-system.

According to Eq. 3.35 the path of the satellite is transformed into the E-system by $\vec{R}_E(T) = \mathbf{L}_{EI}(T)\vec{R}_I(T)$, the satellite velocity vector with respect to the E-system is given by

$$\vec{V}_E(T) = \Omega_{EI}(T)\vec{R}_I(T) + \mathbf{L}_{EI}(T)\vec{V}_I(T) \tag{3.40}$$

with the angular velocity matrix $\Omega_{EI}(T)$ being the time derivative of $\mathbf{L}_{EI}(T)$.

As illustrated in Fig. 3.13, we additionally introduce an antenna fixed Cartesian coordinate system (x_A, y_A, z_A) with its origin at the position $\vec{R}_E(T)$. An arbitrary look direction is denoted in antenna coordinates by the unit vector $\vec{u} = (u, v, w)^t$

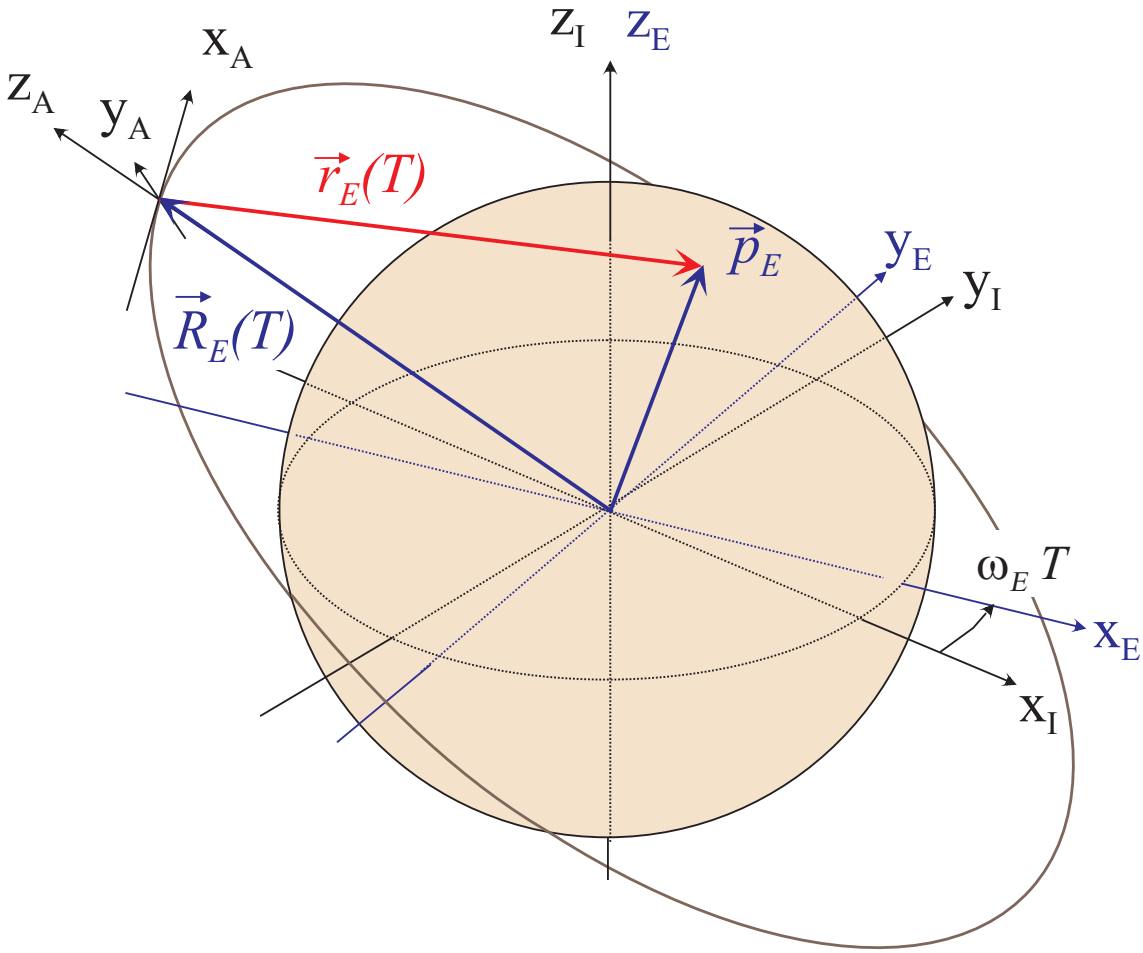

Figure 3.13: *Geometry for space based radar*

originating in the center of the antenna coordinate system. For phased array systems, the main beam direction can be steered by the phase shifters corresponding to a unit vector $\vec{u}_0$.

Let $\mathbf{L}_{AE}(T)$ and $\Omega_{AE}(T)$ be the rotational matrix and its time derivative describing the orientation of the antenna with respect to the earth, and the angular velocities, respectively.

3.5.3 Range and radial velocity of clutter points

For any point on the earth surface, denoted by a vector $\vec{p}_E$ with length equal to the radius ρ_E of the earth, the look direction in the E-system is given by

$$\vec{u}_E(T) = \frac{\vec{p}_E - \vec{R}_E(T)}{\|\vec{p}_E - \vec{R}_E(T)\|} \tag{3.41}$$

(3.42)

and its path, the look direction and its velocity vector in the A-system are

$$\vec{r}_A(T) = \mathbf{L}_{AE}(T)\left(\vec{p}_E - \vec{R}_E(T)\right) \tag{3.43}$$

$$\vec{u}_A(T) = \frac{\vec{r}_A(T)}{\|\vec{r}_A(T)\|} = \mathbf{L}_{AE}(T)\vec{u}_E(T) \tag{3.44}$$

$$\vec{v}_A(T) = \Omega_{AE}(T)\vec{r}_A(T) - \mathbf{L}_{AE}(T)\vec{V}_E(T) \tag{3.45}$$

The radial velocity of this point is

$$v_r(T) = \frac{d}{dT}\left\|\vec{p}_E - \vec{R}_E(T)\right\| \tag{3.46}$$

$$= -\left\langle \vec{V}_E(T), u_E\vec{(T)} \right\rangle \tag{3.47}$$

$$= \langle \vec{v}_A(T), \vec{u_A}(T) \rangle . \tag{3.48}$$

In the following, we regard the geometrical situation at a fixed point of time and don't express the dependency on t explicitly. $V_E = \|\vec{V}_E\|$ denotes the scalar velocity of the platform in earth coordinates, $R_E = \|\vec{R}_E\|$ the distance from the earth center to the satellite. Inverse to the previous derivations, we can determine the point $\vec{p}_E(\vec{u}_A)$ where the LOS-vector $\vec{u}_A$ hits the earth surface. With the LOS-vector $\vec{u}_E = \mathbf{L}_{EA}\vec{u}_A$ in the E-system the necessary condition is formulated as the quadratic equation

$$\left\|\vec{R}_E + \eta\vec{u}_E\right\|^2 = \rho_E^2 \tag{3.49}$$

which has to be solved with respect to the real parameter η. This equation is solvable only if the LOS-vector points into the silhouette of the earth, which is satisfied when

$$\left\langle \vec{u}_E, \vec{R}_E \right\rangle \leq -\sqrt{R_E^2 - \rho_E^2} \tag{3.50}$$

which can be seen in Fig. **??**. Otherwise the LOS-vector misses the earth. Let the set of all 'admissible directions' characterized by Eq.(3.50)be denoted by $\mathbf{U}$.

For an admissible direction $\vec{u}_E$ we get from Eq.(3.49) the solutions

$$R_E^2 + 2\eta\left\langle \vec{u}_E, \vec{R}_E \right\rangle + \eta^2 = \rho_E^2 \tag{3.51}$$

$$\eta_\pm = -\left\langle \vec{u}_E, \vec{R}_E \right\rangle \pm \sqrt{\left\langle \vec{u}_E, \vec{R}_E \right\rangle^2 - (R_E^2 - \rho_E^2)} \tag{3.52}$$

Since $\eta_+ \geq \eta_-$ only the second solution η_- is valid, since η_+ is related to the point where the LOS hits the surface on the earth's backside. The range $r(\vec{u}_A)$ to

the hit point on the front side is simply given by η_-, i.e.

$$r(\vec{u}_A) = -\left\langle \vec{u}_A, \vec{R}_A \right\rangle - \sqrt{\left\langle \vec{u}_A, \vec{R}_A \right\rangle^2 - (R_E^2 - \rho_E^2)} \tag{3.53}$$

since the rotation of a vector pair doesn't change their scalar product.

The radial velocity at this point can be deduced from Eq. (3.46):

$$v_r(\vec{u}_A) \;=\; -\left\langle \vec{V}_E, \mathbf{L}_{EA}\vec{u_A} \right\rangle \tag{3.54}$$

Chapter 4

Synthetic Aperture Radar

In this chapter we will deal the basics of SAR as a pre-requisite for SAR moving target recognition. Starting from a tight expos'e of the SAR principles we will introduce a general model of SAR signals gathered with a SAR system and deduce data processing techniques.

4.1 SAR history and applications

The technique of Synthetic Aperture Radar (SAR) permits the imaging of the earth' surface with high resolution performed from a moving platform (aircraft, satellite). In contrast to other remote sensing methods, for instance optical systems, advantages of SAR comprise on one hand the independency from weather and day light, and on the other hand the provision of additional features such as polarimetry and multi-frequency. The imaging geometry of SAR is hereby different to the optical geometry, as the imaging plane is rather spanned by azimuth and range instead of azimuth and elevation. By means of SAR-Interferometry for instance it is possible to determine the third dimension and hence to chart the terrain height for each resolution cell.

The SAR principle and its first demonstration date back into the fifties. C.A. Wiley of *Goodyear Ltd* exhibited the first system in 1952 and applied for a patent in 1954. In the early days the data recording and imaging was performed with optical lenses due to a lack of digital signal processors. Only recently prevailed the digital processor owing to achievable computation power and its palpable advantages. In 1987 the first SAR-satellite called 'SeaSAT' was launched; today numerous satellites with outstanding imaging performances exist for civilian remote sensing as well as military surveillance. It has been a long journey from the rather 'prosaic' beginnings of SAR towards today's possible. Its evolution, however, is still rousingly advancing and is definitely not at the end!

Glossary for this chapter

α	Chirp rate
β	Doppler slope of azimuth chirp
δu_a	Beamwidth of real antenna
φ	Phase function
λ	Wavelength
λ_0	Wavelength related to the reference frequency
σ^2	Noise variance
ω	Angular velocity of aspect angle
ξ	xPosition of the platform along motion axis
ξ_0	Position at stationary phase
a	Complex Amplitude
$a(x)$	Reflectivity
$\tilde{a}(T)$	Reflectivity scaled to slow time
$A(K)$	Fourier transform of reflectivity
$\tilde{A}(T)$	Fourier transform of reflectivity as time function
b	Bandwidth fast time
B	Bandwidth slow time
c_0	Velocity of light
$D(u)$	Two-way characteristics
f	Radio frequency
f_0	Reference frequency
F	Doppler frequency
F_0	Instantaneous Doppler frequency of the model signal
$F_s = PRF$	Sampling frequency slow-time = Pulse repetition frequency
$h(T)$	Pulse response of azimuth compression filter
$H(F)$	Transfer function of azimuth compression filter
I_M	Indicator function of the set M
k	Spatial frequency in the baseband domain
$k_0 = 2\pi/\lambda_0$	Wavenumber related to the reference frequency
$k_r = 2\pi/\lambda$	Wavenumber in the RF domain
k_x	Spatial frequency along the aperture
K	Spatial frequency
$\mathbf{K} = (K_x, K_y, K_z)^t$	Vector of spatial frequencies
$\mathcal{K}$	Wave number set, k-set
L_a	Azimuth extension of the antenna footprint
l_x	Length of the real antenna
$p(T)$	Azimuth point spread function
$P(F)$	Fourier transform of $p(T)$
$r(\xi; x, \rho)$	Range history
$r_0(\xi; \rho)$	Range history of model signal
r_s	Spatial pulse length

$\mathsf{s}(.)$	Transmitted waveform
$s(k_r, \xi; x, \rho)$	Signal of a scatterer
$s_0(k_r, \xi; \rho)$	Model signal
$s_0(T)$	Azimuth signal
$S_0(F)$	Fourier transform of azimuth signal
$s^{d_1,d_2}(.)$	Signal in the (d_1, d_2)-domain
T_s	Time duration of azimuth chirp
T_0	Time point of stationary phase
$u(\xi; x, \rho)$	Direction history
$u_0(\xi; \rho)$	Direction history of model signal
V	Platform velocity
$w_T(T)$	Window in the time domain
$w_F(F)$	Window in the frequency domain
(x, ρ)	Coordinates of a scatterer
$x(T)$	Measured azimuth signal without noise
$X(F)$	Fourier transform of $x(T)$
$z(T)$	Measured azimuth signal including noise

4.1.1 Application

Today, applications are mainly found in various areas of remote sensing:

- *Geology, Cartography*: Chartering of areas which are permanently under dense cloud cover, surveying of geological structures, worldwide surveying of human settlings and cultivated land.

- *Oceanography:* Analysis of ocean waves, conclusions on wind fields, research on tsunamis.

- *Hydrology*: Surveying of floodings and soil moisture.

- *Glaciology*: Monitoring of ice in the arctic regions, icebergs, and snow coverage.

- *Nautical shipping and economy*: Recording of the sea states, monitoring of shipping lanes, chartering of seaweed appearances.

- *Agriculture and Forestry:* Identification of cultivation types, control of fallowing schemes, monitoring of planting states, observation of grasshopper swarms.

- *Emergency management:* Recognition of surface changes, e.g. cost erosion, Detection of earth- and seaquakes, search and rescue of missing people.

- *Environmental monitoring:* In addition to the applications mentioned above: Recognition and imaging of pollution, e.g. oil films on water surfaces, chartering of damage to forests.

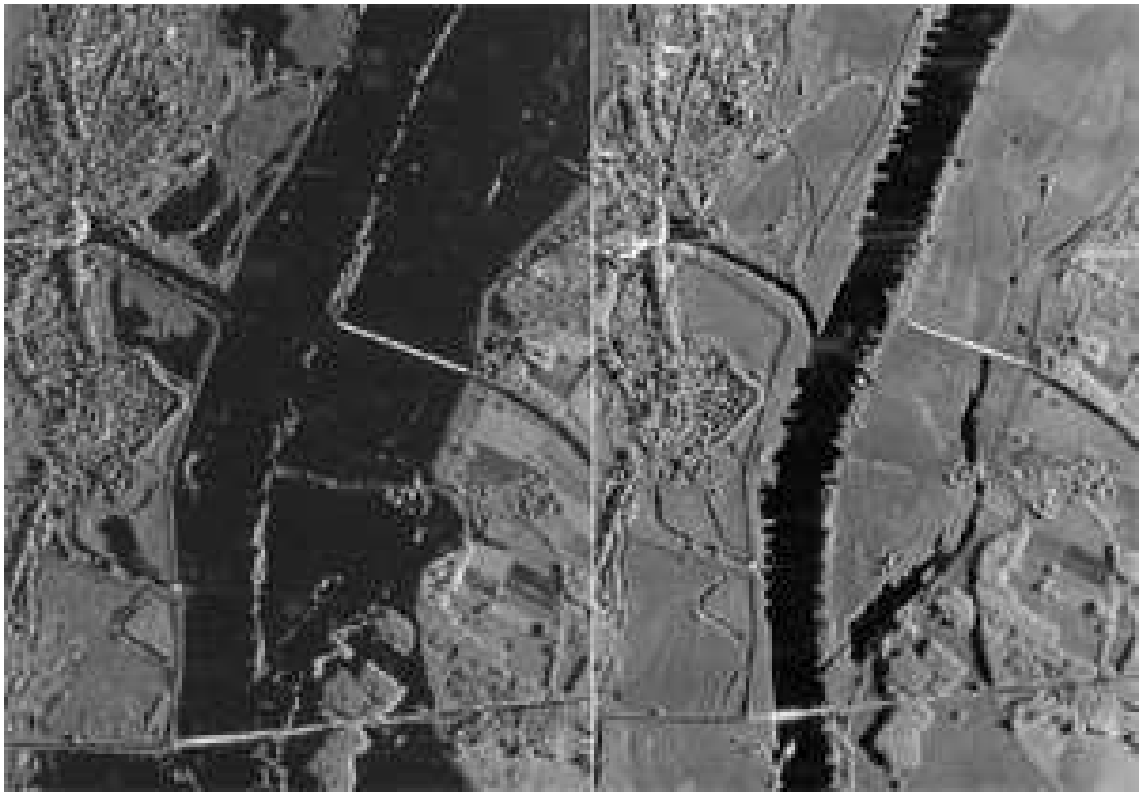

Figure 4.1: *SAR-image of the Elbe river near Dömitz at times of a disastrous flooding. Left: 29 August 2002, Right: 22 October 2003.* ©*Fraunhofer FHR*

4.2 Introduction to imaging Radar

4.2.1 Imaging small scenes and objects

To understand imaging radar, it is favorable to start with techniques to image small scenes and objects, like turntable imaging and inverse synthetic aperture radar (ISAR) . As a pre-requisite we will address the properties of the spatial Fourier transform.

Spatial Fourier transform

If $a(x)$ is a complex function of a spatial variable x, so

$$A(K_x) := \int a(x) e^{-jK_x x} dx \tag{4.1}$$

is defined as the spatial Fourier transform of $a(x)$. K_x is a *spatial frequency* measured in the units rad/m stating the change of phase with the spatial progress. Eq. (4.1) represents the function $a(x)$ as the superposition of *spatial harmonic functions* $w_{K_x}(x) = e^{jK_x x}$.

A function $a(\vec{r})$ in d spatial variables ($d \in \{1, 2, 3\}$) given by the vector $\vec{r}$ is transformed by the multi-dimensional Fourier transform

$$A(\vec{K}) := \int a(\vec{r}) e^{-j\langle \vec{K},\vec{r}\rangle} d\vec{r} \tag{4.2}$$

into the domain of *spatial frequency vectors* $\vec{K}$. The back-transform is performed by

$$a(\vec{r}) = \frac{1}{(2\pi)^d} \int A(\vec{K}) e^{j\langle \vec{K},\vec{r}\rangle} d\vec{K}. \tag{4.3}$$

The spatial Fourier transform of a spatial Dirac function $a(\vec{r}) = \delta(\vec{r} - \vec{r}_0)$ leads to the harmonic function $e^{-j\langle \vec{K},\vec{r}_0\rangle}$. The phase of this function changes most rapidly in the direction of $\vec{r}_0$.

Vice versa, if $A(\vec{K}) = \delta(\vec{K} - \vec{K}_0)$ is a Dirac distribution in the wave-number domain, the back-transform represents the time harmonics of a wave propagating in the direction of $\vec{K}_0$ and a wavelength $\lambda = 2\pi/|\vec{K}_0|$.

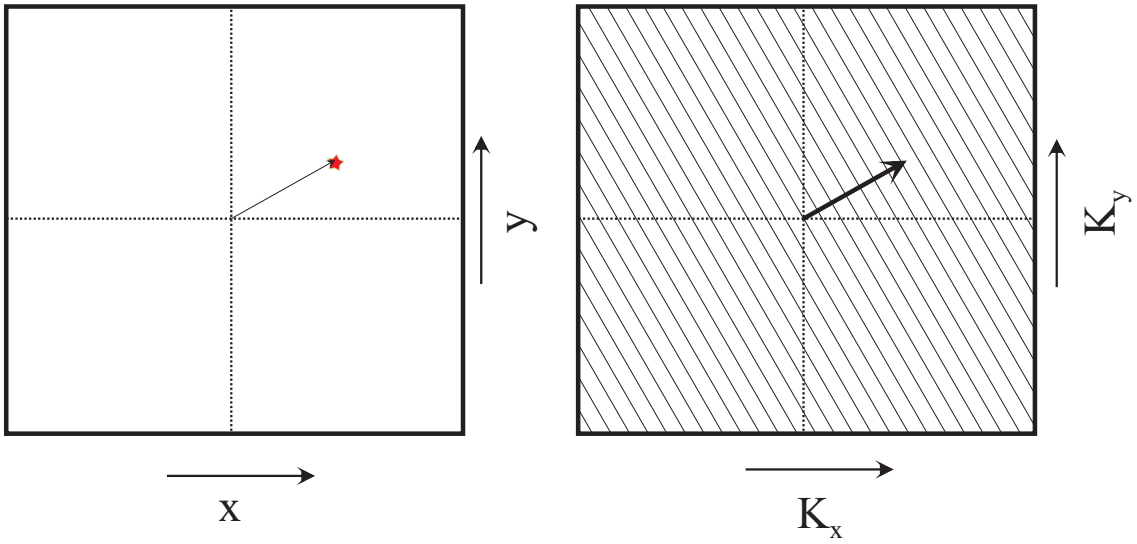

Figure 4.2: *Spatial Fourier correspondence*

Fig. 4.2 illustrates this correspondence. All properties known from the Fourier partners time - frequency can be transferred to the Fourier partners space / wavenumber. Spatial functions $a(\vec{r})$ vanishing outside a cube $[\vec{r}_0, \vec{r}_0 + \Delta\vec{r}]$ with $\Delta\vec{r} = (\Delta x, \Delta y, \Delta z)^t$ lead to 'band limited' functions $A(\vec{K})$, which are - following the Nyquist/Shannon theorem - uniquely determined by sampling on a grid

$$\vec{K}_{\nu\mu\kappa} = \vec{K}_0 + \begin{pmatrix} \nu\Delta K_x \\ \mu\Delta K_y \\ \kappa\Delta K_z \end{pmatrix}, \tag{4.4}$$

if $\Delta K_x \leq 2\pi/\Delta x, \Delta K_y \leq 2\pi/\Delta y, \Delta K_z \leq 2\pi/\Delta z$.

Incomplete back-transform If the back transform is performed only over a subset $\mathcal{K}$

$$\hat{a}_{\mathcal{K}}(\vec{r}) = \frac{1}{(2\pi)^d} \int_{\mathcal{K}} A(\vec{K}) e^{j\langle \vec{K}, \vec{r} \rangle} d\vec{K}, \tag{4.5}$$

so $\hat{a}_{\mathcal{K}}(\vec{r})$ is an - though unsharp - reconstruction of $a(\vec{r})$. Nevertheless, it is a famous property of the Fourier transform that cutting the transform for any subset always lead to the same image! This property is used for radar imaging with the *multi look technique*.

4.3 SAR Terminology

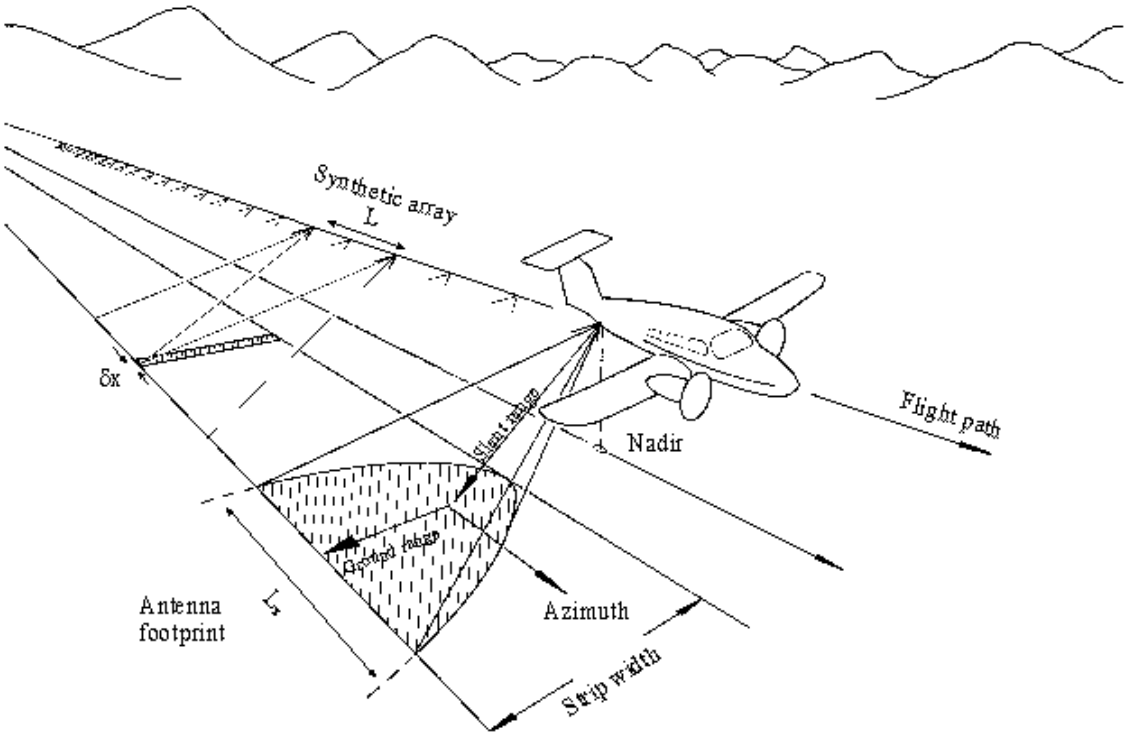

Figure 4.3: *Synthetic Aperture Radar in the stripmap mode*

We will explain some usual expressions used in the SAR terminology by means of Fig. 4.3. Ideally, the platform moves along a straight line. The antenna is mounted to achieve a *side looking geometry* , i.e. the beam points orthogonal to the motion direction - or with a certain *squint angle* - to the earth surface. The look direction is tilted by the *depression angle* from the horizontal plane downwards. The area on ground covered by the antenna main beam is called *antenna footprint* .

The aim of a SAR mission in the *stripmap mode* is to image a strip of a certain *swath width* slipped by the antenna footprint. Besides this mode the imaging of a

smaller area with finer resolution can be obtained by the *spotlight mode* where the beam center is fixed to a point on the earth surface or the *sliding mode* where the antenna footprint moves with a lower (sometimes higher) velocity than the platform.

High resolution in range is obtained by modulated transmit signals and pulse compression. We have to discriminate the range in line-of-sight, which is called *slant range* and the range projected to the earth surface, the *ground range*. The *ground range resolution* of course is coarser than the *slant range resolution*.

To obtain sufficient resolution parallel to the flight direction the beamwidth of the antenna for *real aperture imaging* normally is not narrow enough, since in the microwave region the antenna length would have to be some hundreds or thousands of meters; to overcome this handicap the principle of synthetic aperture is used: due to the motion of the platform it is possible to generate a *synthetic aperture*. By the platform's movement time is transformed into space - a *synthetic array* is spanned, the recorded echoes are processed similar as for a real array summing up the returns after compensating the phases. In this way a *synthetic beam* is generated effecting a fine resolution in azimuth direction.

4.4 Heuristical approach

We consider a synthetic array, as in section 3.3, generated by the motion of the platform with velocity V at a pulse repetition interval ΔT. The positions of this synthetic array are $\xi_n = n\Delta x, n = -\infty, \ldots, \infty$ with the spacing $\Delta x = V\Delta T$. In Fig. 4.4 the principle of a synthetic array is illustrated.

Let a point scatterer be placed at the x-coordinate $x = 0$ at a distance ρ to the flight path. By compensation of the phases effected by the varying distances from the scatterer to the elements of the synthetic array, the received signals can be focused to this point. In contrary to the situation in chapter 3 we don't restrict the length of the synthetic array according to the far field condition. So we have to take into account phase terms of higher orders than linear.

The distance of an element of this synthetic array at position ξ to the point scatterer is given by $r_0(\xi;\rho) = \sqrt{\rho^2 + \xi^2}$. To focus a beam to the scatterer, the phase $\varphi(\xi;\rho) = -2k_r r_0(\xi;\rho)$ has to be compensated by a 'phase shifter'. Since the array is synthetic, this phase shift has to be performed in the processor.

If we take into account all elements of the synthetic array along a synthetic aperture of size L_X, a beam is generated with a beamwidth in terms of directional cosine of size $\delta_u = \lambda/(2L_x)$. The achieved resolution of the scene in direction of the flight (*azimuth resolution*) will be $\delta x = \rho\delta_u = \rho\lambda/(2L_x)$.

Clearly, this requires that the scatterer is illuminated during the whole time where the platform is moving along the synthetic aperture of length L_x. If the antenna has a fixed look direction - as it is the case for stripmap SAR - and has the real beamwidth δu_a, only a restricted azimuth length L_a of the scene is illuminated, i.e. the azimuth length of the *antenna footprint*. This length is roughly given by $L_a = \rho\delta u_a$.

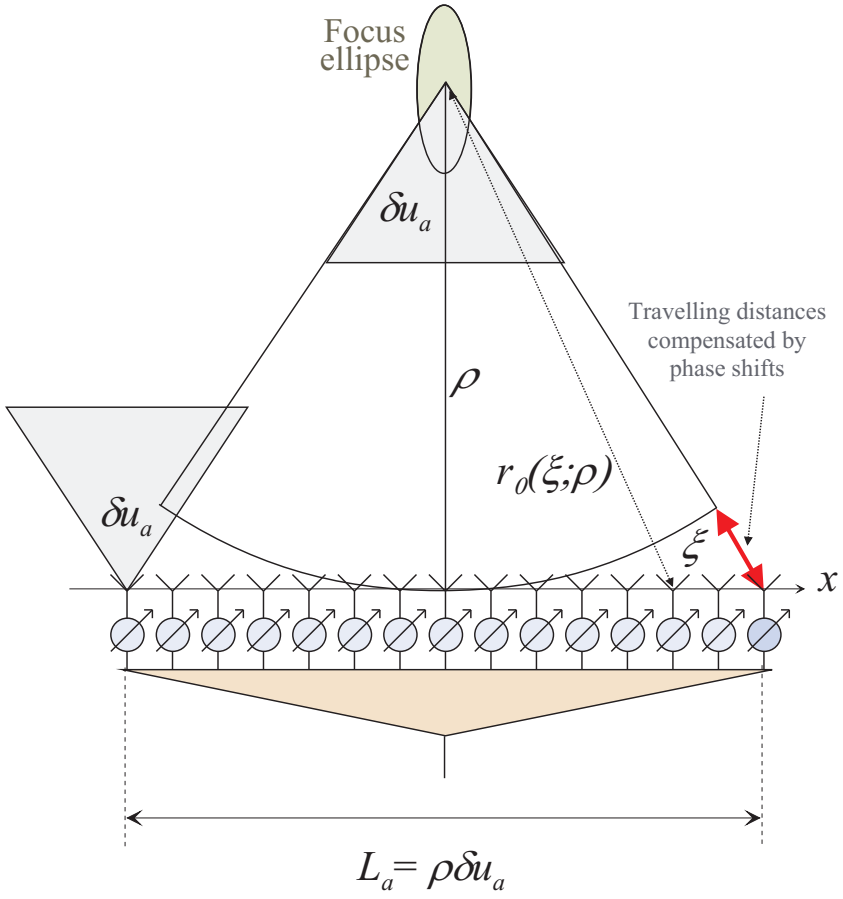

Figure 4.4: *Focused SAR as synthetic antenna*

For stripmap SAR, the distance the platform is flying from a scatterer entering into the mainbeam until its disappearance is L_a, too. So for this mode, the length of the synthetic array L_x is bounded by $L_x \leq L_a$. Consequently, the achievable azimuth resolution for stripmap SAR is

$$\delta x_{min} = \rho \frac{\lambda}{2L_a} = \rho \frac{\lambda}{2\rho \delta u_a} = \frac{\lambda}{2\delta u_a}. \tag{4.6}$$

Obviously, the azimuth resolution is independent on the range, since the length of the available synthetic aperture increases proportional to ρ. Because of the azimuth resolution being proportional to ρ and inverse proportional to L_x, the range ρ cancels out.

The last interesting step is done by inserting the equality $\delta u_a = \lambda / l_x$ for the beamwidth of an antenna with real aperture l_x:

$$\delta x_{min} = \frac{\lambda}{2\delta u_a} = \frac{\lambda}{2\lambda / l_x} = \frac{l_x}{2}. \tag{4.7}$$

Essence 4.1 *The minimum obtainable azimuth resolution of a SAR in stripmap mode with an antenna of length l_x is independent on the range and the wavelength*

equal to the half length of the antenna.

There are some differences compared to a real array:

- The phase terms always are related to two-ways travelling. Compared to a real array always the double phase has to be inserted. As a consequence, for the same aperture the half beamwidth is obtained. On the other hand, the minimum spatial sampling interval is reduced by the factor 2. Omnidirectional antennas would have to be spaced at the raster $\lambda/4$. The phase centers of directed antennas with the real aperture l_x are not allowed to move more than $l_x/2$ from pulse to pulse, see Eq.(3.15).
- The pattern of the synthetic antenna shows only to a one-way characteristics, since the way forward and backward had been regarded in the phase terms. Unfortunately, this leads to a higher side lobe level compared to the two-way pattern of a real array!
- Because of the long synthetic aperture a far field focusing is no longer possible. The quadratic term of the phase along the synthetic aperture is related to a distinct range. Like for an optical lens a high quality focusing is obtained only in a certain range interval, the *depth of focus.*

The depth of focus can be roughly estimated by the following consideration: The range *variation* for a scatterer at the slant range ρ is approximately $r_0(\xi;\rho) - \rho \approx \xi^2/(2\rho)$, that of a scatterer at slant range $\rho \pm d/2$, where d will be the depth of focus, is approximated in an analogue way. To keep the difference between the variations below $\gamma\lambda$, where γ is a fraction, e.g. $\gamma = 1/8$, the following inequation has to be fulfilled:

$$\left|\frac{\xi^2}{2\rho} - \frac{\xi^2}{2(\rho \pm d/2)}\right| \leq \gamma\lambda \text{ for all } \xi \in \left[-\frac{L_x}{2}, \frac{L_x}{2}\right]. \tag{4.8}$$

This leads to the condition

$$\gamma\lambda \geq \left(\frac{L_x}{2}\right)^2 \left|\frac{1}{2\rho} - \frac{1}{2(\rho - d/2)}\right| \approx \left(\frac{L_x}{2}\right)^2 \frac{d}{4\rho^2} \tag{4.9}$$

and finally to the depth of focus:

$$d_{max} = \frac{16\gamma\lambda\rho^2}{L_x^2}. \tag{4.10}$$

4.5 The azimuth signal

In this section, we will investigate the signal in the slow time domain effected by an azimuthal reflectivity distribution along a line parallel to the flight path, the focusing by a temporal filter and the resulting point spread function. We will start at a three-dimensional geometry which can be reduced to two dimensions, if the flight path is exactly a straight line.

4.5.1 Cylinder coordinates

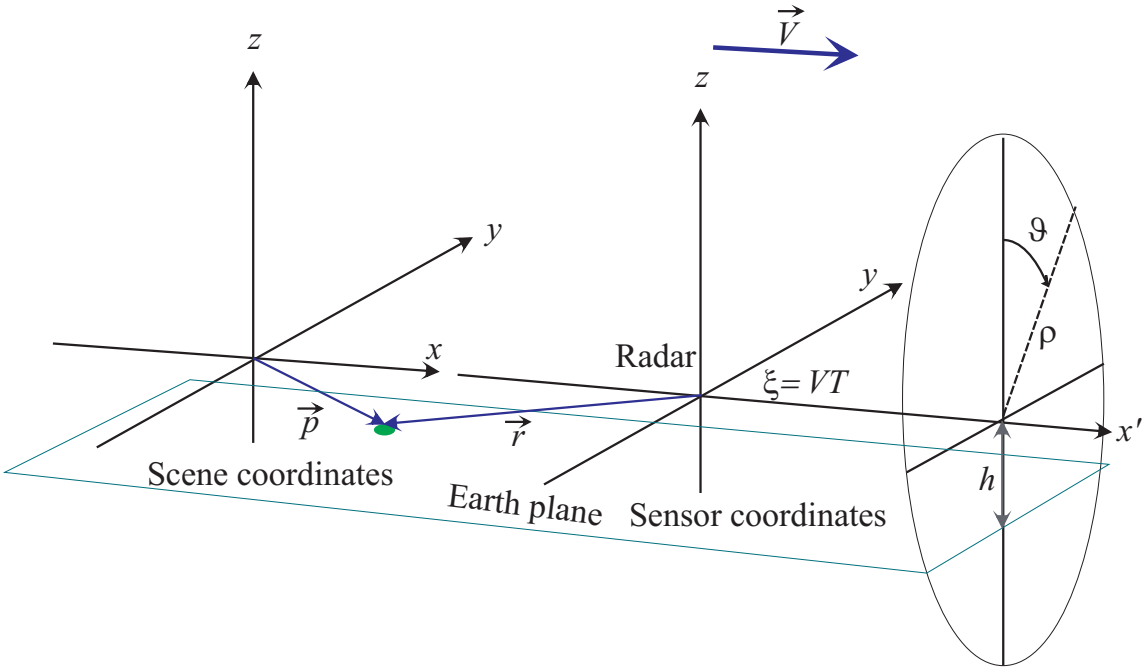

Figure 4.5: *Cylinder coordinates* (x, ρ, ϑ) *for the description of signals from point scatterers*

The three dimensional geometry is illustrated in Fig. 4.5. The phase center of the antenna is placed in the origin of the sensor coordinate system (x', y, z), which is identically orientated as the scene coordinate system (x, y, z). The platform moves at an altitude h with the constant velocity $\vec{V}$ in direction of the x-axis, so the phase center is at the time T at the position $\vec{R}(T) = (VT, 0, 0)^t$ measured in the scene coordinate system. We denote the x-component with $\xi = VT$. A scatterer at the position $\vec{p}$ in sensor coordinates is seen by the radar at the vector $\vec{r}(\xi)$ whose length depends only on the x-position and the *slant range* $\rho = \sqrt{y^2 + z^2}$. Therefore it is convenient to introduce a cylindric coordinate system (x, ρ, ϑ), where the third parameter, the *elevation angle* does not influence the range function. It merely modulates the signal amplitude by the antenna characteristics.

So we can reduce the geometry to two dimensions (x, ρ) and (x', ρ), see Fig. 4.6.

4.5.2 Range and direction history

Let the position of a fixed scatterer be at (x, ρ). Range and directional cosine to this scatterer as functions of ξ are given by

$$r(\xi; x, \rho) = \sqrt{(x - \xi)^2 + \rho^2}, \qquad u(\xi; x, \rho) = \frac{x - \xi}{r(\xi; x, \rho)}. \tag{4.11}$$

where $u(\xi; x, \rho) = \cos \alpha(\xi; x, \rho)$ is the x-component of the LOS vector $\vec{u}(\xi; x, \rho)$

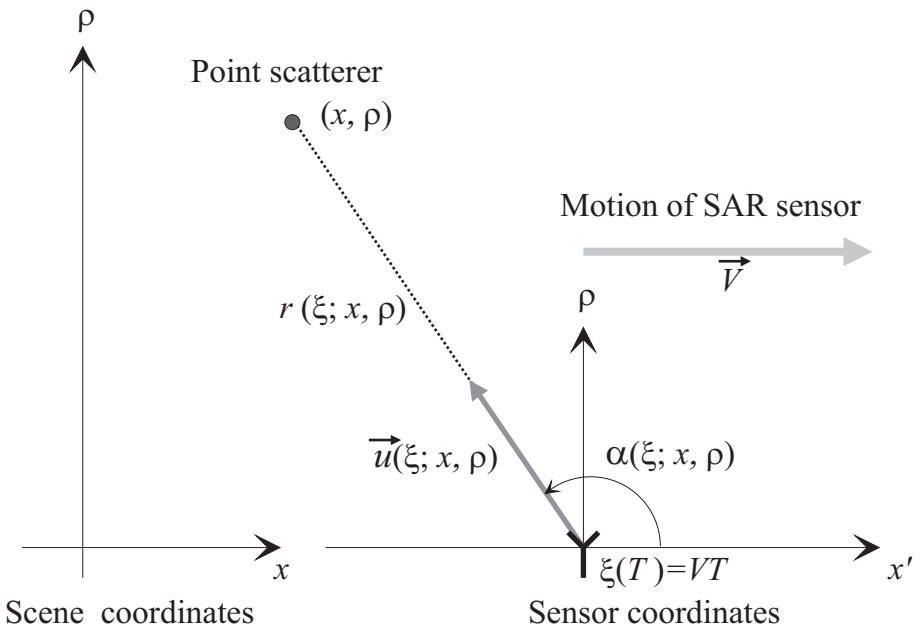

Figure 4.6: *SAR geometry in two dimensions*

pointing to the scatterer. α is again the angle between x-axis and scatterer, the cone-angle. We will call the range- and directional cosine functions of ξ *range history* and *directional cosine history.*

If we regard a scatterer at $x = 0$, its histories are representative for any scatterer with arbitrary x-coordinate, since they only have to be shifted in the ξ-variable by x to get the histories of this scatterer. We define the representative histories by $r_0(\xi;\rho) := r(\xi;0,\rho)$ and $u_0(\xi;\rho) := u(\xi;0,\rho)$, so $r(\xi;x,\rho) = r_0(\xi - x;\rho)$ and $u(\xi;x,\rho) = u_0(\xi - x;\rho)$. We get

$$r_0(\xi;\rho) = \sqrt{\xi^2 + \rho^2}, \qquad u_0(\xi;\rho) = -\frac{\xi}{r_0(\xi;\rho)}. \tag{4.12}$$

The later needed derivatives of these histories with respect to ξ are

$$r_0'(\xi;\rho) = -u_0(\xi;\rho), \qquad u_0'(\xi;\rho) = -\frac{\rho^2}{r_0^3(\xi;\rho)} \tag{4.13}$$

$$r_0''(\xi;\rho) = -u_0'(\xi;\rho) \tag{4.14}$$

and they take following values at $\xi = 0$:

$$r_0'(0;\rho) = 0, \qquad u_0'(0;\rho) = -\frac{1}{\rho}, \qquad r_0''(0;\rho) = \frac{1}{\rho}. \tag{4.15}$$

Evaluation of the range history

For some rough estimates it is practical to use the second order Taylor approximation of the range history with respect to ξ:

$$r_0(\xi;\rho) \approx \rho + \frac{1}{2} r_0''(0;\rho)\xi^2 = \rho + \frac{1}{2\rho}\xi^2 \tag{4.16}$$

$$r_0'(\xi;\rho) \approx \frac{\xi}{\rho}. \tag{4.17}$$

Note that these approximations are only valid for small angular deviations from the normal direction! The area of validity is constrained by the condition that the sinus (ξ/r_0) and the tangens (ξ/ρ) of that angle can be regarded as equal - or that the exact *range hyperbola* Eq.(4.12) can be sufficiently approximated by the *range parabola* Eq.(4.16).

Essence 4.2 *The azimuth signal of any point scatterer at (ξ, ρ) is a shifted version of the model signal of a point scatterer at $(0, \rho)$. The range hyperbola can be approximated by the range parabola for sufficiently small angular deviations from the normal direction. In this region, the directional cosine can be regarded as a linear function of the position ξ.*

4.5.3 The azimuth chirp

The signal for this scatterer in dependence on the slow time (*azimuth signal*) for a fixed wave number k_r is given by the range history and the modulation by the two-way antenna characteristics $D(u)$:

$$s_0(T) = \exp\left\{-j2k_r r_0(VT;\rho)\right\} D\left(u_0(VT;\rho)\right). \tag{4.18}$$

If the antenna is steered during the flight, as it is the case for example for the *spotlight mode*, the antenna characteristics has to be replaced by $D(u_0(VT;\rho), u_s(VT))$ where $u_s(\xi)$ means the steering direction at platform position ξ. But, for the time, we remain at the stripmap mode, where the antenna look direction is fixed.

If the quadratic approximation is used, one gets the form

$$s_0(T) \approx e^{-j2k_r\rho} \exp\left\{-jk_r \frac{(VT)^2}{\rho}\right\} D(u_0(VT;\rho)). \tag{4.19}$$

We state that not only the transmit signal can have a chirp shape but also in the slow-time domain we get a chirp the so called *azimuth chirp* which is nearly linear around the direction perpendicular to the flight direction.

The histories of range ($\hat{=}$ negative phase), Doppler frequency ($\hat{=}$ directional cosine) and the real part of the model signal itself are depicted in Fig. 4.7. We will see that analogue to the compression of the transmit signal this can be compressed, when the received azimuth signal is correlated with the azimuth chirp.

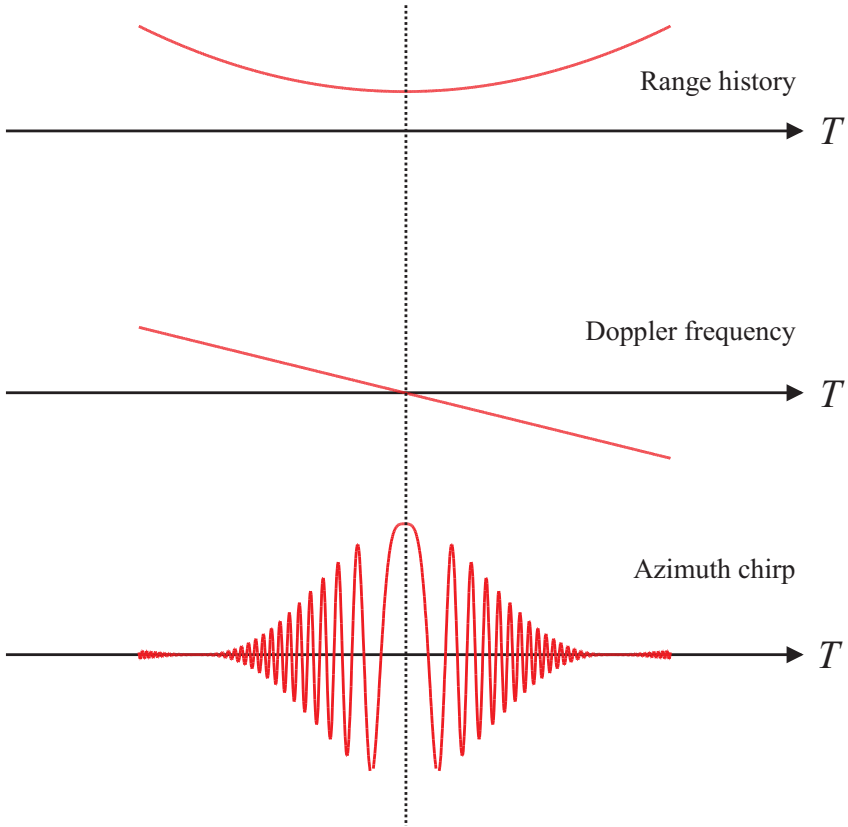

Figure 4.7: *Time histories of the range (phase), the angle, the Doppler frequency and the azimuth chirp*

4.5.4 Temporal parameters of the azimuth signal

Phase and Doppler history

From Eq.(4.18) the phase and Doppler histories of the model signal can be derived:

$$\begin{aligned} \varphi(\xi;\rho) &= -2k_r r_0(\xi;\rho) && (4.20)\\ F_0(\xi;\rho) &= -\frac{1}{2\pi}2k_r V r_0'(\xi;\rho) && (4.21)\\ &= -\frac{2V}{\lambda}r_0'(\xi;\rho) && (4.22)\\ &= F_{max}u_0(\xi;\rho) && (4.23) \end{aligned}$$

with $F_{max} = 2V/\lambda$. In the second order approximation, this is

$$\begin{aligned} \varphi(\xi;\rho) &\approx -2k_r(\rho + \frac{1}{2\rho}\xi^2) && (4.24)\\ F_0(\xi;\rho) &\approx -F_{max}\frac{\xi}{\rho}. && (4.25) \end{aligned}$$

Summary of the interdependencies between the variables

For fixed ρ and k_r each of the four variables ξ,r_0,u_0 and F_0 determines the state. For a better survey we summarize all of the interdependencies in the following table.

Variable	Position			Range		
ξ		$\equiv$		$r_0(\xi)$	$=$	$\sqrt{\rho^2+\xi^2}$
r_0	$\xi(r_0)$	$=$	$\pm\sqrt{r_0^2-\rho^2}$		$\equiv$	
u_0	$\xi(u_0)$	$=$	$-\rho\frac{u_0}{\sqrt{1-u_0^2}}$	$r_0(u_0)$	$=$	$\rho\frac{1}{\sqrt{1-u_0^2}}$
F_0	$\xi(F_0)$	$=$	$\rho\frac{F_0}{\sqrt{F_{max}^2-F_0^2}}$	$r_0(F_0)$	$=$	$\rho\frac{F_{max}}{\sqrt{F_{max}^2-F_0^2}}$
	Direction			Doppler		
ξ	$u_0(\xi)$	$=$	$-\frac{\xi}{\sqrt{\rho^2+\xi^2}}$	$F_0(\xi)$	$=$	$F_{max}\frac{\xi}{\sqrt{\rho^2+\xi^2}}$
r_0	$u_0(r_0)$	$=$	$\pm\frac{\sqrt{r_0^2-\rho^2}}{r_0}$	$F_0(r_0)$	$=$	$\mp F_{max}\frac{\sqrt{r_0^2-\rho^2}}{r_0}$
u_0		$\equiv$		$F_0(u_0)$	$=$	$F_{max}u_0$
F_0	$u_0(F_0)$	$=$	$\frac{F_0}{F_{max}}$		$\equiv$	

(4.26)

Duration of illumination Let u_1 and u_2 be the directional cosines bounding the main beam. Then by Eq. (4.26) the illuminated ξ-interval - i.e. the azimuth-extension of the *antenna footprint* - at slant range ρ is $L_a = \rho\left(u_2/\sqrt{1-u_2^2} - u_1/\sqrt{1-u_1^2}\right)$. We get a temporal duration of

$$T_s = L_a/V. \tag{4.27}$$

For narrow beams of width δu_a directed to the broadside, L_a can be approximated by $\rho\delta u_a = \rho\lambda/l_x$ resulting in

$$T_s \approx \delta u_a \frac{\rho}{V} = \frac{\rho\lambda}{l_x V}. \tag{4.28}$$

Note that $\frac{\rho}{V}$ is the inverse to the *aspect angular velocity* $\omega = V/\rho$ at the point of closest approach.

Doppler modulation rate From Eq. (4.20) the time derivative of the Doppler-history is

$$\frac{\partial}{\partial T}F_0(VT;\rho) = F_{max}Vu_0'(VT;\rho) \tag{4.29}$$

$$= -F_{max}V\frac{\rho^2}{r_0^3(VT;\rho)} \tag{4.30}$$

At time $T = 0$ the *Doppler slope* reaches the maximum magnitude and takes the value

$$\beta = \frac{\partial}{\partial T}F_0(VT;\rho)|_{T=0} = -F_{max}\frac{V}{\rho} = -\frac{2V^2}{\lambda\rho}; \tag{4.31}$$

Doppler bandwidth The Doppler varies between $F_{max}u_1$ and $F_{max}u_2$, so the bandwidth is - in agreement with Eq. (3.15) - given by

$$B = F_{max}(u_2 - u_1) = F_{max}\delta u_a = \frac{2V}{\lambda}\delta u_a. \tag{4.32}$$

For a real aperture of length l_x we get

$$B \approx \frac{2V}{\lambda}\frac{\lambda}{l_x} = \frac{V}{l_x/2} \tag{4.33}$$

This again shows that the spatial sampling interval in slow time must not be larger than $l_x/2$. Since the bandwidth given in Eq. (4.33) is independent on the direction of the main beam, the sampling condition is valid also for squinted beams.

Time-bandwidth product From Eq.(4.27) and (4.32) the time-bandwidth product is calculated to

$$BT_s = \frac{L_a}{V}\frac{2V}{\lambda}\delta u_a = \frac{2L_a\delta u_a}{\lambda} = \frac{L_a}{l_x/2}. \tag{4.34}$$

Since the time-bandwidth product equals the compression ratio, we can read that the maximum compression ratio of the azimuth chirp can be expressed as the number of half real apertures fitting into the synthetic aperture. For narrow beams directed to broadside we get approximately

$$BT_s \approx \frac{2L^2}{\lambda\rho} = \frac{2\lambda\rho}{l_x^2}. \tag{4.35}$$

4.5.5 Numerical example

The following numerical example should give us a feeling for the order of magnitude of the parameters:

given			deducted		
V	150	m/s	δu_a	0,01	rad
λ	3	cm	L_a	1,5	km
l_x	3	m	T_s	10	s
ρ	150	km	β	10	Hertz/s
			B	100	Hertz
			BT_s	1000	

Essence 4.3 *The azimuth signal has the form of a chirp over slow-time with approximately linear frequency modulation around the direction perpendicular to the flight direction, multiplied with the two-way characteristics of the antenna in the instantaneous direction to the scatterer passing by. It is called 'azimuth chirp'.*

4.6 The principle of stationary phase

In the following treatment of SAR we will make use of the *principle of stationary phase*. Because of the importance of this tool this section will be dedicated to this method.

4.6.1 The basic statement

The principle of stationary phase This states that for a sufficiently smooth signal $s(t)$ and a rapidly changing two times differentiable phase $\varphi(t)$ with exactly one local extremum at the point $t = t_0$ the integral $\int \exp\{j\varphi(t)\}s(t)dt$ can be approximated by

$$\int \exp\{j\varphi(t)\}s(t)dt \approx C\exp\{j\varphi(t_0)\}s(t_0) \tag{4.36}$$

with $C = \frac{1+j}{\sqrt{2\alpha}}$ and $\alpha = \frac{1}{2\pi}\frac{d^2}{dt^2}\varphi(t)|_{t=t_0}$.

If the phase function is strictly convex, α is positive and the above formula can be applied directly. If it is strictly concave, α is negative and the expression for C may be replaced by $C = \frac{1-j}{\sqrt{2|\alpha|}}$. If there are more than one *points of stationary phase* all contributions have to be summed up to replace the integral in Eq. 4.36.

4.6.2 Application to the Fourier transform

If a signal $z(t)$ is the product of a function $\exp\{j\varphi(t)\}$ with a rapidly changing phase term with the above stated properties and a slowly varying complex signal $s(t)$, the Fourier transform $Z(\omega)$ of $z(t)$ can be approximated by

$$\begin{aligned} Z(\omega) &= \int \exp\{-j\omega t\}\exp\{j\varphi(t)\}s(t)dt && (4.37)\\ &= \int \exp\{j\Phi(t)\}s(t)dt && (4.38)\\ &\approx C(\omega)\exp\{j\Phi(t_0)\}s(t_0) && (4.39) \end{aligned}$$

with

$$\begin{aligned} \Phi(t) &= -\omega t + \varphi(t) && (4.40)\\ \frac{d}{dt}\varphi(t)|_{t=t_0} &= \omega && (4.41)\\ C(\omega) &= \frac{1+j}{\sqrt{2\frac{1}{2\pi}\frac{d^2}{dt^2}\varphi(t)|_{t=t_0}}}. && (4.42) \end{aligned}$$

4.6.3 Application to a SAR-relevant phase term

This result is often applied to SAR where the phase term $\varphi(t)$ is of the form

$$\varphi(t) = -K\sqrt{\rho^2 + \beta t^2} \tag{4.43}$$

where the square root represents the range history and $K = 2k_r$ for the monostatic case. The related signal is

$$f(t; K, \rho, \beta) = \exp\left\{-jK\sqrt{\rho^2 + \beta t^2}\right\} s(t). \tag{4.44}$$

The application of Eq.(4.37) yields the Fourier transformation $F(\omega)$:

$$F(\omega; K, \rho, \beta) \approx C(\omega) \exp\{j\Phi(t_0)\} s(t_0). \tag{4.45}$$

In the Fourier transform of the azimuth chirp Eq. (4.18)

$$S_0(F) = \int e^{-j2\pi FT} s_0(T) dT \tag{4.46}$$

$$= \int e^{-j2\pi FT} \exp\{-j2k_r r_0(VT; \rho)\} D\left(u_0(VT; \rho)\right) dT \tag{4.47}$$

the accumulated phase term - neglecting phase variations of the antenna pattern - is given by

$$\phi(T) = -2\pi FT + \varphi(T) \text{ with } \varphi(T) = -2k_r r_0(VT; \rho). \tag{4.48}$$

$\varphi(T)$ is the phase of the model signal.

Problem Determine the point of stationary phase T_0, the phase $\phi(T_0)$, and its second derivative at this point!

4.7 Azimuth compression

4.7.1 The flying radar as a time-invariant linear operator

The signal $s_0(T)$ is a normalized model signal for a scatterer placed at $x = 0$. If $a(x)$ denotes the reflectivity along a line parallel to the flight path at a distance ρ, and $\tilde{a}(T) = a(VT)$ is the same function scaled to slow time, the measured azimuth signal of this line will be of the form

$$z(T) = \int s_0(T - T')\tilde{a}(T')dT' + n(T) = x(T) + n(T) \tag{4.49}$$

where $x(T) = (s_0 \star \tilde{a})(T)$ is the deterministic part of $z(T)$ and $n(T)$ is the realization of a white-noise process $N(T)$. Obviously the flying radar acts on the azimuth reflectivity

signal like a time-invariant linear filter, whose pulse response is $s_0(T)$. The corresponding transfer function is its Fourier-transform $S_0(F)$. If the Fourier transforms of the signals $x(T)$ and $\tilde{a}(T)$ are denoted by the corresponding capital letters, we get

$$X(F) = S_0(F)\tilde{A}(F). \tag{4.50}$$

Essence 4.4 *The moving radar responds to the azimuth reflectivity like a time-invariant linear filter with pulse response $s_0(T)$ and transfer function $S_0(T)$.*

We know from the investigation of pulse compression, that a way to compress the azimuth signal will be to apply a time-invariant compression filter with the pulse response $h(T)$ to the data according to $y(T) = (h \star z)(T)$. The noise-free output of the filter is $y(T) = (h \star x)(T)$, in the Doppler frequency region

$$Y(F) = H(F)X(F) = H(F)S_0(F)\tilde{A}(F). \tag{4.51}$$

Analogue to the pulse compression in fast time, the point spread function in azimuth is the response of the compression filter to the azimuth model signal:

$$p(T) = (h \star s_0)(T), \quad P(F) = H(F)S_0(F). \tag{4.52}$$

where the capital letters again denote the Fourier transforms.

4.7.2 The spectrum of the azimuth chirp

Rough estimate of the spectral power

A rough estimation of the square magnitude of $S_0(F)$ can be obtained in the following way: In the survey equations Eq.(4.26) the direction coupled to the Doppler frequency F was given by $u_0(F) = F/F_{max}$. Here the power effected by the two-way antenna pattern is $P(u_0) = |D(u_0)|^2$. So we draw the simple conclusion

$$|S_0(F)|^2 \sim |D(u_0(F))|^2 = \left| D\left(u_0\left(\frac{F}{F_{max}} \right) \right) \right|^2. \tag{4.53}$$

Again, the Doppler power spectrum is a scaled version of the square magnitude of the two-ways antenna pattern, as similar stated in Eq. (3.15). In those investigations we regarded the *clutter spectrum* generated by many ground based scatterers at different azimuth positions, observed over a short time. Here, we assumed a single scatterer observed for the whole time of illumination. Obviously, the simultaneous echoes of the whole illuminated ground and the long term observation of the echo of one scatterer varying its direction over the whole beam width lead to the same result.

The usable bandwidth again corresponds to the main beam of the real antenna, leading to the Doppler bandwidth given in Eq.(4.32)

Azimuth point target reference spectrum

Up to now, we only presented statements about the power spectrum. For the compression filter the phase is much more important. Since it is difficult or impossible to evaluate the Fourier transform of $s_0(T)$ analytically, we apply the 'trick' of the *stationary phase*.

dfafadadffaadfafsdsdf

Solution The necessary condition $\frac{d}{dT}\phi(T)|_{T=T_0} = 0$ is equivalent to

$$\begin{aligned} 0 &= -2\pi F + \frac{d}{dT}\varphi(T)|_{T=T_0} && (4.54)\\ F &= F_0(VT_0;\rho). && (4.55) \end{aligned}$$

So the principle of stationary phase demands that the point of time $T = T_0$ is found where the instantaneous Doppler frequency $F_0(VT_0;\rho)$ is equal to the frequency F of the Fourier cell.

Using the survey Eq. (4.26) at this point the time, we get by inserting $2\pi F = \frac{d}{dT}\varphi(T)|_{T=T_0} = 2k_rVu_0$ (the dependencies on the variables are omitted for better clarity):

$$\begin{aligned} \phi(T_0) &= -2\pi FT_0 + \varphi(T_0) = -2k_rVT_0u_0 + \varphi(T_0)\\ &= -2k_r\xi_0u_0 - 2k_rr_0 = 2k_rr_0u_0^2 - 2k_rr_0\\ &= -2k_rr_0(1-u_0^2) = -2k_r\rho\sqrt{1-u_0^2}\\ &= -2k_r\rho\sqrt{1-\left(\frac{F}{F_{max}}\right)^2} && (4.56) \end{aligned}$$

Further

$$\begin{aligned} \frac{d^2}{dT^2}\phi(T)|_{T=T_0} &= 2k_rV^2u_0' = -2k_rV^2\frac{\rho^2}{r_0^3}\\ &= -2k_rV^2(1-u_0^2)^{3/2}\frac{1}{\rho}\\ &= -\frac{2k_rV^2}{\rho}\left(1-\left(\frac{F}{F_{max}}\right)^2\right)^{3/2}. && (4.57) \end{aligned}$$

From these derivations follows the azimuth point target reference spectrum as stationary-phase approximation:

$$S_0(F) \approx C(F)\exp\left\{-j2k_r\rho\sqrt{1-\left(\frac{F}{F_{max}}\right)^2}\right\} D\left(\frac{F}{F_{max}}\right) \qquad (4.58)$$

with

$$C(F) = \frac{1+j}{\sqrt{2\alpha(F)}} \tag{4.59}$$

$$\alpha(F) = \frac{1}{2\pi}\frac{2k_r V^2}{\rho}\left(1-\left(\frac{F}{F_{max}}\right)^2\right)^{3/2} \tag{4.60}$$

Essence 4.5 *The power spectrum of the azimuth chirp is a scaled version of the square magnitude of the two-way antenna characteristics Eq.(4.53). The complex azimuth point target reference spectrum $S_0(F)$ can be approximated by the principle of the stationary phase by Eq. (4.58) and (4.59). This approximation can be used to perform the azimuth compression in the Doppler domain.*

4.7.3 Filters for azimuth compression

Matched filter On the basis of the model Eq.(4.49) the SNR-optimum filter is - in analogy to the pulse compression in fast time - given by the time inverted complex conjugated azimuth model signal: $h_{mf}(T) = s_0^*(-T)$. In this case, $H_{mf}(F) = S_0^*(F)$, and the point spread function is derived by

$$p_{mf}(T) = (s_0 \diamondsuit s_0)(T), \quad P_{mf}(F) = |S_0(F)|^2, \tag{4.61}$$

where '$\diamondsuit$' means correlation. Eq.(4.51) shows that the response of this compression filter to an arbitrary azimuth reflectivity with Fourier transform $\widetilde{A}(F)$ is in the Doppler frequency domain given by $Y_{mf}(F) = |S_0(F)|^2\widetilde{A}(F)$.

To decrease the numerical effort, the matched filter mostly is applied in the frequency domain. In this case, the transfer function $S_0(F)$ has to be calculated for each ρ or for a variety of range strips each within the depth of focus zones. A fast method to evaluate $S_0(F)$ without Fourier transformation is the *method of stationary phase* which will be explained later.

Windowed matched filter In the time domain as well as in the Doppler frequency domain window functions can be applied to lower the sidelobes or to get independent subbands for *multilook processing*. The corresponding pulse response or transfer function, are

$$h_w(T) = s_0^*(T)w_T(T), \quad H_w(F) = S_0^*(F)w_F(F). \tag{4.62}$$

Inverse filter Similar as for pulse compression, an inverse filter can be applied according to

$$H_{inv}(F) = \begin{cases} \frac{1}{S_0(F)} \text{ if } F \in \mathbf{F}, \\ 0 \text{ else.} \end{cases} \tag{4.63}$$

Here $\mathbf{F}$ is a set of frequency values with $|S_0(F)| > 0$. The Fourier transform of the point spread function for the inverse filter is

$$P_{inv}(F) = I_{\mathbf{F}}(F)\frac{1}{S_0(F)}S_0(F)(F) = I_{\mathbf{F}}(F), \tag{4.64}$$

and the response to the azimuth reflectivity spectrum

$$Y_{inv}(F) = P_{inv}(F)\widetilde{A}(F) = I_{\mathbf{F}}(F)\widetilde{A}(F), \tag{4.65}$$

where $I_{\mathbf{F}}(F)$ is the indicator function of $\mathbf{F}$. If $Y_{inv}(F)$ is regarded as the reconstruction of $\widetilde{A}(F)$ the inverse filter is obviously the most accurate one with the best results if $\mathbf{F}$ is as large as possible.

Essence 4.6 *If the azimuth compression filter is chosen as the matched filter, the azimuth point spread function is the autocorrelation function of the azimuth chirp, it is the Fourier back transform of the square magnitude of the azimuth chirp spectrum. If the compression filter is chosen as the inverse filter, the point spread function is the Fourier back transform of the Indicator function of the Doppler frequency band.*

4.7.4 Azimuth resolution

In Eq. (4.6) it was already shown in a more or less heuristical manner that the achievable azimuth resolution in the stripmap mode is equal to $\delta x = \lambda/\delta u_a$.

This can be confirmed by inspecting the point spread function generated by the inverse filter. The usable frequency band $\mathbf{F}$ for non vanishing signal power will correspond to the main beam of the antenna, so it will be a frequency interval of length B given in Eq. (4.32) and (4.33). So the Fourier back transform will yield an si-function as point spread function with the Rayleigh width $\delta T = 1/B$. This leads to the azimuth resolution

$$\delta x = \delta T V = \frac{V}{B} = V\frac{\lambda}{2V\delta u_a} = \frac{\lambda}{2\delta u_a} = l_x/2. \tag{4.66}$$

This result is independent on the focusing direction of the real antenna.

4.7.5 Spotlight and sliding mode

As we have seen in section 4.7.4, for the stripmap mode the antenna must not be longer then twice the desired azimuth resolution. That means that a very short antenna has to be used to obtain a fine resolution. But this is a problem in several aspects: The antenna gain will be low leading to a poor SNR. At the same time the Nyquist condition for azimuth sampling (at least one pulse per movement of the half antenna length) requires a high PRF leading to a high data rate and perhaps range ambiguities.

Spotlight mode

For this problems, the *spotlight mode* affords relief: The antenna beam is steered to a fixed point at the earth. In this way the synthetic aperture can be elongated nearly arbitrarily to achieve fine resolution. The instantaneous Doppler bandwidth is still given by $B = 2V/l_x$ and the PRF has to be adopted to this bandwidth, while the center Doppler frequency changes according to the varying look direction. A disadvantage of the spotlight mode is the restriction of the azimuth length of the scene to the width of the antenna footprint.

Sliding mode

A continuous intermediate state between stripmap and spotlight mode can be obtained by the *sliding mode*. Here the center point of the antenna footprint moves along the earth surface with a velocity which is normally between zero and the platform velocity, but sometimes it is also desirable to let the footprint slide over the earth with a higher velocity or even opposite to the flight direction. In all these cases, a feasible balance between azimuth extension of the scene and azimuth resolution can be achieved.

4.8 The signal in two dimensions

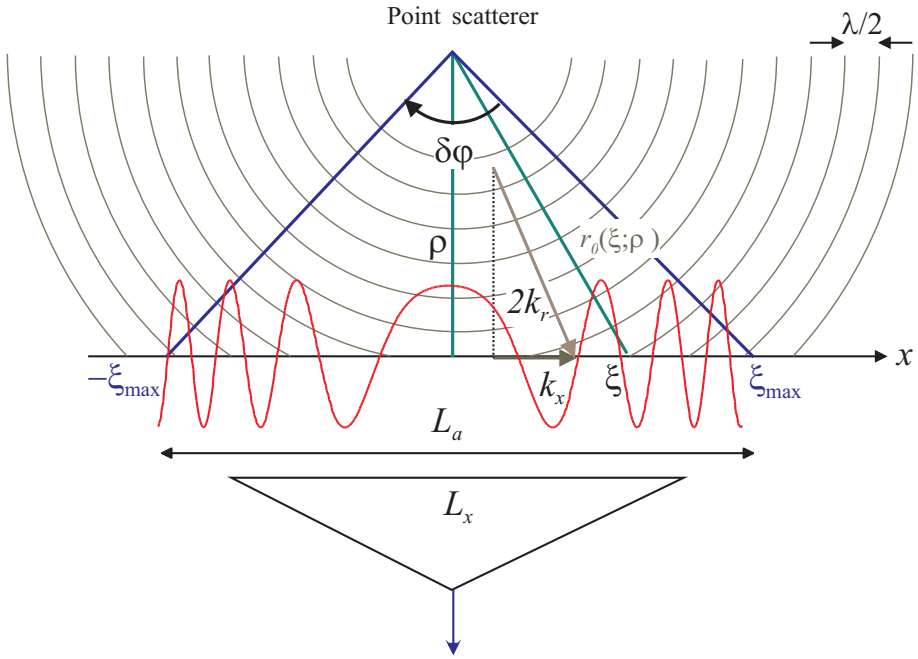

Figure 4.8: *Azimuth chirp and synthetic aperture*

At this stage of the chapter we have regarded only one-dimensional signal processing, we have seen the similarity of pulse compression in the fast-time domain and the compression of the azimuth chirp in the slow-time domain. The two dimensions

cannot be separated: e.g. after range compression the echoes of a point scatterer are not aligned in a straight row of the data matrix, but will migrate through the range lines due to the hyperbolic variation of range along slow time (*range curvature*). So it is necessary to analyze the signal simultaneously in two dimensions.

Since there are several distinct two-dimensional domains, it is not feasible to create for each of these domains a new symbol for the signal. For this reason we will use superscripts indicating the concerned domain, like s^{ξ,k_r} indicating that the signal is regarded in the (ξ, k_r)-domain.

4.8.1 The signal in the $\xi - r$ domain

We go back to the original raw data before pre-processing to the normal form. If the transmit signal $\mathsf{s}(r)$ - written as function of the spatial variable r - is used, the following raw data signal in the (ξ, r)-plane from a point scatterer at the position (x, ρ) is got:

$$\begin{aligned} s^{\xi,r}(\xi, r; x, \rho) &= \mathsf{s}\left(r - r_0(\xi - x; \rho)\right) && (4.67)\\ &\quad \times \exp\left\{-j2k_0 r_0(\xi - x; \rho)\right\} D\left(u_0(\xi - x; \rho)\right) && (4.68) \end{aligned}$$

where k_0 again is the wave number for the reference frequency.

Fresnel figures If the transmit signal is a chirp, written in the spatial variable as

$$\mathsf{s}(r) = \operatorname{rect}\left(\frac{r}{r_s}\right) \exp\left\{j\alpha\pi \left(\frac{r}{r_s}\right)^2\right\}, \tag{4.69}$$

where the temporal duration of the signal t_s is transferred to a spatial extension $r_s = t_s c_0/2$, the signal takes the form

$$\begin{aligned} s^{\xi,r}(\xi, r; x, \rho) &= \operatorname{rect}\left(\frac{r - r_0(\xi - x; \rho)}{r_s}\right) \exp\left\{j\alpha\pi \left(\frac{r - r_0(\xi - x; \rho)}{r_s}\right)^2\right\}\\ &\quad \times \exp\left\{-j2k_0 r_0(\xi - x; \rho)\right\} D\left(u_0(\xi - x; \rho)\right) \end{aligned} \tag{4.70}$$

If the antenna characteristics is assumed to be real, the phase of this expression is

$$\begin{aligned} \varphi(\xi, r) &= \alpha\pi \left(\frac{r - r_0(\xi - x; \rho)}{r_s}\right)^2 - 2k_0 r_0(\xi - x; \rho)\\ &\approx \alpha\pi \left(\frac{r - \rho}{r_s}\right)^2 - 2k_0 \left(\rho + \frac{1}{2\rho}(\xi - x)^2\right) && (4.71)\\ &= -2k_0\rho + \frac{\alpha\pi}{r_s^2}(r - \rho)^2 - \frac{2k_0}{2\rho}(\xi - x)^2 && (4.72) \end{aligned}$$

where the approximation is valid in the vicinity of (x, ρ). In the two-dimensional representation, the range shifted transmitted chirp is multiplied with the azimuth chirp in the ξ dimension. Since the exponents, which are both approximately quadratic in their respective variables add, the lines of equal phases are approximately ellipses, if the signs of the quadratic terms coincide, otherwise they are hyperbolas. Since the azimuth chirp is always a down-chirp, ellipses appear if the transmit signal is also a down chirp, and hyperbolas, otherwise. In Fig. 4.9 the real part of a simulated signal at $x = 0$ is presented.

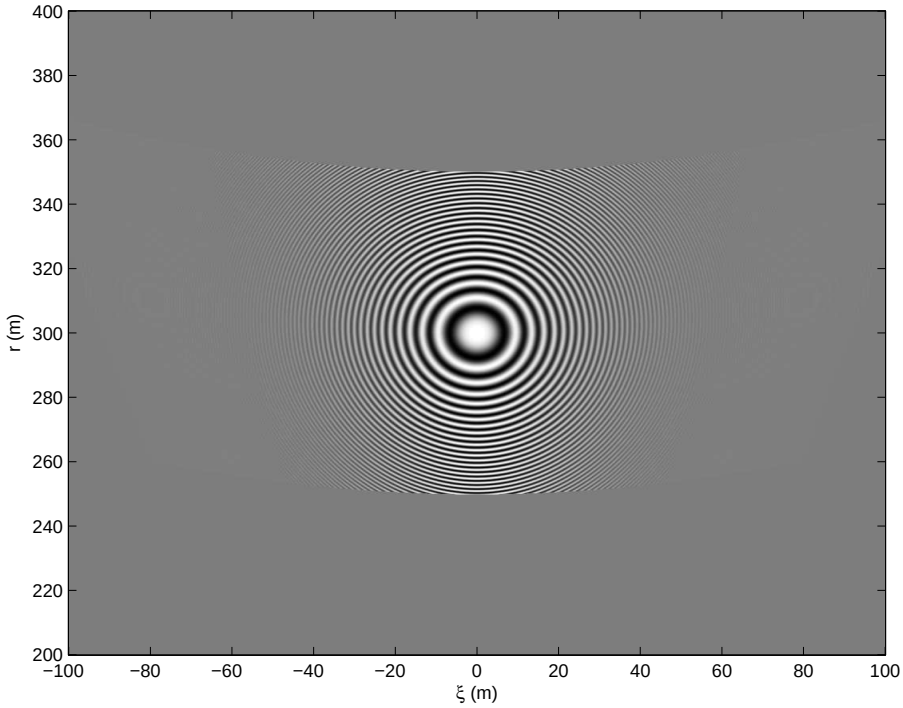

Figure 4.9: *Model signal in the $\xi - r$-plane (real part). Note the deformation along the azimuth coordinate due to the range hyperbola.*

Fig. 4.10 shows the raw data of a real SAR measurement, exhibiting these ellipse pattern accompanying every dominant point scatterer.

Around a fixed point targets we observe in the first case a sequence of concentric ellipses, which have the same sequence of radius as the fringes of a *Fresnel zone plate* which are the cuts of concentric sphere shells with equidistantly growing radius. These interference fringes are known from holography. Since such Fresnel interference patterns can be focused using coherent light, can SAR raw data, exposed on a photographic film, be focused to an image using optical methods, as it was done in the early period of SAR processing.

4.8.2 The signal in the $\xi - k_r$ domain

After the application of a Fourier transform from the r- to the k_r-dimension followed by an inverse filtering, the signal assumes the form

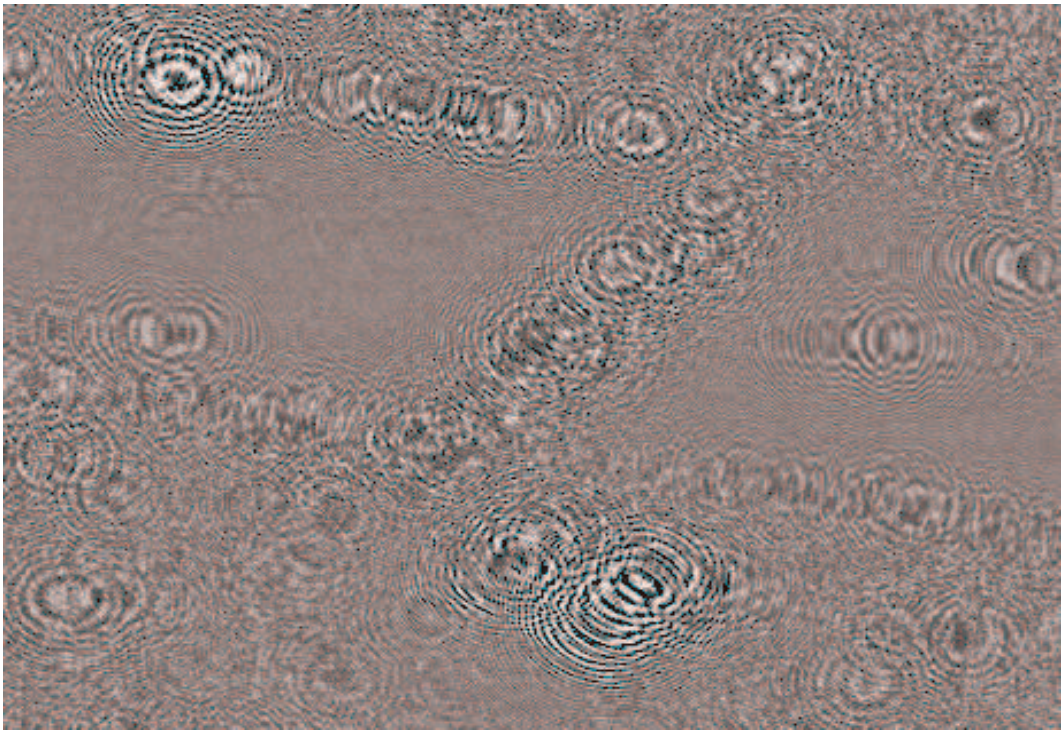

Figure 4.10: *Real raw data in the azimuth-range domain*

$$s^{\xi,k_r}(\xi,k_r;x,\rho)=\exp\left\{-j2k_r r_0(\xi;\rho)\right\}D\left(u_0(\xi;\rho)\right). \tag{4.73}$$

This equation expresses the same as Eq.(4.18) apart from the use of the spatial variable ξ instead of the slow time variable T. Fig. 4.11 shows the model signal in the $k_r-\xi$ domain.

4.8.3 The signal in the k_x-k_r domain

A spatial Fourier transform along ξ yields

$$\begin{aligned} s^{k_x,k_r}(k_x,k_r;x,\rho) &= e^{-jk_x x}s^{k_r,k_x}(k_r,k_x;0,\rho) \\ &= e^{-jk_x x}\int e^{-jk_x\xi}\exp\left\{-j2k_r r_0(\xi;\rho)\right\}D\left(u_0(\xi;\rho)\right)d\xi \end{aligned} \tag{4.74}$$

$$\tag{4.75}$$

Again, the principle of stationary phase can be applied. Not to repeat the derivations of section 4.7.2 we follow a little different way using geometrical interpretations.

The complete phase is given by

$$\phi(\xi)=-k_x\xi-2k_r r_0(\xi;\rho). \tag{4.76}$$

For each k_x, a position ξ_0 has to be determined where the derivation of $\phi(\xi)$ is zero, resulting in

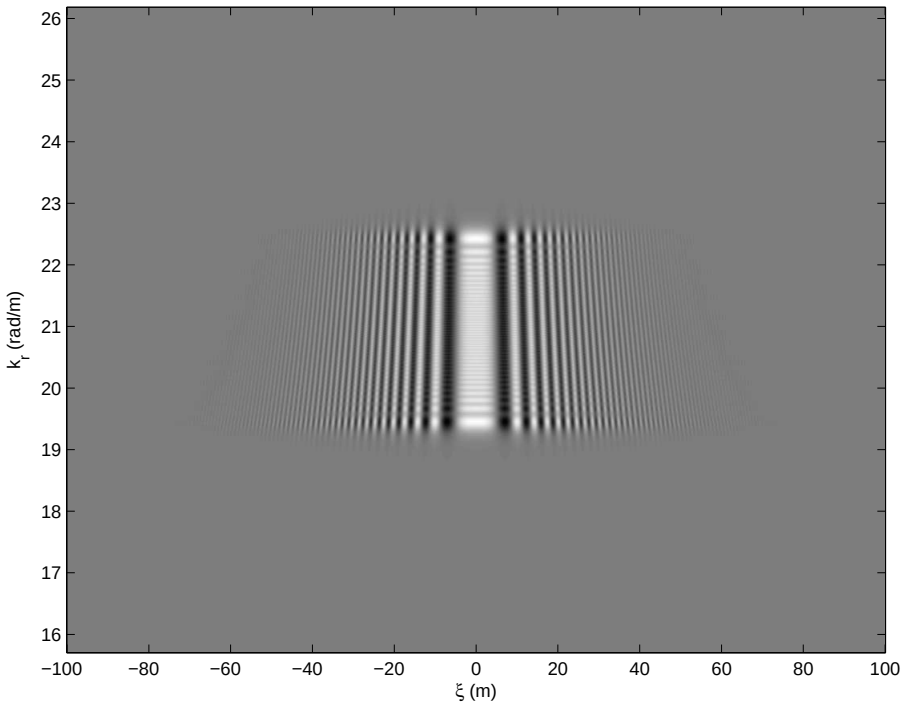

Figure 4.11: *Model signal in the $\xi - k_r$-plane (real part).*

$$
\begin{aligned}
0 &= -k_x - 2k_r r_0'(\xi_0;\rho) && (4.77)\\
\Longrightarrow k_x &= 2k_r u_0(\xi_0;\rho) && (4.78)\\
& && (4.79)
\end{aligned}
$$

The right side of this equation is the phase gradient along the synthetic aperture. Obviously, that position ξ_0 is searched for which this phase gradient is equal to k_x.

Since the absolute value of the phase gradient is always lower or equal to $2k_r$, we can characterize k_x as the abscissa component of a vector $\mathbf{k}$ with length $2k_r$ in the k-domain (k_x, k_ρ), see Fig. 4.12 top. In this plane, $k_x = 2k_r \cos\beta$ where β is the angle from the k_x-axis to the vector.

According to Eq.(4.76) the phase $\phi(\xi)$ may be written as $\phi(\xi) = -2k_r g(\xi)$ where $g(\xi) = \xi\cos\beta + r_0(\xi;\rho)$ can be interpreted as a way length, see Fig. 4.13. For arbitrary ξ the part $r_0(\xi;\rho)$ is the distance between the points A and B in the drawing. The distance between B and C is equal to $|\xi|\cos\beta$. Since we regard the left upper quadrant, the ξ-values are negative, so $g(\xi)$ will be the difference between the length of the lines $\vec{AB}$ and $\vec{BC}$, i.e. the length of the line $\vec{BC'}$. For varying ξ the point C' travels along the marked path, the minimum distance to the point A is reached at $C = C_0$, where the line of sight and the line through the origin and the points C defined by the ratio $k_x/(2k_r)$ are perpendicular.

This is easily proven by inspecting Eq.(4.77). From this follows

$$\cos\beta = u_0(\xi_0;\rho) = \cos\alpha \qquad (4.80)$$

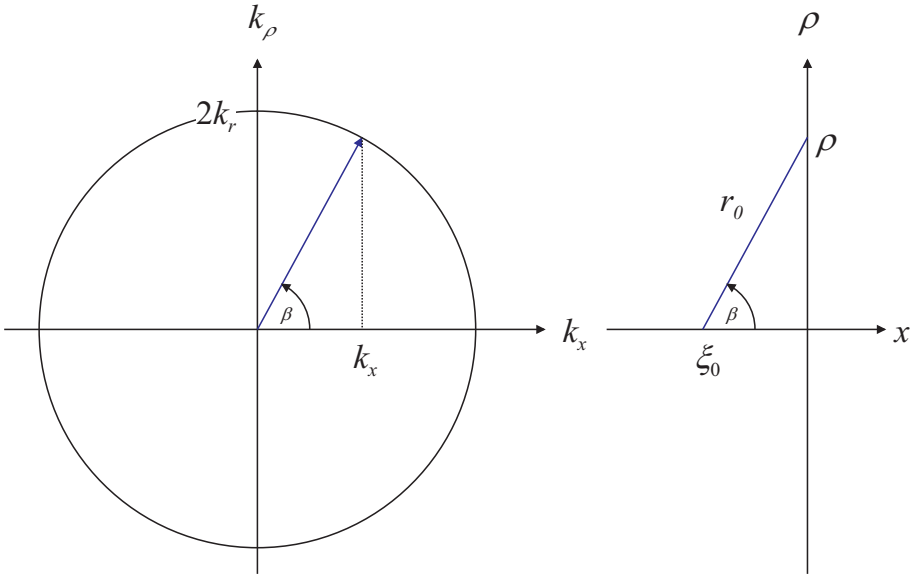

Figure 4.12: *Correspondence from the spatial domain to the domain of spatial frequencies.*

where α is the cone-angle corresponding to the point of the stationary phase. So the direction of the defined **k**-vector and the look direction at the point of the stationary phase coincide. From this we get immediately the values for ξ_0 and $r_0(\xi_0;\rho)$:

$$\xi_0 = -\rho\cot\beta, \quad r_0(\xi_0;\rho) = \rho/\sin\beta. \tag{4.81}$$

Also the value of $g(\xi_0)$ is easily obtained:

$$\begin{aligned} g(\xi_0) &= \rho\sin\beta \\ &= \rho\sqrt{1-\cos^2\beta} \\ &= \rho\sqrt{1-\frac{k_x^2}{4k_r^2}} \end{aligned} \tag{4.82}$$

and the corresponding phase is

$$\phi(\xi_0) = -2k_r g(\xi_0) = -\rho\sqrt{4k_r^2 - k_x^2}. \tag{4.83}$$

Fig. 4.13 bottom shows the behavior of the distance $g(\xi_0)$ in dependence on the variable k_x: In the right bottom quadrant the coordinate system (k_x, k_ρ) is sketched. A specific value of k_x defines the angle β in the circle with radius $2k_r$. In the left upper quadrant we see in the spatial coordinate system (x, ρ) the way of the point C_0 corresponding to the stationary phase for the actual value of k_x. Because of the

orthogonal angle to the line of sight this point moves on the half circle of Thales between the origin and the point A. The length of the cathetus emanating from A defines the stationary phase.

Essence 4.7 *Using the principle of the stationary phase, the phase of the Fourier transform of the azimuth chirp in dependence on the spatial frequency along the azimuth can be deduced to the cathetus length in the half circle of Thales as illustrated in Fig. 4.13.*

For the final formula we still need the second derivative of the phase:

$$\begin{aligned}
\phi''(\xi_0) &= -2k_r r_0''(\xi_0;\rho) \\
&= -2k_r \frac{\rho^2}{r_0^3(\xi_0;\rho)} \\
&= -2k_r \frac{\rho^2}{(\rho/\sin\alpha)^3} \\
&= -2k_r \frac{\sin^3\alpha}{\rho} \\
&= -\frac{2k_r}{\rho}\left(1-\frac{k_x^2}{4k_r^2}\right)^{3/2} \\
&= -\frac{1}{\rho 4k_r^2}\left(4k_r^2-k_x^2\right)^{3/2}. \qquad (4.84)
\end{aligned}$$

The final result for the signal in the $k_x - k_r$ domain now is

$$s^{k_x,k_r}(k_x,k_r;x,\rho) \approx C(k_x)\exp\left\{-j\left(k_x x+\rho\sqrt{4k_r^2-k_x^2}\right)\right\} D\left(\frac{k_x}{2k_r}\right) \qquad (4.85)$$

with

$$C(k_x) = (1+j)\sqrt{\frac{\pi\rho 4k_r^2}{\left(4k_r^2-k_x^2\right)^{3/2}}}. \qquad (4.86)$$

Essence 4.8 *Using the principle of the stationary phase, the signal in the $k_x - k_r$-domain can be approximated by Eq.(4.85) and (4.86).*

Fig. 4.14 shows the model signal in the double-wavenumber domain.

4.8.4 k-set and point spread function

We return to the three dimensional model and regard a reference point, which is at the coordinates $\vec{p}_0$, further a scattering center at the coordinates $\vec{p} = \vec{p}_0 + \vec{p}'$ in

the neighborhood of the reference point. The platform motion is described by the vector $\vec{R}(\xi)$. The range history to this scatterer is now

$$\begin{aligned} r(\xi;\vec{p}) &= \|\vec{R}(\xi)-\vec{p}\| && (4.87)\\ &= \|\vec{R}(\xi)-\vec{p}_0-\vec{p}'\| && (4.88)\\ &\approx r(\xi;\vec{p}_0)+\langle\vec{u}_0(\xi),\vec{p}'\rangle && (4.89)\end{aligned}$$

with the direction vector $\vec{u}_0(\xi)=\frac{\vec{R}(\xi)-\vec{p}_0}{|\vec{R}(\xi)-\vec{p}_0|}$ pointing from the radar to the position $\vec{p}_0$. The signal is given by

$$s(\xi,k_r;\vec{p}')=e^{-j2k_r r(\xi;\vec{p}_0)}\exp\{-j2k_r\langle\vec{u}_0(\xi),\vec{p}'\rangle\}D(2k_r\vec{u}_0(\xi)), \tag{4.90}$$

with the two-ways characteristics $D(2k_r\vec{u})$ written as function of the double k-vector and the measurements (without noise) by

$$z(\xi,k_r)=\int a(\vec{p}')s(\xi,k_r;\vec{p}')d\vec{p}', \tag{4.91}$$

where $a(\vec{p}')$ describes the reflectivity in the vicinity of the reference point. The first exponential function in Eq. (4.90) is equal for all $\vec{p}'$, the phase can be motion-corrected according to $r(\xi;\vec{p}_0)$ by

$$\begin{aligned} z_{mc}(\xi,k_r) &:= e^{j2k_r r(\xi;\vec{p}_0)}z(\xi,k_r) && (4.92)\\ &= \int a(\vec{p}')s_{mc}(\xi,k_r;\vec{p}')d\vec{p}' && (4.93)\\ \text{with } s_{mc}(\xi,k_r;\vec{p}') &= e^{j2k_r r(\xi;\vec{p}_0)}s(\xi,k_r;\vec{r}') && (4.94)\\ &= \exp\{-j2k_r\langle\vec{u}_0(\xi),\vec{p}'\rangle\}D(2k_r\vec{u}_0(\xi))). && (4.95)\end{aligned}$$

The SNR optimum processor correlates with the model signal:

$$\hat{a}(\vec{p}')=\frac{\int\int z_{mc}(\xi,k_r)\exp\{j2k_r\langle\vec{u}_0(\xi),\vec{p}'\rangle\}D(2k_r\vec{u}_0(\xi)))d\xi dk_r}{\int\int|D(2k_r\vec{u}_0(\xi)))|^2d\xi dk_r}. \tag{4.96}$$

By variation of the wavenumber in the interval $[k_{r1},k_{r2}]$ and by variation of the antenna position $\xi\in[\xi_1,\xi_2]$ a k-set

$$\mathcal{K}=\{2k_r\vec{u}_0(\xi):k_r\in[k_{r1},k_{r2}],\xi\in[\xi_1,\xi_2]\} \tag{4.97}$$

is generated and Eq. (4.96) using the variable $\vec{K}:=2k_r\vec{u}_0$ can be written as:

$$\hat{a}(\vec{p}')=\frac{\int_{\mathcal{K}}e^{j\langle\vec{K},\vec{p}'\rangle}z_{mc}(\vec{K})D(\vec{K})d\vec{K}}{\int_{\mathcal{K}}|D(\vec{K})|^2d\vec{K}}. \tag{4.98}$$

The k-set is a circular ring segment as illustrated in Fig. 4.15. If the antenna characteristics is assumed to be rectangular and a ξ-area is admitted which covers the

bounds of the main beam, the k-set can be restricted to the ring segment referring to the main beam. If this restricted k-set is denoted by $\mathcal{K}_0$, the equation Eq. (4.98) becomes

$$\hat{a}(\vec{p}\,') = \frac{\int_{\mathcal{K}_0} e^{j\langle \vec{K},\vec{p}\,'\rangle} z_{mc}(\vec{K}) d\vec{K}}{\int_{\mathcal{K}_0} d\vec{K}}. \tag{4.99}$$

Obviously the reconstruction is obtained by the Fourier transformation of the motion compensated data over the k-set.

If for z_{mc} the motion compensated signal of a point scatterer at $\vec{p} = \vec{p}_0$ is inserted, we get the point spread function

$$p(\vec{p}\,') = \frac{\int_{\mathcal{K}_0} e^{j\langle \vec{K},\vec{p}\,'\rangle} d\vec{K}}{\int_{\mathcal{K}_0} d\vec{K}}. \tag{4.100}$$

Essence 4.9 *The point spread function is the Fourier transform of the indicator function of the k-set.*

4.9 SAR-Processing

4.9.1 Generic SAR processor

The measured signal $z(\xi, r)$ consists of the superposition of the echoes of many point scatterers with the reflectivity at $a(x, \rho)$:

$$z(\xi, r) = \int\int a(x, \rho) s_0(\xi, r; x, \rho) dx d\rho, \tag{4.101}$$

or, after transformation into the (ξ, k_r)-domain,

$$z^{\xi,k_r}(k_r, \xi) = \int\int a(x, \rho) s^{\xi,k_r}(\xi, k_r; x, \rho) dx d\rho. \tag{4.102}$$

Principally, the raw data could be processed to an image optimally, if for each possible position of a point scatterer the two-dimensional normalized matched filter for the model signal in Eq. (4.67), and (4.73), respectively, would be applied:

$$\hat{a}(x, \rho) = \frac{\int\int s^*(\xi, r; x, \rho) z(\xi, r) dr d\xi}{\int\int |s(\xi, r; x, \rho)|^2 dr d\xi} \tag{4.103}$$

or

$$\hat{a}(x, \rho) = \frac{\int\int s^{\xi,k_r *}(\xi, k_r; x, \rho) z^{\xi,k_r}(\xi, k_r) dr d\xi}{\int\int |s^{\xi,k_r}(\xi, k_r; x, \rho)|^2 dr d\xi}. \tag{4.104}$$

The computational effort would be much to high. The first approach is to apply *separated processing*, i.e. range compression and azimuth compression are applied one after the other.

In Fig. 4.17 the essential building blocks of such a separated processor are illustrated.

4.9.2 Range-Doppler processor

The *range-Doppler processor* starts with the classical range compression as a rule as 'fast correlation' performed in the range frequency domain. Now the effect that the signal runs along a hyperbolic curve through the range cells - the range curvature problem - has to be solved.

Curvature correction in the k_x-domain

There is a possibility to reduce the numerical effort of the described interpolation along the range hyperbolas: First the data are transformed by an azimuth FFT into the k_x domain. The signals of scatterers with the same ρ but varying x-coordinates are shifted in slow time; but by the Fourier transform the pathes in the k_x-domain are overlayed[1]. For this reason, the *range curvature correction* can be performed in the k_x-domain simultaneously.

From Eq.(4.83) the phase for a certain k_x can be transferred to the range:

$$r(\xi_0, \rho) = -\frac{1}{2k_r}\phi(\xi_0) = \frac{\rho\sqrt{4k_r^2 - k_x^2}}{2k_r}. \tag{4.105}$$

From this, we get the range variation over k_x. All echoes are shifted back to the value ρ, see Fig. 4.19. This can be performed either by interpolation or by an approximate range curvature relating to the mean distance which can be executed in the range frequency domain. The result for the last possibility is depicted in Fig. 4.19. Only for the reference-ρ the correction is perfect. For smaller or larger slant ranges errors remain which can be neglected for small swathwidths. In the other case, a procedure called *differential range correction* has to be performed. Finally, the azimuth compression is completed by fast convolution along the rows.

4.9.3 Range-migration processor

The range-Doppler processing is based on a classical primary range compression. Since all transformations are linear, the order of application can be altered. Let us start with a pre-processing to the normal form (range FFT and inverse filtering) and an azimuth Fourier transform.

The signal of a point scatterer at (x, ρ) in the k_x, k_r-domain was calculated in Eq.(4.85) using the principle of stationary phase to

[1] Shift in time means multiplication by an exponential in the frequency domain!

$$s^{k_x,k_r}(k_x,k_r;x,\rho) \approx C(k_x)\exp\left\{-j\left(k_x x+\rho\sqrt{4k_r^2-k_x^2}\right)\right\}D\left(\frac{k_x}{2k_r}\right) \quad (4.106)$$

so the data will be the superposition of these signals with the azimuth reflectivity:

$$\begin{aligned} z^{k_x,k_r}(k_x,k_r) &= \int\int s^{k_x,k_r}(k_x,k_r;x,\rho)a(x,\rho)dxd\rho \quad (4.107)\\ &\approx C(k_x)\int\int \exp\left\{-j\left(k_x x+\rho\sqrt{4k_r^2-k_x^2}\right)\right\}D\left(\frac{k_x}{2k_r}\right)a(x,\rho)dxd\rho. \end{aligned}$$

Stolt-interpolation

If we set $k_\rho := \sqrt{4k_r^2-k_x^2}$ and perform the variable substitution

$$z^{k_x,k_\rho}(k_x,k_\rho) := z^{k_x,k_r}(k_x,2\sqrt{k_x^2+k_\rho^2}) \quad (4.108)$$

we get in the new (k_x,k_ρ)-domain:

$$\begin{aligned} z^{k_x,k_\rho}(k_x,k_\rho) &\approx C(k_x)D\left(\frac{k_x}{\sqrt{k_x^2+k_\rho^2}}\right)\int\int \exp\left\{-j\left(k_x x+k_\rho\rho\right)\right)\right\}a(x,\rho)dxd\rho.\\ &= C(k_x)D\left(\frac{k_x}{\sqrt{k_x^2+k_\rho^2}}\right)A(k_x,k_\rho) \quad (4.109) \end{aligned}$$

with $A(k_x,k_\rho)$ being the two-dimensional Fourier transformation of the reflectivity. This substitution has changed the data in the (k_x,k_r)-domain into the 2D Fourier transformation of the reflectivity distribution, modulated by the antenna characteristics.

Similar as for the polar reformatting the grid in (k_x,k_r) has to be transferred into a grid in the (k_x,k_ρ)-domain. For this the *Stolt-interpolation* is applied. At the end only a two-dimensional inverse Fourier transformation has to be performed to get the focused SAR image.

4.9.4 Back-projection processor

The *back projection processor* starts with a usual range compression. A two-dimensional array relating to the later image in the x,ρ-domain is initially filled with zeros. For each pulse the data are distributed along the related range rings and accumulated, see Fig. 4.21).

4.10 The radar equation for SAR imaging

In the power budget Eq. (1.196) we got an SNR of

$$\gamma = \frac{P_{tx} G_{tx} G_{rx} \lambda^2 q}{(4\pi)^3 r^4 \mathsf{k}\mathsf{T} b n_f} \eta \tag{4.110}$$

where P_{tx} is the transmit power, G_{tx} and G_{rx} are the gains of the transmit and receive antennas, λ the wavelength, q the radar cross section of the target, r the range, k the Boltzman constant, T the absolute temperature of the receiver, b the bandwidth, n_f the noise figure of the receiver chain and η the accumulated efficiency of the whole system. This forms the basis for completion of the power budget for SAR imaging.

Instead of a radar cross section q for SAR purposes we take the reflectivity density σ_0, defined by $q = \sigma_0 A$ being the cross section of an area A with constant σ_0. For SAR we chose the area $A = \delta x \times \delta r$ of a resolution cell, so $q = \sigma_0 \delta x \times \delta r$ can be inserted into Eq. (1.196).

The bandwidth b is the inverse illumination time $T_{compl} d$ of the patch where d is the duty factor and T_{compl} is the observation time which is related to the synthetic aperture via $T_{compl} = L_x / V$. On the other hand, the azimuth resolution is given by $\delta x = r\lambda/(2L_x)$ resulting in

$$b = \frac{1}{T_{compl} d} = \frac{V}{L_x d} = \frac{2V\delta x}{r\lambda d}. \tag{4.111}$$

By inserting also this expression into Eq. (1.196) we get the final result, the *radar equation for SAR*:

$$\gamma = \frac{P_{tx} G_{tx} G_{rx} \lambda^3 \sigma_0 \delta r d}{(4\pi)^3 r^3 \mathsf{k}\mathsf{T} n_f 2V} \eta. \tag{4.112}$$

The *noise-equivalent sigma-zero* (NESZ) is defined as that σ_0 which leads to the same power density as the noise. From this we can solve Eq. (4.112) to the maximum range where a specified NESZ is obtained:

$$r_{max} = \sqrt[3]{\frac{P_{tx} G_{tx} G_{rx} \lambda^3 \sigma_0 \delta r d}{NESZ (4\pi)^3 \mathsf{k}\mathsf{T} n_f 2V} \eta} \tag{4.113}$$

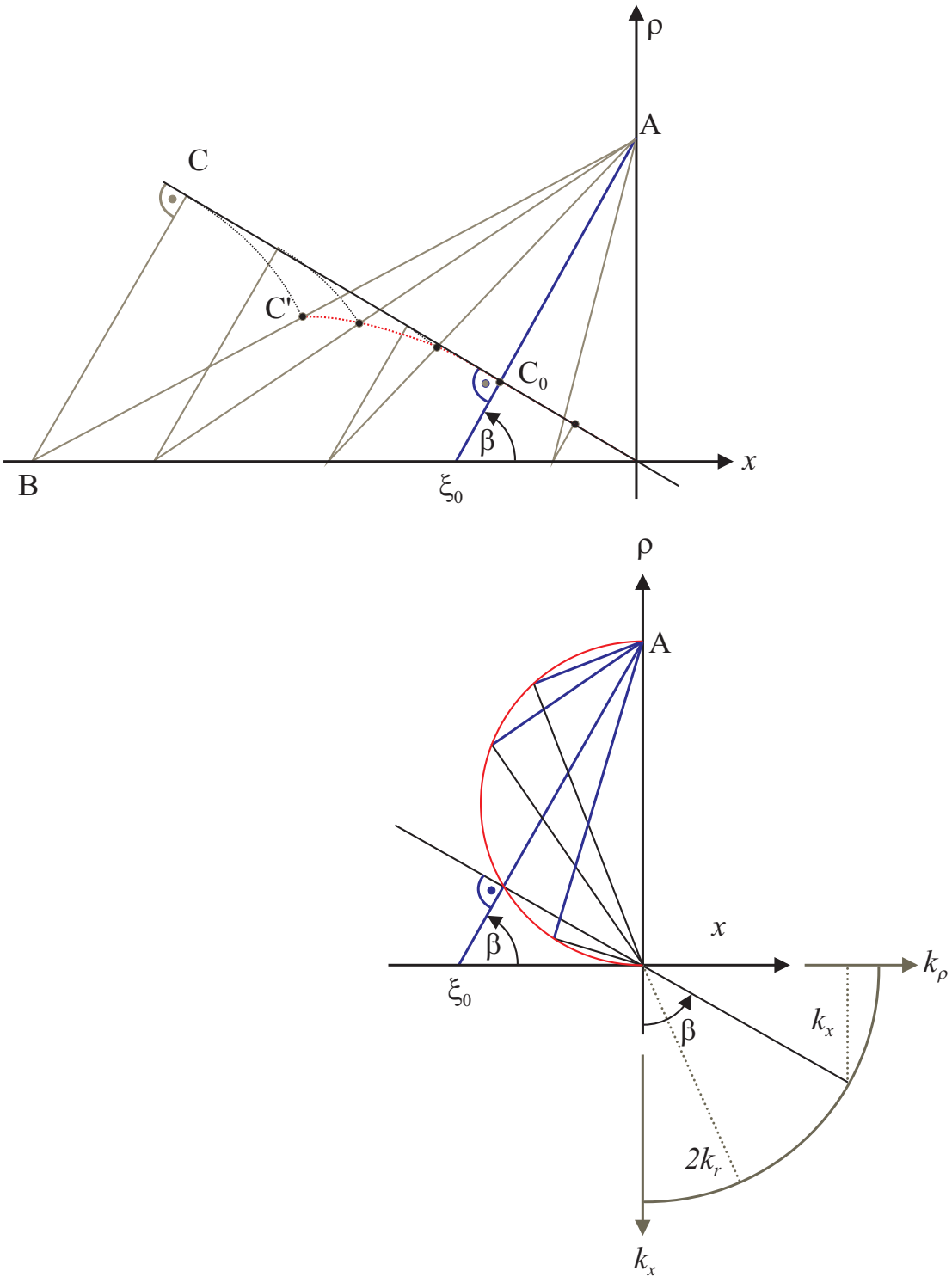

Figure 4.13: *Geometrical interpretation of the stationary phase*

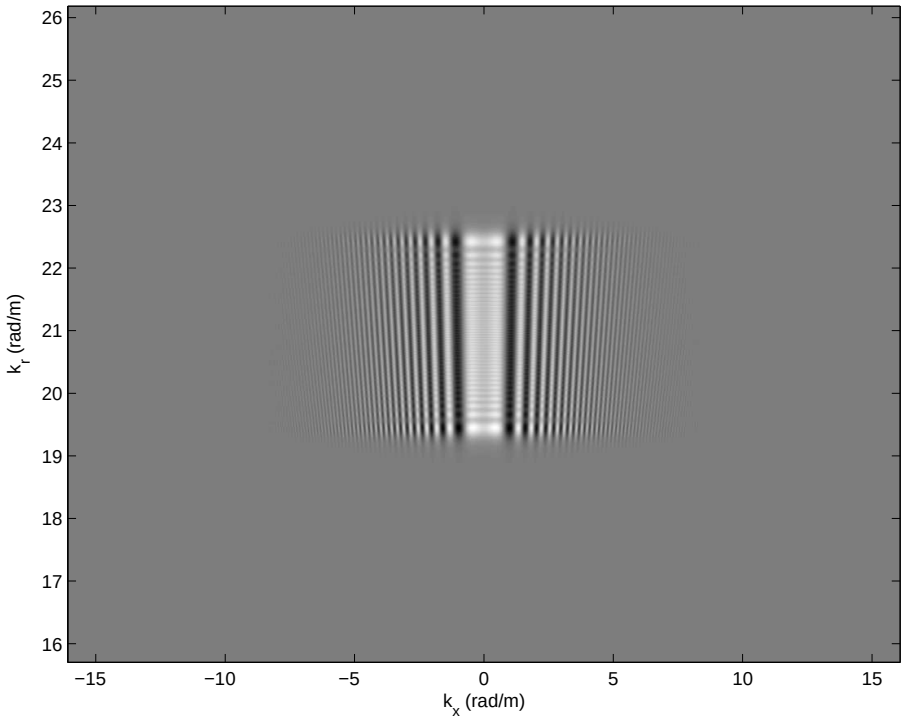

Figure 4.14: *Model signal in the $k_r - k_x$-plane (real part).*

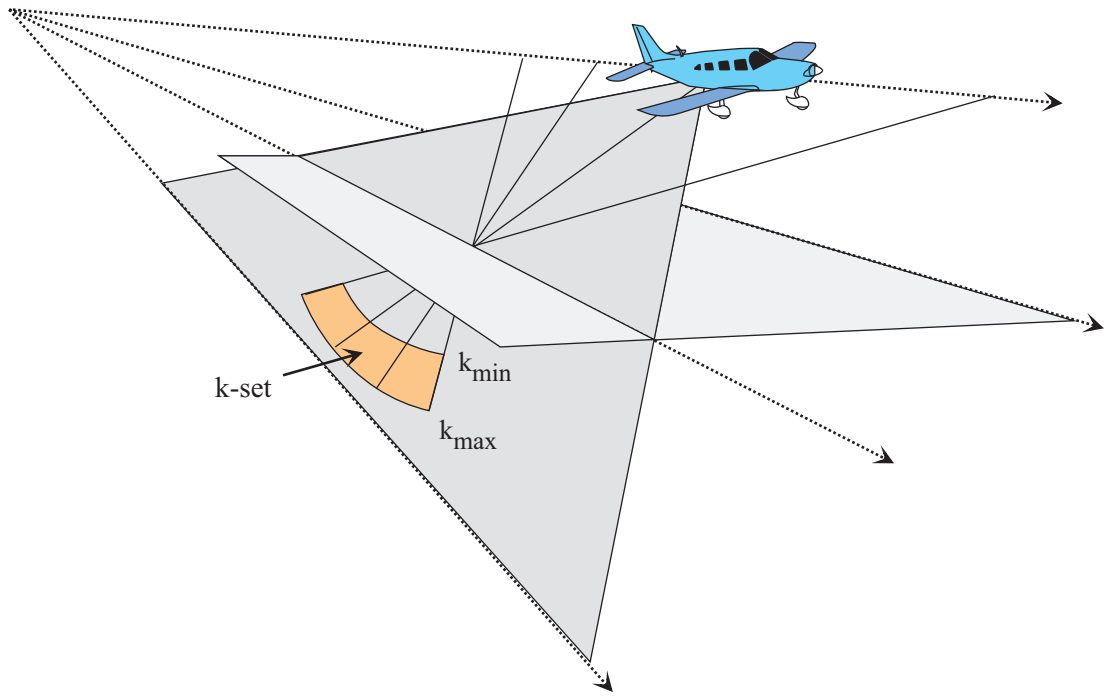

Figure 4.15: *The k-set in three dimensions generated by a stripmap SAR at a reference point at the surface*

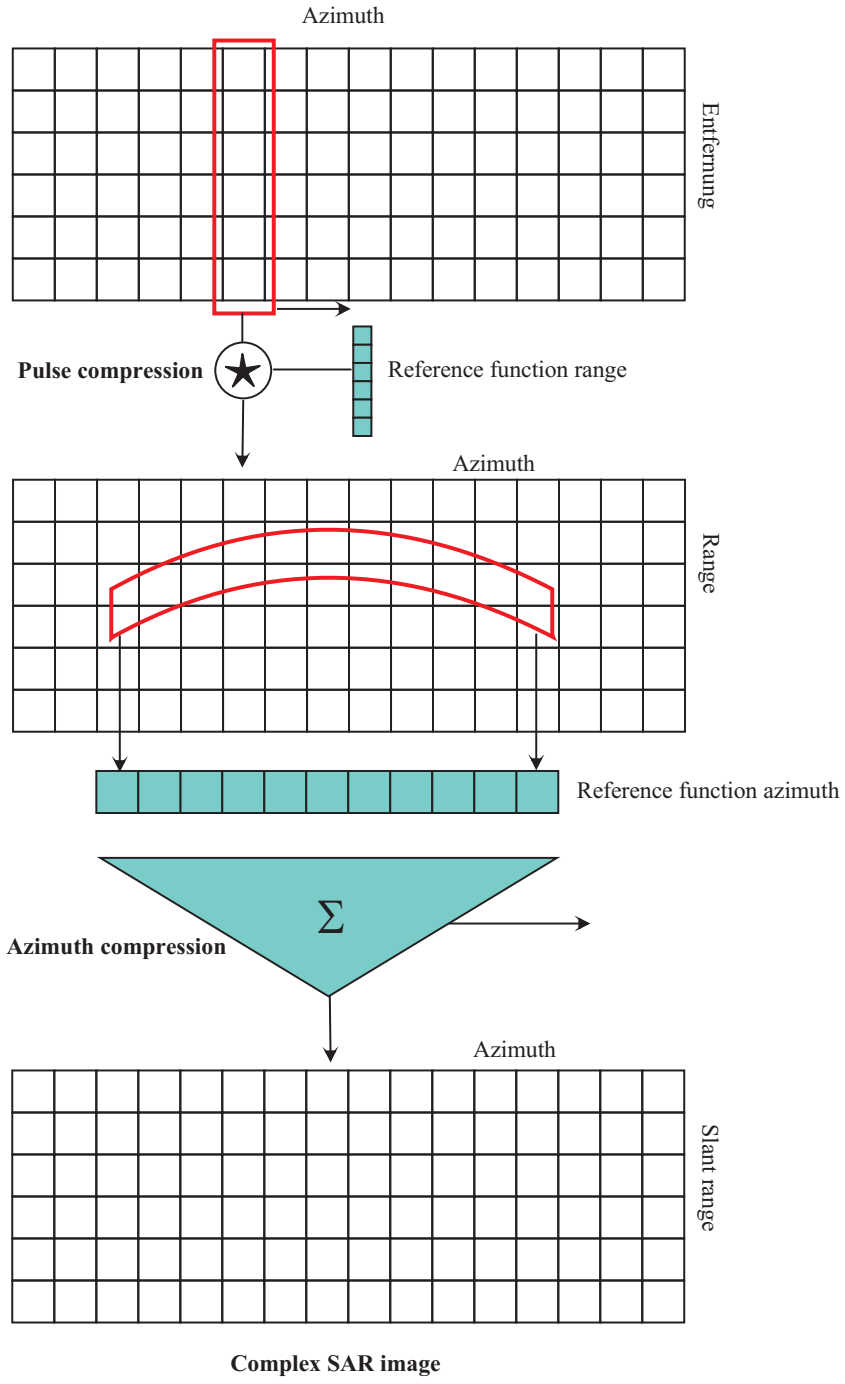

Figure 4.16: *Principle range Doppler processing*

Figure 4.17: *Principal steps in SAR processing*

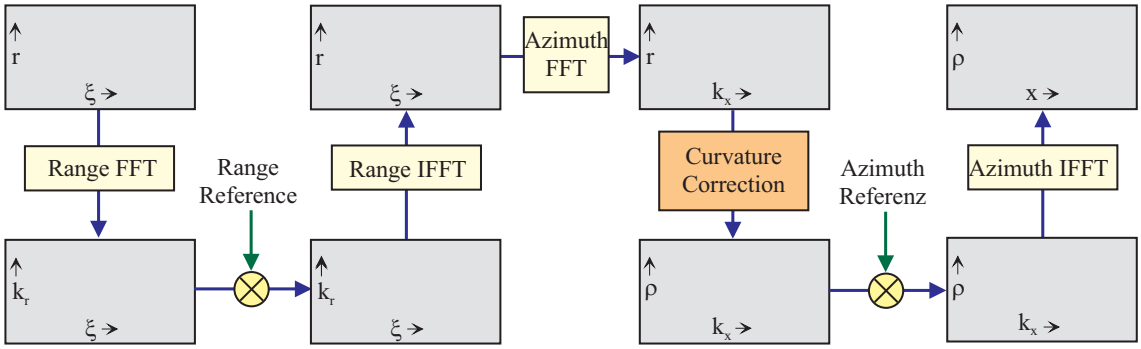

Figure 4.18: *Range Doppler processor*

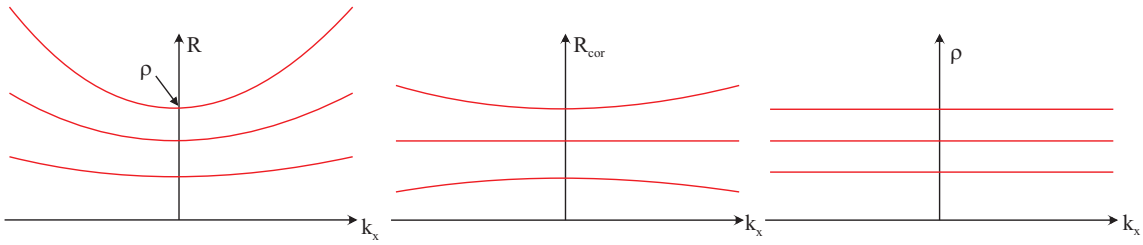

Figure 4.19: *Range curvature over k_x; Center: After correction; right: perfect correction*

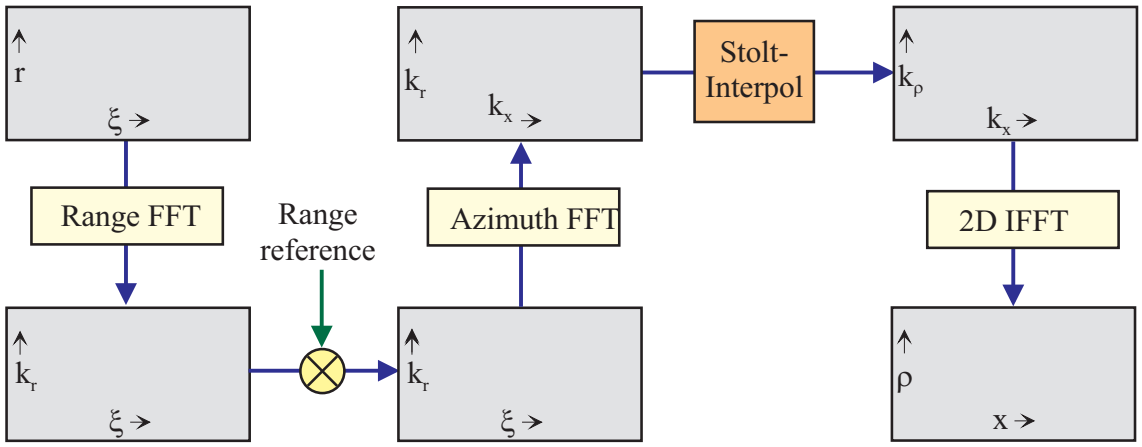

Figure 4.20: *Range migration (omega-k) processor*

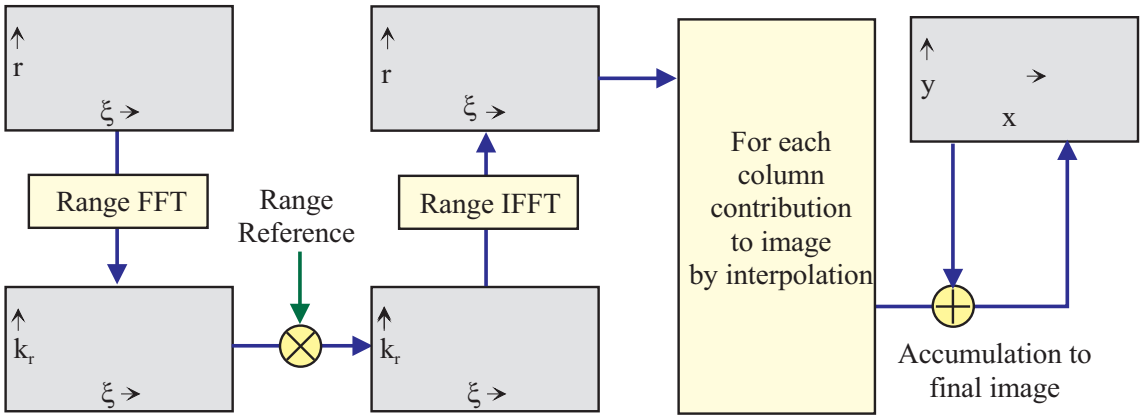

Figure 4.21: *Back projection processor*

Appendix A

Mathematical Annex

A.1 Complex linear algebra

A.1.1 Products of matrices

The vector space $\mathbb{C}^n$ is defined as the set of n-dimensional with elements in $\mathbb{C}$, where

$$\mathbb{C}^n := \left\{ \begin{pmatrix} a_1 \\ \cdots \\ a_n \end{pmatrix} : a_1, \cdots, a_n \in \mathbb{C} \right\}. \tag{A.1}$$

$\mathbb{C}^{n\times m}$ describes the set of all $n \times m$ matrices with complex coefficients. The matrix product is defined as common.

The superscript $*$ denotes complex conjugate, such as

$$\begin{pmatrix} a_{11} & \cdots & a_{1m} \\ \cdots & \cdots & \cdots \\ a_{n1} & \cdots & a_{nm} \end{pmatrix}^* = \begin{pmatrix} a_{11}^* & \cdots & a_{n1}^* \\ \cdots & \cdots & \cdots \\ a_{1m}^* & \cdots & a_{nm}^* \end{pmatrix}. \tag{A.2}$$

For matrices $\mathbf{A}$ and $\mathbf{B}$ yields

$$(\mathbf{AB})^* = \mathbf{B}^*\mathbf{A}^* \tag{A.3}$$

and for invertible quadratic matrices

$$(\mathbf{AB})^{-1} = \mathbf{B}^{-1}\mathbf{A}^{-1}. \tag{A.4}$$

Please note that for vectors $\mathbf{a}, \mathbf{b} \in \mathbb{C}^n$ the expression $\mathbf{a}^*\mathbf{b}$ represents a complex number and $\mathbf{ab}^*$ a complex matrix with rank one (a so-called *dyad*).

The *trace* of matrices is defined as the sum of all diagonal elements. It yields:

$$trace(\mathbf{AB}) = trace(\mathbf{BA}). \tag{A.5}$$

A.1.2 Scalar product and the inequality of Cauchy-Schwarz

The *scalar product (inner product, dot product)* $\mathbf{a}, \mathbf{b} \in \mathbb{C}^n$ is defined as

$$< \mathbf{a}, \mathbf{b} >:= \mathbf{b}^* \mathbf{a} = \sum_{\nu=1}^{n} b_\nu^* a_\nu, \tag{A.6}$$

and the L_2-norm as

$$\|\mathbf{a}\| := \sqrt{< \mathbf{a}, \mathbf{a} >} = \sqrt{\sum_{\nu=1}^{n} |a_\nu|^2}. \tag{A.7}$$

A vector $\mathbf{a} \in \mathbb{C}^n$ is called a *unit vector* when $\|\mathbf{a}\| = 1$; Two vectors $\mathbf{a}, \mathbf{b} \in \mathbb{C}^n$ are called *orthogonal* when $< \mathbf{a}, \mathbf{b} >= 0$. Two orthogonal unit vectors are denoted *orthonormal*.

The *correlation coefficient* of two non-zero vectors $\mathbf{a}, \mathbf{b} \in \mathbb{C}^n$ is given by

$$\rho(\mathbf{a}, \mathbf{b}) := \frac{< \mathbf{a}, \mathbf{b} >}{\|\mathbf{a}\| \|\mathbf{b}\|}. \tag{A.8}$$

Using *Cauchy-Schwarz' inequality* it follows that $|\rho(\mathbf{a}, \mathbf{b})| \leq 1$, with '=' if both vectors are linearly dependent.

A.1.3 Linear Subspaces

A *linear subspace* (LSS) U in $\mathbb{C}^n$ is a non-zero subset which is closed against the summation and multiplication with complex scalars.

If $\mathbf{s}_1, \cdots, \mathbf{s}_K$ are vectors in $\mathbb{C}^n$, the *linear hull* of these vectors is defined by the set of all *linear combinations*:

$$Lin\left(\mathbf{s}_1, \cdots, \mathbf{s}_K\right) := \left\{a_1 \mathbf{s}_1 + \cdots + a_K \mathbf{s}_K : a_1, \cdots, a_K \in \mathbb{C}\right\}. \tag{A.9}$$

The *dimension* od an LSS is the minimum number of vectors which span this space:

$$dim(U) := min\left\{K : \text{ It exist } \mathbf{s}_1, \cdots, \mathbf{s}_K \in \mathbb{C}^n \text{ mit } Lin\left(\mathbf{s}_1, \cdots, \mathbf{s}_K\right) = U\right\}. \tag{A.10}$$

$\mathbf{s}_1, \cdots, \mathbf{s}_K$ are linear independent, if $dim(Lin\left(\mathbf{s}_1, \cdots, \mathbf{s}_K\right)) = K$. In this case, the vectors constitute a *basis* of this space.

A system $\mathbf{u}_1, \cdots, \mathbf{u}_K$ is called an *orthogonal system* if these vectors are mutually orthogonal, and called *orthonormal system* if they are additionally unit vectors:

$$\mathbf{u}_k^* \mathbf{u}_l = \delta_{kl}. \tag{A.11}$$

A orthonormal system $\mathbf{u}_1, \cdots, \mathbf{u}_K$, combined in the $n \times K$-matrix $\mathbf{U} = (\mathbf{u}_1, \cdots, \mathbf{u}_K)$, consists the property

$$\mathbf{U}^* \mathbf{U} = \mathbf{I}_K, \tag{A.12}$$

where $\mathbf{I}_K$ denotes the $K \times K$ identity matrix. Every orthonormal system is linearly independent and the spanned space constitutes a basis.

Let U be A LSS of $\mathbb{C}^n$. Then $U^\perp$ denotes the LSS of all vectors, which are orthogonal to each vector of U.

A.1.4 Properties of Matrices

Hermitian Matrices

A matrix $\mathbf{A} \in \mathbb{C}^{n \times m}$ is called *Hermitian* if and only if $\mathbf{A}^* = \mathbf{A}$.

It is called *positive semidefinite* if each *quadratic form* $\mathbf{x}^*\mathbf{A}\mathbf{x}$ is non-negative:

$$\mathbf{x}^*\mathbf{A}\mathbf{x} \geq 0 \text{ for each } \mathbf{x} \in \mathbb{C}^n. \tag{A.13}$$

It is called *positive definite* if and only if each of those quadratic form is greater than zero for arbitrary vectors $\mathbf{x} \in \mathbb{C}^n$ with $\mathbf{x} \neq \mathbf{0}$.

Unitary Matrices

A $n \times n$-matrix $\mathbf{U}$ of n vectors of a orthonormal system is called *unitary*. It yields:

$$\mathbf{U}^*\mathbf{U} = \mathbf{U}^* = \mathbf{I}_n, \tag{A.14}$$

$$\mathbf{U}^* = \mathbf{U}^{-1}. \tag{A.15}$$

Projectors

A $n \times n$-matrix $\mathbf{P}_U$ is called *projector* or projection matrix if $\mathbf{P}_U\mathbf{P}_U = \mathbf{P}_U$. Let U the subspace spanned by the columns of $\mathbf{P}$. Then it yields:

$$\mathbf{P}_U\mathbf{s} = \mathbf{s}, \text{ if } \mathbf{s} \in U, \tag{A.16}$$

$$\mathbf{P}_U\mathbf{s} = \mathbf{0}, \text{ if } \mathbf{s} \in U^{\perp}. \tag{A.17}$$

$\mathbf{P}_{U^{\perp}} := \mathbf{I} - \mathbf{P}_U$ is also a projector, namely onto the orthogonal space to U. It yields:

$$\mathbf{P}_{U^{\perp}}\mathbf{P}_U = \mathbf{0}. \tag{A.18}$$

Futher, it yields that for each $\mathbf{s} \in \mathbb{C}^n$:

$$\mathbf{s} = \mathbf{P}_U\mathbf{s} + \mathbf{P}_{U^{\perp}}\mathbf{s}. \tag{A.19}$$

The two vectors $\mathbf{s}_U := \mathbf{P}_U\mathbf{s}$ and $\mathbf{s}_{U^{\perp}} := \mathbf{P}_{U^{\perp}}\mathbf{s}$ are orthogonal to each other and with the generalized Pythagoras' theorem:

$$\|\mathbf{s}\|^2 = \|\mathbf{s}_U\|^2 + \|\mathbf{s}_{U^{\perp}}\|^2. \tag{A.20}$$

Eigen-Decomposition

A vector $\mathbf{v}$ is called *eigenvector to the eigenvalue* λ of the matrix $\mathbf{A}$, if

$$\mathbf{A}\mathbf{v} = \lambda\mathbf{v}. \tag{A.21}$$

Eigenvectors to different eigenvalues are orthogonal. Each Hermitian matrix $\mathbf{A}$ can be *diagonalized*:

$$\mathbf{A} = \mathbf{U}\mathbf{\Lambda}\mathbf{U}^*, \tag{A.22}$$

where $\mathbf{U}$ is a unitary matrix and Λ is a diagonal matrix with real diagonal elements λ_ν.

It is easy to see that the column vectors $\mathbf{u}_\nu$ of $\mathbf{U}$ constitute a complete system of eigenvectors to the eigenvalues λ_ν. Eq. A.22 can also be written as a sum of dyads:

$$\mathbf{A} = \sum_{\nu=1}^{n} \lambda_\nu \mathbf{u}_\nu \mathbf{u}_\nu^*. \tag{A.23}$$

A projector $\mathbf{P}_U$ onto a K-dimensional subspace U can be written to

$$\mathbf{P}_U = \sum_{\nu=1}^{K} \mathbf{u}_\nu \mathbf{u}_\nu^*, \tag{A.24}$$

where $\mathbf{u}_\nu, \nu = 1, \cdots, K$ is a orthonormal basis of U. Consequently, $\mathbf{P}_U$ has K eigenvalues $= 1$ and $n - K$ eigenvalues $= 0$.

On a Hermitian matrix $\mathbf{A}$ functions can be applied such as potentiate, logarithmal etc., if the values of the diagonal matrix are used:

$$f(\mathbf{A}) = \mathbf{U} \begin{pmatrix} f(\lambda_1) & \cdots & 0 \\ \cdots & \cdots & \cdots \\ 0 & \cdots & f(\lambda_n) \end{pmatrix} \mathbf{U}^*, \tag{A.25}$$

e. g.

$$\mathbf{A}^x = \mathbf{U} \begin{pmatrix} \lambda_1^x & \cdots & 0 \\ \cdots & \cdots & \cdots \\ 0 & \cdots & \lambda_n^x \end{pmatrix} \mathbf{U}^*. \tag{A.26}$$

Matrix inversion

A positive definite Hermitian matrix $\mathbf{A}$ is invertible. Using the eigen decomposition $\mathbf{A} = \mathbf{U}\mathbf{\Lambda}\mathbf{U}^*$ it yields

$$\mathbf{A}^{-1} = \mathbf{U} \begin{pmatrix} \frac{1}{\lambda_1} & \cdots & 0 \\ \cdots & \cdots & \cdots \\ 0 & \cdots & \frac{1}{\lambda_n} \end{pmatrix} \mathbf{U}^*. \tag{A.27}$$

A matrix of the form $\mathbf{A} = \mathbf{I}_n + \mathbf{s}\mathbf{s}^*$ is positive definite and invertible. The inverse is computed to

$$\mathbf{A}^{-1} = \mathbf{I}_n - \frac{1}{\mathbf{s}^*\mathbf{s} + 1}\mathbf{s}\mathbf{s}^* \tag{A.28}$$

If $\mathbf{S}$ is a $n \times k$-matrix with $k \leq n$ and $\mathbf{D}$ a invertible $k \times k$-matrix, then is a matrix of the form $\mathbf{A} = \mathbf{I}_n + \mathbf{S}\mathbf{D}\mathbf{S}^*$ invertible and it yields:

$$\mathbf{A}^{-1} = \mathbf{I}_n - \mathbf{S}\left(\mathbf{I}_k + \mathbf{D}\mathbf{S}^*\mathbf{S}\right)^{-1}\mathbf{D}\mathbf{S}^*. \tag{A.29}$$

Please note, that in the so called (*Matrix-Inversion-Lemma*) (A.29) the inversion in the n-dimensional space has been transformed into the k-dimensional space.

Differentiating of complex vectors

Let x be a real variable, and $\mathbf{F}(x)$ a complex vector depending on x. Then

$$\frac{d}{dx}\|\mathbf{F}(x)\|^2 = 2\Re\left\{\left(\frac{d}{dx}\mathbf{F}(x)\right)^* \mathbf{F}(x)\right\}. \tag{A.30}$$

Best linear approximations

If $\mathbf{z}$ and $\mathbf{s}$ are n-dim. column vectors and a is a complex constant, then

$$\hat{a}(\mathbf{z}) := \operatorname{argmin}\{\|\mathbf{z} - a\mathbf{s}\|^2 : a \in \mathbb{C}\} = \frac{\mathbf{s}^*}{\mathbf{s}^*\mathbf{s}}\mathbf{z}. \tag{A.31}$$

The best approximation of $\mathbf{z}$ by a scalar multiple of $\mathbf{s}$ in the minimum square error sense is

$$\hat{a}(\mathbf{z})\mathbf{s} = \frac{\mathbf{s}\mathbf{s}^*}{\mathbf{s}^*\mathbf{s}}\mathbf{z}. \tag{A.32}$$

$\mathbf{P}_{<\mathbf{s}>} := \frac{\mathbf{s}\mathbf{s}^*}{\mathbf{s}^*\mathbf{s}}$ is the projector to the subspace spanned by $\mathbf{s}$. Using the generalized Pythagoras' equation

$$\|\mathbf{z}\|^2 = \|\mathbf{P}_{<\mathbf{s}>}\|^2 + \|\mathbf{P}_{<\mathbf{s}>^\perp}\|^2. \tag{A.33}$$

shows that $\|\mathbf{P}_{<\mathbf{s}>^\perp}\|^2$ is the remaining quadratic error.

If $\mathbf{s}_1, \ldots, \mathbf{s}_k$ are linear independent n-dim. column vectors we search for the best approximation of $\mathbf{z}$ by a linear combination of $\mathbf{s}_1, \ldots, \mathbf{s}_k$ with complex coefficients $a_1, \ldots, a_k$:

$$\|\mathbf{z} - (a_1\mathbf{s}_1 + \cdots + a_k\mathbf{s}_k)\|^2 = \text{Min!} \tag{A.34}$$

Let $\mathbf{S} = (\mathbf{s}_1, \ldots, \mathbf{s}_k)$ be the $n \times k$-matrix composed of the signal vectors and $\mathbf{a} = (a_1, \ldots, a_k)^t$ the k-dim. vector of coefficients. Then Eq. (A.34) can be written in the form

$$\hat{\mathbf{a}}(\mathbf{z}) := \operatorname{argmin}\{\|\mathbf{z} - \mathbf{S}\mathbf{a}\|^2 : \mathbf{a} \in \mathbb{C}^k\}. \tag{A.35}$$

The solution is

$$\hat{\mathbf{a}}(\mathbf{z}) = (\mathbf{S}^*\mathbf{S})^{-1}\mathbf{S}^*\mathbf{z}. \tag{A.36}$$

The best approximation of $\mathbf{z}$ can be written in the form

$$\begin{aligned} \hat{\mathbf{a}}(\mathbf{z}) &= \mathbf{S}(\mathbf{S}^*\mathbf{S})^{-1}\mathbf{S}^*\mathbf{z} && \text{(A.37)} \\ &= \mathbf{P}_{<\mathbf{s}_1,\ldots,\mathbf{s}_k>}\mathbf{z} && \text{(A.38)} \\ &= \mathbf{P}_{U_S}\mathbf{z} && \text{(A.39)} \end{aligned}$$

if $U_S :=< \mathbf{s}_1, \ldots, \mathbf{s}_k >$ denotes the subspace spanned by the columns of $\mathbf{S}$. $\mathbf{P}_{U_S} = \mathbf{S}\left(\mathbf{S}^*\mathbf{S}\right)^{-1}\mathbf{S}^*$ is the projector to this space.

A.1.5 Order of matrices

For a Hermitean matrix $\mathbf{A} \in \mathbb{C}^{N\times N}$ it is defined $\mathbf{A} \geq \mathbf{0}$ if for all $\mathbf{x} \in \mathbb{C}^N$ the inequality $\mathbf{x}^*\mathbf{A}\mathbf{x} \geq 0$ is valid. This is identical to the property that all eigenvalues of $\mathbf{A}$ are greater or equal to 0, i.e. $\mathbf{A}$ is positive semidefinite.

For two Hermitean matrices $\mathbf{A}, \mathbf{B}$ the half order $\mathbf{A} \geq \mathbf{B}$ is defined by $\mathbf{A} - \mathbf{B} \geq \mathbf{0}$.

A.2 Energy signals

The space $L_2(\mathbb{C})$ is defined as the set of all square-integrable signals $s : \mathbb{R} \to (\mathbb{C})$. For $s, s_1, s_2 \in L_2(\mathbb{C})$ we define

$$\begin{aligned} < s_1, s_2 > &:= \int s_1(t)\, s_2^*(t)\, dt \quad \text{(dotproduct)}, \\ \|s\| &:= \sqrt{< s, s >} = \sqrt{\int |s(t)|^2\, dt} \quad (\|s\|^2 = \textit{signalenergy}.) \end{aligned} \tag{A.40}$$

It yields

$$< as_1 + bs_2, s > = a < s_1, s > + b < s_2, s > \tag{A.41}$$

$$< s, as_1 + bs_2 > = a^* < s, s_1 > + b^* < s, s_2 > \text{ for all } a, b \in \mathbb{C}, \tag{A.42}$$

$$\|s\| = 0 \text{ if and only if} s(t) = 0 \text{ (almost everywhere) .} \tag{A.43}$$

Possess s_1, s_2 non-vanishing signal energy, then

$$\rho(s_1, s_2) := \frac{< s_1, s_2 >}{\|s_1\|\,\|s_2\|} \quad \text{(correlationcoefficient, generalized cosine).} \tag{A.44}$$

It yields

$$|\rho(s_1, s_2)| \leq 1 \tag{A.45}$$

with equality if and only if an $a \in \mathbb{C}$ exists with $s_1(t) = as_2(t)$ almost everywhere (Cauchy-Schwarz' inequality).

The *convolution* of s_1 with s_2 is defined to

$$(s_1 * s_2)(t) := \int s_1(\tau)\, s_2(t-\tau)\, d\tau = \int s_1(t-\tau)\, s_2(\tau)\, d\tau, \tag{A.46}$$

the *cross-correlation function* to

$$r_{s_1 s_2}(t) := \int s_1(t+\tau)\, s_2^*(\tau)\, d\tau = \int s_1(\tau)\, s_2^*(\tau - t)\, d\tau, \tag{A.47}$$

and the *auto-correlation function* to

$$r_{ss}(t) := \int s_1(t+\tau)\, s^*(\tau)\, d\tau. \tag{A.48}$$

It yields

$$r_{s_1 s_2} = s_1^* \tilde{s}_2 \text{ with } \tilde{s}_2(t) := s_2^*(-t) \tag{A.49}$$

$$r_{s_1 s_2}(t) = < s_1, s_2^{(t)} > \text{ with } s_2^{(t)}(\tau) := s_2(\tau - t) \tag{A.50}$$

The *Fourier transform of a signal* is defined to

$$S(\omega) := \int s(t) e^{-j\omega t} dt. \tag{A.51}$$

with the *back transformation*

$$s(t) = \frac{1}{2\pi} \int S(\omega) e^{j\omega t} d\omega. \tag{A.52}$$

The application of the Fourier transform is written as $S = \mathcal{F}(s)$, $s = \mathcal{F}^{-1}(S)$ and $S(\omega) = \mathcal{F}(s(t)), \quad s(t) = \mathcal{F}^{-1}(S(\omega))$, respectively.

For the Fourier pairs $S = F(s)$, $S_1 = F(s_1)$, and $S_2 = F(s_2)$ yields:

$$\|s\|^2 = \frac{1}{2\pi} \|S\|^2 \textit{ (Parzeval's Lemma),} \tag{A.53}$$

$$< s_1, s_2 > = \frac{1}{2\pi} < S_1, S_2 >, \tag{A.54}$$

$$F(s_1 * s_2) = S_1 S_2 \;\; F(s_1 s_2) = S_1 * S_2, \tag{A.55}$$

$$F(r_{s_1 s_2}) = S_1 S_2 \;\; F(r_{ss}) \quad = |S|^2. \tag{A.56}$$

A.3 Special Functions

Rectangular function:

$$\text{rect}(t) := \begin{cases} 1 \text{ for } |t| \leq \frac{1}{2} \\ 0 \text{ else} \end{cases} \tag{A.57}$$

$\sin x/x$-function:

$$\text{si}(x) := \begin{cases} 1 \text{ for } x = 0 \\ \sin(x)/x \text{ else} \end{cases} \tag{A.58}$$

Integral sine:

$$\text{Si}(x) := \int_0^x si(t) dt \tag{A.59}$$

Modified Bessel function:

$$I_\nu(x) := \frac{1}{2\pi} \int_0^{2\pi} \cos^\nu(\varphi) e^{x\cos(\varphi)} d\varphi \tag{A.60}$$

Fresnel-Integrals:

$$S(x) := \int_0^x \sin\left(\frac{\pi}{2} t^2\right) dt \tag{A.61}$$

$$C(x) := \int_0^x \cos\left(\frac{\pi}{2} t^2\right) dt \tag{A.62}$$

A.4 Probability distributions

A.4.1 Random variables, realizations, probability distributions and densities

Let X be a random variable with values in Ω^X. If x is the result of a 'random experiment' performing X, x is called a *realization* of X. If the random experiment is repeated n times, we observe the realizations $x_1, \cdots, x_n$.

The probability to get a result x is characterized by the *probability distribution* P^X. The probability that X falls into a (measurable) subset $A \subseteq \Omega^X$ is given by $P^X(A)$. If X takes continuous values, the *probability density function (pdf)* $p^X(x)$ defines the distribution via

$$P^X(X \in M) = \int_M p^X(x)dx. \tag{A.63}$$

Expectation and *Variance* of a random variable X with values in $\mathbb{R}$ and the pdf p^X are defined by

$$\begin{aligned} E[X] &= \int x p^X(x)dx && \text{(A.64)} \\ \mathrm{Var}[X] &= \int (x - E[X])^2 p^X(x)dx && \text{(A.65)} \\ &= \int x^2 p^X(x)dx - \left(\int x p^X(x)dx\right)^2. && \text{(A.66)} \end{aligned}$$

For each function $f(x)$ we get

$$E[f(X)] = \int f(x) p^X(x)dx. \tag{A.67}$$

Random variables X and Y are *(statistically, stochastically) independent* if

$$P^{(X,Y)}(X \in M_X, Y \in M_Y) = P^X(X \in M_X) P^Y(Y \in M_Y) \tag{A.68}$$

for all (measurable) subsets M_X and M_Y. If there exists the common pdf of (X, Y) this is equivalent to

$$p^{(X,Y)}(x, y) = p^X(x) p^Y(y) \tag{A.69}$$

(almost everywhere).

If X and Y are independent, also functions of these $f(X)$ and $g(Y)$ are independent. Further independent random variables have the following properties:

$$\begin{aligned} E[XY] &= E[X]E[Y] && \text{(A.70)} \\ \mathrm{Var}[X + Y] &= \mathrm{Var}[X] + \mathrm{Var}[Y] && \text{(A.71)} \end{aligned}$$

For random variables X and Y with values in $\mathbb{R}$ *Jensen's Inequality* is valid:

$$E[XY] \leq \sqrt{E[X^2]E[Y^2]}. \tag{A.72}$$

Complex random variables

For random variables Z, W with values in $\mathbb{C}$ expectation and variance are defined by analogy:

$$\begin{aligned} E[Z] &:= E[\Re\{Z\}] + jE[\Im\{Z\}] && \text{(A.73)} \\ \mathrm{Var}[Z] &:= E|Z - EZ|^2 = E|Z|^2 - |EZ|^2 && \text{(A.74)} \\ \mathrm{Cov}[Z, W] &:= E[Z - EZ]E[W - EW]^* = E[ZW^*] - E[Z]E[W]^* && \text{(A.75)} \end{aligned}$$

Variance and Covariance have the properties $\mathrm{Var}[Z] \in \mathbb{R}$, $\mathrm{Var}[Z] \geq 0$ with 0 if and only if $Z = 0$ almost everywhere. $\mathrm{Cov}[W, Z] = \mathrm{Cov}[Z, W]^*$ and $\mathrm{Cov}[Z, Z] = \mathrm{Var}[Z] \in \mathbb{R}$.

If $\mathrm{Cov}[W, Z] = 0$ the random variables are called *uncorrelated*. If W and Z are independent, they are also uncorrelated.

The covariance properties of real- and imaginary part of a complex random variable are uniquely determined under the condition

$$\mathrm{Cov}[\Re\{Z\}, \Im\{Z\}] = 0, \quad \mathrm{Var}[\Re\{Z\}] = \mathrm{Var}[\Im\{Z\}]. \tag{A.76}$$

It follows $\mathrm{Var}[Z] = 2\mathrm{Var}[\Re\{Z\}] = 2\mathrm{Var}[\Im\{Z\}]$.

Covariance matrix of complex random vectors Let $\mathbf{Z}$ be an n-dimensional complex random column vector with expectation $\boldsymbol{\mu} := E\mathbf{Z}$. The *covariance matrix* of $\mathbf{Z}$ is defined by

$$\begin{aligned} \mathbf{R_Z} &:= E\left[(\mathbf{Z} - \boldsymbol{\mu})(\mathbf{Z} - \boldsymbol{\mu})^*\right] && \text{(A.77)} \\ &= \begin{pmatrix} E\left[(Z_1 - \mu_1)(Z_1 - \mu_1)^*\right] & \dots & E\left[(Z_1 - \mu_1)(Z_n - \mu_n)^*\right] \\ \dots & \dots & \dots \\ E\left[(Z_n - \mu_n)(Z_1 - \mu_1)^*\right] & \dots & E\left[(Z_n - \mu_n)(Z_1 - \mu_1)^*\right] \end{pmatrix} && \text{(A.78)} \\ &= \begin{pmatrix} \mathrm{Var}[Z_1] & \dots & \mathrm{Cov}[Z_1, Z_n] \\ \dots & \dots & \dots \\ \mathrm{Cov}[Z_n, Z_1] & \dots & \mathrm{Var}[Z_n] \end{pmatrix} && \text{(A.79)} \end{aligned}$$

A covariance matrix of a complex random vector is always Hermitean since

$$\begin{aligned} \mathbf{R}_\mathbf{Z}^* &= \left(E\left[(\mathbf{Z} - \boldsymbol{\mu})(\mathbf{Z} - \boldsymbol{\mu})^*\right]\right)^* && \text{(A.80)} \\ &= E\left[(\mathbf{Z} - \boldsymbol{\mu})(\mathbf{Z} - \boldsymbol{\mu})^*\right] && \text{(A.81)} \\ &= \mathbf{R_Z} && \text{(A.82)} \end{aligned}$$

Further it is *positive semidefinit* since

$$\begin{aligned}
\mathbf{x}^* \mathbf{R}_{\mathbf{Z}} \mathbf{x} &= \mathbf{x}^* E\left[(\mathbf{Z}-\boldsymbol{\mu})(\mathbf{Z}-\boldsymbol{\mu})^*\right]\mathbf{x} && \text{(A.83)}\\
&= E\left[\mathbf{x}^*(\mathbf{Z}-\boldsymbol{\mu})(\mathbf{Z}-\boldsymbol{\mu})^*\mathbf{x}\right] && \text{(A.84)}\\
&= E\left|(\mathbf{Z}-\boldsymbol{\mu})^*\mathbf{x}\right|^2 && \text{(A.85)}\\
&\geq 0 \text{ for all } \mathbf{x} \in \mathbb{C}^n. && \text{(A.86)}
\end{aligned}$$

Special distributions

Gaussian distribution, normal distribution of a real valued random variable: A real valued random variable is called *normal distributed* or *Gaussian distributed* with expectation μ and variance σ_X^2 if it has the pdf

$$p^X(x) = \frac{1}{\sqrt{2\pi\sigma_X^2}} \exp\left\{-\frac{(x-\mu)^2}{2\sigma_X^2}\right\} \tag{A.87}$$

We write $X \sim \mathcal{N}_{\mathbb{R}}(\mu, \sigma_X^2)$.

Gaussian distribution, normal distribution of a real valued random vector: A real valued random vector is called *normal distributed* or *Gaussian distributed* with expectation $\boldsymbol{\mu}$ and covariance matrix $\mathbf{R}_{\mathbf{X}}$ if it has the pdf

$$p^{\mathbf{X}}(\mathbf{x}) = \frac{1}{\sqrt{(2\pi)^n \det \mathbf{R}_{\mathbf{X}}}} \exp\left\{-\frac{1}{2}(\mathbf{x}-\boldsymbol{\mu})^t \mathbf{R}_{\mathbf{X}}^{-1}(\mathbf{x}-\boldsymbol{\mu})\right\} \tag{A.88}$$

We write $\mathbf{X} \sim \mathcal{N}_{\mathbb{R}^n}(\boldsymbol{\mu}, \mathbf{R}_{\mathbf{X}})$.

Gaussian distribution, normal distribution of a complex valued random variable: The random variable Z is called *complex Gaussian distributed* with expectation μ and variance σ^2, if $\Re\{Z\}$ and $\Im\{Z\}$ are uncorrelated and have the same variances $\sigma^2/2$. The density p^Z is given by

$$p^Z(z) = \frac{1}{\pi\sigma^2} \exp\left\{-\frac{|z-\mu|^2}{\sigma^2}\right\}. \tag{A.89}$$

We write $Z \sim \mathcal{N}_{\mathbb{C}}(\mu, \sigma^2)$.

Gaussian distribution, normal distribution of a complex valued random vector: A complex valued random vector $\mathbf{Z}$ is called *normal distributed* or *Gaussian distributed* with expectation $\boldsymbol{\mu}$ and covariance matrix $\mathbf{R}_{\mathbf{X}}$ if it has the pdf

$$p^{\mathbf{Z}}(\mathbf{z}) = \frac{1}{\pi^n \det \mathbf{R}_{\mathbf{Z}}} \exp\left\{-(\mathbf{z}-\boldsymbol{\mu})^* \mathbf{R}_{\mathbf{Z}}^{-1}(\mathbf{z}-\boldsymbol{\mu})\right\} \tag{A.90}$$

We write $\mathbf{Z} \sim \mathcal{N}_{\mathbb{C}^n}(\boldsymbol{\mu}, \mathbf{R}_{\mathbf{Z}})$.

Uncorrelated and stochastically independent Gaussian random variables If two real- or complex valued random variables are uncorrelated, they are independent. The phase of a $N_{\mathbb{C}}(0,\sigma^2)$-distributed random variable is rectangular distributed on $[0,2\pi]$ and independent on the amplitude.

Rectangular distribution: A real valued random variable R is distributed according to a *rectangular distribution* (or *uniformly distribution*) on the interval $[a,b]$, if the pdf is given by

$$p^R(r) = \begin{cases} \frac{1}{b-a}, \text{ if } r \in [a,b] \\ 0 \text{ else} \end{cases} \tag{A.91}$$

We write $R \sim \mathcal{R}(a,b)$.

Rayleigh distribution: Distribution of the amplitude of a $\mathcal{N}_{\mathbb{C}}(0,1)$ distributed random variable $X = |Z|$:

$$\begin{aligned} F^{Rayleigh}(x) &= Pr(|Z| \le x) \\ &= \frac{1}{\pi}\int e^{-|z|^2} dz = \frac{1}{\pi}\int_0^x \int_0^{2\pi} e^{-r^2} r d\varphi dr \, \{|z| \le x\} \\ &= 2\int_0^x e^{-r^2} r dr = 1 - e^{-x^2} \end{aligned} \tag{A.92}$$

$$\text{Density: } p^X(x) = 2xe^{-x^2} \tag{A.93}$$

Rician distribution: Distribution of $X = |a + Z|$ with $a \in \mathbb{C}$ and $Z \sim \mathcal{N}_{\mathbb{C}}(0,1)$.

$$\begin{aligned} F_a^{Rice}(x) &= \frac{1}{\pi}\int e^{-|z-a|^2} dz \, \{|z| \le x\} \\ &= \frac{1}{\pi}\int_0^x \int_0^{2\pi} e^{-r^2|a|^2 + 2|a| r\cos\varphi} r d\varphi dr \\ &= 2e^{-|a|^2}\int_0^x e^{-r^2} I_0(2|a| r) r dr \end{aligned} \tag{A.94}$$

$$\text{Density: } p^X(x) = 2x\, e^{-x^2-|a|^2} I_0(2|a| x) \tag{A.95}$$

A.5 Stochastic processes

For complex valued processes $Z(t)$ the definitions are analogue to the real valued case:

$$\begin{array}{ll}
\mu_Z(t) := E[Z(t)] & \text{deterministic part} \\
Z(t) - \mu_Z(t) & \text{stochastic part} \\
\sigma^2_{ZZ}(t) := \mathrm{Var}[Z(t)] & \text{variance function} \\
r_{ZZ}(t_1, t_2) := E[Z(t_1)Z^*(t_2)] & \text{correlation function} \\
c_{ZZ}(t_1, t_2) := \mathrm{Cov}[Z(t_1), Z(t_2)] & \text{covariance function} \\
\rho_{ZZ}(t_1, t_2) := \frac{c_{ZZ}(t_1,t_2)}{\sqrt{\sigma^2_{ZZ}(t_1)\sigma^2_{ZZ}(t_2)}} & \text{normalized covariance function}
\end{array} \tag{A.96}$$

For wide sense stationary complex valued stochastic processes the following definitions are given:

$$r_{ZZ}(\tau) := E[Z(t+\tau)Z^*(t)] \tag{A.97}$$

$$c_{ZZ}(\tau) := \mathrm{Cov}[Z(t+\tau), Z^(t)] \tag{A.98}$$

$$\rho_{ZZ}(\tau) := \frac{c_{ZZ}(\tau)}{\sigma^2_{ZZ}} \tag{A.99}$$

$$C_{ZZ}(\omega) := \int C_{ZZ}(\tau)e^{-2\pi j\omega\tau}d\tau \text{ spectral power density} \tag{A.100}$$

A.6 Estimation

A.6.1 The general estimation problem

If the model for the distribution of the random variable X contains an unknown parameter vector $\boldsymbol{\vartheta} \in \boldsymbol{\Theta}$, the basic problem is to estimate this parameter vector with an estimator $\hat{\boldsymbol{\vartheta}}(x)$ for a given realization x of X.

For each $\boldsymbol{\vartheta}$ the distribution $P^X_{\boldsymbol{\vartheta}}$ of X and the probability distribution function (pdf) $p^X_{\boldsymbol{\vartheta}}(x)$ are parametrized by this parameter vector.

A.6.2 Approaches to estimators

Performance of estimators

If $\hat{\boldsymbol{\vartheta}}(x)$ is an estimator of $\boldsymbol{\vartheta}$, the *bias* is defined by

$$\mathbf{B}_{\hat{\boldsymbol{\vartheta}}}(\boldsymbol{\vartheta}) = E_{\boldsymbol{\vartheta}}\left[\hat{\boldsymbol{\vartheta}}(X)\right] - \boldsymbol{\vartheta}. \tag{A.101}$$

If the bias is zero for all $\boldsymbol{\vartheta} \in \boldsymbol{\Theta}$, we call this estimator *bias-free*.

As a performance measure of the estimator we introduce the expectation of the quadratic deviation from the true value:

$$\mathbf{Q}_{\hat{\boldsymbol{\vartheta}}}(\boldsymbol{\vartheta}) := E_{\boldsymbol{\vartheta}}\left[\left(\hat{\boldsymbol{\vartheta}}(X) - \boldsymbol{\vartheta}\right)\left(\hat{\boldsymbol{\vartheta}}(X) - \boldsymbol{\vartheta}\right)^t\right] \tag{A.102}$$

$$= \mathbf{R}_{\hat{\boldsymbol{\vartheta}}}(\boldsymbol{\vartheta}) + \mathbf{B}_{\hat{\boldsymbol{\vartheta}}}(\boldsymbol{\vartheta})\mathbf{B}^t_{\hat{\boldsymbol{\vartheta}}}(\boldsymbol{\vartheta}) \tag{A.103}$$

where $\mathbf{R}_{\hat{\boldsymbol{\vartheta}}}$ is the covariance matrix of the estimator $\hat{\boldsymbol{\vartheta}}(x)$ as a function of $\boldsymbol{\vartheta}$.

Best unbiased estimator. Weights of estimation. Order of matrices.

Best unbiased estimators

A desired property of an estimator is that its expectation is equal to the parameter vector itself. The *bias* is defined by

$$B_{\boldsymbol{\vartheta}}(\hat{\boldsymbol{\vartheta}}) = E_{\boldsymbol{\vartheta}}\left[\hat{\boldsymbol{\vartheta}}(X)\right] - \boldsymbol{\vartheta}. \tag{A.104}$$

The subscript $\boldsymbol{\vartheta}$ at the expectation operator means that the probability distribution according to this parameter vector is assumed. An estimator is called *bias free* if $B_{\boldsymbol{\vartheta}}(\hat{\boldsymbol{\vartheta}}) = 0$ for all $\boldsymbol{\vartheta} \in \boldsymbol{\Theta}$.

The second desired property of an one-dimensional real valued estimator is that its variance is minimum. If the parameter vector has a dimension larger than 1, the variance has to be replaced by the covariance matrix, and the half order of covariance matrices is defined according to section A.1.5.

So an estimator $\hat{\boldsymbol{\vartheta}}$ is called *best unbiased estimator*, if it is unbiased and has the minimum covariance matrix among all unbiased estimators for all $\boldsymbol{\vartheta} \in \boldsymbol{\Theta}$.

Maximum likelihood estimators

Unfortunately, for the most estimation problems in radar signal processing, best unbiased estimators don't exist. A more practical way is the *maximum likelihood estimator* which mostly leads to a feasible near optimum algorithm. This approach chooses as estimator the parameter vector for which the realization has a 'maximum likelihood' (illustrated in Fig. 1.21):

$$\hat{\boldsymbol{\vartheta}}(x) = \operatorname{argmax}\left\{p^X_{\boldsymbol{\vartheta}}(x) : \boldsymbol{\vartheta} \in \boldsymbol{\Theta}\right\}. \tag{A.105}$$

$p^X_{\boldsymbol{\vartheta}}(x)$ is called *likelihood function* (as function of $\boldsymbol{\vartheta}$), $\hat{\boldsymbol{\vartheta}}(x)$ is the *maximum-likelihood estimator (ML estimator)*. Equivalent with the maximization of the likelihood function is the maximization of the logarithm of the pdf: $L^X_{\boldsymbol{\vartheta}}(x) := \ln\left(p^X_{\boldsymbol{\vartheta}}(x)\right)$, called *log-likelihood function*.

$$\hat{\boldsymbol{\vartheta}}(x) = \operatorname{argmax}\left\{L^X_{\boldsymbol{\vartheta}}(x) : \boldsymbol{\vartheta} \in \boldsymbol{\Theta}\right\}. \tag{A.106}$$

If the partial derivatives of the log-likelihood function with respect to $\boldsymbol{\vartheta}$ exist, the necessary condition for an extremum is

$$\frac{\partial}{\partial \boldsymbol{\vartheta}} L^X_{\boldsymbol{\vartheta}}(x)|_{\boldsymbol{\vartheta}=\hat{\boldsymbol{\vartheta}}(x)} = \mathbf{0}. \tag{A.107}$$

A.6.3 Cramér-Rao Bounds

The *Cramér-Rao Bounds* offer the possibility to obtain a lower bound for the expected quadratic error of an estimator without specifying an estimation algorithm. The quality of any estimator is dependent on the *information* implicitly contained in the probability distribution as function of the parameter to be estimated. This information is measurable: The *Fisher-information* relates to a single real parameter, the *Fisher-information matrix* represents the information about a parameter vector. For a family of pdf's $p^X_{\boldsymbol{\vartheta}}, \boldsymbol{\vartheta} \in \boldsymbol{\Theta}$ the Fisher-information matrix is defined by:

$$\mathbf{J}(\boldsymbol{\vartheta}) = E\left[\left(\frac{\partial}{\partial \boldsymbol{\vartheta}} \ln p^X_{\boldsymbol{\vartheta}}(X)\right)\left(\frac{\partial}{\partial \boldsymbol{\vartheta}} \ln p^X_{\boldsymbol{\vartheta}}(X)\right)^t\right]. \tag{A.108}$$

This matrix has remarkable properties appropriate to an information measure; so invertible transformations of a statistic do not change the Fisher-information matrix, the information of an independent pair of distributions is the sum of the individual information measures and so on.

For any unbiased estimator $\hat{\boldsymbol{\vartheta}}$ for $\boldsymbol{\vartheta}$ the following inequation is valid, if Fisher's information matrix is invertible:

$$\mathbf{R}_{\hat{\boldsymbol{\vartheta}}}(\boldsymbol{\vartheta}) \geq \mathbf{J}^{-1}(\boldsymbol{\vartheta}). \tag{A.109}$$

If the equality sign holds, the estimator is called *efficient*.

If we use the statistical model **??**

$$\mathbf{Z} = \mathbf{m}(\boldsymbol{\vartheta}) + \mathbf{Q} \tag{A.110}$$

with a deterministic complex vector $\mathbf{m}(\boldsymbol{\vartheta})$ and interference $\mathbf{Q} \sim \mathcal{N}_{\mathbb{C}^n}(\mathbf{0}, \mathbf{R})$, Fisher's information matrix is given by

$$\mathbf{J}(\boldsymbol{\vartheta}) = \frac{2}{\sigma^2} Re\left\{\mathbf{m}^*_{\boldsymbol{\vartheta}}(\boldsymbol{\vartheta})\mathbf{R}^{-1}\mathbf{m}_{\boldsymbol{\vartheta}}(\boldsymbol{\vartheta})\right\} \tag{A.111}$$

where $\mathbf{m}_{\boldsymbol{\vartheta}}(\boldsymbol{\vartheta})$ means the gradient of $\mathbf{m}_{\boldsymbol{\vartheta}}$ with respect to $\boldsymbol{\vartheta}$ written as $n \times k$ matrix.

Proof: The log-likelihood Function is

$$L^{\mathbf{Z}}_{\boldsymbol{\vartheta}}(\mathbf{z}) = -\ln(\pi^n \sigma^{2n}) - \frac{1}{\sigma^2}\left\|\mathbf{z} - \mathbf{m}(\boldsymbol{\vartheta})\right\|^2 \tag{A.112}$$

and the Fisher-information matrix is calculated using $\mathbf{m}_{\boldsymbol{\vartheta}}(\boldsymbol{\vartheta}) := \frac{\partial}{\partial \boldsymbol{\vartheta}}\mathbf{m}(\boldsymbol{\vartheta}) :=$

$\left(\frac{\partial}{\partial\vartheta_1}\mathbf{m}(\boldsymbol{\vartheta}),\cdots,\frac{\partial}{\partial\vartheta_K}\mathbf{m}(\boldsymbol{\vartheta})\right)$ to

$$\begin{aligned}
\mathbf{J}(\boldsymbol{\vartheta}) &= E_{\boldsymbol{\vartheta}}\left[\left(\frac{\partial}{\partial\boldsymbol{\vartheta}}L^{\mathbf{Z}}_{\boldsymbol{\vartheta}}(\mathbf{Z})\right)\left(\frac{\partial}{\partial\boldsymbol{\vartheta}}L^{\mathbf{Z}}_{\boldsymbol{\vartheta}}(\mathbf{Z})\right)^t\right] && \text{(A.113)}\\
&= \frac{1}{\sigma^4}E_{\boldsymbol{\vartheta}}\left[\left(\frac{\partial}{\partial\boldsymbol{\vartheta}}\left\|\mathbf{Z}-\mathbf{m}(\boldsymbol{\vartheta})\right\|^2\right)\left(\frac{\partial}{\partial\boldsymbol{\vartheta}}\left\|\mathbf{Z}-\mathbf{m}(\boldsymbol{\vartheta})\right\|^2\right)^t\right] && \text{(A.114)}\\
&= \frac{1}{\sigma^4}E_{\boldsymbol{\vartheta}}\left[2Re\left\{\mathbf{N}^*\mathbf{m}_{\boldsymbol{\vartheta}}(\boldsymbol{\vartheta})\right\}^t 2Re\left\{\mathbf{N}^*\mathbf{m}_{\boldsymbol{\vartheta}}(\boldsymbol{\vartheta})\right\}\right] && \text{(A.115)}\\
&= \frac{1}{\sigma^4}E_{\boldsymbol{\vartheta}}\left[\left(\mathbf{N}^*\mathbf{m}_{\boldsymbol{\vartheta}}(\boldsymbol{\vartheta})+\mathbf{m}^*_{\boldsymbol{\vartheta}}(\boldsymbol{\vartheta})\mathbf{N}\right)^t\left(\mathbf{N}^*\mathbf{m}_{\boldsymbol{\vartheta}}(\boldsymbol{\vartheta})+\mathbf{m}^*_{\boldsymbol{\vartheta}}(\boldsymbol{\vartheta})\mathbf{N}\right)\right]. && \text{(A.116)}
\end{aligned}$$

We get

$$\mathbf{J}(\boldsymbol{\vartheta}) = \frac{2}{\sigma^2}Re\left\{\left(\mathbf{m}_{\boldsymbol{\vartheta}}(\boldsymbol{\vartheta})\right)^*\mathbf{m}_{\boldsymbol{\vartheta}}(\boldsymbol{\vartheta})\right\} \quad \text{(A.117)}$$

A.7 Power of filtered noise

Let N be white noise, t.i. $C_{NN}(f)=\sigma^2$ for all frequencies f, which is passed through a filter with pulse response $h\in L_2(\mathbb{C})$. The expected power of the filter output is evaluated over the spectral density:

$$\begin{aligned}
E\left|(h\star N)(0)\right|^2 &= E\left|\int h(-t)N(t)dt\right|^2 && \text{(A.118)}\\
&= E\int\int h^*(-t)N^*(t)h(-t')N(t')dtdt' && \text{(A.119)}\\
&= E\int\int h^*(-t)N^*(t)h(-t-\tau)N(t+\tau)dtd\tau && \text{(A.120)}\\
&= \int\left(\int h^*(t)h(t-\tau)dt\right)r_{NN}(\tau)d\tau && \text{(A.121)}\\
&= \int\left(\int |H(f)|^2\exp\{-j2\pi f\tau\}df\right)r_{NN}(\tau)d\tau && \text{(A.122)}\\
&= \int |H(f)|^2 C_{NN}(f)df && \text{(A.123)}\\
&= \sigma^2\int |H(f)|^2 df && \text{(A.124)}\\
&= \sigma^2\|h\|^2 && \text{(A.125)}
\end{aligned}$$

Index

Bibliography

[1] F. Le Chevalier: 'Principles of Radar and Sonar Signal Processing', Artech House 2002, ISBN 1-58053-338-8

[2] A. Farina: 'Antenna-Based Signal Processing Techniques for Radar Systems', Artech House 1992, ISBN 0-89006-396-6

[3] N. Fourikis: 'Phased Array-Based Systems and Applications', Wiley series in microwave and optical engineering, 1997, ISBN 0-471-01212-2

[4] A. Papoulis: 'Signal analysis', McGraw-Hill, New York, 1977

[5] A. W. Rihaczek: 'Principles of High-Resolution Radar', Artech House 1996, ISBN 0-89006-900-X

[6] M. I. Skolnik: 'Introduction to Radar Systems', third edition 2001, McGraw-Hill, ISBN 0-07-290980-3

[7] D. R. Wehner: 'High-Resolution Radar', second edition, Artech House, 1995, ISBN 0-89006-727-9

[8] W. D. Wirth: 'Radar techniques using array antennas', IEE Radar, Sonar, Navigation and Avionics Series 10, London 2001, ISBN 0 85296 798 5

[9] R. E. Collin, F. J. Zucker: 'Antenna Theory', McGraw Hill 1969

[10] J. Ender, D. Cerutti-Maori: *Position Estimation of Moving Vehicles for Space-Based Multi-Channel SAR/MTI Systems,* European Conference on Synthetic Aperture Radar, European Conference on Synthetic Aperture Radar, EUSAR 2006, Dresden, May 2006

[11] J. Ender, C. Gierull, D. Cerutti-Maori, "Improved Space-Based Moving Target Indication via Alternate Transmission and Receiver Switching," Geoscience and Remote Sensing, IEEE Transactions on , vol. 46, no.12, pp.3960-3974, Dec. 2008.

[12] J. Neyman, E. Pearson: 'On the Problem of the Most Efficient Tests of Statistical Hypotheses', Philosophical Transactions of the Royal Society of London. Series A, Containing Papers of a Mathematical or Physical Character 231, pp. 289-337, 1933

[13] U. Nickel: *An Overview of Generalized Monopulse Estimation*, IEEE A&E System Magazine Vol. 21, No.6 June 2006, Part 2:Tutorials, pp. 27-55

[14] R. K. Raney, H.Runge, R. Bamler, I. G. Cumming, F. H. Wong: 'Precision SAR Processing using Chirp Scaling', IEEE Transactions on Geoscience and Remote Sensing, vol. 32, No. 4, pp. 786-799, July 1994

[15] J. Ward, G. F. Hatke: *An Efficient Rooting Algorithm for Simultaneous Angle and Doppler Estimation with Space-Time Adaptive Processing Radar* ASILOMAR97, Nov. 1997, Pacific Grove, CA

Appendix B

Exercises

B.1

How large is the maximum signal-to-noise-ratio for a matched filter in the RF domain if a narrow band signal with fixed carrier frequency and triangular envelope is used? The additive noise is assumed to be white with the spectral power density $N_0/2$.

B.2

Calculate the point spread function for a Gaussian base band signal
$s(t) = \frac{1}{\sqrt{2\pi t_s^2}} \exp\left\{-\frac{t^2}{2t_s^2}\right\}$ for matched filtering!

B.3

Let $\mathbf{Z} = a\mathbf{s} + \mathbf{N}$ be a vector composed by N complex samples with a known deterministic signal $\mathbf{s}$ and $\mathcal{N}_{\mathbb{C}^N}(\mathbf{0}, \sigma^2\mathbf{I}_N)$-distributed noise $\mathbf{N}$. Derive with the method of minimum mean squares an estimator $\hat{a}(\mathbf{z})$ of a and calculate its expectation and variance!

B.4

As exercise B.3, but as superposition of known signals with unknown complex amplitudes:
$\mathbf{Z} = \sum_{k=1}^{K} a_k\mathbf{s}_k + \mathbf{N}$ with $K \leq N$. In matrix notation: $\mathbf{Z} = \mathbf{Sa} + \mathbf{N}$ with
$\mathbf{S} = (s_1, \ldots, s_K), \mathbf{a} = (a_1, \ldots, a_K)^t$.
Determine

1) $\hat{\mathbf{a}}(\mathbf{z}) = \operatorname{argmin}\left\{\|\mathbf{z} - \mathbf{Sa}\|^2 : \mathbf{a} \in \mathbb{C}^K\right\}$

2) $\mathbf{z} - \mathbf{S}\hat{\mathbf{a}}(\mathbf{z})$

3) $\|\mathbf{z} - \mathbf{S}\hat{\mathbf{a}}(\mathbf{z})\|^2$

and the expectations of these quantities!

B.5

For the base band signal $s(t) = rect(t/t_s)$ with subsequent matched filtering and sampling with $\Delta t = t_s$ determine the maximum-likelihood estimate of the time delay τ for unknown complex amplitude a. It is assumed to be known that

$\tau/\Delta t \in [\nu_0 - 1/2, \nu_0 + 1/2]$.

B.6

Let a coherent pulse radar with RF frequency ($f_0 = 3GHz$) be operated with rectangular pulses of the width $t_s = 1\mu s$ at a PRF of 1 kHz. How large is the unambiguous range interval if the transmit-receive switch causes a 'dead time' of 2 μs? How many range cells with full integration are obtainable at a sampling with $\Delta t = t_s$? At which radial velocity rotates the phase from pulse to pulse by 360° ('blind velocity')? Which shape has the spectrum of the received base band signal if a pulse train of ten pulses is transmitted? How does this change if the object is moving at a radial velocity $v_r = 10m/s$? (A sketch with declaration of the relevant frequencies is sufficient!).

B.7

At the output of a quadrature modulator the band limited signal s_{RX} with bandwidth b is superposed by noise with power density $C_{NN}(f) = N_0 rect(f/b_n)$ and $b_s < b_n$. Let this signal be sampled an filtered by a digital filter with transfer function $H(f) = S^*(f)$. Discuss the deterministic signal spectrum and the noise power spectral density of the output signal for the cases $b_s < f_s < b_n$ and $b_n < f_s$! What does this mean for the signal-to-noise ratio of the filtered signal (heuristics and sketches are sufficient!).

B.8

Let a continuous-wave (CW) radar transmit a signal s which is repeated with the period ΔT: $q(t) = \sum_{\nu=\infty}^{\infty} \mathsf{s}(t - \nu\Delta T)$.

At the receiver baseband output a filter is applied matched to one cycle. Which point spread function can be stated for a phase coded base band signal of the

form $\mathsf{s}(t) = e^{j\psi_\mu}$ for $t \in [\mu\Delta t, (\mu+1)\Delta t]$, $\mu = 0, \ldots, m-1$ with $m = k^2$ and $k \in \mathbb{N}, \Delta t = \Delta T/m$? ψ_μ is defined by $\psi_\mu = (\mu \bmod k)(\mu \operatorname{div} k)\, 2\pi/k$ *(Frank code).*

B.9

Evaluate the ambiguity function for a chirp with rectangular envelope $\mathsf{s}(t) = t_s^{-1/2}\mathrm{rect}(t/t_s)\, e^{j\pi\alpha t^2}$.

a) How large is the range resolution, defined by the first null, for $\nu = 0$ (no Doppler shift) as a function of α? Regard also the limiting cases $\alpha = 0$ and $\alpha \to \infty$.

b) For which τ decreases $\chi(\tau, \nu(\tau))$ to the half power? Here, $\nu(\tau)$ is defined as the Doppler shift for which the power ambiguity is maximum for fixed τ.

B.10

Design a detector for the model

$Z_\nu = ae^{j\phi_\nu} + N_\nu$ for $\nu = 1 \ldots n$, ϕ_ν, N_ν stoch. independent for $\nu = 1 \ldots n$, $\phi_\nu \sim \mathcal{R}(0, 2\pi)$,$N_\nu \sim \mathcal{N}_{\mathbb{C}}(0, \sigma^2)$ for $\nu = 1 \ldots n$. a is assumed to be non-negative real valued, and the test problem is to decide between H: $a = 0$ and K: $a > 0$ (*incoherent detection*).

Approximate the distribution of the obtained test by a normal distribution and derive the approximated threshold and detection probability for n tending to ∞. For fixed P_E and P_F a signal-to-noise ratio $\gamma_n = (a/\sigma)^2$ is necessary. Determine the rate of γ_n tending to zero and compare this with the analogue result for coherent detection!

B.11

Let a Doppler filter bank for a data vector of the length N consist of $2N$ filters for a uniform distribution of the Doppler angle increment over $[0, 2\pi]$. Calculate the covariance matrix of the $2N$ dimensional output vector, if the input is given by a deterministic signal plus noise with covariance matrix $\sigma^2\mathbf{I}_N$! Further, derive the eigenvalues of this covariance matrix!

B.12

Let $\mathbf{Z}$ be $\mathcal{N}_{\mathbb{C}^N}(\mathbf{0}, \sigma^2\mathbf{I}_N)$-distributed. Develop a test for H: $\sigma^2 = \sigma_0^2$ against K:$\sigma^2 = \sigma_1^2$ with $\sigma_1 > \sigma_0$!

B.13

Develop a maximum-likelihood-ratio test for the model
$\mathbf{Z} = \mathbf{Sa} + \mathbf{N}$, $\mathbf{N} \sim \mathcal{N}_{\mathbb{C}^N}(\mathbf{0}, \sigma^2 \mathbf{I}_N)$ with a known $N \times K$ matrix $\mathbf{S}$ and an unknown amplitude vector $\mathbf{a} \in \mathbb{C}^K$ for H: $\mathbf{a} = \mathbf{0}$ against K: $\mathbf{a} \neq \mathbf{0}$! Which distribution has the test statistic under the hypothesis?

B.14

Often the temporal behavior of clutter echoes can be modelled by an autoregressive stochastic process. Let the process $C_\nu := C(\nu \Delta T), \nu \in \mathbb{Z}$ be modelled as autoregressive of order one:

$C_\nu = \rho C_{\nu-1} + M_\nu$ for $\nu \in \mathbb{Z}$ with identical independent excitations $M_\nu \sim \mathcal{N}_{\mathbb{C}}(0, \sigma^2)$ and $|\rho| < 1$.

a) Which transfer function has the linear system that transforms the time series $(M_\nu)_{\nu \in \mathbb{Z}}$ into the process $(C_\nu)_{\nu \in \mathbb{Z}}$?

b) Calculate the Doppler spectrum of the clutter!

c) Determine a sequential clutter filter which transforms $(C_\nu)_{\nu \in \mathbb{Z}}$ into white noise and calculate its transfer function!

d) Which SCR gain obtains this filter?

B.15

Show that the de-ramping technique does not change the range resolution compared to direct matched filtering according to the transmitted chirp!

B.16

Recall that the point spread function for matched filtering is equal to the Fourier back transform of the square magnitude of the signal spectrum ($P(f) = |\mathsf{S}(f)|^2$). As you know, the application of a 'well-shaped' window in the frequency domain before the Fourier back transform effects low side lobes of the point spread function. But this is connected to a loss of SNR. It would be preferable to design the transmitted waveform in order to get a 'well-shaped' magnitude-square spectrum $|\mathsf{S}(.)|^2$ from the beginning. On the other hand, the amplitude of the waveform should be constant in the time domain to drive the last amplifier to maximum output power. How can you construct a waveform $\mathsf{s}(t) = \exp\{j\varphi(t)\}, t = -t_s/2, \cdots, t_s/2$ with phase modulation only to obtain approximately a given shape $W(.)$ of $|\mathsf{S}(.)|^2$?

B.17

Let the sampling of a signal from pulse to pulse modelled by an N dimensional random vector $\mathbf{Z} = a\mathbf{s}(F) + \mathbf{N}$,$\mathbf{N} \sim \mathcal{N}_{\mathbb{C}^N}(\mathbf{0}, \sigma^2\mathbf{I}_N)$, where

$$\mathbf{s}(F) = \begin{pmatrix} \exp\{j2\pi \left(1 - \frac{N+1}{2}\right) F\Delta T\} \\ \vdots \\ \exp\{j2\pi \left(N - \frac{N+1}{2}\right) F\Delta T\} \end{pmatrix}.$$

The complex amplitude $a = \alpha e^{j\psi}$ is unknown as well as the Doppler frequency F. Derive the maximum-likelihood estimator for F and calculate the Cramér-Rao Bounds for the estimation of F at unknown a!

B.18

For a simple monopulse radar with the aperture divided into two equal parts the two receive signals can be modelled by a vector $\mathbf{Z} = a \begin{pmatrix} e^{jk_r du_0/2} \\ e^{-jk_r du_0/2} \end{pmatrix} + \mathbf{N}$ with $\mathbf{N} \sim \mathcal{N}_{\mathbb{C}^2}(\mathbf{0}, \sigma^2\mathbf{I}_2)$.

The estimation of the directional cosine is performed by

$\hat{u}(\mathbf{z}) = \frac{2}{k_r d} \Im\{Q(\mathbf{z})\}$ with $Q(\mathbf{z}) = \frac{\Delta}{\Sigma} = \frac{z_1 - z_2}{z_1 + z_2}$.

Calculate the variance of $\hat{u}$, if the real direction is $u_0 = 0$ in the approximation for SNR $\to \infty$. Compare the result with the Cramér-Rao Bounds from exercise B.17 with $N = 2$ and equivalent replacement of the Doppler frequency by the directional cosine!

B.19

We regard an object in the object coordinate system (x, y) which is rotated on a turntable in clock sense while a radar measures this object from a large (far field) distance R_0 to the origin. The direction of the transmitted wave is described by the unit vector

$$\mathbf{u}(\varphi) = \begin{pmatrix} \cos\varphi \\ \sin\varphi \end{pmatrix}. \tag{B.1}$$

in the object-fixed coordinate system. Now we assume a point scatterer at position $\vec{r} = (x, y)^t$. For the azimuth angle φ the distance to the point scatterer is given by

$$\begin{aligned} R(\varphi; x, y) &= \sqrt{(R_0 \cos\varphi + x)^2 + (R_0 \sin\varphi + y)^2} \\ &\approx R_0 + (x\cos\varphi + y\sin\varphi) \\ &= R_0 + \langle \vec{u}(\varphi), \vec{r} \rangle . \end{aligned} \tag{B.2}$$

Now a Fourier transform is performed over φ:
$S(k_\varphi, k_r; x, y) := \frac{1}{2\pi} \int_0^{2\pi} e^{-jk_r\varphi} s(\varphi, k_r; x, y) d\varphi$. Using the principle of stationary phase, approximate this signal!